Dissertation

submitted to the

Combined Faculty of Mathematics, Engineering and Natural Sciences

of Heidelberg University, Germany

for the degree of

Doctor of Natural Sciences

Put forward by

Rachel A. Hanley

born in: Dublin, Ireland

Oral examination: $15^{th}$ February 2022

# Radio-Resistance of Hypoxic Tumours: The Effects of Oxygen and Radiation on Cancer Cell Metabolism, Oxidative Stress, and DNA Repair

Referees:

Prof. Dr. Joao Seco

Prof. Dr. Christian Karger

# Abstract

Cancers are often riddled with areas of low oxygen concentration (i.e. hypoxic regions) and these are, in fact, more resistant to treatments such as photon radiation which primarily relies on oxygen for the production of reactive oxygen species (ROS) to induce damage on the DNA. Cancer cells adapt to hypoxia by activating complex changes in their cellular processes, for example, in the oxidant environment and DNA damage response (DDR) as well as modifying their metabolism. The present study showed that hypoxic tumour cells from various organs have strong, albeit different, reducing capabilities and can adequately alter their energy production processes for enhanced survival and resistance to irradiation (IR). Hypoxic lung cancer cells have reduced DNA damages which correlated with their enhanced clonogenic survival. In addition, their antioxidant capacity was upregulated, resulting in a reduced cytosolic $H_2O_2$ content. Moreover, nuclear $H_2O_2$ induction of DNA double strand breaks (DSBs) was oxygen dependent, highlighting the reliance of photon IR on oxygen to generate ROS for indirect DNA damage. In conclusion, our findings highlight common and/or distinctive traits in different tumours with regions of hypoxia and elucidate the resistant behaviour of these cells, and can therefore possibly provide insight into improving radiation sensitivity.

# Zusammenfassung

Krebsgeschwüre sind oft von Gebieten mit niedriger Sauerstoffkonzentration durchlöchert (hypoxische Gebiete), die eine erhöhte Resistenz für Behandlungen wie Photonen-Strahlentherapie besitzen, welche primär auf Sauerstoff für die Produktion von reaktiven Sauerstoffspezies (ROS) angewiesen sind um DNA Schäden zu induzieren. Krebszellen passen sich an Sauerstoffmangel durch komplexe Veränderungen in ihren zellulären Prozessen an, zum Beispiel in der Redox-Umgebung und DNA-Schadensantwort, sowie durch Modifikation ihres Metabolismus. Diese Arbeit hat gezeigt dass hypoxische Krebszellen von verschiedenen Organen starke, wenn auch unterschiedliche, Reduktionsmöglichkeiten besitzen und ihre Energieproduktionsprozesse verändern können, um ihr Überleben und den Widerstand gegen ionisierende Strahlung zu verbessern. Hypoxische Lungenkrebszellen haben reduzierte DNA-Schäden, welche mit ihrem verstärkten koloniebildenden Überleben korrelierten. Zusätzlich war ihre antioxidative Kapazität hochreguliert, was in einer reduzierten Menge von $H_2O_2$ im Zytosol resultierte. Außerdem war die nukleare $H_2O_2$ Induktion von DNA-Doppelstrangbrüchen sauerstoffabhängig, was den wichtigen Einfluss von Sauerstoff auf Photonen-Strahlentherapie zeigte welcher nötig ist um ROS für indirekte DNA-Schäden zu generieren. Zusammengefasst zeigen unsere Resultate gemeinsame und/oder charakteristische Eigenschaften in verschiedenen Tumoren mit sauerstoffarmen Regionen, verdeutlichen das resistente Verhalten dieser Zellen und können somit möglicherweise helfen die Genauigkeit von Strahlentherapie zu verbessern.

# Contents

**Abstract** ii

**Zusammenfassung** iv

**1 Introduction** 1
- 1.1 Radiotherapy . . . 1
  - 1.1.1 Basic physics of radiotherapy . . . 1
  - 1.1.2 Linear quadratic model of cell survival . . . 9
  - 1.1.3 The target of radiotherapy - The DNA . . . 10
- 1.2 Cellular Oxidants and Antioxidants . . . 12
  - 1.2.1 Water radiolysis and $H_2O_2$ production . . . 12
  - 1.2.2 Reactive oxygen species (ROS) . . . 14
  - 1.2.3 Anti-oxidant response . . . 14
- 1.3 DNA Damage Response (DDR) and Repair . . . 17
  - 1.3.1 Cell cycle checkpoints . . . 18
  - 1.3.2 DNA repair pathways: an overview . . . 18
  - 1.3.3 ROS involvement in the DDR . . . 21
- 1.4 Tumour Hypoxia and Metabolic Reprogramming . . . 23
  - 1.4.1 Tumour Hypoxia and Oxygen Enhancement Ratio . . . 24
  - 1.4.2 Hypoxia Inducible Factors (HIFs) and their role in radiation responses . . . 25
  - 1.4.3 DNA damage and DDR in Hypoxia . . . 28
  - 1.4.4 Energy metabolism and oxygen consumption . . . 29
  - 1.4.5 Redox metabolism: Mitochondrial ROS, Pentose Phosphate Pathway . . . 34

**2 Overview of Thesis** 38
- 2.1 Motivation of current research . . . 38
- 2.2 Aims and objectives of research . . . 40

**3 Metabolic adaption of cancer cell lines to different levels of hypoxia and photon radiation** 41
- 3.1 Introduction . . . 41
- 3.2 Materials & Methods . . . 42
  - 3.2.1 Cell Culture . . . 42

3.2.2 Oxygen concentration measurements using oxygen sensor spots . . . . . 43
3.2.3 Oxygen removal rate of cells using oxygen sensor spots . . . . . 45
3.2.4 Membrane and Nuclear Staining . . . . . 45
3.2.5 Confocal Microscopy . . . . . 45
3.2.6 ATP Assay . . . . . 46
3.2.7 Redox Assay . . . . . 46
3.2.8 Propidium Iodide (PI) Staining for Cell Cycle Analysis . . . . . 47
3.2.9 Clonogenic Assays . . . . . 47
3.2.10 RNA extraction, cDNA sythesis and RT-qPCR . . . . . 48
3.2.11 Image Processing: IMARIS . . . . . 49
3.2.12 Statistical Analysis . . . . . 50
3.3 Results: Hypoxia Adaption . . . . . 51
3.3.1 Measurement of oxygen removal rate (ORR) in-vitro using $O_2$ sensors . . 51
3.3.2 Morphological changes of cell and nucleus volumes in response to acute and chronic hypoxia . . . . . 53
3.3.3 Cell cycle changes in response to acute and chronic hypoxia . . . . . 56
3.3.4 Energy (i.e. ATP) metabolism changes in response to acute and chronic hypoxia . . . . . 58
3.3.5 Reducing power of cancer cell lines in response to acute and chronic hypoxia . . . . . 59
3.4 Results: Radiation Effect . . . . . 62
3.4.1 Clonogenic survival ability of different cancer cell lines in normoxia and hypoxia . . . . . 62
3.4.2 Morphological changes of cell and nucleus volumes of irradiated cancer cells in normoxia and severe chronic hypoxia . . . . . 67
3.4.3 Cell cycle progression of irradiated cancer cells in normoxia and severe chronic hypoxia . . . . . 69
3.4.4 Energy (ATP) metabolism of irradiated cancer cells in normoxia and severe chronic hypoxia . . . . . 70
3.4.5 Reducing power of irradiated cancer cell lines in normoxia and severe chronic hypoxia . . . . . 73
3.4.6 RT-qPCR analysis of genetic expression of irradiated cancer cells in normoxia and severe chronic hypoxia . . . . . 75
3.5 Discussion . . . . . 84

**4 Measurement of the radio-response of non-small cell lung cancer (NSCLC) cell lines exposed to chronic hypoxia 92**
4.1 Introduction . . . . . 92
4.2 Materials & Methods . . . . . 94
4.2.1 Cell Culture . . . . . 94
4.2.2 Clonogenic Assay: Hypoxia & Normoxia . . . . . 95

4.2.3 Immunofluorescent Assay: $\gamma$H2AX Foci Staining . . . 96
4.2.4 Nuclear $H_2O_2$ Staining/Cell cycle staining . . . 97
4.2.5 Nuclear Extraction for Flow Cytometric Analysis . . . 98
4.2.6 Cytosolic $H_2O_2$ Staining . . . 98
4.2.7 GSH/GSSG Assay . . . 100
4.2.8 Cell Death Assay using Propidium Iodide . . . 101
4.2.9 RNA extraction, cDNA sythesis and RT-qPCR . . . 101
4.2.10 Confocal and Widefield Microscopy . . . 102
4.2.11 Image Processing: Imagej . . . 103
4.2.12 Statistical Analysis . . . 103
4.3 Results . . . 104
4.3.1 Cell growth of lung cancer cell lines under different oxygen conditions . . 104
4.3.2 Radio-response of lung cancer cell lines under different oxygen conditions 106
4.3.3 DSB detection after IR in normoxia and hypoxia . . . 110
4.3.4 Nuclear hydrogen peroxide ($H_2O_2$) levels of lung cancer cell lines evaluated in normoxia and hypoxia . . . 117
4.3.5 Cytosolic hydrogen peroxide ($H_2O_2$) levels of lung cancer cell lines evaluated in normoxia and hypoxia . . . 120
4.3.6 Measurement of glutathione levels of lung cancer cells in normoxia and hypoxia . . . 122
4.3.7 Cell cycle progression after IR in normoxia and hypoxia . . . 128
4.3.8 RT-qPCR analysis of gene alteration in the antioxidant pathways after irradiation in normoxia and hypoxia . . . 133
4.3.9 RT-qPCR analysis of gene alteration in the repair pathways after irradiation in normoxia and hypoxia . . . 141
4.4 Discussion . . . 149

**5 Conclusion and Future Perspectives** **159**

**Scientific Contributions** **163**

**Conference Contributions** **165**

**Acronyms** **167**

**List of Figures** **171**

**List of Tables** **177**

**Bibliography** **179**

# 1 Introduction

## 1.1 Radiotherapy

Radiation therapy (RT) is one of the common modalities used to treat malignant tumours. It is often combined with chemotherapy and/or surgery, to destroy microscopic regions of the cancerous tissue that are not visible to the human eye and thereby maximise the therapeutic response. In order to comprehend the therapeutic benefits of using ionising radiation to treat cancer, an understanding of the basic physics of radiation is necessary. This includes the biological effects that occur when radiation interacts with matter and the models used to define cell survival, which will be outlined in the following section.

### 1.1.1 Basic physics of radiotherapy

RT has become one of the primary treatments of cancer as it non-invasively penetrates tissue and deposits energy to destroy cancerous cells by damaging cellular DNA and preventing further cell division and proliferation. When radiation interacts with matter, or biological systems, it is interacting with the atoms that they are composed of. Atoms are made of electrons orbiting a nucleus (consisting of protons and neutrons), held in orbit by electrostatic forces of attraction. The removal of one of these electrons from the orbiting shell is known as ionisation and is illustrated in figure 1.1. Ionisation, can only occur if an applied energy is stronger than the electron binding energy, which is proportional to the atomic number (Z) of the element in question. In the context of biological systems, which are mainly composed of living tissue and therefore 70-90% water, this energy needs to be approximately 13.6 eV (i.e. ionisation of water molecule).

In RT, radiation is split into two main categories, directly ionising and indirectly ionising. Directly ionising, including charged particles like protons and heavy ions, can directly cause

biological or a chemical changes to the atoms of the absorbing material through which they pass. Indirectly ionising radiation, on the other hand, does not produces changes to the atomic structures themselves but instead they release their energy in the material and produce secondary charged particles which thereby induce the electron removal and resulting ion formation to cause damage. Both X-rays and $\gamma$-rays are considered indirectly ionising radiation. The processes that the X-ray photons undergo in the absorbing material is largely dependent on the energy of the incident photon as well as the absorbing materials chemical composition. (1) These processes will be discussed in more detail in the next section 1.1.1.

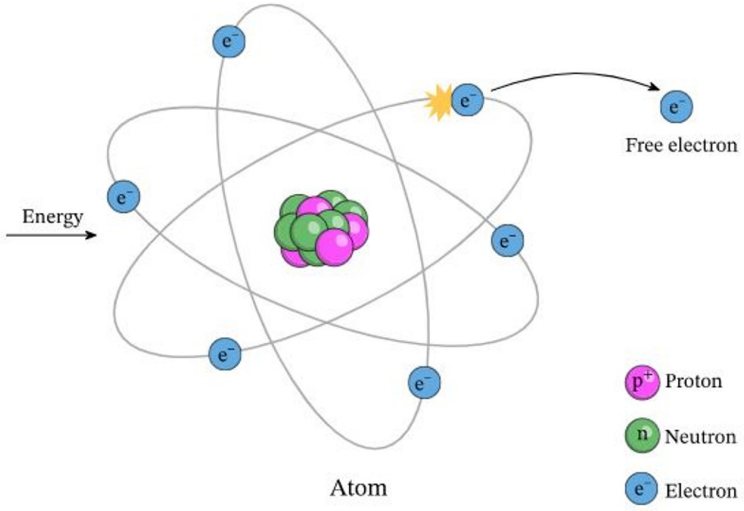


**Figure 1.1:** Schematic illustration of an external energy source causing ionisation of an atom by ejecting an electron from the shell orbiting its nucleus. (2)

Although heavy charged particles can transfer energy more efficiently than lighter particles, increasing their ability to ionise and therefore lead to higher amounts of biological damage, high energy photons or X-rays continue to be the most widely used radiation type around the world in RT. They are easy and cheap to produce, and are by far the most well understood type of radiation. For this thesis, we will mainly focus on the latter and the following sections will continue on how photons interact with matter and the associated biological effects in RT.

### Interaction of photons with matter

Photons used for treatment can be produced using a linear accelerator (LINAC), where electrons are accelerated by an oscillating electric potential along a vacuumed wave-guide towards a tungsten target. The quick deceleration of the electrons in the target material produces x-rays via Bremsstrahlung radiation with a maximum energy corresponding to the kinetic energy of the incident electron ($E_k$) (3).

The energy of the photons is dependent on the electron kinetic energy which is given by:

$$E_k = h \cdot v = \frac{h \cdot c}{\lambda} \tag{1}$$

where $h$ is Planck's constant, $v$ is the frequency of the wave, $c$ is the speed of light and $\lambda$ is the photon wavelength.

The kinetic energy of the electrons accelerated in a clinical LINAC are in the range of 4 and 25 MeV, depending on the voltage applied to accelerate the electrons (4). The minimum wavelength produced in a LINAC is given by:

$$E_{kin_{electron}} = e \cdot U = \frac{h \cdot c}{\lambda} \rightarrow \lambda_{min} = \frac{c \cdot h}{e \cdot U} \tag{2}$$

where $U$ is the voltage applied to accelerate the electron and $e$ is the charge of the elementary particle (3).

The energy ($hv$) of the incoming photon and the atomic number ($Z$) of the attenuating material will determine the probability of nuclear or orbital interaction and therefore the different processes whereby damage can be produced. For therapeutic energy ranges, the more dominant processes include the (i) photoelectric effect, (ii) Compton scattering and (iii) pair production (5) and vary as a function of the atomic number (Z) as indicated in figure 1.2, with the photoelectric effect dominates at low energies, Compton at intermediate, and pair production at very high energies.

**(i) Photoelectric Effect**

In the photoelectric effect the photon is completely absorbed by the attenuating material. During this process the photon interacts with a tightly bound electron, imparting some of its energy to overcome the binding energy of the electron ($E_B$), transferring the rest to kinetic energy of the ejected electron ($E_k$) given by:

$$E_k = h \cdot v - E_B \tag{3}$$

The probability that a photon will undergo the photoelectric effect is proportional to $\frac{(Z)^4}{(hv)^3}$,

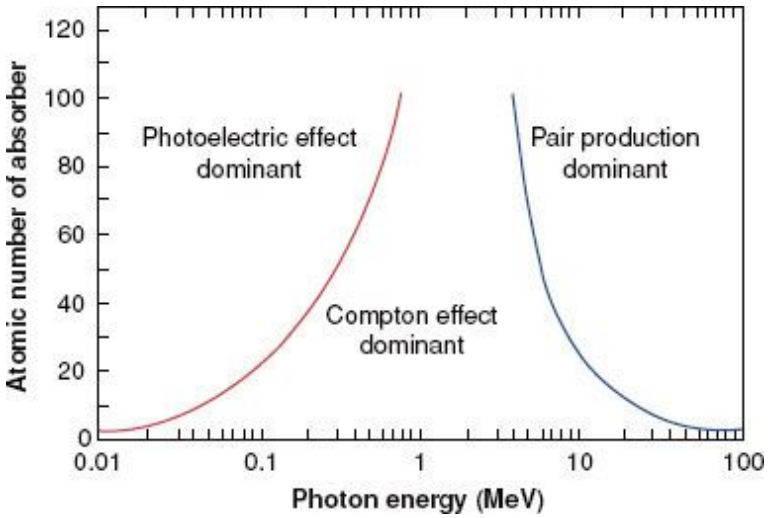


**Figure 1.2:** Illustration of the dominant processes of photon interaction (i.e. photoelectric effect, Compton effect, pair production) with matter, as a function of energy ranging from 0.1 MeV to 100 MeV (6).

where $Z$ is the atomic number of the attenuating material and $hv$ is the energy of the photon, thereby indicating that this process is more prevalent at lower energies and highly sensitive to the attenuating material with which it interacts (4).

**(ii) Compton Scattering**

Compton scattering or incoherent scattering occurs when the incident energy of the incoming photon is much greater than the binding energy of the free orbiting electron (i.e. $hv >> E_B$). When the photon interacts with a weakly bound electron it loses some of its energy to a recoil electron (Compton) with kinetic energy $E_k$, scattered at an angle $\phi$, and the photon itself is scattered through an angle $\theta$ (5). A schematic of the Compton scattering process can be seen in figure 1.3 (4).

The photon and electron are treated as relativistic particles and are therefore assumed to obey the laws of total energy and momentum conservation during their collisions (7), with this, the energy of the scattered photon is derived as:

$$h \cdot v^{'} = h \cdot v - E_k \tag{4}$$

where the kinetic energy of the recoil electron is given by:

$$E_k = h \cdot v \cdot \frac{\varepsilon(1 - cos\theta)}{1 + \varepsilon(1 - cos\theta)} \tag{5}$$

and $\varepsilon$ is the normalised photon energy using the mass of the electron ($m_e$):

$$\varepsilon = \frac{h \cdot v}{m_e \cdot c^2} \tag{6}$$

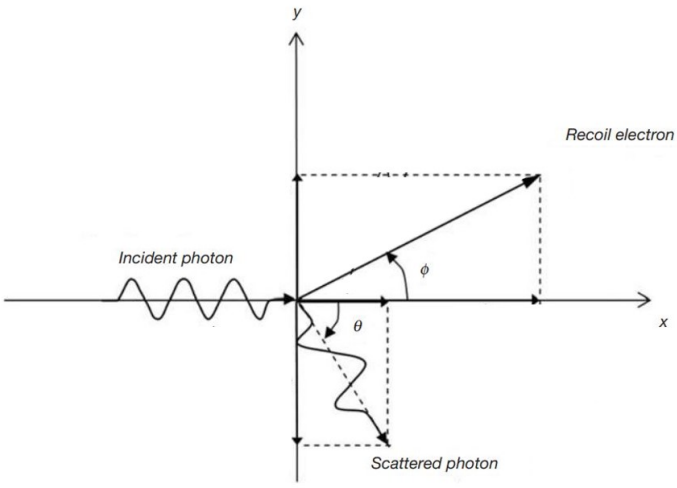


**Figure 1.3:** Schematic of Compton scattering whereby an incoming incident photon on path x is scattered at an angle $\theta$ following interaction with a loosely bound electron, resulting in a recoil electron ejected at an angle $\phi$ with a kinetic energy $E_k$.

**(iii) Pair Production**

When a photon comes into the vicinity of the nucleus, it may undergo a process called pair production, when exposed to the nuclear coulomb field. In this process the photon is converted to an electron-positron pair with a kinetic energy of $hv - 2m_e c^2$. The interaction with the nuclear field varies with the square of the nuclear charge ($Z^2$) (8). The minimum energy of the photon required for pair production to occur is 1.022 MeV (4), which equals the rest mass of an electron and a positron. Below this threshold there is zero probability of this process occurring, however, it rapidly increases above this threshold. When energies exceed 30 MeV, pair production dominates the atomic interaction in tissue as indicated in figure 1.2, but it only has a minor contribution to the effects of low LET radiation treatment (9).

**Photon beam attenuation**

The attenuation of a photon beam passing through a material can be described using **Beer Lambert's Law** which states that the reduced intensity of a light beam passing through a medium of thickness x is directly proportional to the initial intensity ($I_0$) and the path length it travels:

$$I(x) = I_0 \cdot e^{-\mu(h\nu,Z)x} \tag{7}$$

where $\mu(h\nu, Z)$ is the linear attenuation coefficient which is dependent on the energy ($h\nu$) of the mono-energetic beam and the atomic number of the attenuating material ($Z$) (3).

The **linear attenuation (μ)** of a photon beam passing a slab of thickness $dx$ is defined by the possible number of interactions per unit volume ($N_a$) and the total cross-section interaction per atom ($\sigma$):

$$\mu = N_a \cdot \sigma dx \tag{8}$$

where $N_a$ is dependant on Avogadro's number ($N_A$), the atomic weight ($A_\Gamma$) and the density ($\rho$) of the attenuator.

The **mass attenuation coefficient**, on the other hand, factors in the density that the linear coefficient is dependent on and is therefore depicted as $\frac{\mu}{\rho}$ with units $m^2/kg$ (3). The effect that the mass attenuation coefficient has on the interaction processes that a photon can undergo when it transverses a material is depicted in figure 1.4.

**Electron interaction with matter**

As mentioned in the previous section, secondary electrons can be created in the aftermath of the photon passing through a material, for example in the Compton process. These electrons lose their kinetic energy through collisional or radiative interactions, which are dependent on the atomic number of the material, Z and $Z^2$, respectively (4). During collisional interaction the electron loses some of its energy to other electrons, resulting in atomic ionisation. Radiative energy loss occurs when the electron interacts with the Coulomb field of a nucleus, thereby being slowed down and emitting Bremsstrahlung radiation.

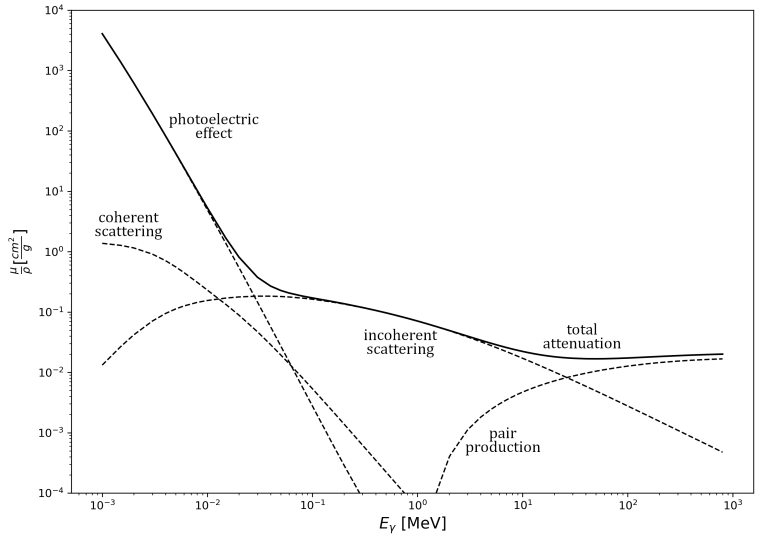


**Figure 1.4:** Interaction of photons in water. Plot represents the mass attenuation coefficient ($\frac{\mu}{\rho}$) as a function of energy ranging from $10^-3$ MeV to $10^3$ MeV (10)

The combined energy loss can be defined as the total stopping power of the electron ($S_{tot}$) with units MeV/cm and is given by:

$$S_{tot} = \left(-\frac{dE_{kin}}{dx}\right)_{tot} = \left(-\frac{dE_{kin}}{dx}\right)_{rad} + \left(-\frac{dE_{kin}}{dx}\right)_{coll} \tag{9}$$

where $E_{kin}$ is its kinetic energy and x is the path it transverses. The total mass stopping power $(\frac{S}{\rho})_{tot}$ with units MeV $\cdot$ cm$^2$/g is defined by the linear stopping power ($S_{tot}$) divided by the density of the absorbing material ($\rho$) (4).

**Dosimetric Quantities**

The energy imparted in the target material or tissue during a treatment of RT is described by additional dosimetric quantities such as fluence, KERMA and absorbed dose.

Fluence ($\phi$) is defined as the amount of particles (dN) that hit a sphere with a cross sectional area (dA) (m$^2$):

$$\phi = \frac{dN}{dA} \tag{10}$$

It is used to derive the amount of photons attenuated by the material as outlined in equation 7. The energy fluence ($\Psi$) is therefore calculated by multiplying the particle fluence ($\phi$) with the energy of the particle (E) with units of (Jm$^{-2}$).

The kinetic energy released per unit mass (KERMA) describes the average energy transfer ($d\bar{E}_{tr}$) from indirect ionising events to charged particles in the medium, evaluated per unit mass (dm) with units of $Jkg^{-1}$ (11):

$$K = \frac{d\bar{E}_{tr}}{dm} \tag{11}$$

KERMA is measured in equivalent units of Gray (i.e. 1 $Jkg^{-1}$ = 1 Gy), which is the same as for absorbed dose. However, here the average energy that is used is the energy imparted ($\bar{\epsilon}$) from the charged particle to the tumour volume (11):

$$D = \frac{d\bar{\epsilon}}{dm} \tag{12}$$

**Linear Energy Transfer (LET)**

Radiation can be sparsely ionising, with spread out particle tracks of ionisation, or densely ionising, with a compact and dense particle track of ionisation. The linear energy transfer (LET) can be used to define whether a radiation type is sparsely or densely ionising (1). The LET is therefore defined as the energy transfer rate (dE) per unit length (dl) of a charged particle track as it transverses through a medium:

$$LET = \frac{dE}{dl} \tag{13}$$

In general, LET can be split up into two categories: (i) Low LET (for example x-rays and $\gamma$-rays) or (ii) high LET (for example $\alpha$-particles and heavy ions). High LET radiation transfers energy more efficiently than low LET radiation, which increases their ability to ionise and leads to higher amounts of biological damage. However, low LET still remains the gold standard in RT (1). For the purpose of this thesis, the effects of low LET radiation, specifically x-ray photons, on cell lines in-vitro will be investigated.

### 1.1.2 Linear quadratic model of cell survival

The linear quadratic model (LQM) was developed over 50 years ago and has been used as a key tool in radiotherapy to define a simple relationship between irradiation dose and cancer cell survival. It has become the preferred mathematical model and method of predicting radiation dose responses of tumours and fractionation of RT, both in the laboratory and in the clinic (12). It is simply defined as the probability of cell survival ($S$) after a single dose of radiation:

$$S = e^{-\alpha D - \beta D^2} \tag{14}$$

where the parameters $\alpha$ and $\beta$ describe the radiosensitivity of the cell, and $D$ is the radiation dose applied. These terms become important when describing the shape of the linear quadratic curve with the $\alpha$ term depicting the linear section of the curve and therefore dominating at low doses, and the $\beta$ term illustrating the quadratic curvature that follows at higher doses (12). This can be seen in figure 1.5.

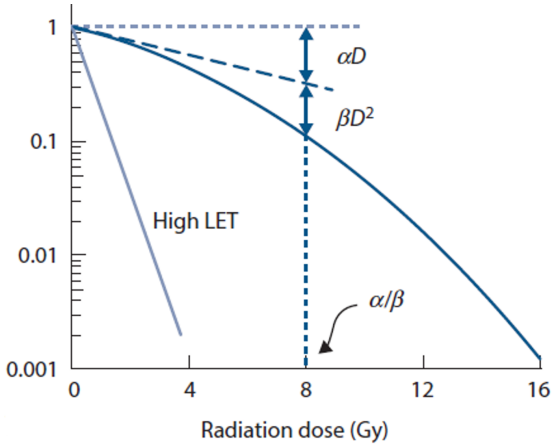


**Figure 1.5:** Representative graph of the Linear quadratic model (LQM) used in radiobiological experiments to determine the fraction of cell survival (SF) following irradiation with a particular dose (Gy). The $\alpha/\beta$ ratio are also defined on the graph as the ratio of the linear and quadratic components of the LQM curve.

The $\alpha/\beta$ ratio is used to describe the degree of curvature and thereby cell killing rate of the radiation. A high $\alpha/\beta$ ratio, where the $\alpha$ term dominates, corresponds to a constant killing rate reflecting "single hit" events. That is when a single incident particle causes lethal cell damage, an event that often occurs with high LET radiation (12). However, when the $\beta$ term dominates and a low $\alpha/\beta$ ratio is calculated, the cell death rate scales with the square of the dose and reflects events from "multiple hits" (i.e. cell damage from multiple radiation tracks)

which is associated with low LET radiation (12) (figure 1.5). The linear quadratic dose response and thereby the $\alpha$ and $\beta$ values can be affected by externally controlled parameters including radiation type (fig. 1.5), but also by internally uncontrolled processes. These uncontrolled processes include: (i) the cell phase, with different phases having varying radio-sensitivities, as well as (ii) the tumour micro-environment, for example, low oxygenation of a tumour (i.e. hypoxia) which has been known to contribute to radioresistance as indicated by the oxygen enhancement ratio (OER).

### 1.1.3 The target of radiotherapy - The DNA

The cell consists of many components which can be damaged by irradiation, but ultimately its main target is the cellular DNA (Deoxyribonucleic acid), a macromolecule that encodes the genetic material of a cell. Structurally, DNA is a double helix bound together by hydrogen bonds. Each helix consists of four types of nucleotides, composed by an alternating sugar-phosphate backbone bound to one of four possible bases: adenine (A), cytosine (C), guanine (G), or thymine (T). The hydrogen bonds are formed between the two complimentary base pairs: adenine and guanine; thymine and cytosine on opposite strands, as indicated in figure 1.6.

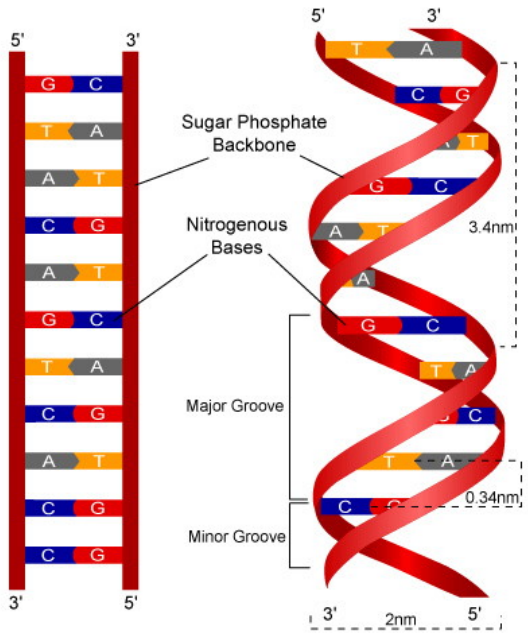


**Figure 1.6:** Illustration of DNA structure showing the **(left)** uncoiled DNA indicating the sugar phosphate backbone with 5′ and 3′ ends, nucleotide bases (adenine (A), cytosine (C), guanine (G), thymine (T)) and their associated complimentary pairs, and **(right)** coiled DNA indicating the major and minor grooves and estimated strand lengths (nm). (13)

### Direct and indirect DNA damage

Radiation can damage the DNA either directly or indirectly. Direct radiation damage occurs when an incoming photon is absorbed by an atom and an electron is released (i.e. secondary electron), which induces damage in the DNA. Indirect action occurs when the secondary electron interacts with a water molecule causing radiolysis and thereby creating radicals or reactive oxygen species (ROS), that can migrate and damage the DNA (14), as indicated in figure 1.7. Through both mechanisms, radiation can induce many different types of DNA damages, including modifications to the sugar- phosphate backbone, inter- or intra-strand DNA crosslinking, Apurinic sites (AP), base damage (BD), as well as single and double strand breaks (SSBs and DSBs, respectively). DSBs are the most difficult lesion for the cell to repair and therefore are more sought after by clinicians. However, the extent and degree of lesion largely depends on the type of radiation, in particular the LET, with an increasing LET inducing a larger proportion of direct DSB damage (15). Low LET on the other hand, for example photons, have a much lower probability of direct damage and thereby largely depend on ROS-induced DSB damage (16).

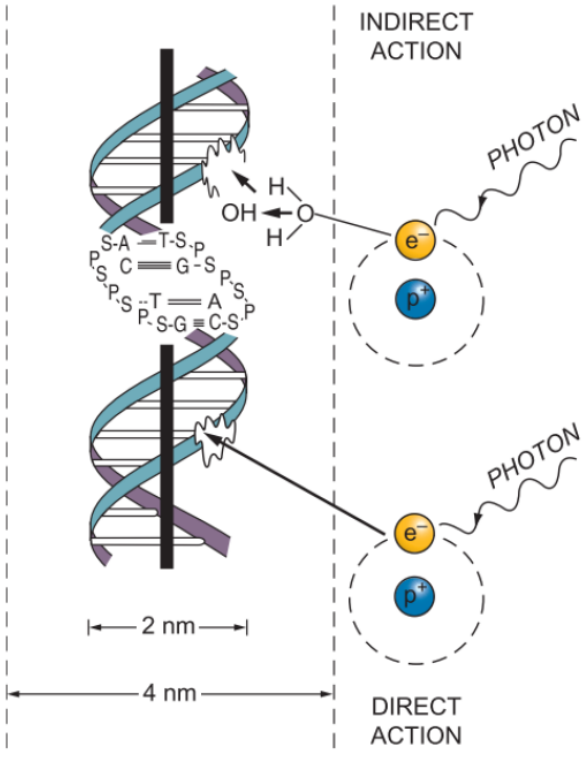


**Figure 1.7:** Illustration of direct and indirect action to damage DNA. Direct action of DNA damage occurs after a photon is absorbed by an atom thereby releasing an electron (secondary $e^-$) which interacts with the DNA strand. Indirect action occurs when the secondary electron interacts with $H_2O_2$ to create radicals or ROS that damage the DNA strand. (1)

## 1.2 Cellular Oxidants and Antioxidants

Cellular oxidants, including hydrogen peroxide ($H_2O_2$), are reactive molecules produced when free radicals are generated and interact with water in the body through a process known as water radiolysis. In general, cancer cells have higher level of oxidants compared to normal healthy cells, either produced by external stimulus (i.e. radiation) or internal cellular processes (i.e. mitochondrial electron transport chain etc.). At very high levels, these oxidants can cause cellular oxidative stress and thereby induce indirect damage on the DNA, however, cancer cells have a very active antioxidant system which neutralises the reactive oxidants and prevents excessive damage. An understanding of how these oxidants are produced in cells, in particular, by irradiation, and the responding antioxidant scavenging system which contributes to cellular radioresistance is outlined in the next section.

### 1.2.1 Water radiolysis and $H_2O_2$ production

As mentioned previously, radiation interacts with atoms or molecules in the cell, most likely water, to produce oxygen-derived free radicals which can either travel short distances to damage critical cellular targets such as the DNA, or continue in further reactions with hydrogen and oxygen. These radiolytic events, however, occur on a very short time-scale. These time-scales can be classified as the: **(i)** physical stage, lasting approximately 1fs (fento-second), **(ii)** physio-chemical stage lasting about $10^{-15}$-$10^{-12}$ s, and **(iii)** chemical stage which has the longest, albeit still short, lifetime of $10^{-12}$-$10^{-6}$ s. The different radiolysis stages and the corresponding reactions are illustrated in a schematic adapted from Lousada et al (17) (figure 1.8).

The potential reactions involved in the radiolysis of water (18) are therefore as follows:

$$H_2O + IR \rightarrow H_2O^+ + e^- \tag{15}$$

$$H_2O^+ \rightarrow H^+ + OH^{\cdot} \tag{16}$$

$$e^- + H_2O \rightarrow OH^- + H^{\cdot} \tag{17}$$

$$H_2O + IR \rightarrow H_2O^* \rightarrow H^{\cdot} + OH^{\cdot} \tag{18}$$

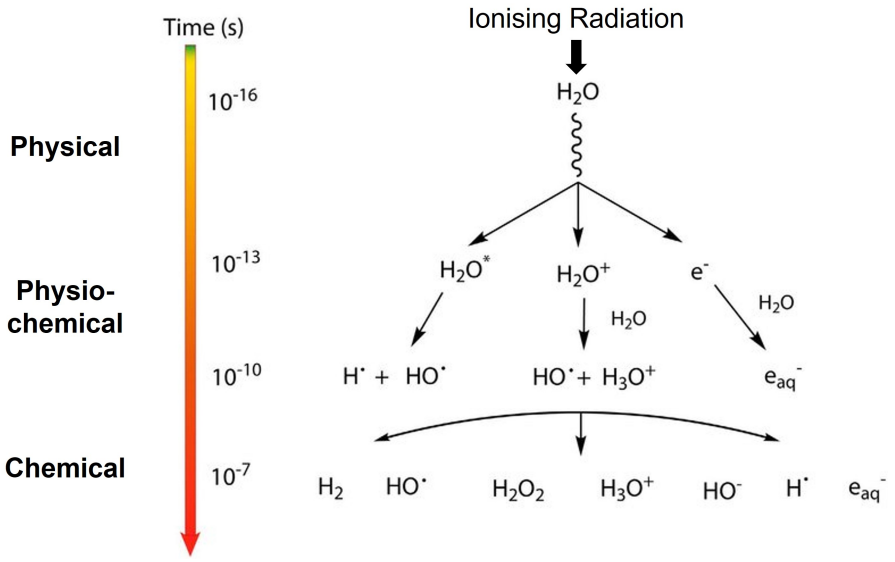


**Figure 1.8:** Illustration of water radiolysis indicating the timescale of the physical, physio-chemical and chemical stages leading to the main products: $H_2O_2$, $H_3O^*$, $HO^-$, $H^\cdot$ and $e^-_{aqua}$ (17)

The free electron produced in equation (15) can become stabilised after polarisation of a water molecule and is referred to as $e^-_{aqua}$. In particular, $H^\cdot$, $OH^\cdot$ and $e^-_{aqua}$, otherwise known as *water radicals*, are very important radiolytic products in biological systems (18). In fact, in the presence of oxygen, theses radicals further react with the oxygen molecule and result in the production of highly reactive oxygen species, including $H_2O_2$. The radiolytic yield of water radicals and ROS following $\gamma$ radiation and accelerated electrons are outlined in table 1.1.

| **Radiation** | $e^-_{aqua}$ | $OH^\cdot$ | $H^\cdot$ | $H_2$ | $H_2O_2$ | $HO_2^\cdot$ |
|---|---|---|---|---|---|---|
| $\gamma$ **electrons (0.1 - 10 MeV)** | 0.28 | 0.28 | 0.06 | 0.047 | 0.073 | 0.0027 |

**Table 1.1:** Water radiolysis yields in µmol $J^{-1}$ following exposure of water (pH 3 - 11) to gamma radiation and electrons with LETs of 0.2 - 0.3 keV $\mu m^{-1}$. Adapted from (19).

A high proportion of water radiolysis yields production of OH radicals (table 1.1), however, due to their high reactivity and short half-life (i.e. approximately $10^{-9}$s (20), their concentrations in the cell post-IR are difficult to detect. Nevertheless, a catalytic reaction can occur with two OH radicals and the enzyme superoxide dismutase (SOD) to produce hydrogen peroxide ($H_2O_2$). $H_2O_2$ is a much more stable ROS molecule that has a longer half-life. Cancer cells have an increased rate of generating $H_2O_2$ (approximately 0.5 nmol/$10^4$ cells/h) compared

to healthy cells and therefore exhibit a higher level of $H_2O_2$ (21). These properties of $H_2O_2$ contribute to its induction of DNA damage and also preventing DNA repair (22) through cell signalling, and thereby highlights necessary research into its contribution to cellular radiosensitivity of cancer cells.

### 1.2.2 Reactive oxygen species (ROS)

DNA is considered damaged if there is a change in its basic structure caused by a chemical modification of the bases. Reactive oxygen species are such molecules that can induce these changes and modifications, and the extent of change is dependant on their concentration within the cell. ROS are a family of short-lived molecules which can be produced through chemical reactions, typically involving hydrogen and oxygen, and can therefore occur in both the nucleus and cytosol of the cell. Important ROS molecules include the highly reactive hydroxyl radical ($OH^-$) and superoxide anion ($O_2^{\cdot -}$), as well as the less reactive non-radical hydrogen peroxide ($H_2O_2$), which is more stable and can therefore diffuse over longer distances in the cell (19, 21). In addition to being created in cancer treatments such as chemotherapy and/or ionising radiation as outlined in the previous section, ROS can also be produced endogenously through the following ways: (i) the electron transport chain in the mitochondria, (ii) enzymatic processes involving the nicotinamide adenine dinucleotide phosphate (NADPH) oxidase family of enzymes (NOXs), and reactions occurring (iii) in the peroxisomes or in the (iv) endoplasmic reticulum whereby $H_2O_2$ is produced during protein folding (23). At low levels, $H_2O_2$ and other ROS molecules can be beneficial to the cell by acting as signalling molecules and maintaining redox balance, however, at high concentrations they can result in oxidative stress and cause damage to cellular bio-constructs (24). ROS have therefore been implicated in mediating the response of RT and chemotherapy treatments due to their knock-on effects on cell signalling of DDR and repair, and thereby overall cell survival (25, 26).

### 1.2.3 Anti-oxidant response

It is well documented that cancer cells show higher basal ROS levels than the normal cells, mainly due to their increased metabolic activity, mitochondrial malfunction and genetic alterations. However, while a modest increase of ROS can favour tumour promotion, an excessive level can induce tumour suppression (27). RT aims at further enhancing the intracellular ROS content thus altering the redox balance of cancer cells over a threshold able to induce cell

death. In response to oxidative stress or an excess of ROS production following radiation treatments, cancer cells activate antioxidant responses which can alter ROS levels and restore redox homeostasis, and thereby enhance resistance to radiation therapy (28, 29). Cellular redox defense includes the increasing generation of enzymatic and non-enzymatic antioxidants for ROS removal. The enzymatic regulation of ROS is carried out by glutathione peroxidase (GPX), catalase (CAT) and superoxide dismutase (SOD), whereas the non-enzymatic contributing portion includes glutathione (GSH) and thioredoxin (TRX).

Nuclear erythroid 2-related factor (NRF2) is one of the leading transcription factors which, drive the antioxidant responses of cancer cells. Several cancer types have also been reported to have an upregulated expression of NRF2, which contributes to radioresistance of the cells (30, 31, 32) and highlights NRF2 as an interesting avenue of research.Under oxidative stress in fact, NRF2 is unbound from its negative regulator, KEAP1 (Kelch-like ECH-associated protein 1) and translocates to the nucleus. This therefore induces the ARE (i.e. antioxidant response element) which instigates the expression of an array of antioxidant genes, involved in the glutathione (33) and thioredoxin systems (34) as well the antioxidant enzymes, catalase and SOD, directly, as indicated in the schematic adapted from Narayanan et al. (figure 1.9).

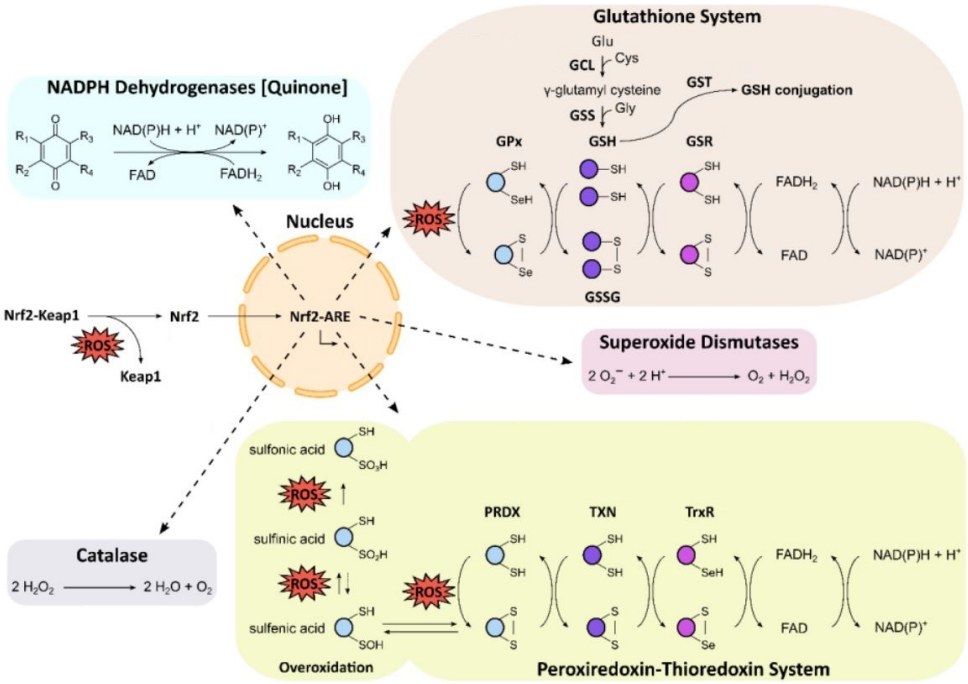


**Figure 1.9:** Overview of the antioxidant response of cancer cells. Reactive oxygen species (ROS) trigger activation of NRF2-KEAP1 pathway. NRF2 translocates to the nucleus where it induces the ARE (antioxidant response element) which thereby stimulates the glutathione (GSH) and thioredoxin (TRX) systems as well as the antioxidant enzymes including superoxide dismutase (SOD), NADPH dehydrogenases and catalase. (28)

In the glutathione system, GPX scavenges the ROS through the oxidation of GSH. GSH is then regenerated by using NADPH and FAD. In the thioredoxin system, ROS scavenging occurs through peroxiredoxin (PRDX) which is continuously regenerated by TRX and thioredoxin reductase (TR = TrxR). Overall, the antioxidant systems work together to rid the cell of the toxic excess ROS, including the more stable $H_2O_2$ as indicated by the equations below. In brief, the removal of excess $H_2O_2$ occurs through a GPX catalysed reaction whereby the $H_2O_2$ reacts with the reduced form of glutathione (GSH) creating oxidised glutathione (GSSG) and $H_2O$ as indicated in equation (19). GSH is then regenerated by the glutathione reductase () catalysed reaction of GSSG with NADPH (equation (20)). High levels of $H_2O_2$ can also be removed by CAT enzyme to form an oxygen and a water molecule (equation (21)).

$$2GSH + 2H_2O_2 \xrightarrow[GPX]{} GSSG + 2H_2O \tag{19}$$

$$GSSG + NADPH + H^+ \xrightarrow[GR]{} 2GSH + NADP^+ \tag{20}$$

$$2H_2O_2 \xrightarrow[CAT]{} O_2 + 2H_2O \tag{21}$$

The schematic below indicates how ROS can be induced through external factors (e.g. Ionising radiation, smoking, pollution etc.) and internal processes (e.g. mitochondria, electron transport chain (ETC), NADPH Oxidase (NOX)) and the corresponding mechanisms for ROS removal via antioxidant compounds and enzymes. This activation of intracellular antioxidant responses following elevated ROS levels within cancer cells can help to reduce the IR-induced DNA damages and therefore favour cancer radioresistance.

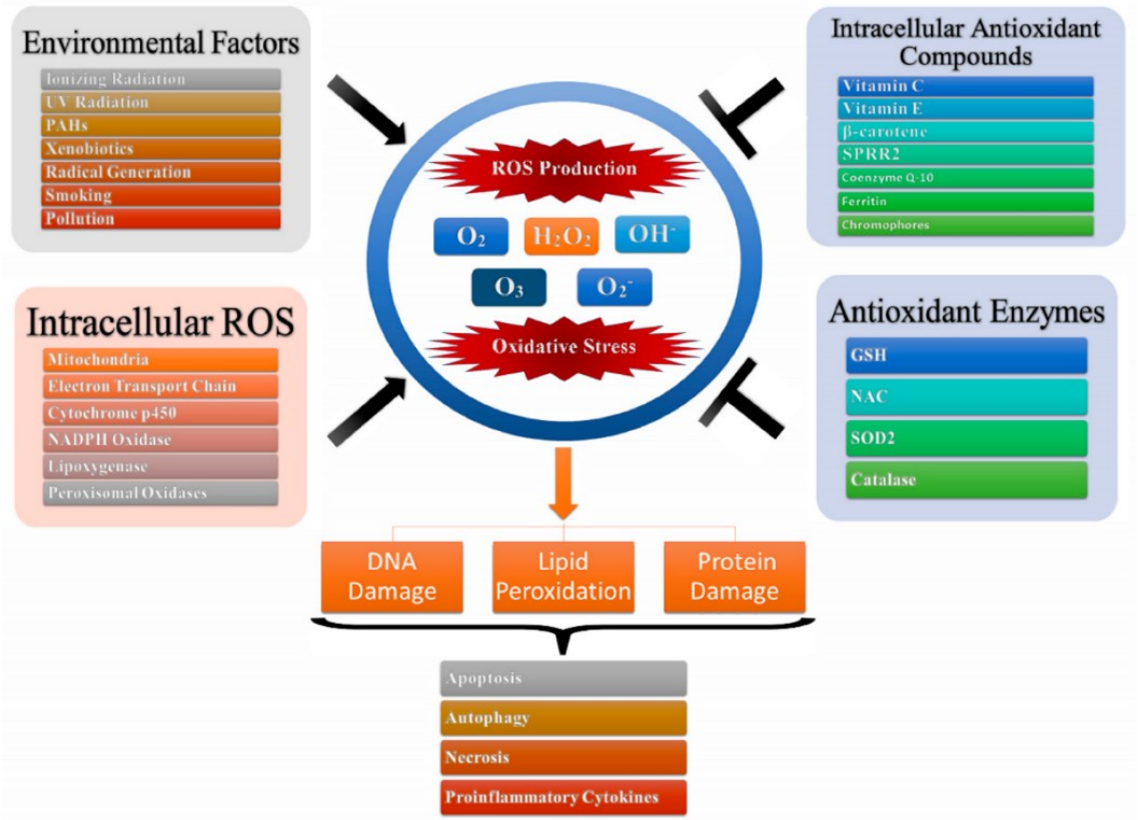


**Figure 1.10:** Illustration of ROS production by environmental factors or intracellular mechanisms and a corresponding ROS scavenging system, comprised of antioxidant compounds and enzymes, which compete to induce/prevent intracellular damage. (35)

## 1.3 DNA Damage Response (DDR) and Repair

The mechanisms for DNA repair following an IR insult involve the activation of a series of biochemical reactions which trigger cellular responses and usually occur within seconds or minutes after irradiation (36). This is known as the DNA damage response (DDR) network of the cell and is a term describing the abundance of inter- and intra-cellular signalling events and enzymatic activities that detect and recruit for DNA repair. To this purpose, the sensory DDR network regulates cell cycle progression, including the cells fate on continued replication or programmed cell death. The level of cellular genomic instability of cells and DDR alterations, which are quite common in cancerous cells, can therefore impact the quality of repair or even bypass repair entirely, leading to sub-optimal repair and replication of defect cells, which eventually result in cancer radioresistance (37).

### 1.3.1 Cell cycle checkpoints

The cell cycle consists of four distinct and sequential phases, called G0/G1 (gap 1), S (DNA synthesis), G2 (gap 2), and M (mitosis) as indicated in figure 1.11. Within each phase, checkpoints ensure the correct DNA replication and segregation of the chromosomes in the two daughter cells. There are three important cell cycle checkpoints in the DDR network: **1.** G1/S, **2.** Intra-S and **3.** G2/M. The main DDR sensors in the G1/S checkpoint include ATM (Ataxia Telangiectasia Mutated, a protein kinase that is considered a central transducer of DDR), Chk2 (checkpoint kinase activated by ATM) and p53 (37). P53 is a tumour suppressor called "the guardian of the genome" because of its crucial and central role in DNA damage responses. It acts by orchestrating transcriptions of genes and initiating cell cycle arrest or apoptosis to prevent the proliferation of damaged DNA (28). However, it is often the case that cancer cells have an altered expression of this protein and in many cases they lack this DNA damage checkpoint due to the loss of p53 function. They are then more reliant on the other two checkpoints (38, 39). The intra-S phase is regulated by ATR (Ataxia Telangiectasia and RAD3 related, key regulator of DDR), Chk1 (checkpoint kinase activated by ATR), DNA-PKcs (DNA-dependant protein kinase catalytic sub-unit) and Wee1 (Wee1 G2 Checkpoint Kinase) (37). Wee1 is mostly known for preventing/protecting cells from early entry into mitosis (i.e. mitotic events) through inactivating cyclin dependent kinase 1 (CDK1) and consequent arrest in G2 phase. However, recent studies have suggested an emerging role of Wee 1 in S-phase in regulating CDK1 and 2 and therefore in delaying the S-phase onset in the case of damage (40). When DNA damages are produced, ATM, ATR, and DNA-PKc recognise the damage site, recruit several downstream proteins and elicit the phosphorylation, among others, of histone H2AX and p53. Such events aim at blocking cell cycle progression and enabling cells to repair the damages prior to DNA replication and mitosis.

### 1.3.2 DNA repair pathways: an overview

After DNA damages have been detected and cell cycle arrest has been induced, DDR sensors activate the DNA repair machinery. The five main DNA repair pathways include nucleotide excision repair (NER), base excision repair (BER), mismatch repair (MMR), non-homologous end joining (NHEJ) and homologous recombination (HR). The dominance of the repair pathway is dependant on the damaging agent (e.g. toxins, replication errors, oxidative damage,

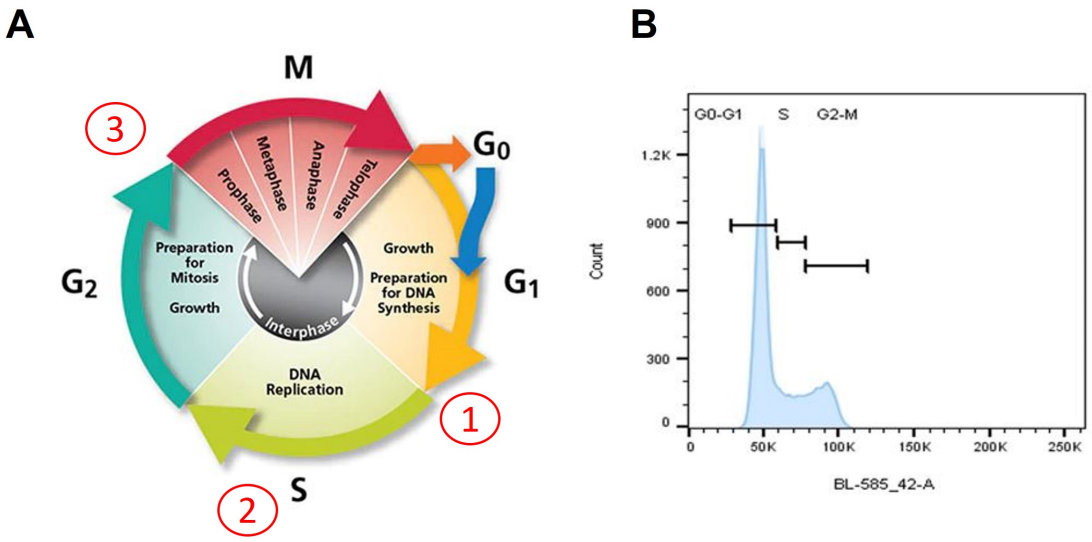


**Figure 1.11: A.** Illustration of cell cycle progression consisting of the following phases: G0/G1 (gap 1), S (DNA synthesis), G2 (gap 2), and M (mitosis). The cell damage checkpoints are located at (1) G1/S , (2) intra-S and (3) G2/M in the cell cycle (41). **B.** Representative image of cell cycle progression profile acquired using flow cytometry after propidium iodide staining. Cell cycle phase sections G0/G1, S and G2/M are indicated on the graph, with cell count on the y-axis and laser intensity on the x-axis.

radiation, hypoxia etc.), the type of damage induced (i.e. mismatches, AB, lesions, SSB, DSB etc.) as well as the stage of the cell cycle that the cells reside in at the point of damage (42). In radiation biology, DSBs are the most cytotoxic lesions and more abundant than SSBs, therefore more sought after by clinicians than the other possible damages. For DSB repair, the most important mechanisms are (i) NHEJ and (ii) HR, and will therefore be discussed in more detail. The HR DNA repair is a more complicated mechanism, involving many more proteins and enzymes compared to the NHEJ. Because of this, HR is also more accurate and error-free. However, if these systems fail to repair DNA lesions and the cells continue to divide, this can result either in cell death by mitotic catastrophe or in an accumulation of damages, responsible for radiation-induced genomic instability. Moreover, cancer cells from different organs can show aberrant activation or increased expression of the DNA repair pathways, which most likely contribute to develop tumour radioresistance (43, 44, 45). As a consequence, the outcome of RT is predominantly based on the extent of the damages produced and the ability of cancer cells to sense and repair them (37).

**(i) Non-Homologous end joining (NHEJ)**

NHEJ works by re-joining two broken ends independently of sequence homology (figure 1.8). It mainly operates in the quiescent G0 and in G1 phases (46) and accounts for the majority of

repaired DSBs in cells. In NHEJ, the damage is initially recognised by Ku70/Ku80 heterodimer which binds to both of the strand breaks. The catalytic sub-unit of DNA protein kinase (DNA-PKcs), which is the main regulator for a small number of proteins involved in NHEJ (47), is then recruited to the damage site. If necessary and depending on the complexity of the DNA damage, Ku recruits a protein known as Artemis which forms a complex with DNA-PKc to activate its endonuclease activity, trimming the 5′ and 3′ overhangs. Otherwise, compatible ends for ligation are created using DNA polymerases (48). Ligation then requires the complex XRCC4-DNA Ligase IV-XLF to complete the repair of the breaks (48).

**(ii) Homologous recombination (HR)**

Unlike NHEJ, HR requires a template that is similar to the broken sequence of DNA in order to achieve accurate repair. For this reason, HR can only operate in the G2 or S phase of the cell cycle after the DNA has been replicated and a sister chromatin template is available (figure 1.11). In HR, the MRN-complex (i.e. MRE11-RAD50-NBS1), recruited by poly(ADP-ribose) polymerase (PARP), acts as a sensor for DSBs and initiates, together with other exonucleases, the DSB end resection in order to create a single strand DNA (ssDNA) tail to be used as a template (i.e. DNA 5′ to 3′-strand). This complex is very important when it comes to DNA repair as it is involved in sensing, signalling and repair of the damage in response to ionising radiation (49). MRE11 of the MRN complex, along with other endonucleases, generates a 3′ single-strand DNA overhang. Subsequently, the tail of the overhang is coated in RPA (Replication Protein A) which protects the ssDNA from nucleases and\or prevents the DNA recoiling in on itself. The MRN complex promotes the activation of ATM, which subsequently phosphorylates the tumour suppressor protein BRCA1 (50), that in turn binds to the DSB site. BRCA2 is therefore attracted by BRCA1 to the damage site, and facilitates the loading of RAD51 to the RPA-coated strand. RAD51 protein helps search for homologous DNA and facilitates the strand exchange with the complimentary strand, thereby creating a D-loop. In this process, RAD51 is also supported by its paralogues, RAD52 and RAD54. Following D-loop formation, either non- or crossover HR repair can occur by extension of the annealed 3′-end to the original damage location (51, 52, 53).

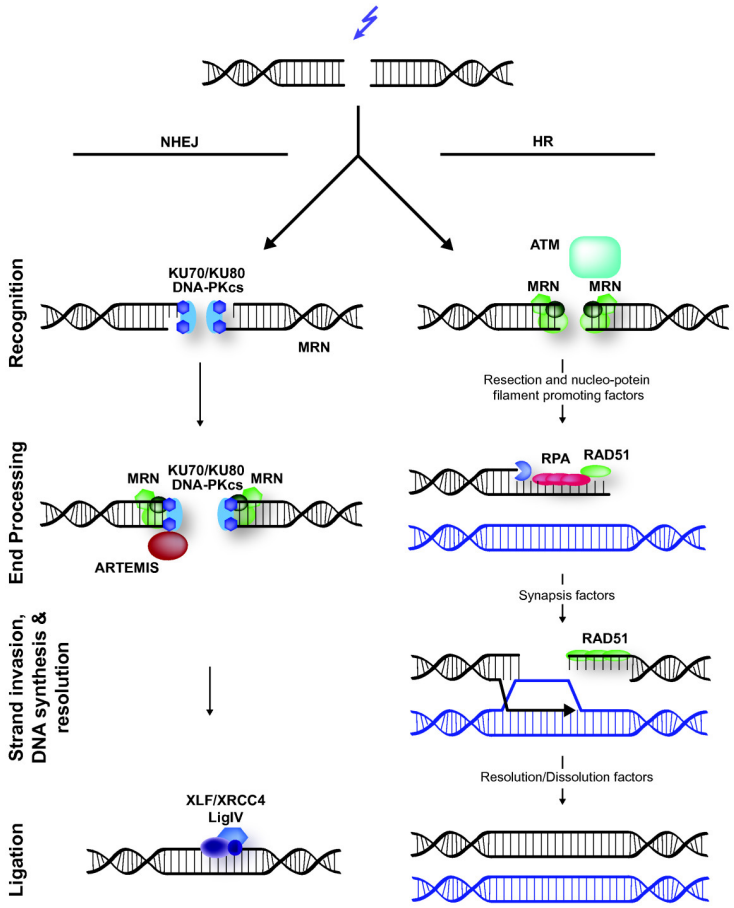


**Figure 1.12:** Illustration of DNA damage repair pathways, non-homologous end joining (NHEJ) and homologous recombination (HR). NHEJ involves recognition of DNA DSB by Ku70/Ku80 complex which recruits DNA-PKcs (catalytic sub-unit of DNA protein kinase) to regulate proteins to complete the repair. HR repair involves MRN complex (MRE11-RAD50-NBS1) which senses the DSB damage and promotes the activation of ATM and subsequently recruits BRCA1 and RAD51 for D-loop formation and thus repair. (54)

### 1.3.3 ROS involvement in the DDR

As mentioned previously, ROS have opposing tendencies in the cell, whereby they can induce DNA damage as well as act as a signalling molecule for important processes within the cell, including initiating responses following cellular damage. For this reason there has been increasing attention on the interplay between ROS and the DDR. In fact, ROS are key molecules in both contributing to redox homeostasis and also activation of DDR reactions (55). On one hand, an accumulation of ROS, such as $H_2O_2$, can enhance the phosphorylation and therefore the activation of ATM-Chk2 and ATR-Chk1 axes, as well as p53, leading to downstream activation of the DDR pathway (56, 57, 58, 59). On the other hand, ROS can inhibit DNA-PKcs activity by interfering with DNA-PKcs/Ku interaction (23). Besides the activation of proteins regulating cell cycle checkpoints, ROS can also directly act on the Cdc25

phosphatase proteins, which promote cell cycle progression and ROS-mediated decrease of their levels (60). The regulation and effect of ROS levels on DSB induction and DDR via sensor, transducer and effector proteins are summarised by Srinivas et al. in figure 1.13 (23).

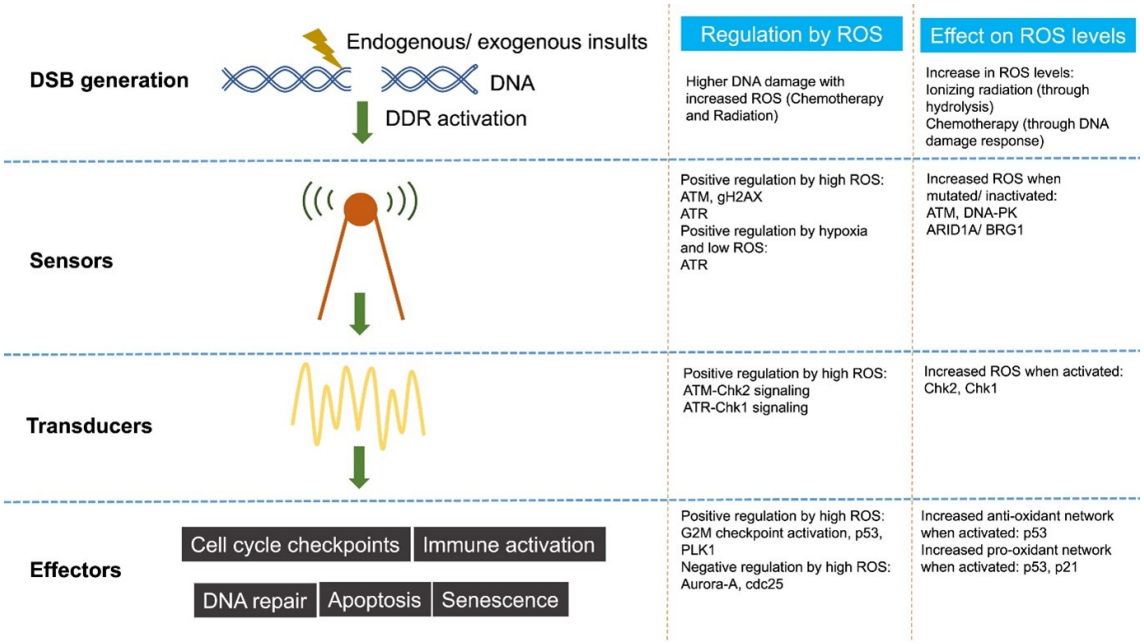


**Figure 1.13:** Illustration of the interaction of ROS, DSB damage and the subsequent initiation of the DDR involving sensor, transducer and effector proteins. (23)

All these phenomena are involved in regulating proteins of DNA repair and cell cycle arrest and are an example of the downstream effects of ROS. As mentioned above, ATM and ATR are involved in the recruitment and phosphorylation of several proteins and of the chromatin factor and $\gamma$H2AX histone. H2AX plays an essential role in signalling, initiating, and facilitating the repair of DSBs in the DDR and for this reason is often used as an early marker of DSBs in radiobiological experiments (61, 62). It has been shown that elevated ROS levels are able to stimulate H2AX phosphorylation ($\gamma$H2AX) and viceversa, which in turn recruits multiple components of the DDR signalling (63). Moreover, increased levels of $H_2O_2$ have also been shown to enhance Polo-like kinase 1 (PLK1) in a p53-dependant manner. PLK1is an important kinase, which mediates entry in M phase and recovery from the G2/M arrest upon DNA repair. PLK1 phosphorylates Glucose-6-phosphate dehydrogenase (G6PD), increasing pentose phosphate pathway (PPP) flux and NADPH production, and thereby enhances the antioxidant ability of the cell (23). However, although a strong correlation between ROS and the DDR has been reported, a mechanistic link between IR-induced ROS and DDR response has not been clearly elucidated.

## 1.4 Tumour Hypoxia and Metabolic Reprogramming

The extent and the outcome of DNA damages caused by ionising radiation are strongly influenced by the tumour microenvironment. In particular, oxygen content plays a critical role in local control in radiotherapy. Many solid tumours are characterised by different and fluctuating $O_2$ levels and when such levels decrease under the oxygenation levels of the respective normal tissues (normoxia), a condition known as "hypoxia" is established. The severity of hypoxia (from mild oxygen deficiency to anoxia) depends on cancer types and changes also within the same tumour mass, where different areas can be characterised by different $O_2$ levels. This is mainly due to the fact that in highly proliferating and expanding tumours, the oxygen demand is not sustained by an adequate $O_2$ supply because of the increasing distance between cells and the vasculature network. This, together with the disorganised and defective rearrangement of the blood vessels in a cancerous tissue, hinders $O_2$ diffusion and creates further more hypoxic milieu (64, 65, 66). In these conditions, tumour cells also tend to quickly exhaust the nutrients and consequently the metabolic demand is not met thus creating regions of the tumour that exhibit also a deprivation of energy and glucose. Therefore, tumour cells undergo a “metabolic shift”, which also results in increased levels of lactate production and an acidic extracellular matrix. Additionally, it is accepted that hypoxic tumour regions will reoxygenate after RT treatment as a result of a reduced oxygen consumption rate, due to death of the more radiosensitive oxygenated cells, and therefore also have a better perfusion (67). However, ionising radiation can also damage the vascular network of the tumour, thus creating a new hypoxic condition or intensifying the existing one and consequently activating hypoxic responses (25).

On one hand, hypoxia can slow down cell proliferation, modify cell cycle distribution and potentially lead to cell death. Nevertheless, on the other hand, the adaptive responses, also including an alteration of the DDR systems and the antioxidant defences, can allow for continued survival, enhanced metastasis, and selection of more aggressive cell sub-populations (64, 68, 69). Taken together, these events contribute to develop cancer cell resistance to radiation treatments (70).

### 1.4.1 Tumour Hypoxia and Oxygen Enhancement Ratio

Cancer cell responses in hypoxia are influenced not only by the severity of the hypoxic environment, but also by the time of exposure. Different forms of tumour hypoxia exist including chronic and acute tumour hypoxia. Acute hypoxia occurs when the blood flow around and inside the tumour region fluctuates periodically, thus exposing cells to a short-term oxygen deprivation. Chronic hypoxia, on the other hand, is associated with regions where oxygen has no access and is thereby a result of the diffusion limit of oxygen (71). The diffusion distance from the blood vessel can also depend on other factors, including the blood ability to carry oxygen (affected by anaemia or smoking) or the oxygen release capacity of the haemoglobin. It can also be tumour dependent involving the intravascular oxygen partial pressure gradient, the tumour growth rate and the oxygen consumption rate of the tumour cells (72).

It is well known that hypoxic cancerous cells at the time of radiation therapy are generally less damaged than the normoxic cells and therefore more radio-resistant. Pre-clinical studies as early as the 1950's demonstrated the association of hypoxia with tumour radioresistance. In these studies, cells became resistant to RT damage when the $O_2$ pp (partial pressure) was below 20 mmHg ( 3% $O_2$) (65). In addition, multiple clinical studies have proven hypoxia to be associated with poor prognosis after RT in patients with different cancers (73, 74, 75). The reason is explained through the role of $O_2$ as a radiosensitizer being able to promote the generation of free radicals, which in turn cause damage to several biomolecules. When the $O_2$ levels are reduced during radiotherapy, the so-called "oxygen-effect" is less pronounced, because ROS generation is limited. Hypoxic tumours therefore require typically a 2.5-3-fold increase in radiation dose to induce a damage equivalent to the damage seen in a normoxic tumour. In radiobiology, this radio-response factor is otherwise known as the oxygen enhancement ratio (OER) which refers to the improvement of the therapeutic effect of RT due to oxygen presence (76). It is determined by the ratio of doses in hypoxia and normoxia to achieve an equivalent cell survival, as shown in the schematic 1.14. This effect and the cellular adaptation promoted by hypoxia contributes to radiotherapy resistance of cancer cells and the majority of such responses is mediated by Hypoxia Inducible Factors (HIFs).

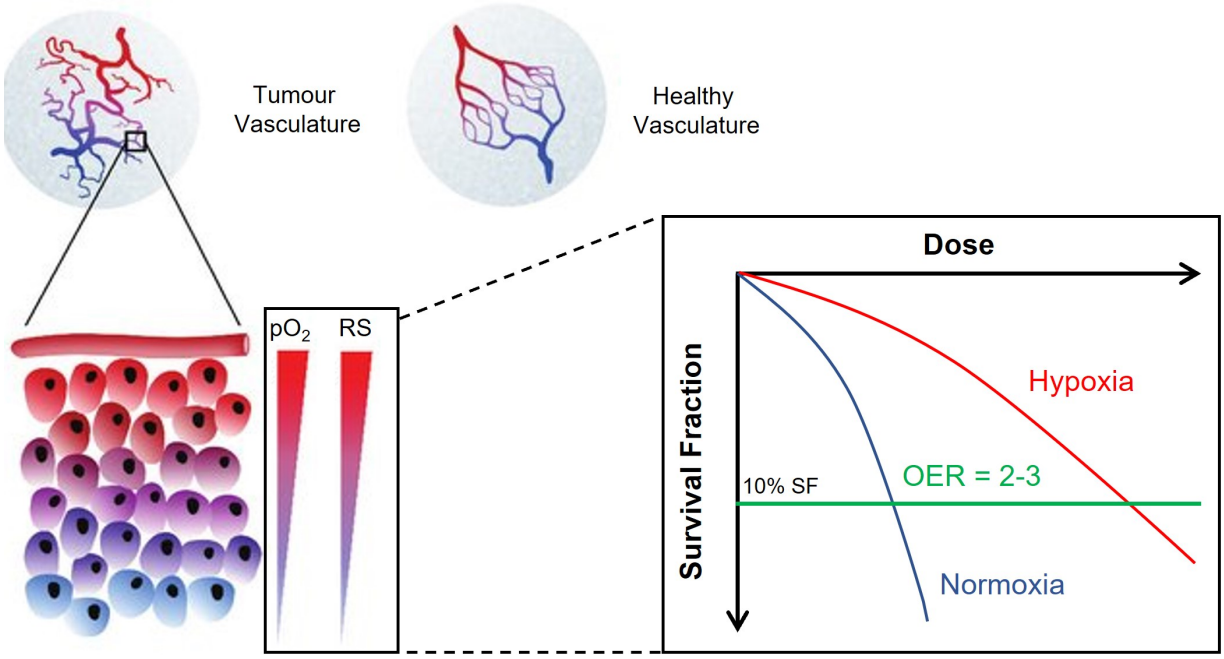


**Figure 1.14:** Illustration of the tumour vasculature indicating that as the distance from the blood vessel increases, the partial pressure of oxygen ($pO_2$) decreases. The increase in oxygen concentration has a high association with radio-sensitivity (RS) and results in a 2-3 fold decrease in the survival of cells post-IR which is otherwise known as the oxygen enhancement ratio (OER).

### 1.4.2 Hypoxia Inducible Factors (HIFs) and their role in radiation responses

The key molecular factors mediating cellular responses to hypoxia are the Hypoxia-inducible factors (HIFs). HIFs are major regulators of gene and protein expression which induce signalling events promoting cell survival under hypoxic exposure. They are heterodimers composed of two sub-units, $\beta$ and $\alpha$, able to bind specific sequence on target genes (77, 78). There are three known HIF-$\alpha$ proteins: HIF1-$\alpha$ (ubiquitously expressed), HIF2-$\alpha$ (tissue specific expression) and HIF3-$\alpha$. HIF1-$\alpha$ has been the most studied of all three since its discovery by Nobel laureates Kaelin, Ratcliffe and Semenza in 1995, who elucidated its role in oxygen sensing and its importance for cell survival at reduced oxygen levels (79). In normoxic environments, HIF1-a protein is continuously synthesised and targeted for proteasomal degradation by the von Hippel-Lindau protein (pVHL). Prior to degradation, proline residues in HIF1-$\alpha$ are hydroxylated through $[O_2^-]$ and $[Fe_2^+]$ dependent proline hydroxylation domain proteins (PHDs) (i.e. PHDs are used to catalyze the reaction). However, in hypoxia these PHDs are no longer active due to the lack of oxygen as a substrate and the proline residues cannot be hydroxylated. Consequently, the lack of interaction between HIF1-$\alpha$ and pVHL results in an accumulation of the HIF1-$\alpha$ transcription factor in the cytoplasm of the cell. The HIF1-$\alpha$

then translocates to the nucleus where it binds to the constitutively expressed HIF1-$\beta$, thus activating or silencing the transcription of certain genes required for survival. These genes can be ones involved in energy production and anaerobic metabolism, in angiogenesis, in protection from oxidative stress, as well as promoting migration and invasion - all of which can in turn influence the cells resistance to therapies (64, 77, 80). Figure 1.15 illustrates the mechanisms by which HIF accumulates under hypoxic conditions.

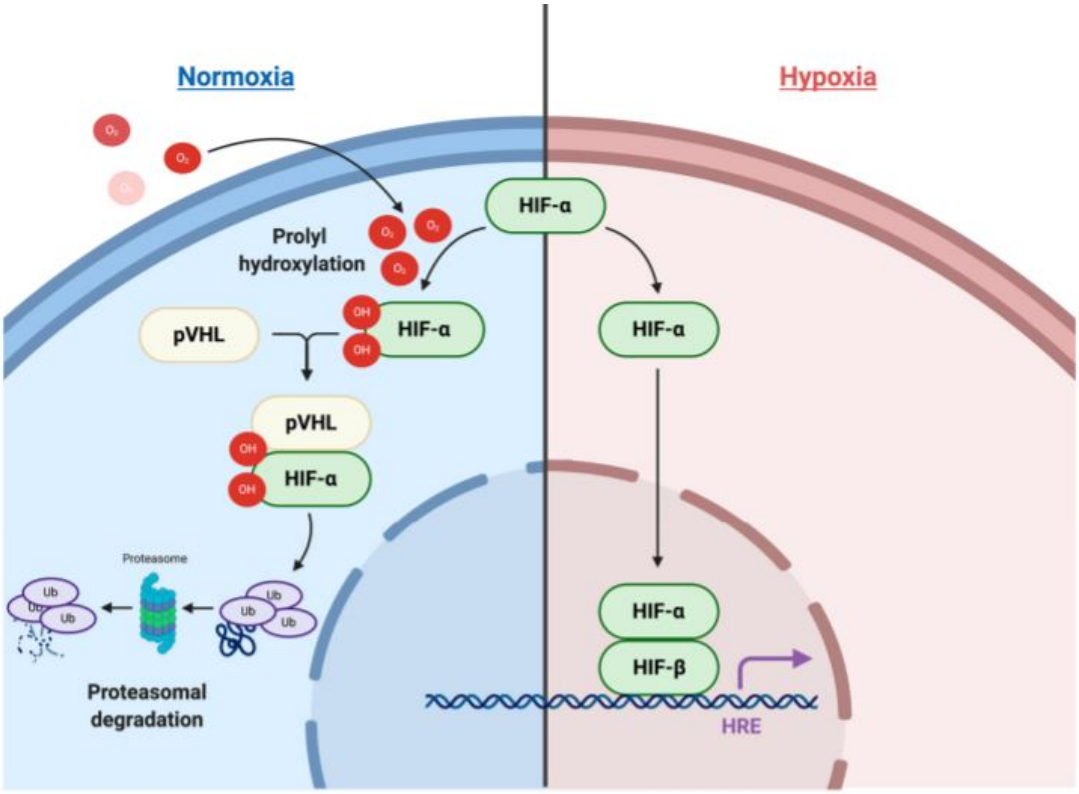


**Figure 1.15:** Illustration of HIF-$\alpha$s activation under hypoxic conditions. In normoxia, HIF are hydroxylated by proline hydroxylation domain proteins (PHDs) and then degraded by the von Hippel-Lindau protein (pVHL). In hypoxia, the PHDs are not activated and thereby HIF translocates to the nucleus, binding to HIF-$\beta$ which activates an array of cell responses. (81)

Cell adaption to hypoxia is mediated by both HIF1-$\alpha$ and HIF2-$\alpha$, which have distinct target genes and their activity can be dependent on the extent (i.e. $pO_2$) and duration (i.e. acute, chronic) of hypoxic exposure (82). Evidence showed that when cells were exposed to a hypoxic environment for a certain period of time, there is in fact a switch from one HIF protein to the other (82, 83). Saxena et al. demonstrated that while both proteins become stabilised at 1% $O_2$, HIF1-$\alpha$ protein remains stabilised only in acute hypoxia with a peak at around 4-8 hrs, whereas in prolonged hypoxia (24 hrs - 72 hrs) its expression decays and HIF2-$\alpha$ remains stable (84). Indeed, a number of studies showed that the downregulation of HIF-1a expression in sustained hypoxia is most likely due to a reduced stability of its mRNA (85, 86). HIF1-$\alpha$, however, has

been targeted and researched far more than its protein sibling HIF2-$\alpha$, even though HIF2-$\alpha$ has been shown to be a key player in chronic hypoxia exposure (83, 87, 88, 89).

Numerous studies have highlighted that most tumours including lung (90, 91), brain (92), breast (93), prostate (94) and bladder (94) along with many others (92, 95), show an over-expression of HIF1-$\alpha$ compared to their normal tissue counterpart with a further increase under hypoxic exposure. Although the over-expression of HIF1-$\alpha$ is associated with poor survival following chemo/radiation chemo/radiation treatment (96, 97, 98, 99), the increase in tumour resistance, however, is not directly influenced by the accumulation of the HIF1-$\alpha$ protein, but rather by the cascade of effects and events that occur following its induction (70). This includes the metabolic switch from strongly active mitochondria, which utilises oxidative phosphorylation (OXPHOS) for energy production, to the highly glycolytic cellular activity and activation of the pentose phosphate pathway (PPP) to establish and maintain redox homeostasis, also in hypoxic conditions. A study by Harada et al. highlighted the importance of investigating metabolic changes post treatment and found that suppression of upregulated HIF post IR had a better therapeutic outcome in comparison to before IR, which in some cases actually increased the radioresistance (100). Nevertheless, the proportionality with which HIF-induced events contribute to the resistance is unknown. For this reason, many researchers have sought to target the HIF protein itself through either direct or indirect inhibition to prevent the events that follow and as a result promote radio-sensitivity. However, it is not only the stabilisation of HIF before radiation that contributes to the radio-response. HIF1-$\alpha$ expression has been known to also increase following radiation in a hypoxia-independent manner (100, 101, 102, 103) due to reoxygenation and the resulting amplified ROS signal (67). Accumulating, but controversial, evidence in fact suggests that ROS influence HIF1-$\alpha$ stabilisation and in particular mitochondrial ROS were shown play a critical role (104, 105, 106). A study carried out by Chandel et al. found that under hypoxic conditions HIF1-$\alpha$ was activated via mitochondrial dependent signalling involving the production of ROS. However, the precise mechanisms still remain to be elucidated and conflicting hypothesis have been proposed. In conclusion, HIF-mediated resistance to RT is a complex phenomenon, which involves both the radiation-induced activation of HIFs and the activation of pro-survival pathways by HIFs.

### 1.4.3 DNA damage and DDR in Hypoxia

Hypoxia reprogramming restricts the efficacy of radiotherapy treatments by altering DDR (107, 108). These changes combined with the fact that oxygen is required for the induction of DNA damage during radiotherapy signify that hypoxia remains a relentless obstacle in the treatment of many solid tumours. Although there has been a considerable amount of research on investigating the DNA repair capabilities of hypoxic cancer cells and how this compares to the oxygenated cancer cell repair system (109), a more thorough understanding about hypoxia contribution to RR is needed, with particular attention to the modulation of targetable complexes in the DDR pathways (107).

Hypoxic cancerous tissues are an embellished form of an aggressive tumour and inevitably have an altered DDR compared with normally oxygenated tumours. According to literature, the number of DSBs induced by an external source are reduced in oxygen conditions which are less than 1% $O_2$, and hypoxia itself does not cause DNA damage as long as no reoxygenation occurs (110, 111). Many studies have shown that some elements of the DDR pathways, whether in the NHEJ or HR repair, can be either upregulated or downregulated in response to hypoxia. This response, however, has crucially been shown to largely depend on the duration (time) and extent ($O_2$%) of hypoxic exposure (109, 112, 113). Previous literature has shown that many proteins involved in DDR pathway (sensors, transducers and effectors) (107) are altered in the presence of hypoxia. For example, the MRN complex was found to be downregulated in medulloblastomas following chronic hypoxic exposure (114) and also in Non-small-cell lung carcinomas (NSCLCs) under severe hypoxia (115). Further, it has been shown that hypoxia can induce activation of both ATM-Chk2 and ATR/Chk1 signalling (110, 116). However, conflicting results have been reported with regard to Ku complexes. In fact, some studies found an upregulation and others a downregulation of Ku in hypoxia. Meng et al. found a decrease in expression levels of DNA PKc and Ku70 in prostate cancer cells under severely chronic hypoxic conditions (i.e. 48 - 72 hrs of 0.2%), whereas Ren et al. found an upregulation in the Ku70 expression levels of an epithelial cancer cell line under their hypoxic conditions (i.e. $< 0.1\%$ $O_2$ for $> 36$ hrs) (117, 118). A study by Um et al. investigated the association of HIF1-$\alpha$ with the NHEJ repair pathway and found an upregulation of the sensor and transducer proteins (i.e. Ku70/Ku80, DNA-PKcs) following acute hypoxic exposure (1% $O_2$, 2 - 8 hrs) (119). Effector proteins involved in HR repair pathway such as BRCA1/2 and RAD51 have also

shown to be downregulated in hypoxia in various studies with ranging oxygen percentages and incubation periods (117, 120, 121). Although many previous studies have investigated the changes in some DDR proteins in response to hypoxia as illustrated in figure 1.13, it is clear that the effects of hypoxia on DNA repair systems are complex and multifaceted and their contribution to a more radio-resistant phenotype is not yet completely known and further research on this topic is therefore required.

### 1.4.4 Energy metabolism and oxygen consumption

It is widely recognised that metabolic reprogramming in cancer is one of the major factors contributing to radioresistance. The majority of tumours in normoxic conditions have an increased dependency on glycolysis, which converts glucose in pyruvate in the cytoplasm, and are less dependent on mitochondrial oxidative phosphorylation (OXPHOS) capacity. Although glycolysis is less energetically efficient than OXPHOS, it provides enough energy in the form of adenosine 5'-triphosphate (ATP) in a fast way and redox regulation for tumour development. This has been termed aerobic glycolysis or Warburg effect (122, 123). Moreover, pyruvate production following glycolysis can fuel the mitochondrial tricarboxylic (TCA or citric acid) cycle, thus generating precursors for lipid and nucleotide synthesis and promoting cancer cell proliferation (124, 125).

In a hypoxic microenvironment, OXPHOS is weakened, while aerobic glycolysis is further enhanced and sustained by HIFs, which also impairs TCA and OXPHOS. Moreover, glycolytic intermediates are substrates for the PPP which is important for the biogenesis of antioxidants like NADPH and glutathione. As a result, the mitochondrial oxygen-consumption is reduced and hypoxic ROS production is attenuated, while optimising glucose uptake and utilisation to generate ATP (77). The interconnection between these concepts (i.e. glyocolysis, TCA cycle and PPP) are highlighted in figure 1.16 and will be better explained in the following sections.

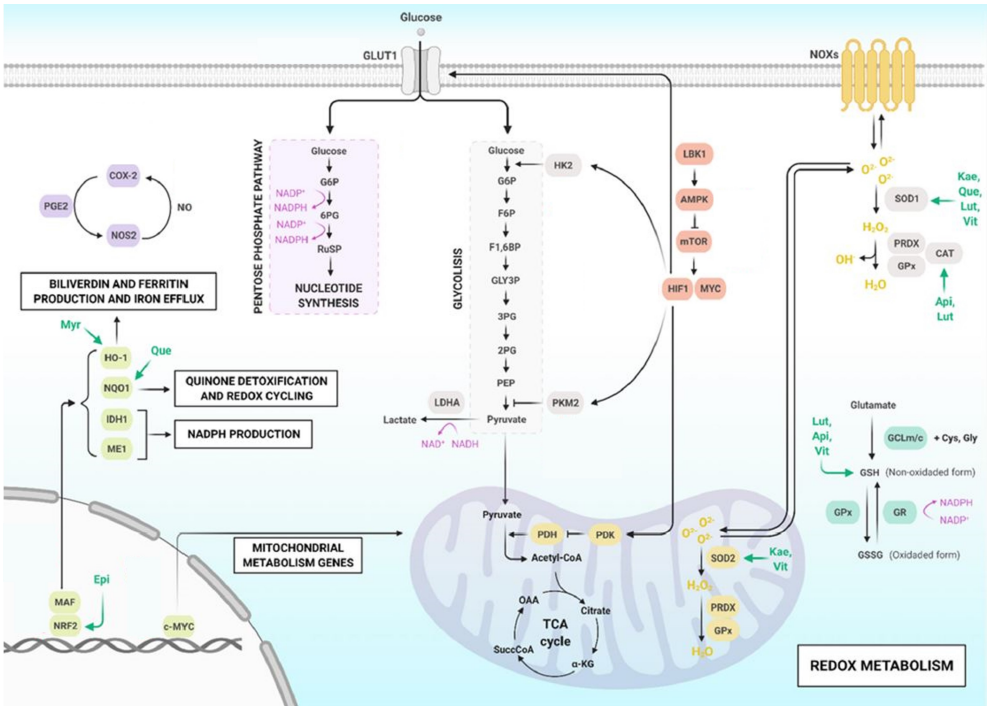


**Figure 1.16:** Illustration of the interconnection between cellular metabolic processes including glycolysis and mitochondrial tricarboxylic (TCA) cycle which are used to produce energy, and also the redox metabolism of the cell including the pentose phostphate pathway (PPP) which produces NADPH. (126)

### Mitochondria and cellular respiration

Although DNA in the nucleus is the main target of ionising radiation, nowadays it has become clear that a critical role in mediating the effectiveness of RT especially in hypoxic tumours is also played by the radiation-induced effects on other subcellular organelles, in particular the mitochondria (127, 128). Mitochondria, as described by author Nick Lane, are "tiny power generators inside living cells that produce virtually all the energy we need to live" (129). They are double membrane organelles found inside the cell cytosol, most often dispersed strategically where energy demand is high. Their inner membrane is extensively folded into ridges called cristae, in which the intermediary metabolism (i.e. fatty acid oxidation and TCA) occurs, with the number of folds present positively correlating to the cell's respiratory activity. It is therefore not surprising that OXPHOS also occurs there, although firmly rooted on the inner part of the mitochondrial membrane (130), as shown in figure 1.17.

Energy production via mitochondrion is far more efficient than glycolysis – 36 molecules of ATP as opposed to 2 ATP produced per cycle – and with it being its central role, mitochodrion is aptly been named "the powerhouse of the cell". In aerobic cells, oxygen dependent ATP synthesis (that is OXPHOS) relies on enzymatic reactions of the TCA cycle, fueled by

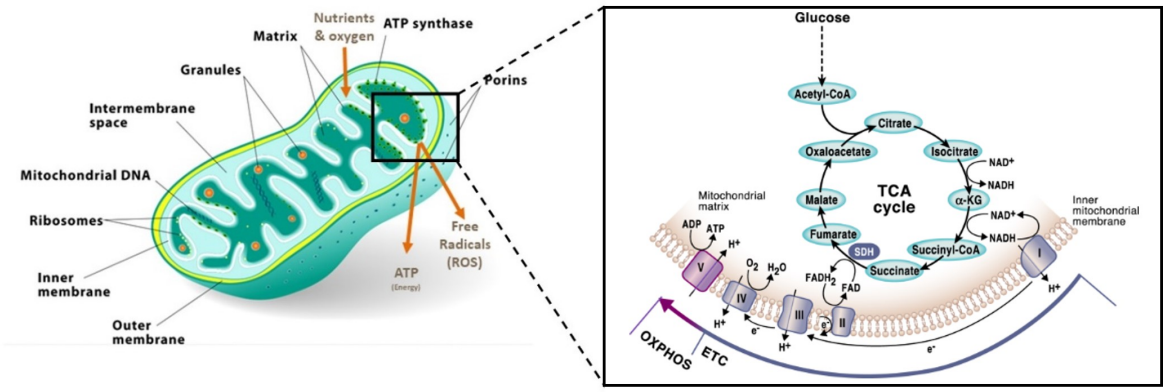


**Figure 1.17: Left:** Illustration of the mitochondria and it's components including the location of the electron transport chain (ETC) and oxidative phosphorylation (OXPHOS) on the inner mitochondrial membrane. **Right:** Schematic of the TCA cycle generating NADH AND FADH2 which transfer electrons to the ETC where they are funnelled through the mitochondrial complexes, creating a membrane potential. ATP is then produced in the presence of oxygen in a process known as oxidative phosphorylation (OXPHOS). Adapted from Martínez-Reyes et al. (131)

acetyl-coenzyme A (acetyl-CoA). Acetyl-CoA is produced by either pyruvate derived from glycolytic pathway or by the oxidation of fatty acids. TCA cycle provides reducing equivalents such as NADH (reduced form of Nicotinamide adenine dinucleotide (NAD)) and $FADH_2$ (hydroquinone form of Flavin adenine dinucleotide (FAD)) used to transfer electrons to the mitochondrial electron transport chain (ETC). This process consumes $O_2$ and it is therefore known as mitochondrial respiratory chain. In fact, electrons are transferred from complex proteins I, II, III and IV along the ETC. In particular, in the transfer from cytochrome c to complex IV (known as cytochrome c oxidase or ) the electrons are used for the reduction of $O_2$ to water. In aerobic cells, the majority, but not all, of oxygen utilisation occurs in the mitochondria. Mitochondrial respiration can be described in the following equation where oxygen is reduced by 4 electrons to produce water (132):

$$O_2 + 4H^+ + 4e^- \rightarrow 2H_2O \tag{22}$$

The partial reduction of an oxygen molecule by a free electron creates a superoxide anion mainly from complex I and III), which is then can be removed by the ROS scavenger superoxide dismutase (SOD). SOD catalyses the following reaction that produces hydrogen peroxide ($H_2O_2$) and oxygen (132):

$$O_2^{(\bullet-)} + O_2^{(\bullet-)} + 2H^+ \rightarrow H_2O_2 + O_2 \tag{23}$$

Afterwards, other antioxidant systems, including Catalase, convert $H_2O_2$ in $H_2O$ and $O_2$ (see section 1.2.3)

These reactive oxygen species produced due to the flow of electrons through the ETC influence the cells redox environment by initiating redox signalling pathways and are important in regulating metabolism (133). The electron transfer steps are coupled to proton translocation across the mitochondrial inner membrane which creates an electrochemical gradient. Such a gradient is in turn used to drive the synthesis of ATP from ADP and inorganic phosphate by complex V (ATP synthase) (figure 1.18). ROS therefore are by-products of ATP production. However, if the production of ATP is inhibited or the mitochondria are defective, the mitochondrial respiration will decrease which leads to a build-up of oxygen partial pressure and thereby contributes to an increase in mitochondrial ROS accumulation.

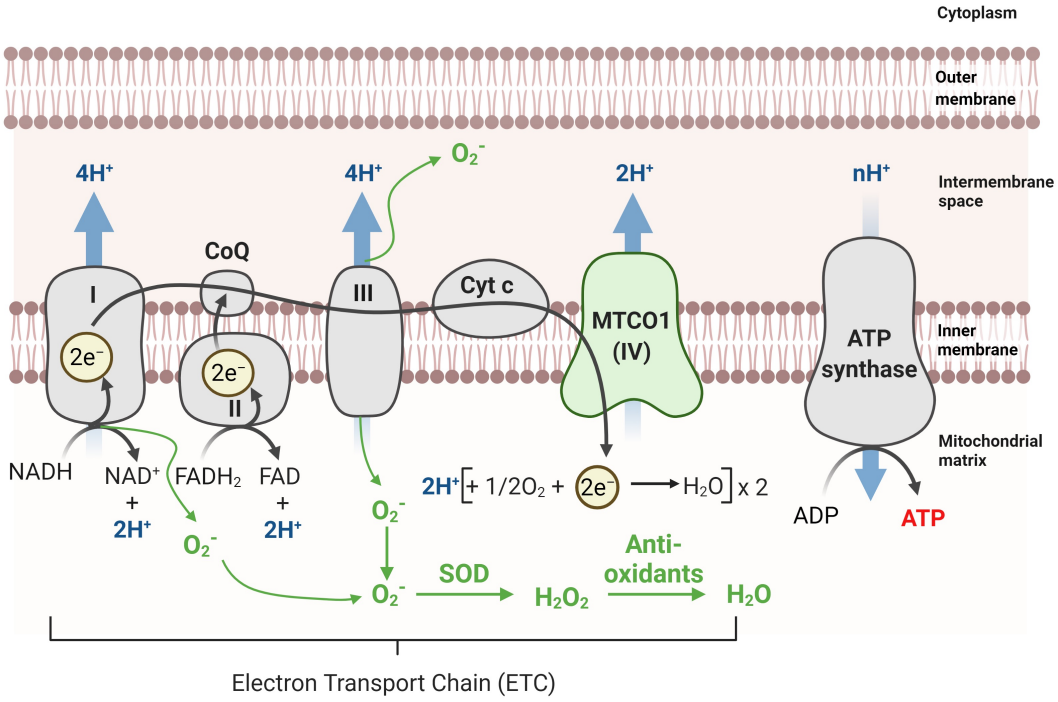


**Figure 1.18:** Illustration of the mitochondrial electron transport chain (ETC) and its protein complexes I - IV. The transport of electrons along the chain causes production of highly reaction radicals (i.e. $O_2^-$) which are converted to less reaction ROS (i.e. $H_2O_2$) by superoxide dismutase (SOD) and further detoxified to $H_2O$ by antioxidants in the cell. Figure was made using Biorender.

### Cellular respiration in cancer cells

As mentioned previously, the oxygenation status of a tumour is dependent on the oxygen diffusion within the cancer tissue and can be limited by the oxygen consumption rate of the cancer cells themselves. Cells use oxygen in many ways and at varying rates depending on the

cell type, function, and environmental conditions. Cancer cells often have altered mitochondrial activity and are known to function anaerobically, favouring glycolysis over OXPHOS in energy production (Warburg effect) also in well oxygenated conditions. Although previously thought to be due to defective mitochondria, a hypothesis that was largely debated, further studies have shown that this is not the case and that it is more likely caused by a suppression of mitochondrial activity and possible that OXPHOS function can be restored (134). Nevertheless, other studies have shown that genetic mutations in cancer cells can result in dysfunctional mitochondria, and p53 in particular has been shown to interfere with the transcription of cytochrome c oxidase 2 and therefore alter mitochondrial respiration (135, 136, 137). However, when $O_2$ levels decrease, cells undergo metabolic adaptations by fine regulating mitochondrial functions and amount. In fact, OXPHOS process is generally weakened due to lack of oxygen and glycolytic pathways are enhanced to ensure cell energy demands are met. Concurrently, together with a reduced ATP supply, the metabolic demand (including protein synthesis) is also diminished which results in decreased need of ATP and rate of oxygen consumption (138).

Low $O_2$ levels can decrease TCA cycle flux in a HIF-dependent manner (139, 140) limiting the generation of NADH and $FADH_2$, which results in a reduced electron flux through the ETC. Conversely, it has been shown that  has a high affinity for $O_2$ (apparent Km value near to 0.1%), thus suggesting that the ETC can function also in severe hypoxia (141) and that cells can thus maintain high levels of ATP production. Indeed, acute hypoxia does not seem to inhibit ETC function, while prolonged hypoxia can decrease it resulting in attenuated mitochondrial activity (142). Therefore, as a result of glycolytic reprogramming, hypoxic tumour cells generate a more protective intracellular environment, and the presence of mitochondrial dysfunctions together with the adaptation to hypoxic micro-environments confers the ability to survive and/or grow and thus to be potentially more radio-resistant (25, 108). Indeed, metabolic adaptive responses in cancer cells have been associated with enhanced radioresistance in hypoxia (108, 143, 144). In fact, radiation-induced ROS production and the effects on mitochondrial metabolism become more detrimental for oxygenated cancer cells than for hypoxic cells (108).

### 1.4.5 Redox metabolism: Mitochondrial ROS, Pentose Phosphate Pathway

In general, in hypoxic conditions, one of the major consequences of the reduced ETC activity and respiratory rate is a corresponding reduction in mitochondrial ROS formation (139). Therefore, the likelihood of an oxygen partial pressure build-up is low and radicals are less likely to accumulate, reducing the probability of cell damage. Whether hypoxia increases or decreases cellular ROS has been the subject of intense debate. Several reports have shown that decreased oxygen availability in hypoxia leads to lower ROS concentrations. In fact, it has been proposed that the hypoxic metabolic responses would mainly serve to prevent the excess of mitochondrial ROS production associated with ETC impairment (145). Although the mechanisms of hypoxic ROS-induction are poorly understood and not straightforward, it has been shown that acute hypoxia increased ROS production within minutes, which stabilises HIF-1$\alpha$ (146), while chronic hypoxia reduced ROS levels to normoxic values (139).

Conflicting studies have also been reported on the role of mitochondria in regulating the adaptation to hypoxic micro-environments. In fact, some studies have shown that mitochondria induce hypoxic responses, in particular HIF-1$\alpha$ protein accumulation and stabilisation, by releasing ROS from complex III (147, 148), while others by regulating $O_2$ cellular availability independently on mitochondrial ROS (149, 150). The main redox species ROS formed in tumour cells are superoxide ($O_2^{\cdot -}$), hydrogen peroxide ($H_2O_2$), nitric oxide (NO) and the non-radical intermediates, such as lipid hydroperoxides, and peroxynitrite. $O_2^{\cdot -}$ and $H_2O_2$ are both produced during mitochondrial respiration as by-products and also by enzymatic reactions involving nicotinamide adenine dinucleotide phosphate (NADPH) oxidases (NOX1 - 5) and dual oxidases (DUOX1 - 2).

Ionising radiation can damage mitochondria and induce further ROS release (128). This mitochondrial ROS production can be delayed and persist for days after IR as compared to the ROS produced by water radiolysis which have short life spans (128, 151). These ROS significantly contribute to perturbing the redox state as well as the DNA repair capacity of the cells and can participate in conferring a radio-resistant phenotype (128). In a study by Yamamori et al. high dose X-ray irradiation of lung cancer cells caused a time-dependent overproduction of ROS, which decreased at 24 hrs. ROS production was associated with an increase of mitochondrial respiration, ATP production and mitochondrial content (152). Moreover, other studies demonstrated an accumulation of total and mitochondrial ROS in

irradiated cells over a period of 24 hrs post-IR (153, 154). However, evidence of a reduction of ATP content and decreased activity of OXPHOS soon after IR has also been reported ((155)). Moreover, radiation-induced HIF-stabilisation further contributes to glycolytic metabolism in hypoxia and to reduced mitochondrial activity, thus indicating that ionising radiation alters the metabolism of the cells and their redox state, but the type of responses is most likely cell-specific and dose and time dependent.

In general, ROS production and removal by antioxidant systems influence cellular redox environment, which is mainly regulated by the two redox couples: NAD+/NADH and NADP+/ NADPH. In this context, the NAD+/NADH redox couple is associated with the metabolic activities of cells. NADH is primarily produced from glycolysis and TCA cycle. The phosphorylated form of NADH is NADPH synthesised by using ATP. Moreover, NADPH is generated through the reduction of NADP+ when glucose is converted into glucose-6-phosphate (glycolytic step) and enters the pentose phosphate pathway (PPP), which will be discussed below. Cells depending on glycolytic metabolism produce more cytoplasmic NADH and NADPH than mitochondrial respiratory dependent cells. These events, associated with the overproduction of antioxidant redox couples derived from intermediates of the upregulated glycolysis (156, 157, 158, 159), are thought to confer radioresistance to hypoxic cancer cell (70).

**Pentose Phosphate Pathway (PPP) and the antioxidant responses in hypoxia**

Reprogramming of cancer cells involves enhanced glycolytic activity, which results in higher production of intermediated to be used in parallel anabolic processes for sustaining cell survival and redox homeostasis. One of these pathways is the Pentose Phosphate Pathway which uses glucose-6-phoshate (G6P), produced during glycolysis, to regenerate nicotinamide adenine dinucleotide phosphate (NADPH) from NADP+ and ribulose-5-phosphate (Ru5P) by the enzymatic activity of glucose-6-phosphate dehydrogenase (G6PD) (160). This is termed oxidative phase and it is followed by a non-oxidative phase in which pentose phosphates are generated for ribonucleotide synthesis used to make up DNA and RNA and is indicated in figure 1.19. These are reversible reactions which can be used for generating additional NADPH or helping in glycolysis, depending on the cell's metabolic demands (157). NADPH is a reducing agent mainly used for biosynthetic processes, such as fatty acid synthesis (161), but it is also involved in antioxidant responses. In fact, NADPH participates in the glutathione

regeneration from the oxidised GSSG by glutathione reductase (GSR) and thereby contributing to ROS elimination (162). Glutathione is an antioxidant frequently increased in many tumours, including lung, breast and ovarian cancer (163, 164). GSH can be oxidised to remove $H_2O_2$ by glutathione peroxidases and GSSG/GSH ratio represents another important indicator of the cellular redox environment. Moreover, NADPH is an essential cofactor required for the activity of the thioredoxin reductase (TR) which reduces the oxidised form of thioredoxin (TRX). TRX is used for $H_2O_2$ removal by peroxiredoxins (165). Hence, NADPH plays a crucial role in counteracting ROS-induced oxidative stress and thus in radiation responses and resistance. However, an excess of glutathione and NADPH can paradoxically lead to reductive stress (97). Additionally, many of these antioxidants are over-expressed in cancer and regulated at both mRNA and activity level. Their expression is under NRF-2 control, which is responsible for GSH synthesis (166, 167). In a study by Singh et al., high expression of NRF-2 non-small-cell lung cancer cell lines has been associated with radioresistance through GSH (31).

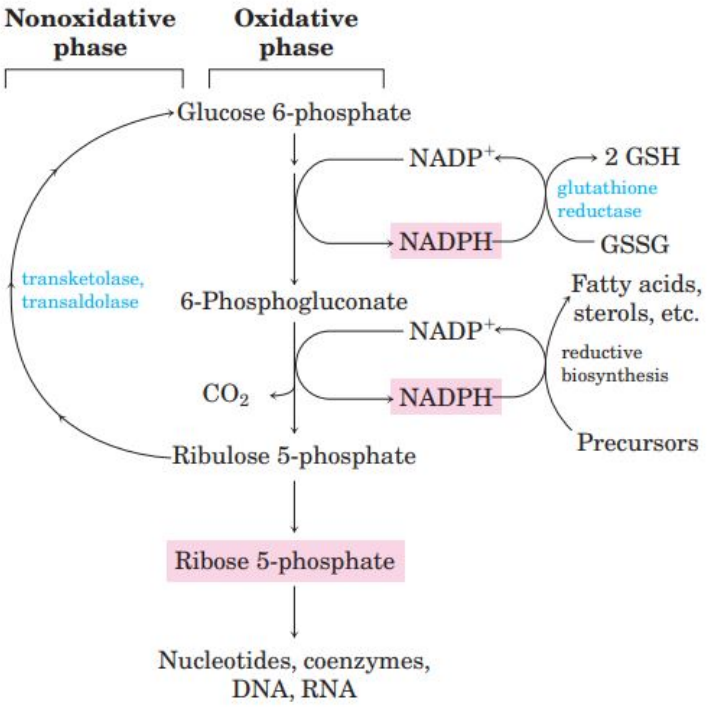


**Figure 1.19:** Illustration of the pentose phosphate pathway (PPP) indicating the non-oxidative and oxidative phases, where the latter consists of the synthesis of NADPH. NADPH is used to convert oxidised glutathione (GSH) into its reduced form (GSSG). Ribose 5-phosphate is used to produce hexose glucose-6-phosphate and allow for continuous production of NADPH. (168)

G6PD is the rate-limiting enzyme in cytosolic NADPH regeneration and consequently its activity affects the redox state of the cells. G6PD has been shown to be overexpressed in several tumours including breast, cervical, colon, liver, prostate, and lung (157) and associated with

tumour angiogenesis, invasion, metastasis, and survival (157, 169) The NADPH/NADP+ ratio is critical for G6PD activity. In fact, high NADPH consumption produces high levels of $NADP^+$ which stabilise G6PD conformation stimulating its activity. On the contrary, NADPH accumulation reduces G6PD activity (169). G6PD expression is also regulated by NRF2, whose knockdown can decrease NADPH/$NADP^+$ ratio (170). Also, Jiang et al. showed direct inhibition of G6PD through interaction with the cytoplasmic tumour suppressor p53, resulting in a decrease of PPP activity and NADPH production, suggesting that p53 deficient cells have an increased consumption of glucose through an enhanced PPP (171). In relation to radiotherapy and resistance, PPP activity may play an important role and the enzymes involved could potentially represent prognostic markers. Therefore, the use of inhibitors in the pathway could decrease the NADPH generation and thereby resistance to intracellular ROS, improving the outcome of therapeutic treatment.

Together with favouring glycolysis, hypoxia can also support PPP and further trigger antioxidant responses (172). It has been shown that HIF-1$\alpha$ is involved in targeting and transactivating G6PD (173) and by acting on other enzymes of the glycolysis can divert glycolytic intermediates to the PPP to generate more reducing equivalents for counteracting oxidative stress. Other factors such as the $pO_2$ and the duration of hypoxia will affect genetic expression and signalling induction levels differently. For example, in a study by Gao et al., chronic mild hypoxia (72 hrs at 3% $O_2$) was required to induce G6PD activity through ROS-mediated activation. However, this was found to be cell type dependent. Gao et al. suggested that G6PD has a low sensitivity to HIF and requires a prolonged low hypoxia exposure to allow ROS accumulation before it becomes activated (174). This again just reiterates the importance of HIF-1$\alpha$ in many aspects of biological signalling and its contributions to radioresistance. Hence, hypoxia can promote the increase of NADPH content which in addition to others concomitant antioxidant strategies can favour ROS detoxification and reduce radiotherapy efficacy.

In conclusion, it appears evident the intricate and complex interplay between hypoxia and tumour metabolic rewiring plays a role in determining cellular responses to radiation therapy. Understanding the way cancer cells utilise oxygen, from ROS production to the antioxidant species that scavenge them, can help to comprehend the intracellular and extracellular redox environments as well as how these processes activate or suppress metabolic signalling pathways and thereby contribute to cancer radio-resistance (175).

# 2 Overview of Thesis

In this section, a brief overview of the concerning topics for this thesis titled "Radio-Resistance of Hypoxic Tumours: The Effects of Oxygen and Radiation on Cancer Cell Metabolism, Oxidative Stress, and DNA Repair" will be outlined, highlighting the motivation for the research and the two main aims that were pursued throughout. An outline of the thesis structure will also be provided.

## 2.1 Motivation of current research

Cancer is one of the leading causes of death in the world and is routinely treated with photon radiotherapy. The purpose of radiotherapy is to induce a high level of damage to cancer cells while sparing the nearby healthy tissue. Radiation aims to ensue damage on the most important macromolecule in the cell, the DNA, by interacting either directly with it or indirectly via induction of cellular oxidative stress and thus formation of reactive oxygen species (ROS). ROS molecules include the highly reactive hydroxyl radical ($OH^{-}$) and superoxide anion ($O_2^{\cdot -}$), as well as the less reactive non-radical hydrogen peroxide ($H_2O_2$), which is more stable and can therefore diffuse over longer distances in the cell. ROS accounts for approximately 80% of cellular damage caused by photon radiation, which includes the induction of DNA double strand breaks (DSBs). DSBs are the most detrimental lesions due to the complexity to efficiently repair the DNA by the two repair pathways, non-homologous end joining (NHEJ) and homologous recombination (HR), and are therefore most sought-after lesion by clinician. However, even with a high amount of oxidative stress and potentially a higher probability of damage, cancer cells can respond by activating their antioxidant systems and scavenge the toxic ROS. Radiation therefore needs to not only overcome the cancer cell DNA repair systems but also their corresponding antioxidant defences.

In addition to this, the efficacy of the radiation with respect to ROS induction and DNA damage depends largely on the tumour microenvironment, with oxygen content playing a particularly crucial role in radiotherapy. Tumours tend to have fluctuating levels of $O_2$, often even varying with the tumour mass itself. Oxygen levels, termed "hypoxia", which are lower than the respective normal cancerous tissue (normoxia) may occur due to the highly proliferative characteristics of cancer cells, resulting in the tumour mass increasing and thereby the diffusion distance between the vasculature network and cells exceeding the cancerous metabolic demand. Conditions such as these result in the cell being deprived of energy and nutrients, however, cancer cells have reprogrammed their metabolism to function anaerobically. This so-called "metabolic shift" enables continuous cell proliferation even under nutrient deprivation, has been known to establish a more aggressive phenotype and enhances resistance to therapies such as radiation, with hypoxic tumours typically requiring 2.5-3-fold increase in radiation dose to induce a damage equivalent to the damage seen in a normoxic tumour.

The strong influence that hypoxia has on establishing a population of cells which are metabolically more resistant to treatment, whereby the damaging effects of radiation are less consequential and the therapeutic outcome is reduced, highlights the need for a better understanding of how these more resistant cancer cells function and respond to treatment.

## 2.2 Aims and objectives of research

The complex mechanisms underlying the development of radio-resistance involve, among others, altered antioxidant properties and DNA repair ability, as well as altered tumour metabolism and micro-environmental factors, in particular the levels of $O_2$ inside the tumour. All of them play central roles and their contribution can vary depending on tissue and organ.

The aim of the present experimental thesis was to investigate the in vitro radio-responses activated by hypoxic cancer cells in diverse tumours or tumours from the same organ in comparison with their normoxic counterparts. The overall goal was to look at some of the mechanisms potentially related to the radio-resistance in order to highlight common and/or distinctive traits in different tumours that might help to better elucidate their behaviour and, in a future perspective, provide input which might be useful for improving the radiotherapy sensitivity.

To these purposes, in the two main chapters it was evaluated:

1. the metabolic behaviour of cancer cell lines, derived from different organs in the body, in presence of different levels of hypoxic severity (i.e. acute and chronic);
2. the metabolic signatures of radio-resistant cancers of different origin, in normoxia and chronic hypoxia;
3. the radio-responses of three different non-small lung cancer cell lines (NSCLC) exposed to hypoxia and their corresponding antioxidant and repair capacity post-IR;.
4. the indirect DNA damage induced by photon radiation on NSCLC and the possible correlation with nuclear radiation-induced ROS.

# 3 Metabolic adaption of cancer cell lines to different levels of hypoxia and photon radiation

## 3.1 Introduction

Cancer cells have an altered metabolism which allows them to thrive in nutrient deprived regions and provides them with characteristics such as being highly proliferative and aggressive, with a strong capability of mitigating genotoxic stress. Tumour cell metabolic reprogramming has been in fact widely recognised as a hallmark of cancer. In this way, cancer cells are also less susceptible to treatments like chemotherapy and/or radiation, making it difficult to treat them effectively. Contrary to healthy cell metabolism, which mainly utilises oxidative phosphorylation (OXPHOS) in the mitochondria for ATP production, cancer cells will almost always favour glycolytic production of ATP, even in the presence of oxygen and even if this process generates less ATP per glucose molecule, otherwise termed "aerobic glycolysis" (122). Nevertheless, recent research has suggested that some cancers also have a relatively high reliance on mitochondrial OXPHOS, in addition to glycolysis, for ATP production (176, 177). Their strong glycolytic behaviour contributes to their rapid proliferation, and as a result they exhaust oxygen and nutrients. For this reason, cancer cells tend to have a lower oxygen ($O_2$) concentration in comparison to their healthy tissue counterpart as indicated in table 3.1.

| | **Median healthy tissue $O_2$%** | **Median tumour $O_2$%** | **Reference** |
|---|---|---|---|
| **Brain** | 3.4 | 1.7 | (178) |
| **Lung** | 5.6 | 2.2 | (179) |
| **Renal (bladder)** | 4.9 | 1.3 | (180) |
| **Prostate** | 3.4 to 3.9 | 0.3 to 1.2 | (181, 182) |

**Table 3.1:** Median oxygen percentage ($O_2$%) in healthy tissue and tumour tissue from different organs in the body including brain, lung, bladder, and prostate. Table adapted from Mckeown et. al (183)

Often within a tumour mass there is a heterogeneous distribution of oxygen content, for example, the exterior parts may have a higher oxygen concentration due to possible access to blood vessels, compared to the centre of the tumour mass, where the diffusion of oxygen can be extremely limited (184). In addition to this, following treatments such as radiotherapy, reoxygenation may occur and alter the oxygen content. These fluctuating amounts of oxygen can result in some cancer cells experiencing a short time of oxygen deprivation, defined as acute hypoxia, while others are without oxygen for a longer period and would be considered a chronic hypoxic situation (84). There are also cancer cells which remain hypoxic even after treatment, which experience severely chronic hypoxia. Hypoxic regions within a tumour function metabolically different to the normally oxygenated regions (185), which can also vary depending on the severity of the hypoxic condition (i.e. depending on the $O_2$ level). Without oxygen, cells are forced to change their cellular bio-energetics and redox state, processes which are intrinsically linked at different levels, in an attempt to restore cellular homeostasis. The adaptive behaviour of hypoxic cancer cells to such stressful conditions can therefore contribute to their enhanced resistance to therapy.

Therefore, this in-vitro study was designed in order to investigate the functional differences that cancer cells, cultured in various hypoxic conditions, adopted in comparison to their normoxic counterparts. Further, the present study aimed at elucidating the potential impact of severe prolonged hypoxia on the metabolic features of the most radioresistant populations. Cell lines derived from different organs (brain, lung, bladder and prostate) were considered, in an attempt to highlight potential common and/or distinctive features, which might shed light on key points in their adaptive behaviours and help to better overcome radio-resistance.

## 3.2 Materials & Methods

### 3.2.1 Cell Culture

Cells were cultured at 37°C in a humidified atmosphere of 5% $CO_2$ and 21% $O_2$, unless otherwise stated, and were sub-cultured using TrypLE Express (Thermo Fisher Scientific, Cat.Nr.: 12604013) when they reached 70 - 80% confluency. The cell lines used in this thesis include human brain neuroglioma cells (H4) from a 37 year old Caucasian male, human urinary blad- der carcinoma cells (T24) from an 81 year Caucasian female, human prostate adenocarcinoma cells (PC-3) from a 62 year Caucasian male and human non-small lung carcinoma cells (H460: pleu-

ral) from a male (age and ethnicity unspecified). All cell lines were purchased from ATCC. H4 cells were cultivated in Dulbecco's Modified Eagle Medium (Thermo Fisher Scientific, Cat.Nr: 11995065), T24 cells in McCoy's 5A (Modified) Medium (Thermo Fisher Scientific, Cat.Nr.: 16600082), H460 cells in Gibco RPMI Medium (Thermo Fisher Scientific, Cat.Nr.: 224000-89), and PC-3 in Ham's F-12K (Kaighn's) Medium (Thermo Fisher Scientific, Cat.Nr.: 21127-022). All media were supplemented with 10% Fetal Bovine Serum (FBS) (Thermo Fisher Scientific, Cat.Nr.: 10082147) and 1% PenStrep ((10,000 U/mL), Thermo Fisher Scientific, Cat.Nr.: 15140122). Additionally, 1% HEPES Buffer (1M) (Thermo Fisher Scientific, Cat.Nr.: 15630056,) was added to T24 medium.

Under normal environmental conditions (i.e. normoxia) and for regular cell culture, cells were incubated at 37°C, 5% $CO_2$ and an oxygen concentration of 21%, whereas in low oxygenated conditions (i.e. hypoxia), cells were incubated and cultured in a hypoxic chamber (HC) (Sci-Tive, Baker Ruskin) as shown in figure 4.1, where nitrogen was used as an oxygen substitute. The HC had the following control settings: 37°C temperature, 5% $CO_2$, 70% humidity and an oxygen concentration of 0.1% - 1%, depending on the experiment. This will be specified throughout the thesis.


**Figure 3.1:** Hypoxic chamber (Sci-Tive, Baker Ruskin) used for all low oxygenated experiments with controlled atmospheric parameters such as oxygen and carbon dioxide percent, temperature and relative humidity.

### 3.2.2 Oxygen concentration measurements using oxygen sensor spots

Oxygen sensor spots (TROXSP5) were obtained from PyroScience and utilised as an additional control to measure the oxygen percentage that the cells were exposed to following hypoxic incubation. The TROXSP5 $O_2$ sensor spots have a measuring range of 0 - 10% $O_2$, with high

precision at oxygen levels close to 0% $O_2$ (186). The working principle of the oxygen sensors is based on the quenching of emitted red light from the optical fibre (wavelengths of 610 - 630 nm) by oxygen molecules, resulting in a returning signal which is in the near infrared range (760 - 790 nm) (186). The sensors were calibrated using a two-point calibration method with 0% $O_2$ for the lower point and 21% $O_2$ for the upper point. OXCAL capsules from PyroScience were used to perform the 0% $O_2$ calibration.

Prior to use the sensor spots were sterilised with ethanol 70%. The senors were then glued to the inner bottom surface of a clean T25 flask (Greiner Bio-One, Cat.Nr.: 690175 and 690160) (figure 3.2(c)). Once the glue was dry, the flask was repeatedly washed with phosphate buffer saline solution (PBS) (SIGMA ALDRICH, Cat.Nr: D8537) and the cells were then seeded in the flask containing the $O_2$ sensor spot. After cell attachment the flask was inserted in the hypoxic chamber as shown in figure 3.2(b). Using an $O_2$ meter and an optical fibre, the $O_2$% was then determined by the quenched fluorescence of the returning signal due to the $O_2$ molecules, and a readout was recorded on a computer beside the hypoxic chamber, as shown in figure 3.2(a). The $O_2$ concentration was measured for approximately 10 - 18 hrs for the different cell lines.

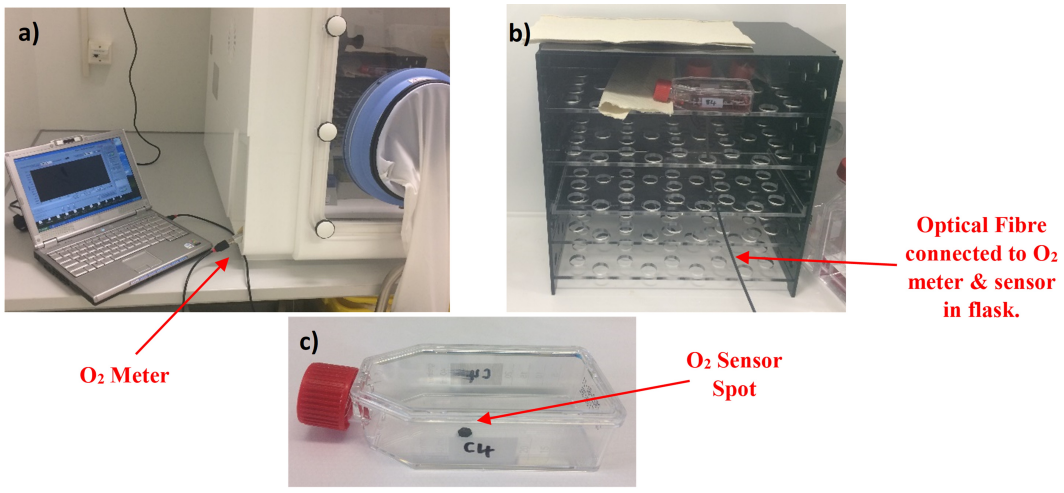


**Figure 3.2:** Oxygen concentration measurements in-vitro using PyroScience $O_2$ sensor spots (TROXSP5). **(a)** Measurements were recorded using an oxygen meter connected to computer which was external to the hypoxic chamber. **(b)** The optical fibre was connected to the $O_2$ meter, transmitting/recording the light to/from the $O_2$ sensor glued to the inner bottom surface of the flask in the hypoxic chamber. **(c)** Image of TROXSP5 $O_2$ sensor spot glued to the inner bottom surface of a cell culture flask.

### 3.2.3 Oxygen removal rate of cells using oxygen sensor spots

The oxygen removal of cells was determined by measuring the removal of oxygen from the media over a period of time using the $O_2$ sensor spots from 3.2.2. Cells were seeded at a density of 600,000 in a T25 flask containing the $O_2$ sensors. After the cells had attached to the flasks, they were placed in the hypoxic chamber which was set at an $O_2$% of 1%, a temperature of 37°C, $CO_2$ of 5% and a relative humidity of 75%. The normoxic media (21% $O_2$) in the flask was replaced with pre-incubated hypoxic media (0.1%). After the flask had equilibrated with the 1% $O_2$ hypoxic environment it was sealed with a non-filtered lid and parafilm to ensure that oxygen diffusion into the flask did not occur. The decrease in oxygen concentration was then measured for a total of 10 - 18 hrs. The slope of the linear fit to theses data points indicated the change in $O_2$% over time (i.e. $dO_2/dt$). The $dO_2/dt$ was then plotted against the logarithmic of the cell concentration (ln(cell count)) which was determined at the end of the experiment. From this plot the oxygen removal rate per cell (%/hr/cell) was defined.

### 3.2.4 Membrane and Nuclear Staining

Cells were seeded in a 12 well plate and cultured in the same way as detailed in section 3.2.1. At their respective time-points, samples were washed with PBS and fixed using 4% Paraformaldehyde (PFA) (Thermo Fisher Scientific, Cat.Nr: 28908) for 15 min. Samples were then washed twice with PBS and kept at 4°C in PBS until staining. Prior to imaging, samples were stained with a 250 µL solution of BioTracker 655 Red Cytoplasmic Membrane Dye (BioTracker, Cat.Nr.: SCT108), using a concentration of 3.5 : 1000 µL for the membrane, and Hoechst 33342 (Thermo fisher Scientific, Cat.Nr.:62249) for nuclear staining using a concentration of 2:1000 µL, for 20 min on a shaker. Samples were then washed three times using PBS and imaged using confocal microscopy as detailed below 3.2.5. The acquired images were then reconstructed using IMARIS software to determine their volume measurements.

### 3.2.5 Confocal Microscopy

Cancer cell lines H4, H460, T24 and PC-3 were stained with BioTracker 655 Red and Hoechst as for measuring the cell membrane and nucleus size, respectively, as outlined in section 3.2.4. Zeiss LSM710 confocal microscope was used to image the cells using a 63x oil immersion objective. For each experiment >20 cells were imaged per well.

### 3.2.6 ATP Assay

The CellTiter-Glo® Luminescent Cell Viability Assay (Promega , G7570) was used to quantify the cellular ATP levels. In this assay, ATP is used as a cofactor in the luciferase reaction as shown in figure 3.3. In the presence of ATP, $Mg^{2+}$ and $O_2$, the luciferase enzyme acts on the luciferin, resulting in the production of oxyluciferin and releasing energy as light.

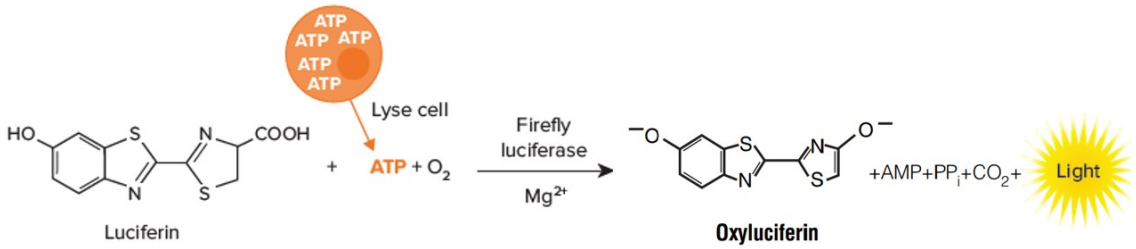


**Figure 3.3:** ATP measurements using CellTiter-Glo® Luminescent Cell Viability Assay. Luciferin is catalysed by $Mg^{2+}$, ATP and oxygen to produce oxyluciferin and a luminescence signal.

The assay for both the normoxic and hypoxic samples was conducted under normal oxygenated atmosphere (i.e 21% $O_2$). The assay was conducted in a 96 well plate as follows: Cell Titer Glo reagent was thawed overnight at 4°C. Prior to use it was equilibrated to RT for 30 min and mixed gently by inverting to homogenise. 100 µL of the reagent was then added to 100 µL of the cell culture media in each well and mixed on an orbital shaker for 2 min to induce cell lysis. The plates were then incubated at RT for 10 min to stabilise the signal and then the luminescence signal was recorded using a plate reader (ClarioStar, BMG LABTECH). All data was normalised to cell number by staining the cells with Hoechst, imaging the plate and counting the number of stained cells with imageJ (version 2.1.0/1.53c).

### 3.2.7 Redox Assay

The PrestoBlue Cell Viability Reagent (Thermo Fisher Scientific, Cat.Nr.: A13262) was used to determine the redox status of the cell by measuring the reduction of resazurin to resorufin by $FMNH_2$, $FADH_2$, NADH, NADPH. The PrestoBlue solution was equilibrated at 37°C in a water bath and an amount of reagent equal to 10% of the media volume was used. 100 µL of the PrestoBlue solution was then added to the corresponding wells in a 96-well plate. The plate was incubated at 37°C for approximately 1 hr, when a colour change had occurred in all wells. The fluorescence signal was then recorded at the spectrophotometer by using filter settings as follows: excitation 560 nm, emission 590 nm.

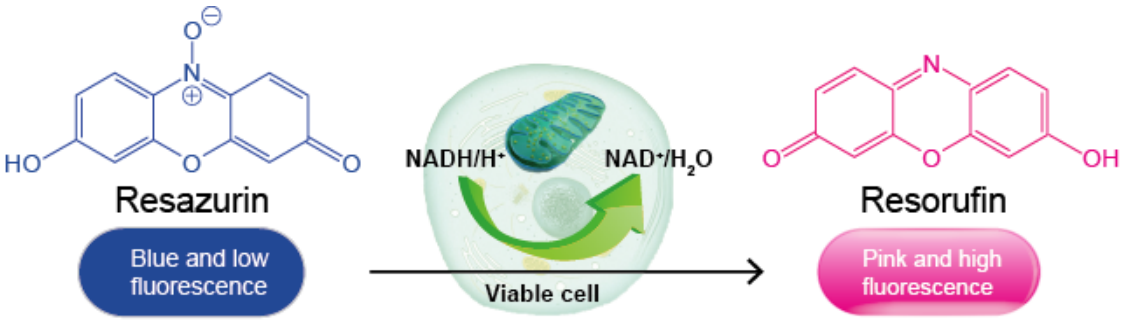


**Figure 3.4:** Reducing agents were measured using PrestoBlue Assay whereby resazurin is converted to resorufin in the presence of NADPH, NADH, FADH2 and FMNH2.

### 3.2.8 Propidium Iodide (PI) Staining for Cell Cycle Analysis

Cells were seeded in a T75 $cm^3$ flask (Greiner-BioOne, Cat. Nr.: 658175 and 658170) for non-IR and IR samples and cultured as per section 2.5.3. At the respective time-points, 1.2 million cells for each sample were collected and pelleted down (1200 RPM, 5 min). The supernatant was then discarded and samples were fixed with 70% ethanol using the drop-by-drop method. Samples were stored at 4°C until the staining (no more than 3 days later).

**PI Staining**: Cells were pelleted down (1300 RPM, 5 min) and the resulting supernatant was discarded. Samples were resuspended in 250 µL of RNase A with a concentration of 100 units/mL and incubated at room temperature for 30 min. Samples were then washed once with 500 µL of PBS, and resuspended in PI solution (SIGMA ALDRICH, Cat.Nr.: P4864) with a concentration of 20 µg/mL. They were stored at 4°C until flow cytometric acquisition at a FACS Canto ™ II flow cytometer (Becton Dickinson). The samples were excited with a 488 nm laser and the fluorescence emission was collected at 585/42 nm. The results were analysed by FlowJo software 8.1.

### 3.2.9 Clonogenic Assays

Cells were irradiated using a 6 MV Siemens linear accelerator with a field size of 20 cm x 20 cm. T75 $cm^2$ flasks were placed horizontally (i.e. cell layer perpendicular to the IR beam) on 5 cm of tissue equivalent phantom slabs with another 3 cm slab placed on top (figure 3.5). The IR doses used were 0, 4, 6, 8 Gy for the normoxic flasks and 0, 4, 7, 11, 16 Gy for the hypoxic flasks, to account for the oxygen enhancement (OER) effect.

**Plating after IR:** Following IR treatment, cells were washed with PBS, detached using TrypLE (2.5 mL for each T75 flask) and counted. After counting, cells were plated in T25 culture flasks with 5mL media using the count corresponding to a particular dose (i.e. 200 – 85,000 cells for low and high doses, respectively). Colonies were left to form over 10 to 14 days in the normoxic incubator (37°C, 5% $CO_2$).

**Fixation & Staining of colonies:** Colony sizes in the lower doses were checked 10 to 14 days after IR, depending on the cell line. Media was removed from the flasks and the cells were washed with 5 mL PBS. Cells were fixed using 5 mL of 100% ethanol for 5 min and stained using crystal violet solution for another 5 min. Flasks were then washed with DI water and allowed to dry before counting. Stained cell clusters of more than 50 cells were considered a colony and included in the data.

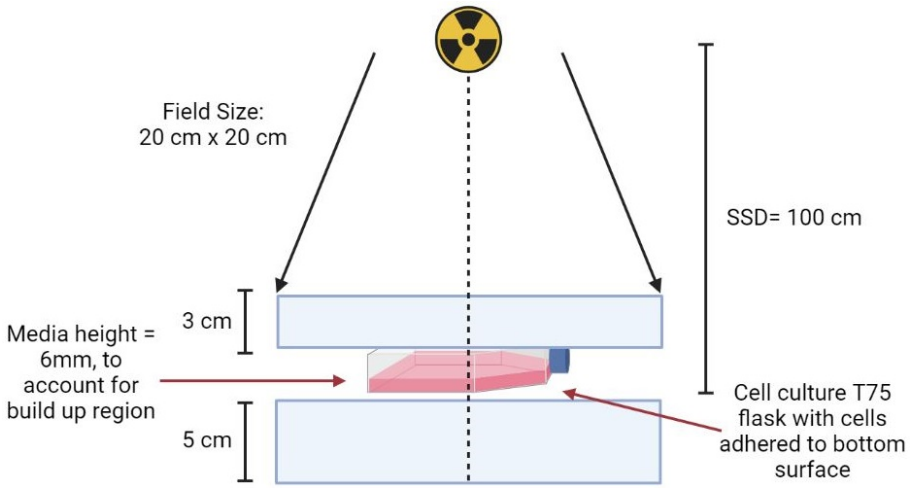


**Figure 3.5:** X-ray exposure setup using the 6 MV Siemens linear accelerator (LINAC), with the cell culture flask lying perpendicular to the beam at a source to skin distance (SSD) of 100 cm and a field size of 20 cm x 20 cm.

### 3.2.10 RNA extraction, cDNA sythesis and RT-qPCR

RNA was isolated from non-irradiated and 4 Gy irradiated normoxic and hypoxic cell lines (H4, H460, T24 and PC-3) 72 hrs after irradiation using High Pure Isolation Kit (Roche, cat.Nr.: 11828665001) as per instruction from the manufacturer. Following extraction, RNA amount, purity and integrity were checked using a Nanodrop ND-1000 (Thermo Fisher Scientific) and by running 2 µL of RNA per sample on a 1% agarose gel. 1 µg of RNA was retrotranscribed in cDNA by using RT2 First Strand Kit (Qiagen, Cat.Nr.:330404). RT-qPCR was then used to analyse the gene expression from the cDNA obtained from the isolated RNA samples.

A reaction mix (15 µL) containing 20 pmol of the forward and reverse primer pairs, Power SYBR Green PCR Master mix (Thermo Fischer Scientific) and nuclease dree water ((Thermo Fischer Scientific, Cat.Nr.: 4368706) was used to amplify 25 ng of cDNA. The RT-qPCR protocol consisted of the following cycles: 1 cycle at 95°C for 10 min, 40 cycles at 95°C for 15 s and finally 60°C for 60 s. The relative gene expression was then normalised to our housekeeping gene HPRT1 (i.e gene which is expressed in all cells and not affected by IR or hypoxia). The 2-ΔΔCt method was used to perform all data analysis.

| **Gene Name** | **Forward Primer** | **Reverse Primer** |
|---|---|---|
| HPRT1 | TTGACACTGGCAAAACAATG | GTCCTTTTCACCAGCAAGC |
| PHD2 | ACCACTGTCCAGGAGTGC | CGAAGAGGGCTGGCAGT |
| HIF-1$\alpha$ | GCTCATCAGTTGCCACTTCC | CCAGAAGTTTCCTCACACGC |
| MTCO-1 | CTACACCCTAGACCAAACCTAC | TGAGCCTACAGATGATAGGATG |
| PGK1 | GTGGTGGAATGGCTTTTAC | CAAAGTCAACAGGCAAGGT |
| G6PD | CTGTCCAACCACATCTCCT | GAAGGTGAGGATAACGCAG |

**Table 3.2:** List of genes used in this study and their corresponding forward and reverse primers for RT-qPCR analysis

### 3.2.11 Image Processing: IMARIS

A z-stack was acquired for all images using Zeiss LSM710 confocal microscope using 63x oil immersion objective. Images were all 12-bit and were post processed using IMARIS software (version 9.3) to reconstruct the cell and nucleus images so that their volumes could be deduced. In brief: All images were imported into IMARIS which consisted of two laser channels (488 nm for Hoechst (i.e. nuclei), and 655 nm for Biotracker Red (i.e. Cell)) and both the cells and nuclei in each image were processed individually. Each cell and nuclei in the image were then defined as a regions of interest (ROI) to be segmented. Smoothing of 0.415 was applied for both laser channels and the threshold was set to absolute intensity. The threshold (absolute intensity) was then manually set to completely cover the ROIs. The image was then fully processed and the surface volume of each cell and nuclei were calculated.

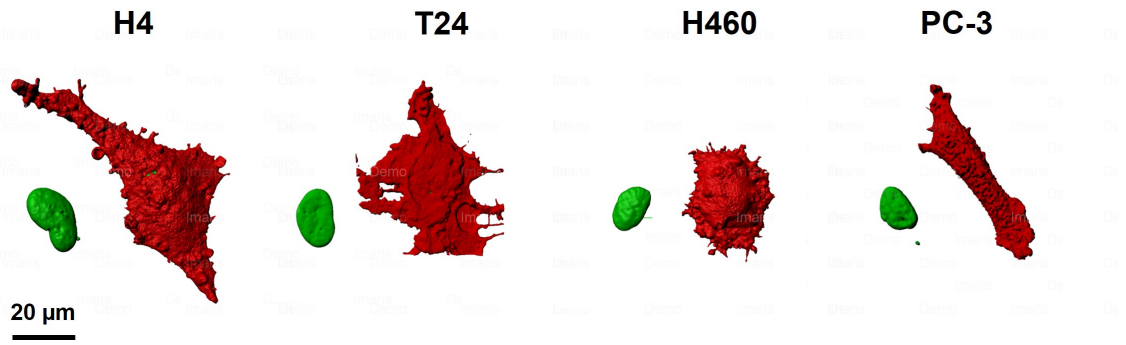


**Figure 3.6:** IMARIS reconstructed images of nucleus (green) and cell (red) volumes for cancer cell lines H4, T24, H460 and PC-3 in hypoxia. Scale bar is represented as 20 µm.

### 3.2.12 Statistical Analysis

Statistical analysis was carried out using Sigmaplot software (Version 14.5). All data was statistically compared to their non-IR control for their respective oxygen conditions unless otherwise stated. Data is presented as mean ± SD or mean ± SEM and will be stated in the figure caption. Statistical significance was assessed on the mean of three individual experiments (i.e. n = 3) using student t-tests and one-way ANOVA with a significance threshold of $p = 0.05$.

## 3.3 Results: Hypoxia Adaption

In the present study, four cancer cell lines from different organs (H4: Brain, H460: Lung, T24: Bladder, PC-3: Prostate) were exposed to different levels of hypoxia, specifically acute (12 hrs at 1% $O_2$) and chronic (72 hrs at 1% $O_2$) to understand how they adapted and dealt with low oxygenated atmospheres. The main hypoxic adaptive processes that will be investigated in the following section include: **(i)** the oxygen removal rate of the cells after an initial hypoxic incubation, **(ii)** changes in the cell and nuclear volume, **(iii)** alterations in the cell cycle progression, as well as changes in **(iv)** the energy metabolism and **(v)** reducing power of the cells. For **(ii), (iii), (iv), (v)**, the acute and chronic conditions were investigated and compared to their normoxic control (21% $O_2$).

### 3.3.1 Measurement of oxygen removal rate (ORR) in-vitro using $O_2$ sensors

Tumours tend to have a much lower oxygen content in comparison to healthy tissue. This oxygen level is organ specific and depends on the cells metabolic demand. The estimated median $O_2$ level obtained from published data (183) for the organs investigated in this study (i.e. Brain, Lung, Bladder (renal), Prostate) are outlined in table 3.1 which can be found in section 3.1. The differences in $O_2$ level observed between tissues make it seem logical to assume that the cancer cell lines derived from these organs would also have a different uptake of oxygen compared to each other. For this reason, the rate of oxygen uptake (i.e. the removal of oxygen from the cell media) was measured using the $O_2$ sensor spots. In this study, the hypoxic chamber (HC) was used for all low oxygen experiments (see section 3.2.1). The HC has a built-in oxygen sensor that constantly measures the oxygen percentage inside the chamber and therefore the oxygen pressure where the cells are cultured is at a set value (i.e for the experiments in this study this would be in the range of 0.1% - 1% $O_2$). As an additional control for these experiments, oxygen sensor spots were used to measure the pericellular dissolved oxygen levels inside the culture flasks over time, where the cells and medium were present. In this way, the oxygen percentage that the cells themselves experienced or were exposed to could be measured. The measurement of the oxygen concentration using the sensor spots is described in section 3.2.2 and the set-up is shown in figure 3.2. In brief, the $O_2$ sensor spots were glued to the inner bottom surface of the culture flask as shown in figure 3.2C and by

using an externally connected optical fibre, an $O_2$ concentration readout was deduced from the returning quenched signal. The four different cancer cell lines were seeded in T25 flasks containing the $O_2$ sensor. Once the cells had attached to the flasks, the flasks were put in the HC of 1% $O_2$ and the oxygen concentration was measured for a period of at least 10 hrs. The starting oxygen percentage was around 21% (i.e. normoxic oxygen level) and decreased in a cell-dependant manner, as measured by the $O_2$ sensor spots and shown in figure 3.7A and B. The oxygen decreased below the set value at (1% $O_2$), indicating that the removal of oxygen by the cells was contributing to the $O_2$ decrease. After 10 hrs of incubation, the measured $O_2$% was 0.24%, 0.21%, 0.28% and 0.23% for H4, H460, T24 and PC-3, respectively (figure 3.7A). The observed decrease in oxygen concentration in these plots (figure 3.7A & B) is therefore a combination of oxygen diffusion out of the media into the HC as well as oxygen removal from the media by the cells that were adhered to the bottom of the flask.

In order to improve the protocol, the media was exchanged with already hypoxic media (i.e 1% $O_2$) for each cell line before the $O_2$% measurements and the flask was sealed with a non-filtered cap. The decrease in the oxygen level measured over a period of 18 hrs and observed in this instance, was solely due to the removal of the cells (i.e. the measured removal of oxygen from the media can be related to the oxygen consumption of the cells). The oxygen decrease rate ($dO_2/dt$)(%/hr) (i.e. the first derivative of the oxygen concentration) for each cell line was then plotted against the cell density as shown in figure 3.7C. The slope indicates the oxygen removal rate per cell (OCR) ($dO_2/dt$) (%/hr/cell) for each cell line. The ORR is more clearly depicted in figure 3.7D and shows the large differences between cell lines. H460 and PC-3 had a large ORR of $2.49 \pm 0.39$ and $1.84 \pm 0.30$, respectively, whereas T24 and H4 had a much slower removal of $0.62 \pm 0.21$ and $1.03 \pm 0.28$, respectively. These results therefore show that in the first 18 hrs of hypoxic exposure (i.e. 1% $O_2$), the four cancer cell lines have different oxygen removal rates, with H460 being the fastest in removing oxygen from the media, and the H4 the slowest. This different behaviour most likely reflected their differing metabolic activity in conditions of decreasing $O_2$% levels.

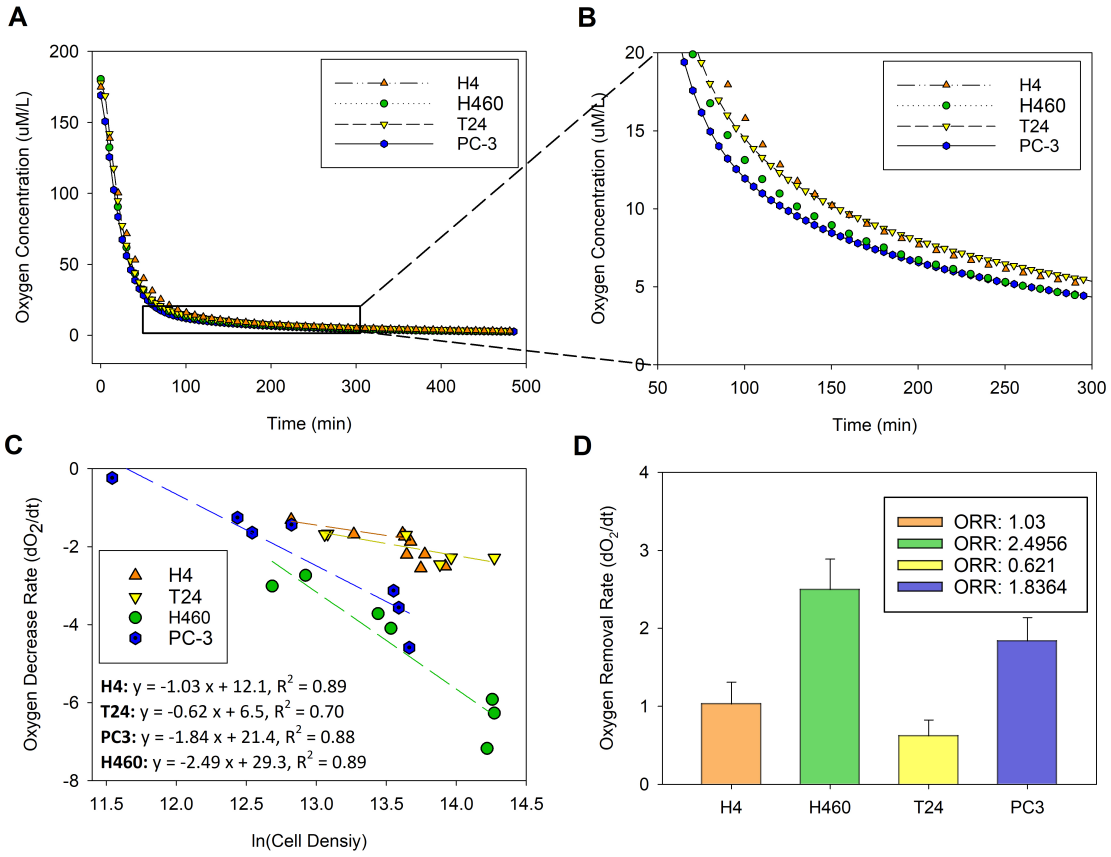


**Figure 3.7:** Oxygen concentration measurements in-vitro using $O_2$ sensor spots and Firesting oxygen meter. **A**) Oxygen concentration (µM/L) measurements of H4, H460, T24 and PC-3 seeded at a density of 600,000 in a T25 over a time-span of 10 hrs. **B**) Oxygen concentration (µM/L) measurements from (**A**) indicating differences between cell lines after 1 hr of incubation until a period of 5 hrs (300 min). **C**) Oxygen decrease rate ($dO_2/dt$) (%/hr) measured over 18 hrs and plotted against cell density for each cell line (H4, H460, T24, PC-3). Prior to measurement, media in the flask (21% $O_2$) was exchanged with hypoxic media (1% $O_2$) and the flasks were sealed with non-filtered caps. **D**) Oxygen removal rate (ORR) per cell (%/hr/cell) determined from the slopes in (**C**) for each cell line.

The next section investigates if differences in cell oxygen removal could depend on volume or other metabolic factors and whether the cell size changes during hypoxic adaption.

### 3.3.2 Morphological changes of cell and nucleus volumes in response to acute and chronic hypoxia

The changes in cell volume were investigated for each cell line after they were exposed to different hypoxic conditions: acute hypoxia (i.e. 1% $O_2$ for 12 hrs) and chronic hypoxia (i.e. 1% $O_2$ for 60 hrs followed by 0.1% $O_2$ for 12 hrs). Each measurement was compared to their normoxic control (i.e. 21% $O_2$). Of note, cells in chronic hypoxia were passaged once and therefore the hypoxic equilibrated media was changed in order to ensure that the cell density

and consequently the exhaustion of nutrients could not affect the results, therefore allowing better comparison with the normoxic samples. In both normoxia and hypoxia, cell cultures were never over-confluent at the end of the time points considered.

The cell membrane and nucleus were stained with fluorescent dyes and then imaged using confocal microscopy as outlined in sections 3.2.4 and 3.2.5, respectively. The images were then reconstructed using IMARIS software as described in section 3.2.11 and the volume measurements were computed and plotted in figure 3.8.

The results showed that, in acute hypoxia, although the volumes among the cell lines were different, the differences between normoxic and hypoxic oxygen conditions for each cell lines were less apparent (figure 3.8A(i) and B(i)). This was the case for both the nucleus and cell volume measurements. In particular, in acute hypoxia, H4 had the largest nucleus with a volume size of (1475 $\pm$ 272) $\mu m^3$ and cell volume size of (5713 $\pm$ 979) $\mu m^3$, compared to the other cell lines which had nuclei volumes of less than 900$\mu m^3$ (figure 3.8A(i)) and cell volumes of (3906 $\pm$ 362) $\mu m^3$ for T24, (2683 $\pm$ 260) $\mu m^3$ for H460 and (2712 $\pm$ 854) $\mu m^3$ for PC-3 (figure 3.8B(i)). Interestingly, in this oxygen condition (1% $O_2$ for 12 hrs) H460 and PC-3 had smaller cell volumes compared to H4 and T24 and since they had the fastest OCR shown in section 3.7, this might be correlated with the reduced volumes. In chronic hypoxia , there were differences observed in the nucleus volume for H460 and PC-3 compared to their normoxic controls, with H460 nuclei decreasing in volume from (717 $\pm$ 124) $\mu m^3$ to (464 $\pm$ 105) $\mu m^3$, and PC-3 nuclei increasing from (521 $\pm$ 63) $\mu m^3$ to (804 $\pm$ 76) $\mu m^3$ (figure 3.8A(ii) ). There were only insignificant changes seen between the cell volumes for all cell lines in normoxia and chronic hypoxia (figure 3.8B(ii)).

The cell size measurements (nucleus and cell membrane) were then normalised to their normoxic control and the change induced by each low oxygen condition was investigated and compared among cell lines. These results are plotted in figure 3.8A(iii) and B(iii) for the nucleus and cell volumes, respectively. The volume of the nucleus was observed to decrease in size with increasing hypoxic stress (i.e. the more severe the hypoxic exposure, the smaller the nucleus) for H4 and H460 cell lines, while it increased for PC-3 (figure 3.8A(iii)). Instead, the cell volume increased with increasing severity of hypoxic exposure for the H460 and PC-3 cell lines (figure 3.8B(iii)). However, for H4 and T24, the cell volume was observed to decrease with longer hypoxic exposure time, although the differences were not significant 3.8B(iii).

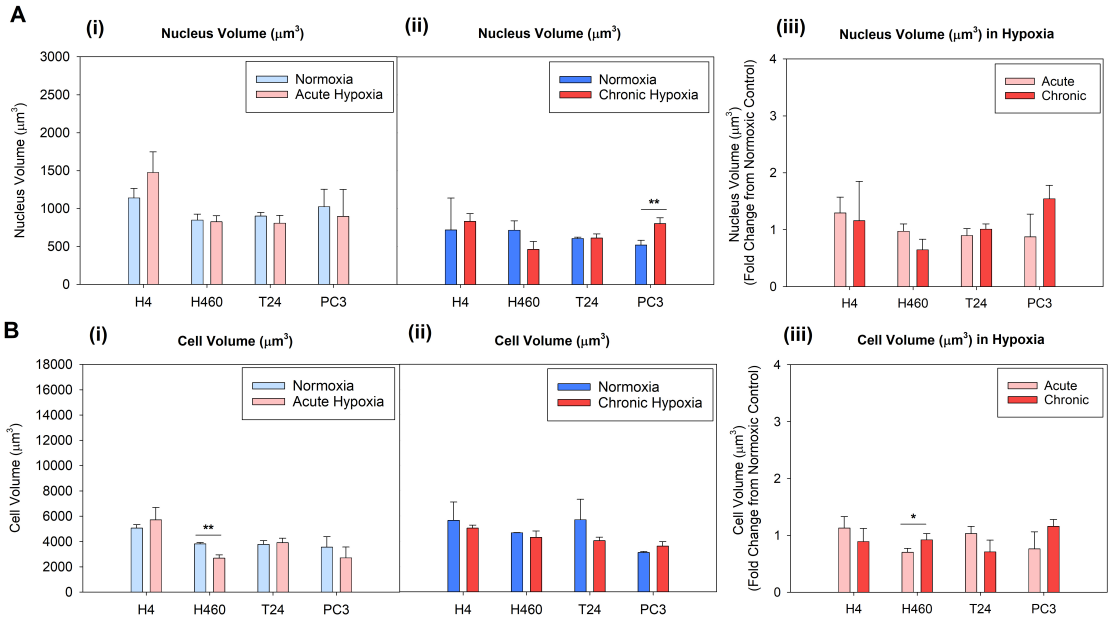


**Figure 3.8:** Nucleus and cell volume measurements of cell lines (H4, H460, T24 and PC-3) following acute (12 hrs at 1% $O_2$) and chronic (60 hrs at 1% $O_2$ + 12 hrs at 0.1% $O_2$) hypoxic incubation compared to samples in normoxia (21% $O_2$). **A)** nuclear volume measurements in: **(i)** acute hypoxia; **(ii)** chronic hypoxia; **(iii)** comparison between acute and chronic hypoxia values, normalised to the normoxic samples. **B)** cell volume measurements in: **(i)** acute hypoxia; **(ii)** chronic hypoxia; **(iii)** comparison between acute and chronic hypoxia values, normalised to the normoxic samples. Each sample was statistically compared to the normoxic control sample (student t-test) and error bars are represented as SD. *P<0.05, **P<0.01, ***P<0.001 (n = 3).

These data reveal that the $O_2$ levels influenced the cell and nucleus volumes mainly when comparing the acute vs the chronic hypoxic condition, suggesting that cells adapted their shape and size accordingly. These physical parameters are in turn strongly influenced by the cellular metabolic adaptations to low oxygen conditions, therefore the volume modifications might assumingly reflect such differences observed in the oxygen removal rate of cells in section 3.3. In fact, after determining the surface area-to-volume ratio of the cells, a somewhat positive correlation could be found with the cell lines, indicating that cells with a high $O_2$ removal rate, tend to also have a larger surface area to volume ratio (figure 3.9A) (i) and (ii)). In addition, the ratio of cell volume to nucleus volume could also play a role in cellular ORR as indicated in the inverse relationship observed in figure 3.9A) (i) and (ii).

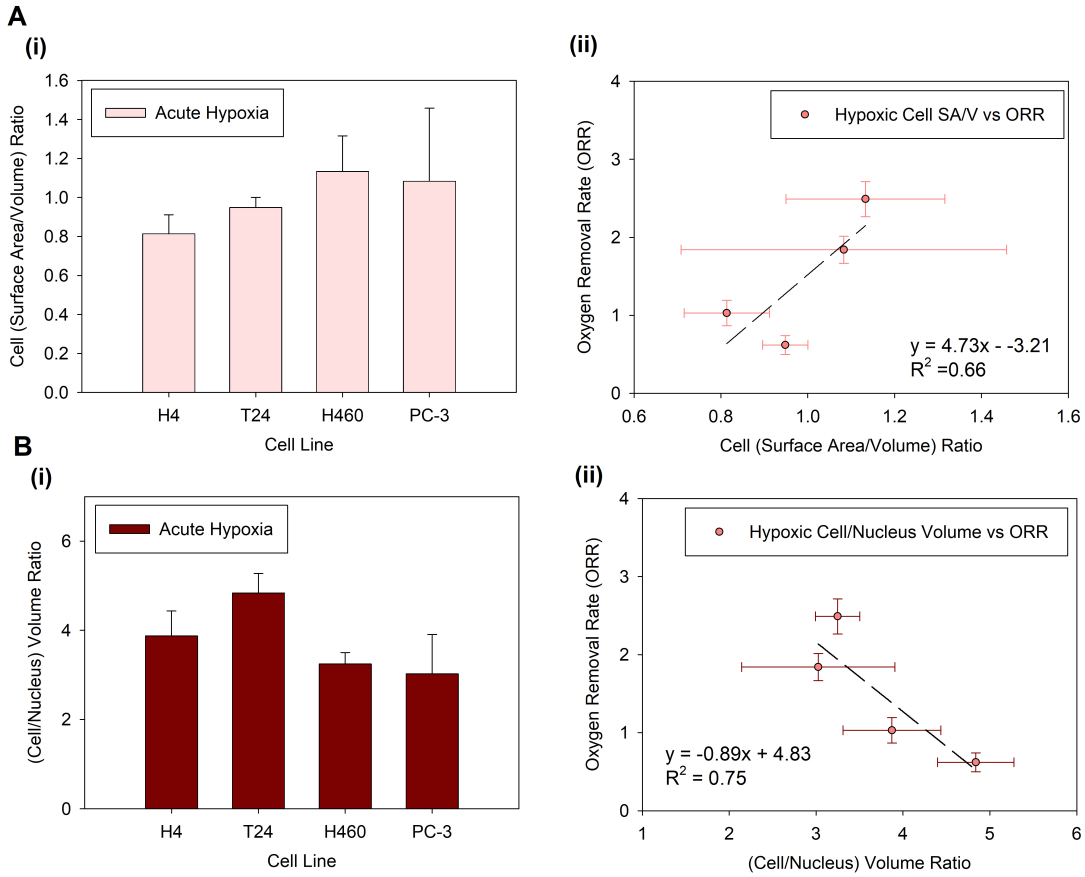


**Figure 3.9:** Nucleus and cell size measurements of cell lines (H4, H460, T24 and PC-3) from acute (12 hrs at 1% $O_2$) hypoxia correlated with the oxygen removal rate (ORR) of cells. **A) (i)** Ratio of cell surface area ($\mu m^2$) (SA) and cell volume (V) ($\mu m^3$) **(ii)** Ratio of cell SA ($\mu m^2$) and cell V ($\mu m^3$) plotted against ORR. **B) (i)** Ratio of cell volume ($\mu m^3$) and nucleus volume ($\mu m^3$) **(ii)** Ratio of cell and nuclear volumes ($\mu m^2$) plotted against ORR. Error bars are represented as standard error of the mean.

### 3.3.3 Cell cycle changes in response to acute and chronic hypoxia

The cell cycle is an important process which ensures error-free replication of cells. In order to avoid errors, the cell has strict control over its progression. However, since cancer cells have a somewhat chaotic metabolic system, often their cell cycle is not without errors and in turn results in a more aggressive behaviour. Apart from the mutations that already exist within many cancers and that can have a direct effect on their cell cycles, the phases of the cell cycle can also be affected by other internal and external stresses. For example, hypoxia or low oxygen availability would be considered an external stress which in turn results in a domino of internal stresses on the cancer cell. Mechanisms exist within cells to deal with these stresses, however, they can depend on the extent and duration of the exposure of the stress, as well as the cell type itself.

To understand whether the cell cycle processes were affected by acute and prolonged hypoxic exposure, the four cancer cell lines were exposed to the same hypoxic conditions, as outlined in the previous sections, and their cell cycle profiles were acquired and compared to the normoxic control. The samples were acquired at a FACs instrument and the corresponding results can be seen in figure 3.10.

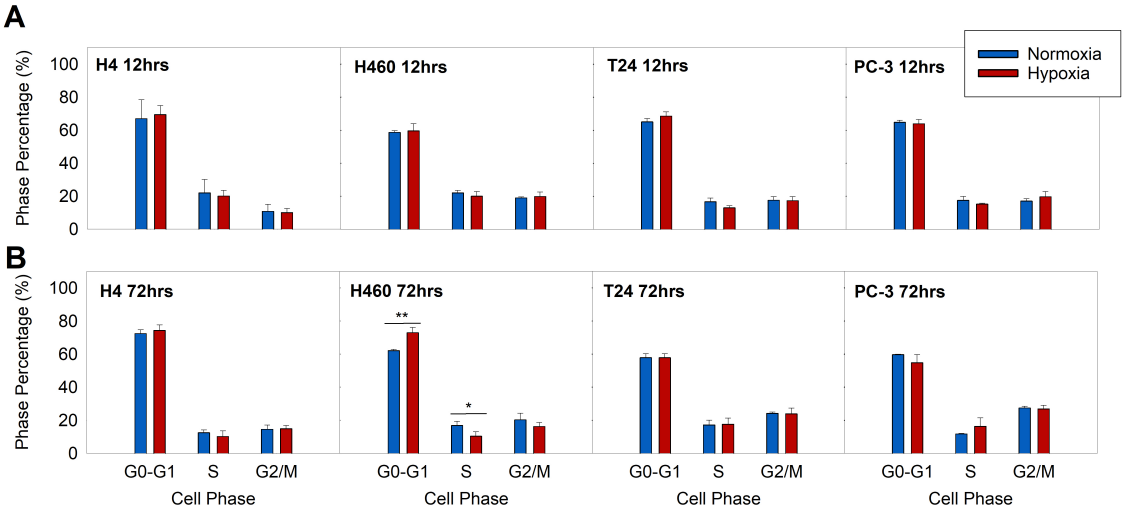


**Figure 3.10:** Cell cycle progression of cell lines (H4, H460, T24 and PC-3) indicating the cell phase (G0-G1, S, G2-M) which the cell resides in following acute and chronic hypoxic incubation compared to samples in normoxia (21% $O_2$). **A)** acute hypoxia and **B)** chronic hypoxia. Samples were stained with propidium iodide (PI) and analysed using flow cytometry. Each sample was statistically compared to the normoxic control sample (student t-test) and error bars are represented as SD. *P<0.05, **P<0.01, ***P<0.001 (n = 3).

As expected, 12 hrs in hypoxia was not a sufficient time to see changes in the cell cycle progression for any of the cell lines (figure 3.10A). However, even in prolonged hypoxia (figure 3.10B), the cell cycle appeared largely unchanged, with the exception of H460, where a significant increase in the G0-G1 and a decrease in the S phases were observed compared to its normoxic control. This indicates that most likely a block at the G0-G1 checkpoint was activated. The results suggest that these cancer cell lines could adapt to the low oxygenated atmosphere at as early as 12 hrs, and that they could maintain the cell cycle progression to a similar extent as in normoxia, even after 72 hrs of chronic hypoxia incubation.

In order to better investigate cell features under reduced oxygen levels, the changes of cellular metabolism, in particular the ATP levels and thereby OXPHOS system, were evaluated and the results reported in the next section.

### 3.3.4 Energy (i.e. ATP) metabolism changes in response to acute and chronic hypoxia

Cancer cells often rely more on aerobic glycolysis than on mitochondrial oxidative phosphorylation (OXPHOS) to produce adenosine triphosphate (ATP) at a high rate also in normoxic conditions, which is otherwise known as "the metabolic shift" as described by the Warburg effect. However, studies have shown that not all tumour cell types depend on glycolysis but they instead can also utilise both OXPHOS and glycolysis to meet the ATP demands. Since OXPHOS relies on the presence of oxygen, and depending on the cancer cell's reliance on OXPHOS, it can be assumed that varying levels of oxygen concentration and the duration of the hypoxic exposure will affect cancer cells metabolism and in turn affect the production of ATP.

For this study, the Cell Titer Glo assay was used. It quantifies intracellular ATP, which reflects the cells ability to produce energy, and also provides an indication of their viability. By normalising the values to the cell numbers for each cell line, this method was used as an indirect measure of the ATP production. The ATP levels were measured under various stages of hypoxia (acute and chronic) and compared to values measured in their normoxic (21% $O_2$) controls. The obtained results can be seen in figure 3.11.

First, the results showed that when comparing the four cell lines in normoxic conditions at the 12 hrs time-point (figure 3.11A), the ATP levels, deduced by normalising the values to the cell numbers, were the highest for H460 and PC-3 ($3.56 \pm 1.04$ and $4.97 \pm 2.61$), compared to the lower ATP produced in H4 and T24 ($1.54 \pm 0.003$ and $1.29 \pm 0.35$, respectively). At a low oxygen concentration (1% $O_2$), these values decreased to $1.22 \pm 0.47$ for H4, $1.69 \pm 0.59$ for H460, $0.72 \pm 0.25$ for T24 and $4.32 \pm 2.03$ for PC-3. Moreover, in acute hypoxia (figure 3.11A), although a decrease was observed in all cell lines compared to their normoxic controls, it was not statistically significant for any of the cell lines. H460 had the largest drop in ATP levels of 52%, followed by T24 with a decrease of 44%, whereas H4 and T24 decreased by only 21% and 13%, respectively. Interestingly, these results loosely correlate with the oxygen removal rate data shown in section 3.7, indicating a faster oxygen removal results in more ATP production. In chronic hypoxia (figure 3.11B), the trend remained the same as previously seen in the acute data, however, the decrease from the normoxic control was slightly larger for H4, H460 and PC-3 with a percent decrease of 26% (not significant (ns)), 62% (significant (*)) and

16%, respectively, whereas the decrease for T24 was slightly less compared to acute hypoxia with a drop of 36% from the normoxic control.

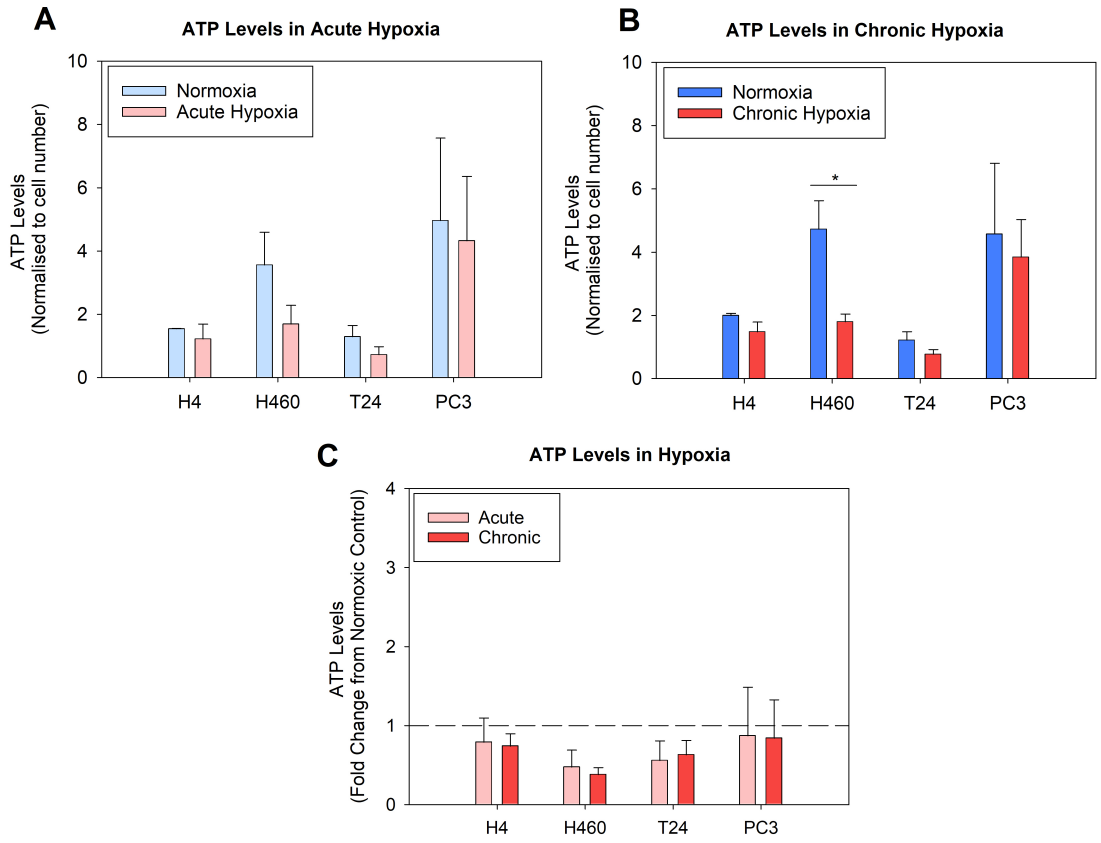


**Figure 3.11:** ATP levels of cancer cell lines (H4, H460, T24, PC-3) under varying levels of hypoxia. Samples were measured using Cell Titer Glo assay kit and luminescence signals were recorded at the plate reader. Data shown were normalised to cell number. **(A)** Acute hypoxia, **(B)** Chronic hypoxia, and **C)** Comparison of ATP levels under different oxygen conditions (acute and chronic hypoxia) following sample normalisation to the normoxic control for each cell line. For the statistical analysis, each cell line was compared to their normoxic control sample (student t-test). Error bars are represented as SD. *P<0.05, **P<0.01, ***P<0.001 (n = 3).

### 3.3.5 Reducing power of cancer cell lines in response to acute and chronic hypoxia

Nicotinamide adenine dinucleotide (NADH) and its phosphorylated form (NADPH), as well as the reduced form of flavin adenine dinucleotide FADH2, are important cofactors involved in many catabolic reactions (NADH and FADH2) to break down lipids and carbohydrates, and anabolic reactions (NADPH) for the biosynthesis of fatty acids and nucleic acids. Moreover, NADH and FADH2 transfer electrons in the ETC and therefore are regulators of metabolic energy processes (glycolysis and OXPHOS). NADH and NADPH are key factors used to maintain the cellular redox balance. NADPH is the most abundant inside the cells and it is also a

central ROS scavenger (187). It can be generated by enzymatic activity in the mitochondria through glycolysis, but the major source is the oxidative pentose phosphate pathway (PPP) which has been shown to play a critical role in cancer cell growth (188). Tumour cells often have a high level of NADPH so they can maintain their rapid proliferation.

In order to indirectly measure the levels of these cofactors in the cancer cells investigated in this study, the presto blue assay was performed (189). The presto blue assay is commonly used to assess the viability of the cells as a measurement of their metabolic activity. It works by measuring the colorimetric/fluorometric change of the resazurin dye which is metabolically reduced by mitochondrial enzyme activity accepting electrons from NADH, NADPH, FADH2, and FMNH2 (the reduced form of flavin mononucleotide) as well as from the cytochromes (189). Therefore, the signal intensity is proportional to the cellular content of such cofactors and can provide an indication of mainly the mitochondrial function and the PPP activity. Similarly to the ATP measurements, the FFNN (FADH2, FMNH2, NADH and NADPH) levels were normalised to the respective cell numbers, thus allowing to indirectly get an indication of the FFNN production and the energy and reducing power of the different cell lines, which, although having different proliferation profiles, could then be compared. The FFNN levels were measured under acute and chronic hypoxic stress conditions and compared to their normoxic (21% $O_2$) control samples. The results obtained are plotted in figure 3.12.

In normoxia, H460 showed a higher baseline level of FFNN compared to the other cell lines (figure 3.12A and B). Figure 3.12A shows the normalised values to cell number for normoxic cell lines, which were as follows: 0.58 $\pm$ 0.15 for H4, 1.42 $\pm$ 0.32 for H460, 0.64 $\pm$ 0.05 for T24 and 0.48 $\pm$ 0.14 for PC-3. In acute hypoxia (figure 3.12A), the FFNN levels increased in all cell lines, which was significant for H4, T24 and PC-3, with fold changes of 2.58, 2.07 and 2.72, respectively, compared to their normoxic control samples. For H460, acute hypoxia only increased the levels by 44% which was by far the lowest increase among the cell lines. The FFNN levels in acute hypoxic following normalisation to cell number were 1.51 $\pm$ 0.07 for H4, 2.06 $\pm$ 0.34 for H460, 1.32 $\pm$ 0.33 for T24 and 1.31 $\pm$ 0.14 for PC-3. Interestingly, the FFNN levels for the majority of cell lines investigated had an even larger fold change increase following exposure to chronic hypoxia compared to their normoxic controls (figure 3.12B and C). This was the case for H4, T24 and PC-3 which had a significant increase with a fold change of 3.15, 3.4 and 3.7, respectively, whereas, for H460, the increase from its normoxic control remained

at 1.4 as in acute hypoxia. The FFNN levels in chronic hypoxic following normalisation to cell number were 2.30 ± 0.66 for H4, 3.49 ± 0.20 for H460, 2.05 ± 0.38 for T24 and 1.54 ± 0.30 for PC-3. In the normoxic control samples, however, these same cell lines expressed normalised FFNN levels of 0.73 ± 0.08 for H4, 2.49 ± 0.33 for H460, 0.60 ± 0.11 for T24 and 0.41 ± 0.08 for PC-3.

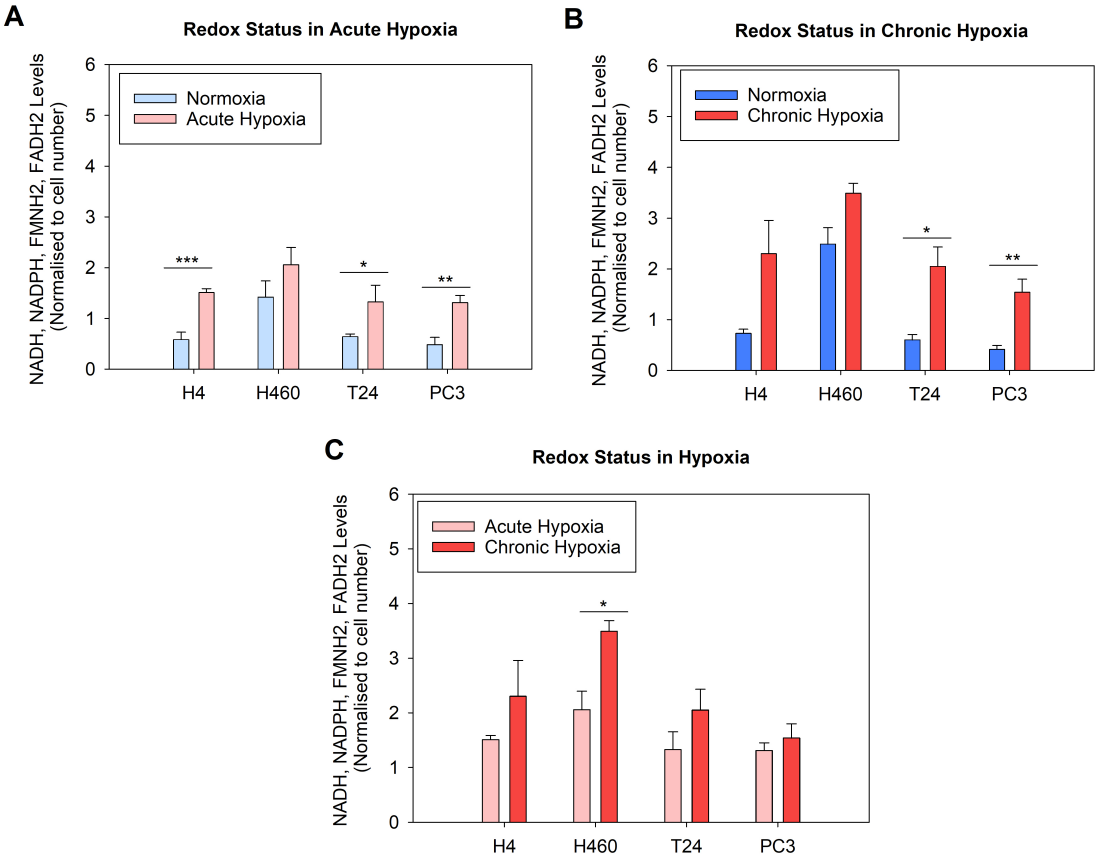


**Figure 3.12:** Reducing power of cancer cell lines (H4, H460, T24, PC-3) indicated by levels of FMNH2, FADHs, NADH, NADPH (FFNN) under varying hypoxic oxygen conditions (**A)** Acute: 12 hrs at 1% $O_2$, **B)** Chronic: 60 hrs at 1% $O_2$ followed by 12 hrs at 0.1% $O_2$, and **C)** Comparison of FFNN levels under different oxygen conditions (acute and chronic) following sample normalisation to each normoxic cell lines control. Samples were measured using prestoBlue viability assay which measures the reduction of resazurin to resorufin and the corresponding fluorescent signal was measured at the plate reader. Data shown were normalised to cell number and each cell line was then statistically compared to their normoxic control sample (student t-test). Error bars are represented as SD. *P<0.05, **P<0.01, ***P<0.001 (n = 3).

Overall, these results show that with prolonged hypoxic stress or hypoxic exposure, the content of reducing molecules was highly affected, and caused an accumulation of FFNN levels which potentially highlights an alternative metabolic strategy in hypoxia compared with normoxia.

Based on the results shown in the previous sections, it is evident that the cancer cell lines in this study adapted to hypoxia by altering their energy metabolism (i.e. reduce ATP levels) and reprogramming their reducing power capabilities (i.e. increase in FFNN levels). This effect was observed to be cell type dependant.

## 3.4 Results: Radiation Effect

Rapidly growing cancer cells and the dysfunctional vasculature network generate chronic hypoxic regions with different $O_2$ gradients, from mild to severe hypoxia, inside the tumour mass. Intratumoural hypoxia is a well-known phenomenon occurring in various solid cancer types and often associated with resistance to radiation treatments and poor prognosis, due to the selection of hypoxia radioresistant cells. Prolonged $O_2$ deprivation can result in specific responses and can distinctively affect the redox balance and the energetic metabolism. Consequently, the responses of hypoxic adapted cells to radiation therapy, which represents a condition present in a solid tumour at the time of radiation treatments, can be distinct and strongly influence the therapy outcomes. Based on that and on the previous results, in the next sections, only chronically adapted hypoxic cells were studied. Therefore, colony formation assays were conducted in different cancer cell lines following exposure to chronic hypoxic conditions before and during X-ray exposure. The changes in energy metabolism and reducing power of the chronically hypoxic cells, which remained hypoxic after irradiation, was also investigated and outlined in the following sections.

### 3.4.1 Clonogenic survival ability of different cancer cell lines in normoxia and hypoxia

The differing radio-responses of H4 (brain), H460 (lung), T24 (bladder) and PC-3 (prostate) cancer cell lines under normal oxygen and low oxygen levels were investigated. First, cell survival after irradiation was determined by clonogenic assays. Cells were incubated in normoxia (21% $O_2$) and in different hypoxic conditions, 0.6% $O_2$ and 0.1% $O_2$, prior to irradiation to observe the effect of low oxygenation on their radio-responses. Despite the fact that cell seeding numbers were the same in all oxygen conditions, higher doses were employed in hypoxia (4, 8, 11 and 16 Gy) compared to normoxia (2, 4, 6 and 8 Gy), to account for the higher cell survival in hypoxia. The corresponding clonogenic assay results can be seen in figure 3.13

and 3.14. Survival curves were fitted with the linear quadratic model, from which the alpha and beta values were deduced and recorded in tables 3.4, 3.5, 3.6, for the 21% $O_2$, 0.6% $O_2$ and 0.1% $O_2$ clonogenics, respectively.

The different survival ability between cell lines and how this is altered in varying degrees depending on the amount of oxygen present is highlighted in figure 3.13A, B and C. In the normoxic cells (figure 3.13A), H460 were found to be the most sensitive cell line to irradiation for all doses and T24 cells were observed to be the most resistant cell line, with H4 and PC-3 cells having similar radio-responses. However, when the oxygen level was reduced to 0.6% (figure 3.13B), differences between the survival of the four cell lines were observed when comparing them to their normoxic data. In fact, H4 cells showed the highest resistance and PC-3 the lowest, particularly at higher doses of 16 Gy (figure 3.13B). Under severe hypoxia (0.1% $O_2$) (figure 3.13C), T24 and H4 cells had the highest survival capacity compared with H460 and PC-3 cells, and were therefore, from a radiobiological point of view, considered more radio-resistant than the other two cell lines.

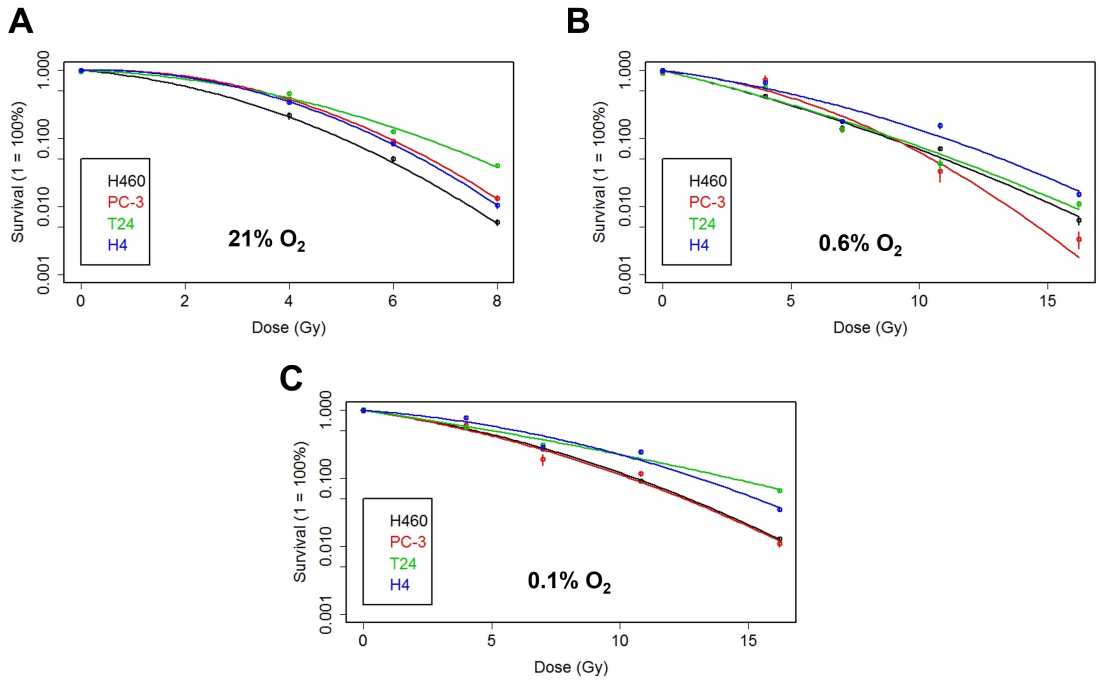


**Figure 3.13:** Clonogenic assays conducted at different oxygen conditions **(A)** 21% $O_2$, **B)** 0.6% $O_2$, and **C)** 0.1% $O_2$ for cancer cell lines H460 (black), PC-3 (red), T24 (green) and H4 (blue). Cell lines were incubated in normoxia (21% $O_2$) or hypoxia (0.1%, 0.6% $O_2$) prior to irradiation with doses of 2, 4, 6, 8 Gy and 4, 8, 11, 16 Gy in normoxia and hypoxia, respectively. Survival curves were fitted with a linear quadratic equation and corresponding alpha, beta values were recorded in table 3.4, 3.5, 3.6. The means ± SD of the experiments are reported.

These results therefore highlight that cancer cells which are derived from different organs in the body not only have differing responses to radiation, but also that their radio-resistance appears to be oxygen-dependant with a group (including H4 and T24) that in both hypoxic conditions could be classified as more resistant mainly at high doses and another group (including H460 and PC-3) being more radio-sensitive compared to the other two cell lines by a small amount.

In order to assess the extent with which a depletion of oxygen contributed to a higher resistance, each cell line was singularly plotted with their normoxic (21% $O_2$) and hypoxic (0.1% and 0.6% $O_2$) clonogenic data, and the corresponding results can be seen in figure 3.14. The graphs show that there was a clear increase in radio-resistance with decreasing oxygen percentage for all cancer cell lines (i.e. more cells survived at high doses of radiation if the oxygen levels are low). The lack of oxygen provides protection for cells from radiation, which is known as the oxygen enhancement ratio (OER). The OER is a parameter known in the radio-biological field which connects radio-resistance with a lower oxygen percentage, at least in the case of low-LET radiation (i.e photons). For the cancer cell lines investigated in this study, the OER (determined by the ratio of hypoxic dose to normoxic dose at the point of 10% cell survival) was highest for H4 with a value of 2.27, followed by T24 and H460 which had OERs of 2.17 and 2.11, respectively. PC-3 cells had an OER of 1.99 and therefore were the lowest among all four cell lines. The OERs were determined at 10% and 50% cell survival for both hypoxic clonogenics (0.1% and 0.6% $O_2$) with the normoxic clonogenic assays (21% $O_2$) (table3.3).

| **OER from 21% $O_2$** | | **H4** | **H460** | **T24** | **PC-3** |
|---|---|---|---|---|---|
| **10% SF** | **0.1%** | 2.27 | 2.11 | 2.17 | 1.996 |
| | **0.6%** | 1.91 | 1.76 | 1.38 | 1.72 |
| **50% SF** | **0.1%** | 1.83 | 1.84 | 1.50 | 1.54 |
| | **0.6%** | 1.37 | 1.29 | 0.93 | 1.52 |

**Table 3.3:** OER cancer cell lines (H460, PC-3, T24, H4) determined from clonogenic results conducted at normoxic oxygen levels (21% $O_2$)

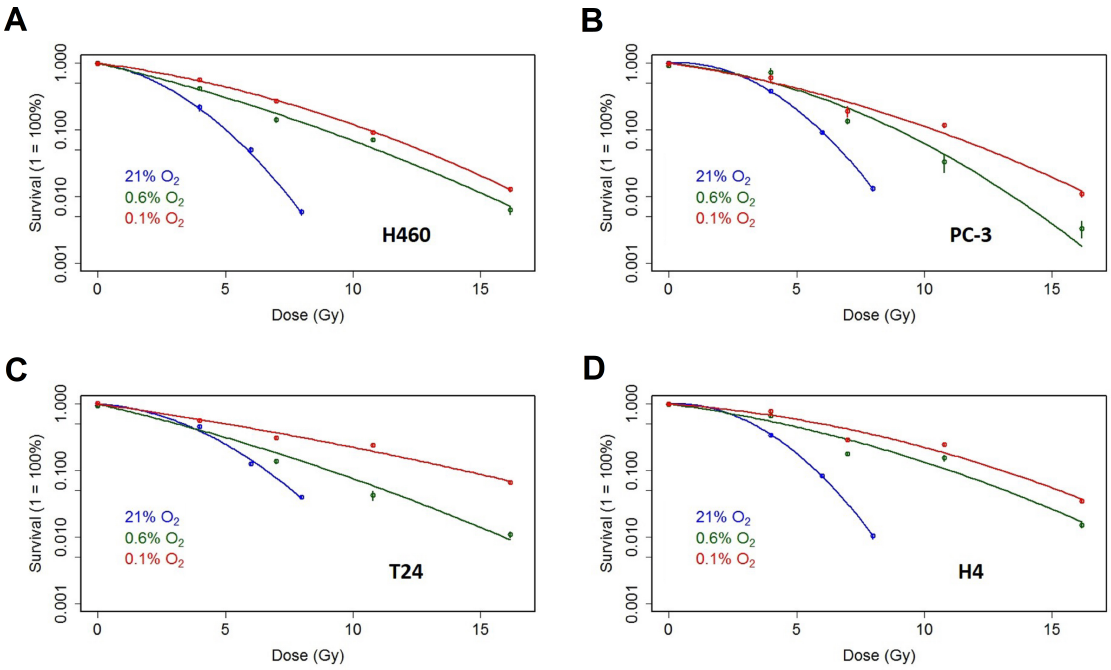


**Figure 3.14:** Clonogenic assays conducted for different caner cell lines (**A)** H460 (lung), **B)** PC-3 (prostate), **C)** T24 (bladder) and **D)** H4 (brain) under normoxia (21% $O_2$ in blue) and hypoxia (0.6% $O_2$ in green; 0.1% $O_2$ in red), highlighting the oxygen-dependant enhancement of resistance to RT treatment (OER = Oxygen Enhancement Ratio). Cell lines were irradiated with doses of 2, 4, 6 and 8 Gy in normoxia and 4, 8, 11 and 16 Gy in hypoxia. Survival curves were fitted with a linear quadratic equation and corresponding alpha, beta values were recorded in tables 3.4, 3.5, 3.6.

The $\alpha$ and $\beta$ values closely correspond to the shape of the survival curves and with that also signify the radio resistance and repair capacity of the irradiated cells. A small $\alpha/\beta$ ratio is associated with late responding tissue having a large repair capacity, which follows from the visible shoulder shape of the related survival curve. Cells with larger $\alpha/\beta$ values on the other hand have a relatively linear profile and are associated with fast responding tissues. These experience a more constant rate of cell killing for increasing dose in comparison to tissues with a low ratio and stronger shoulder.

Low levels of oxygen induced a more radio-resistant phenotype in the cancer cell lines analysed and in fact had higher $\alpha/\beta$ ratios as indicated in table 3.6 and 3.5 compared with the data obtained from the clonogenics conducted in normoxia (table 3.4). The negative $\alpha$ value, and thereby negative $\alpha/\beta$ ratio determined for H4 in normoxia (table 3.4), is not realistic from a radio-biological point of view and is possibly due to statistical variation (190).

| **21% $O_2$** | **H460** | **PC-3** | **T24** | **H4** |
|---|---|---|---|---|
| **alpha ($\alpha$)** | 0.139 $\pm$ 0.016 | 0.053 $\pm$ 0.022 | 0.058 $\pm$ 0.0496 | -0.039 $\pm$ 0.024 |
| **beta ($\beta$)** | 0.064 $\pm$ 0.0023 | 0.075 $\pm$ 0.0029 | 0.044 $\pm$ 0.0059 | 0.076 $\pm$ 0.0032 |
| **ratio ($\alpha/\beta$)** | 2.192 | 0.717 | 1.325 | -0.521 |

**Table 3.4:** $\alpha$ and $\beta$ values for cancer cell lines (H460, PC-3, T24, H4) determined from clonogenic results conducted at normoxic oxygen levels (21% $O_2$)

| **0.6% $O_2$** | **H460** | **PC-3** | **T24** | **H4** |
|---|---|---|---|---|
| **alpha ($\alpha$)** | 0.206 $\pm$ 0.024 | 0.092 $\pm$ 0.063 | 0.205 $\pm$ 0.034 | 0.116 $\pm$ 0.041 |
| **beta ($\beta$)** | 0.0062 $\pm$ 0.0017 | 0.0185 $\pm$ 0.0056 | 0.0053 $\pm$ 0.0024 | 0.0084 $\pm$ 0.0027 |
| **ratio ($\alpha/\beta$)** | 33.27 | 5.01 | 38.95 | 13.87 |

**Table 3.5:** $\alpha$ and $\beta$ values for cancer cell lines (H460, PC-3, T24, H4) determined from clonogenic results conducted at hypoxic oxygen levels (0.6% $O_2$)

| **0.1% $O_2$** | **H460** | **PC-3** | **T24** | **H4** |
|---|---|---|---|---|
| **alpha ($\alpha$)** | 0.116 $\pm$ 0.012 | 0.128 $\pm$ 0.035 | 0.124 $\pm$ 0.018 | 0.063 $\pm$ 0.033 |
| **beta ($\beta$)** | 0.0095 $\pm$ 0.00084 | 0.0089 $\pm$ 0.0024 | 0.0025 $\pm$ 0.0010 | 0.0087 $\pm$ 0.0020 |
| **ratio ($\alpha/\beta$)** | 12.21 | 14.35 | 49.43 | 7.27 |

**Table 3.6:** $\alpha$ and $\beta$ values for cancer cell lines (H460, PC-3, T24, H4) determined from clonogenic results conducted at hypoxic oxygen levels (0.1% $O_2$)

### 3.4.2 Morphological changes of cell and nucleus volumes of irradiated cancer cells in normoxia and severe chronic hypoxia

Following the clonogenic assays, the radiation dose of 4 Gy was chosen for the next analyses in normoxia (21% $O_2$) and in severe chronic hypoxia (0.1% $O_2$). In particular, cell responses were evaluated on both non-irradiated and irradiated cell lines after 72 hrs from ionising radiation treatment with the hypoxic cells maintained in severe hypoxia after the irradiation. This time-point was set in order to select only for the most radioresistant sub-populations and to investigate their adaptive responses, as they represent one of the reasons, if not the principal, of radiotherapy failure and potentially recurrence. Also, media were changed each day, so that all possible dead cells were removed and only the highly radio-resistant cells were included in the measurements. Initially, at 72 hrs post-IR, the effect of radiation on the size of the cell nucleus and membrane volumes was investigated. The chronically hypoxic cells and their normoxic counterparts were stained as per section 3.2.4 and imaged using confocal microscopy (section 3.2.5). The corresponding images were then reconstructed and volume measurements were deduced. The results obtained are plotted in figure 3.15.

In normoxia, irradiation induced an increase in cell volume for H4 and H460 cell lines, increasing from (9027 $\pm$ 619) $\mu m^3$ and (5491 $\pm$ 542) $\mu m^3$ in the non-IR samples (0 Gy), to (13664 $\pm$ 1690) $\mu m^3$ and (21749 $\pm$ 704) $\mu m^3$ in the IR samples, respectively (figure 3.15A(i)). On the contrary, there was no change observed in the cell volume of the irradiated PC-3 cell line (**0 Gy:** (4826 $\pm$ 747) $\mu m^3$, **4 Gy:** (4458 $\pm$ 1233) $\mu m^3$) and T24 cell line (**0 Gy:** (5709 $\pm$ 1618) $\mu m^3$, **4 Gy:** (6200 $\pm$ 2015) $\mu m^3$). In hypoxia, an increase in cell volumes compared to non-IR cells was observed in all cell lines with a significant increase for H460 (**0 Gy:** (6829 $\pm$ 487) $\mu m^3$, **4 Gy:** (10839 $\pm$ 939) $\mu m^3$), T24 (**0 Gy:** (6055 $\pm$ 1563) $\mu m^3$, **4 Gy:** (18677 $\pm$ 2436) $\mu m^3$) and PC-3 (**0 Gy:** (4376 $\pm$ 873) $\mu m^3$, **4 Gy:** (8846 $\pm$ 1281) $\mu m^3$) (figure 3.15A(ii)). H4 also increased with IR although it was not significant (**0 Gy:** (10674 $\pm$ 2039) $\mu m^3$, **4 Gy:** (15341 $\pm$ 2336) $\mu m^3$).

The nucleus volume measurements (figure 3.15B) showed that in normoxia, there were no significant changes induced by IR compared to the non-IR controls for any of the cell lines. In the normoxic samples, H4 (**0 Gy:** 751 $\pm$ 266 $\mu m^3$, **4 Gy:** 1035 $\pm$ 479 $\mu m^3$) and H460 (**0 Gy:** 860 $\pm$ 152 $\mu m^3$, **4 Gy:** 1089 $\pm$ 149 $\mu m^3$) nucleus volumes increased in size due to IR by 284 $\mu m^3$ and 228 $\mu m^3$, whereas the PC-3 (**0 Gy:** (758 $\pm$ 123) $\mu m^3$, **4 Gy:** (571 $\pm$ 92) $\mu m^3$) nuclei decreased in size by 187 $\mu m^3$. However, for T24 nuclei there was no difference in size observed

post-IR (**0 Gy:** (608 ± 17) μm$^3$, **4 Gy:** (590 ± 58) μm$^3$). In hypoxia, on the other hand, T24 had a significantly large increase of nuclei volume post-IR (**0 Gy:** (722 ± 153) μm$^3$, **4 Gy:** (1801 ± 66) μm$^3$), and H460 also had a slight increase, although not significant (**0 Gy:** (474 ± 11) μm$^3$, **4 Gy:** (811 ± 262) μm$^3$) (figure 3.15B(ii)). In contrast, however, there were no changes observed in the nucleus volumes of H4 (**0 Gy:** 722 ± 152 μm$^3$, **4 Gy:** (812 ± 140) μm$^3$) and PC-3 (**0 Gy:** (441 ± 40) μm$^3$, **4 Gy:** (450 ± 61) μm$^3$) post-IR compared to their non-IR hypoxic controls (figure 3.15B(ii)).

These data show that in general the effect of irradiation on the size of the more resistant cells was more evident for the total cellular volume than for the nuclear volume both in normoxia and in hypoxia. Although the results were not always significant or consistent and differences were present among cell lines, for example, the H460 total volume was more influenced in normoxia, whereas for T24 and PC-3 the cellular volume was not affected in normoxic conditions, but increased in hypoxia.

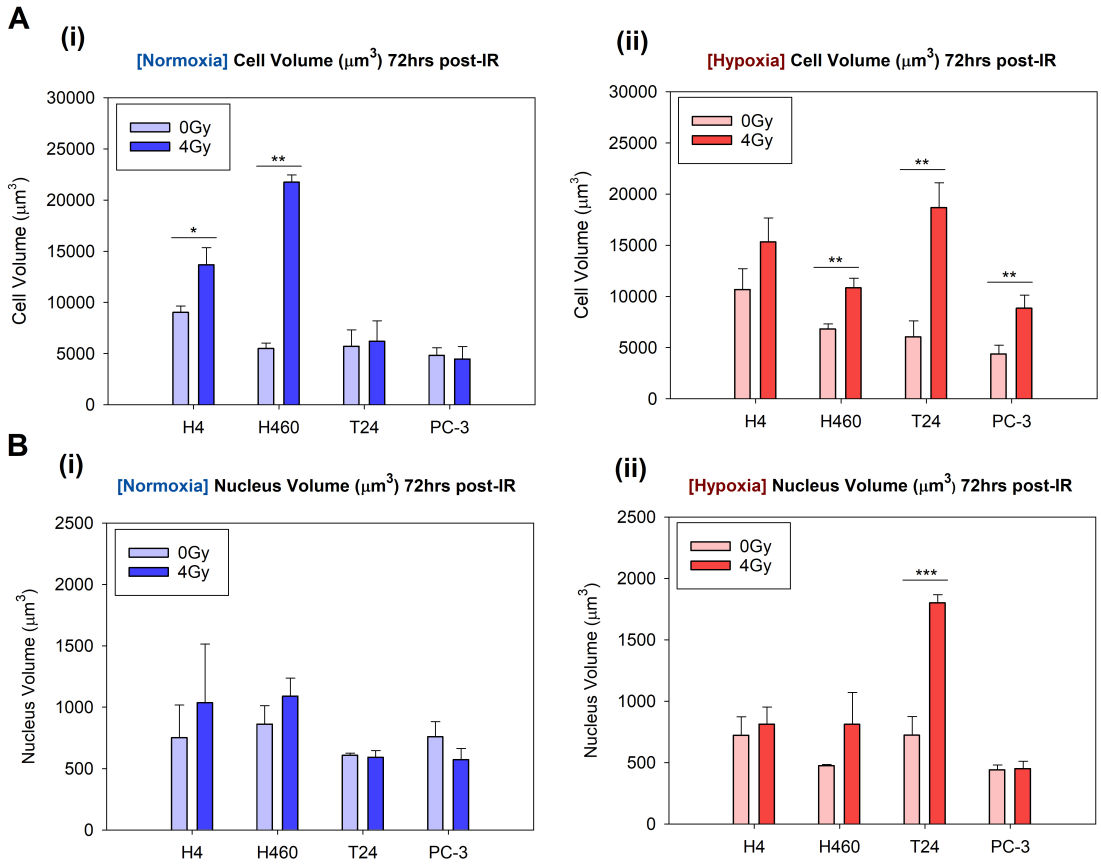


**Figure 3.15:** Volume measurements of the **A)** cell and **B)** nucleus for cell lines (H4, H460, T24 and PC-3) at 72 hrs after irradiation with 4 Gy photons in **(i)** normoxia (21% $O_2$) and **(ii)** hypoxia (0.1% $O_2$). Each sample was statistically compared to the normoxic control sample (student t-test) and error bars are represented as SD. *P<0.05, **P<0.01, ***P<0.001 (n = 3).

### 3.4.3 Cell cycle progression of irradiated cancer cells in normoxia and severe chronic hypoxia

After IR-induced damages, cells usually tend to accumulate at a cell cycle checkpoint within one or more of the cell cycle phases to be repaired or programmed to die. The G2-M damage checkpoint is particularly important because it is the penultimate checkpoint before cell mitosis. For this reason, a block in the G2-M often occurs if cells are under intense stress or the amount of damage is particularly high. The effect IR has on the cell cycle progression of the four cell lines (H4, H460, T24, PC-3) was investigated both after normoxic (21% $O_2$) and severely chronic hypoxic (0.1% $O_2$) incubation at 72 hrs from irradiation. The corresponding results can be seen in figure 3.16A for the normoxic samples and 3.16B for the hypoxic samples.

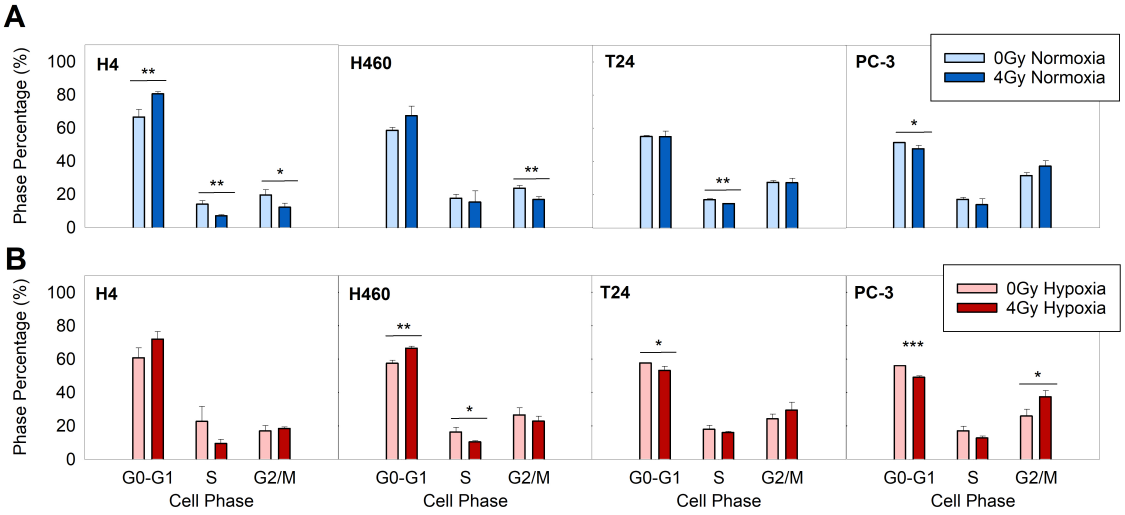


**Figure 3.16:** Cell cycle progression of cell lines (H4, H460, T24 and PC-3) indicating the cell checkpoints (G0-G1, S, G2-M) which the cell resides in following irradiation with a dose of 4 Gy. Cell lines were cultured for 72 hrs after IR in **A)** normoxia (21% $O_2$) or in **B)** severe chronic hypoxia ((21% $O_2$)). Samples were stained with propidium iodide (PI) and analysed using flow cytometry. Each sample was statistically compared to the non-irradiated control sample (student t-test) and error bars are represented as SD. *P<0.05, **P<0.01, ***P<0.001 (n = 3).

In normoxia (figure 3.16A, first panel), the H4 cell line had a significant accumulation of cells in the G0-G1 checkpoint with an increase of 14% from the non-IR control and resulting decrease of approximately 7% for the other two phases (S, G2-M). On the contrary, H4 cells that were maintained under hypoxic conditions after IR appeared to have a higher accumulation in the G2-M phase with an increase of approximately 1.5%, as compared to their lines from their non-lR control hypoxic sample (figure 3.16B, first panel). A similar trend as H4 had was observed for the H460 cell line in normoxia (figure 3.16A, second panel), with an accumulation of cells

in the G0-G1 phase and a decrease of 6.8% of cells in the G2-M. When H460 were cultured in chronic severe hypoxia, cells were significantly arrested in G0-G1 (+9% increase), while G2-M phase had a decrease of cells compared to the non-IR control. For the normoxic T24 cell line, a slight but significant decrease in the S-phase was observed, whereas no change was observed in the other phases (figure 3.16A, third panel). In prolonged hypoxia and after 72 hrs from irradiation, there was only a slight increase of T24 cells in the G2-M phase (+5.2%) accompanied by a decrease of cells in the G0-G1 (-4.5%) (figure 3.16B, third panel). PC-3 cells in normoxia did not show significant changes in the cell cycle distribution after 72 hrs from IR (figure 3.16A, fourth panel). Nevertheless, they were the only cell lines which had an increase (+11.6%) of cells accumulated in the G2-M and a significant decrease of approximately 7% in the G0-G1 phase (figure 3.16B, fourth panel).

These results therefore highlight the differing dominance of cell cycle checkpoints present after damage induction for different cell lines, which is also affected by the oxygen condition. In summary, the results show that after 72 hrs from radiation the normoxic cell cycle distribution of the surviving cells from almost all cell lines was similar to the control cells, except for H4 which were the only cell line still maintaining a significant, yet marginal, arrest in the G0-G1 phase. In hypoxia, however, the distribution was different, in fact in low oxygen the surviving H4 behave similarly to the control, although the slight increase in the G0-G1 was still present but not significant. Instead, the hypoxic H460 were arrested in the G0-G1 phase and the PC-3 in the G2-M. Therefore, the severe hypoxic conditions influenced the cells ability to sense the damages and consequently activate the blocks of these cells which resulted in a long arrest in the mentioned phases. On the contrary, T24 cell cycle was not affected at 72 hrs post-IR in both normoxia and hypoxia demonstrating their ability to resolve all the potential damages and to reenter in their cycle after 72 hrs from the insult, independently on the oxygen levels tested in this study.

### 3.4.4 Energy (ATP) metabolism of irradiated cancer cells in normoxia and severe chronic hypoxia

The effect that photon radiotherapy treatment had on the ATP content in different cancer cells, both oxygen-enriched (21% $O_2$) and oxygen-deprived (0.1% $O_2$), surviving IR was also investigated in this study and the corresponding results can be seen in figure 3.17. The ATP

levels of the cells were measured 72 hrs after irradiation. The signals were measured at the plate reader and then normalised to cell number to account for the different proliferation rates of the cells following IR in normoxia and hypoxia.

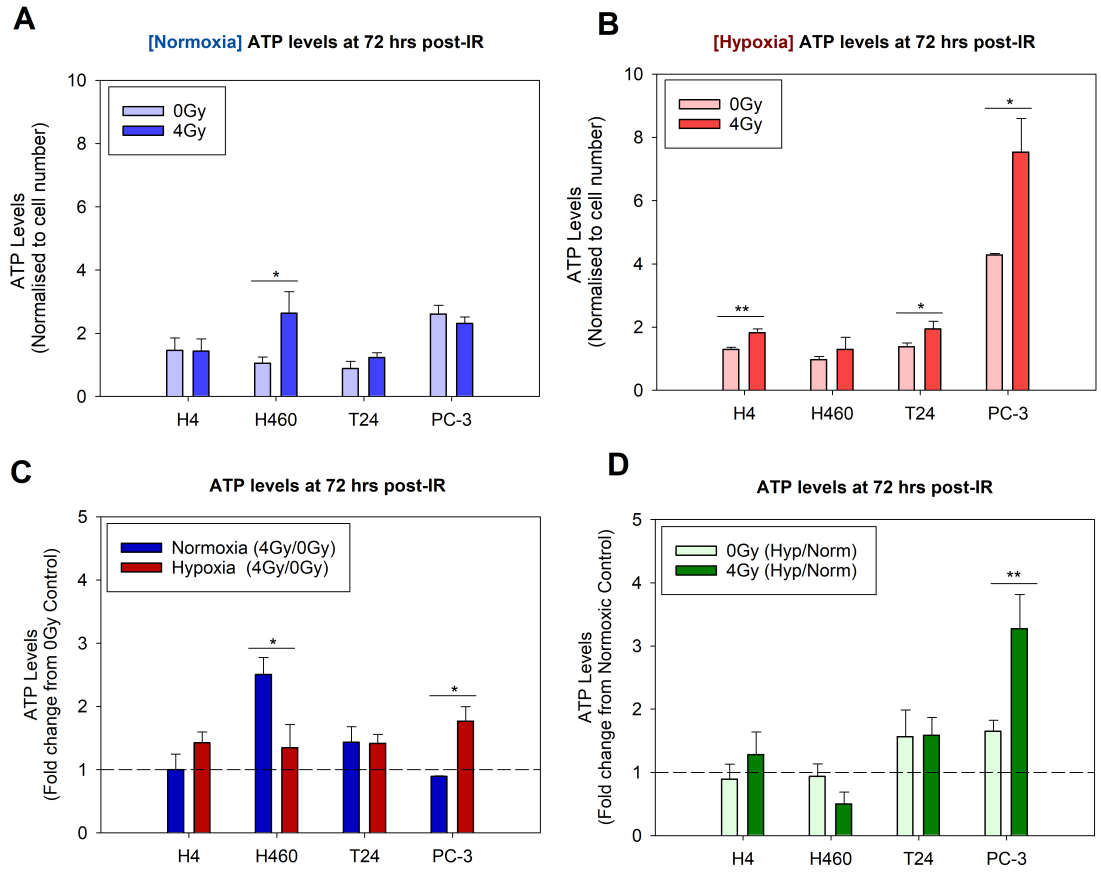


**Figure 3.17:** Luminescence ATP detection of cancer cell lines (H4, H460, T24, PC-3) at 72 hrs following irradiation with photons (4 Gy) assessed by using Cell Titer Glo assay kit and recorded at the plate reader. **A)** ATP levels in normoxia (21% $O_2$); **B)** ATP levels in severe hypoxia (0.1% $O_2$); **C)** ATP data normalised to the respective (normoxic or hypoxic) 0 Gy control to compare fold increase between oxygen conditions. **D)** ATP data normalised to normoxic control to compare fold increase between irradiation conditions. Data shown were normalised to cell number and each cell line was then statistically compared to their non-IR (A, B, D) or normoxic control sample (C) (Student t-test). Error bars are represented as SD. *P<0.05, **P<0.01, ***P<0.001 (n = 3).

In the normoxic cells (figure 3.17A), a significant increase of 152% in the ATP levels was observed in the H460 cell line following a dose of 4 Gy IR with a normalised value of 2.63 $\pm$ 0.69 compared to the normoxic control value of 1.02 $\pm$ 0.20. In contrast to the normoxic data, H460 had the lowest ATP levels after IR compared to the other cell lines, and also the smallest increase of 34% (ns) from the 0 Gy hypoxic control (1.29 $\pm$ 0.4 for 4 Gy sample, and 0.97 $\pm$ 0.1 for the 0 Gy sample) (figure 3.17B). For T24 cells, a smaller increase of 39% (ns) was observed after irradiation with normalised values of 1.23 $\pm$ 0.16 and 0.88 $\pm$ 0.23 for the

irradiated and control samples, respectively. On the contrary, there was no change in the ATP content for normoxic H4 after IR and in PC-3 the levels decreased by 11% after IR compared to the normoxic control, although the difference was not statistically significant.

In hypoxia on the other hand (figure 3.17B), PC-3 had the highest ATP levels compared to the other cell lines and in addition also had the largest increase of 76% following IR with a normalised value of 7.53 $\pm$ 1.06 in comparison to the non-IR hypoxic control, whose value was 4.28 $\pm$ 0.05. An increase of 41% was also observed for both H4 (1.82 $\pm$ 0.13) and T24 (1.94 $\pm$ 0.25) cell lines compared to their non-IR hypoxic control (1.29 $\pm$ 0.07 and 1.38 $\pm$ 0.13, respectively). The fold-change of ATP levels in normoxia and hypoxia were compared by normalising each cell line to their non-irradiated control sample as shown in figure 3.17C. In this plot the fold change for H460 was much smaller in hypoxia (1.34 $\pm$ 0.37) compared with the normoxic sample (2.52 $\pm$ 0.28). In contrast, the PC-3 fold change was significantly larger in hypoxia (1.76 $\pm$ 0.24) compared to normoxia (0.88$\pm$ 0.06). Instead, the difference for the other two cell lines (T24, H4) between oxygen condition was found to be statistically insignificant. The hypoxic and normoxic samples were then compared by normalising the hypoxic data to the normoxic data for both non-irradiated and irradiated samples to highlight the oxygen dependency, as shown in figure 3.17D. The plot shows that the fold change was larger for the irradiated samples of H4 (1.27 $\pm$ 0.36) and PC-3 (3.27 $\pm$ 0.19) compared to the non-IR controls (0.88 $\pm$ 0.24 and 1.66 $\pm$ 0.18, respectively). The ATP fold change did not vary between hypoxic 0 Gy and 4 Gy T24, while for H460 it decreased in comparison to the non-IR control (0.93 $\pm$ 0.21) and it was the smallest fold change among cell lines with a value of 0.49 $\pm$ 0.19.

These data suggest that irradiation affected the cellular metabolic response, in terms of energy production, with a dependency on the oxygen condition. Moreover, although there was a cell-type dependency, in general an increase of the ATP content was observed in all cell lines, albeit by differing extents. Although the method used did not enable to discriminate between the main pathways producing ATP (glycolysis or OXPHOS) or how much each pathway was contributing in energy production, it gives an indication that the resistant cells surviving radiation in a severe hypoxic environment were still metabolically active and stimulated by irradiation to produce ATP.

### 3.4.5 Reducing power of irradiated cancer cell lines in normoxia and severe chronic hypoxia

The effect of 4 Gy photon irradiation on the cellular reducing power (FADH2, FMNH2, NADH, NADPH = FFNN) was also investigated for all four cell lines (H4, H460, T24, PC-3) under both normoxia and hypoxia (severe chronic) conditions. The corresponding results which were obtained 72 hrs after IR can be seen in figure 3.18.

In normoxia, irradiation induced a statistically significant increase in the FFNN levels of H4 and H460 with levels of 0.55 $\pm$ 0.08 and 0.88 $\pm$ 0.19 in the irradiated normoxic samples, respectively, compared with 0.30 $\pm$ 0.05 and 0.42 $\pm$ 0.07 in the non-IR normoxic control samples (figure 3.18)A. However, there were no differences observed between the FFNN levels in the irradiated and non-irradiated normoxic samples of T24 (**0 Gy**: 0.32 $\pm$ 0.02, **4 Gy:** 0.31 $\pm$ 0.04) and PC-3 (**0 Gy**: 0.29 $\pm$ 0.04, **4 Gy:** 0.28 $\pm$ 0.05). In hypoxia, however, an increase in the FFNN levels was observed for H4 (**0 Gy**: 1.97 $\pm$ 0.48, **4 Gy:** 2.34 $\pm$ 0.48), H460 (**0 Gy**: 3.10 $\pm$ 0.17, **4 Gy:** 4.48 $\pm$ 1.10) and T24 (**0 Gy**: 2.12 $\pm$ 0.18, **4 Gy:** 2.63 $\pm$ 0.48), although none were found to be statistically significant (figure 3.18B). PC-3 (**0 Gy**: 1.32 $\pm$ 0.31, **4 Gy:** 0.96 $\pm$ 0.01), on the other hand, decreased with IR compared to its non-IR hypoxic control.

Furthermore, the fold-change in FFNN levels in normoxia and hypoxia were compared by normalising each cell line to their non-IR control sample as shown in figure 3.18C. From this plot, it is clear that IR induced a larger increase of FFNN levels in normoxia than it did in hypoxia for H4 and H460 cell lines, with a statistically significant difference between the fold changes. H4 FFNN levels increased by a factor of 1.88 $\pm$ 0.17 as a result of IR in normoxia compared with 1.19 $\pm$ 0.27 in hypoxia. For H460, IR induced a factor increase of 2.11 $\pm$ 0.24 in the normoxic samples, but only a factor of 1.44 $\pm$ 0.25 in hypoxia. The differences in the FFNN fold change levels observed for T24 and PC-3 were statistically insignificant. The irradiated and non-irradiated samples were then compared by normalising the hypoxic data to the normoxic data as shown in figure 3.18D, thus enabling to better highlight the differences in the FFNN content due to the oxygen deprivation. In this plot, it is quite apparent that for all cell lines there was an increase in FFNN levels in hypoxia compared with the normoxia, as indicated by the large fold changes observed in figure 3.18D. However, when irradiated, these fold changes were significantly reduced for the most resistant and surviving H4, H460 and PC-3. For these cell lines the non-IR samples had a fold change of 6.69 $\pm$ 0.29, 7.43 $\pm$

0.17 and 4.53 $\pm$ 0.27, respectively, compared with 4.23 $\pm$ 0.25, 5.09 $\pm$ 0.33 and 3.41 $\pm$ 0.17, respectively, in the IR samples. Interestingly, T24 was the only cell line where irradiation significantly increased the fold change between oxygen conditions, compared with the non-IR sample with fold changes of 6.74 $\pm$ 0.10 and 5.09 $\pm$ 0.33, respectively.

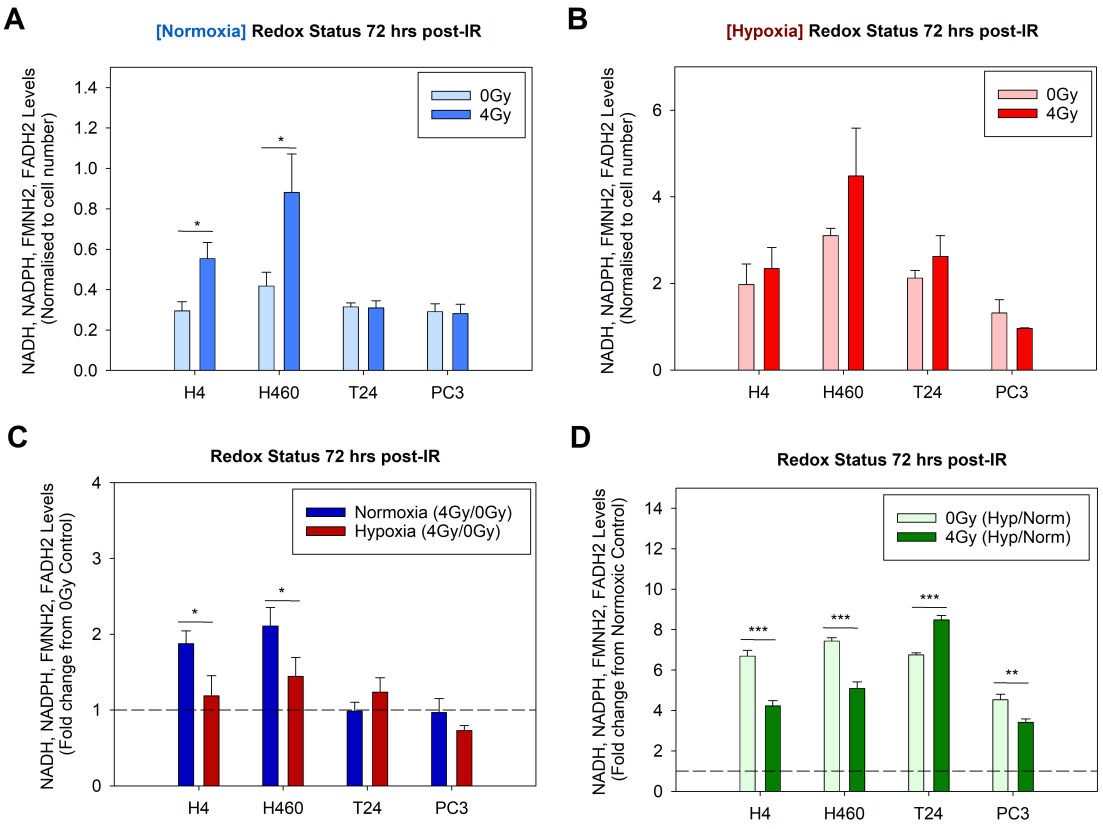


**Figure 3.18:** Reducing power of cancer cell lines (H4, H460, T24, PC-3) indicated by levels of FMNH2, FADH2, NADH, NADPH (that is, FFNN) in normoxia (21% $O_2$) and severe hypoxia (0.1% $O_2$) at 72 hrs following irradiation with photons (4 Gy). **A)** FFNN levels in normoxia **B)** FFNN levels in severe hypoxia **C)** FFNN data normalised to 0 Gy control to compare fold increase between oxygen conditions. **D)** FFNN data normalised to normoxic control to compare fold increase between irradiation conditions. Samples were incubated with prestoBlue viability reagent and the fluorescent signal was measured at the plate reader. Data shown were normalised to cell number and each cell line was then statistically compared to their non-IR (A, B, D) or normoxic control sample (C) (Student t-test). Error bars are represented as SD. *P<0.05, **P<0.01, ***P<0.001 (n = 3).

These results therefore indicate that IR has an effect on the redox metabolism, specifically the FFNN levels, and that the oxygen levels strongly influenced the FFNN pool inside the cells. In fact, increasing signals from the presto blue assay are indicative of a high content of the FFNN molecules that represent the reducing power of the cells. Hypoxia increased the FFNN levels in cells cultured in chronic severe hypoxia, which might be a result of either a stimulation of the metabolic pathways associated with their production or a reduction of their consumption which would result in an accumulation of the reduced molecules. Once irradiated, the effect

of IR on the FFNN levels was cell-type dependant, but in hypoxia a general decrease in the most radioresistant cells, compared with the hypoxic non-IR samples, was reported with the exception represented by T24, where IR induced an increase of the FFNN content.

### 3.4.6 RT-qPCR analysis of genetic expression of irradiated cancer cells in normoxia and severe chronic hypoxia

The results from the previous sections indicate that both oxygen and radiation played a role in altering the metabolism of the cancer cell lines investigated in this study (H4, H460, T24, PC-3), although to differing degrees. Decreased levels of oxygen are said to be "sensed" by the hypoxia inducible factor (HIF), which in previous research has been shown to have a high association with altered metabolic pathways and energy supply (173). For this reason, the expression at mRNA level of the most studied HIF gene, HIF-1$\alpha$, and its regulator PHD2, were investigated using RT-qPCR analysis. Other key genes investigated were genes which are involved in metabolic and energy producing processes, such as glycolysis and OXPHOS. In particular, the phosphoglycerate kinase 1 (PGK1), for the glycolysis, and the mitochondrial encoded cytochrome c oxidase 1 (MTCO-1) for the OXPHOS, were analysed. The gene PGK1 is the enzyme which produces ATP through catalysing the chemical reaction of 1,3-diphosphoglycerate to 3-phosphoglycerate in the glycolytic pathway (191). MTCO-1, otherwise known as cytochrome c oxidase 1 (COX1), is the main subunit of the mitochondrial respiratory complex IV. This is the final enzyme in the electron transport chain transferring electrons from cytochrome c to $O_2$, thus producing $H_2O$ which drives OXPHOS for ATP production (192). Moreover, the expression of the gene encoding for the rate limiting enzyme involved in the PPP (e.g. Glucose-6-phosphate dehydrogenase (G6PD)) was also investigated. G6PD is necessary for the first step in the PPP to generate ribose and NADPH and is therefore essential in maintaining redox homeostasis (193).

The gene expression alterations of cancer cell lines (H4, H460, T24, PC-3) incubated in normoxia or severely chronic hypoxia after 72 hrs from 4 Gy X-ray treatment were analysed using RT-qPCR as outlined in section 4.2.9. The mRNA results obtained for H4, H460, T24 and PC-3 under both oxygen conditions can be seen in figure 3.19, 3.20, 3.21 and 3.22, respectively. Each figure also includes a heatmap (figure 3.19B, 3.20B, 3.21B and 3.22B) and a schematic outlining the up- and down-regulation of the investigated genes involved in glycolysis and PPP (figure 3.19D, 3.20D, 3.21D and 3.22D) as well OXPHOS (figure 3.19E, 3.20E, 3.21E and 3.22E).

**H4**

The H4 results in figure 3.19 show a statistically significant upregulation of PHD2 in hypoxia compared with the normoxic samples with a 2.5-fold increase ($\pm$ 0.1) (0 Gy Hypoxia vs 0 Gy normoxia) (figure 3.19A(i)). Interestingly, the HIF-1$\alpha$ levels decreased under severe chronic hypoxic exposure by 0.73-fold ($\pm$ 0.03) (figure 3.19A(ii)), potentially indicating that, even though an opposite trend was expected at low $O_2$ levels, the enhanced PHD levels continued to degrade the HIF-1$\alpha$. Irradiation induced an upregulation in normoxia for both PHD2 and HIF-1$\alpha$ mRNA levels, with a 1.25-fold increase ($\pm$ 0.07) and 1.45-fold change ($\pm$ 0.03), respectively. In hypoxia, there were no differences observed post-IR in the mRNA levels of PHD2 (2.43-fold change ($\pm$ 0.07)) compared to the hypoxic non-IR sample (2.49-fold change ($\pm$ 0.1)), thus suggesting that the modulation of this gene expression was more driven by the oxygen content than by the IR. However, IR exhibited an effect on the normoxic samples, where, as reported above, the levels were increased for both PHD2 and HIF-1$\alpha$. Again, IR did not change the expression of HIF-1$\alpha$ in the irradiated hypoxic sample (0.90-fold ($\pm$ 0.09)) compared with the non-IR hypoxic sample (0.73-fold ($\pm$ 0.03)).

Glycolysis appeared to be significantly enhanced for adapted hypoxic H4 cells (0 Gy hypoxia) as indicated by the statistically significant upregulation of the PGK1 gene by 2.23-fold increase ($\pm$ 0.009) (figure 3.19C(i)). Interestingly, after 72 hrs from irradiation, the normoxic H4 showed increased levels of PGK1 (1.17-fold increase ($\pm$ 0.009))(figure 3.19C(i)). When cultured in hypoxia and irradiated with 4 Gy X-rays, the surviving cells after 72 hrs maintained high levels of PGK1 expression (2.22-fold increase ($\pm$ 0.03)), similar to the non-irradiated hypoxic sample (0 Gy hypoxia) (figure 3.19C(i)). Therefore, in a situation of oxygen deprivation, glycolysis in H4 was most likely stimulated and the irradiation treatment did not significantly modify this condition in hypoxia, as instead was observed in normoxia. Concurrently in the same cell line, MTCO-1 expression was downregulated in hypoxic cells compared to the normoxic control, as indicated by a 0.67-fold decrease ($\pm$ 0.02) (figure 3.19C(ii)). After 72 hrs from IR, the MTCO-1 expression in normoxic surviving cells was not affected, whereas, similarly to the hypoxic non-irradiated cells, it was still downregulated in the hypoxic radioresistant samples (0.63-fold ($\pm$ 0.03)) compared to the normoxic control sample (4 Gy hypoxia vs 0 Gy normoxia) (figure 3.19C(ii)). As a consequence, this suggests that the OXPHOS process could be affected in hypoxia. As far as the expression of G6PD is concerned, it was slightly but

significantly downregulated in hypoxia compared to the normoxic control sample (0.70-fold (± 0.06)) (figure 3.19C(iii)). However, on the contrary, the gene expression of G6PD was strongly stimulated in radioresistant normoxic H4 cells (1.78-fold increase (± 0.07)), but it remained downregulated in hypoxic cells after 72 hrs from radiation with no differences to the non-irradiated hypoxic cells (0.51-fold (± 0.16)) (figure 3.19C(iii)). This indicates that the expression of the main enzyme involved in PPP was influenced by radiation only in normoxia, while in hypoxia its level of gene expression was more controlled by the reduced oxygen content and tended to slightly decrease.

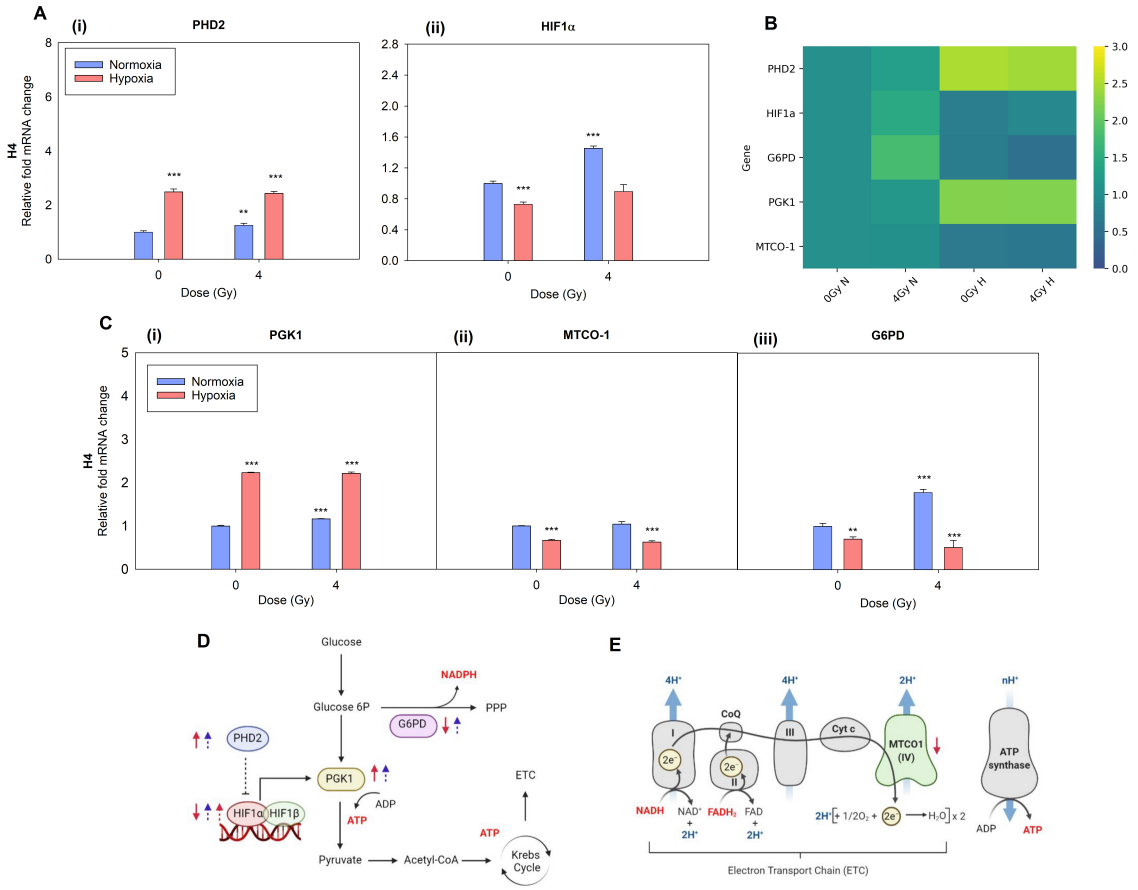


**Figure 3.19:** mRNA expression levels of genes evaluated using RT-qPCR in **H4** cancer cell line at 72 hrs following 4 Gy X-rays in normoxia (21% $O_2$) and hypoxia (0.1% $O_2$). **A)** Gene expression of **(i)** PHD2, **(ii)** HIF-1$\alpha$. **B)** Heatmap summary indicating upregulation and downregulation of investigated genes (PHD2, HIF1$\alpha$, MTCO-1, PGK1 and G6PD). **C)** Gene expression analysis of **(i)** PGK1, **(ii)** MTCO-1 and **(iii)** G6PD **D)** Schematic summary of the intracellular metabolic processes involving HIF-1$\alpha$, PHD2, PGK1 and G6PD following IR treatment. **E)** Electron transport chain (ETC) indicating the response of MTCO-1, which is a subunit of complex IV of the ETC, to radiation and oxygen level. In the schematic **D** & **E)**, a dose response is indicated by a dotted arrow and an oxygen response by a solid arrow (normoxia = blue, hypoxia = red). Up-arrow = upregulation, down-arrow = downregulation. The data was normalised to the non-IR normoxic control sample and the means and error bars (SD values) are presented. Each sample was statistically compared to the non-IR normoxic control sample (one-way ANOVA test). *P<0.05, **P<0.01, ***P<0.001 (n = 3).

**H460**

In the H460 cell line, RT-qPCR results (figure 3.20) show that the mRNA levels of PHD2 were largely upregulated by a fold change of 4.5 ($\pm$ 0.15) compared to the normoxic non-IR control samples (figure 3.20A(i)), which was similar to the results seen for the H4 cell line, although with a smaller increase. Following treatment with IR, there were no changes observed in the PHD2 mRNA levels compared to the non-IR samples for either oxygen condition (figure 3.20A(i)). In contrast to the previous results seen for H4, however, the HIF-1$\alpha$ mRNA levels actually increased by 1.78-fold ($\pm$ 0.01) in response to severe chronic hypoxia compared to the normoxic control (figure 3.20A(ii)). After 72 hrs from radiation exposure, HIF-1$\alpha$ on the other hand, increased in normoxia by 1.12-fold ($\pm$ 0.076) compared to the normoxic non-IR control sample (figure 3.20A(ii)). Nevertheless, in hypoxia its mRNA levels decreased compared to the non-IR hypoxic samples (1.2-fold ($\pm$ 0.05) and 1.77-fold ($\pm$ 0.01) from normoxic 0 Gy, respectively) but remained higher than the normoxic control (0 Gy) (figure 3.20A(ii)). The PGK1 mRNA levels, which provide a potential indication for the glycolytic pathway, were significantly upregulated by 2.61-fold increase ($\pm$ 0.017) following exposure to prolonged hypoxia (figure 3.20C(i)). However, irradiation moderately decreased this fold change to 2.25 ($\pm$ 0.01) compared to the non-IR normoxic control sample (figure 3.20C(ii)). This decrease of the PGK1 mRNA levels due to IR was also observed in normoxic surviving cells with a fold-decrease of 0.79 ($\pm$ 0.01) in comparison to the non-IR normoxic control sample (figure 3.20C(ii)). Also for the H460 hypoxic cells, the MTCO-1 levels decreased by 0.70-fold ($\pm$ 0.016) (figure 3.20C(ii)). However, irradiation induced an upregulation in both oxygen conditions compared to their respective non-IR controls with a fold change of 1.61 ($\pm$ 0.016) for the normoxic samples and 0.92 ($\pm$ 0.012) in the hypoxic samples (figure 3.20C(iii)). Therefore, the gene encoded for one of the complex IV sub-units, which uses $O_2$ and favours the OXPHOS, was downregulated in hypoxia, most likely due to the reduced level of oxygen, and marginally upregulated by the IR in the radioresistant cells at a level similar to the normoxic non-irradiated cells. Conversely, the mRNA levels of G6PD did not undergo significant changes following hypoxic exposure (0.88-fold $\pm$ 0.08) nor following treatment with IR in normoxia (1.14 $\pm$ 0.06). Conversely, a significant downregulation was observed in the hypoxic radio-resistant cells with a fold decrease of 0.49 ($\pm$ 0.07) in comparison to the normoxic non-IR control sample (figure 3.20C(iii)). This indicates that, for the H460 cancer cell line, the PPP was was probably less affected by hypoxia

than in H4 and the X-ray exposure only induced a reduction of the key gene expression in hypoxia, thus most likely decreasing the flux of metabolites and NADPH production through this pathway.

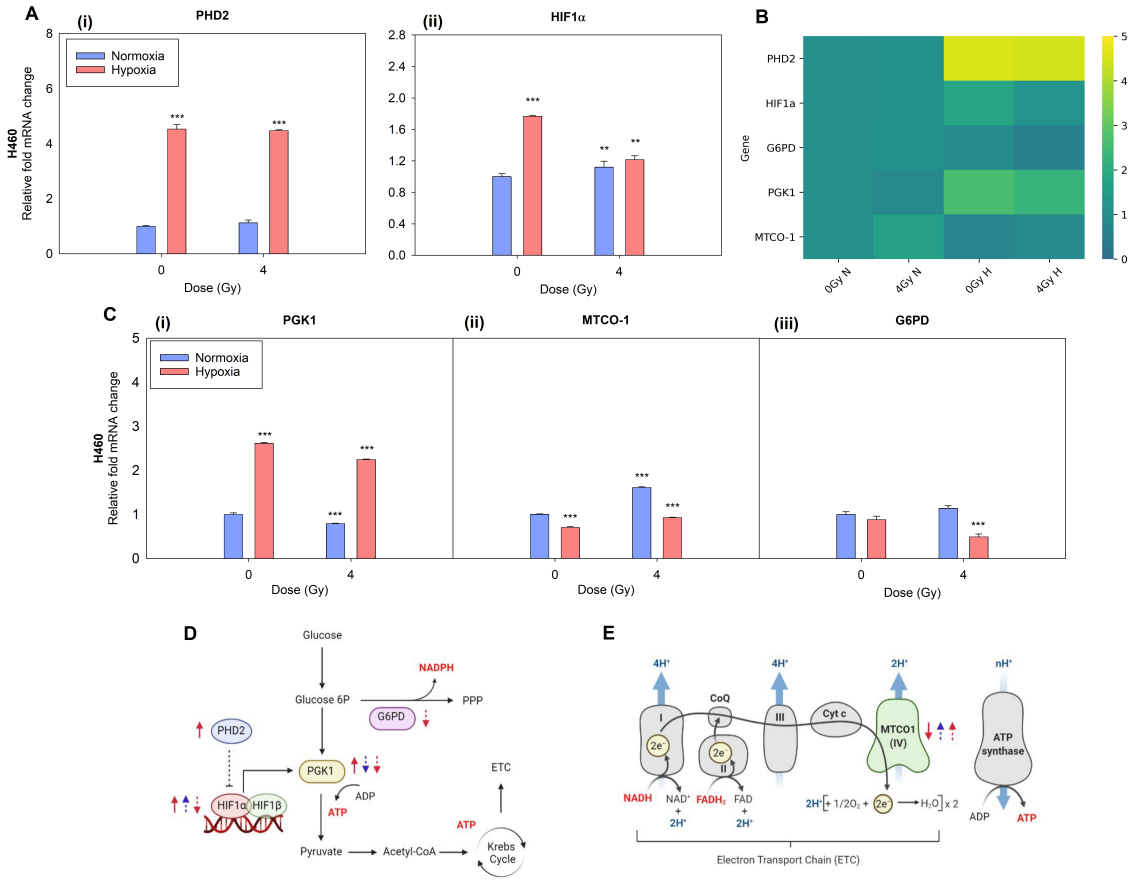


**Figure 3.20:** mRNA expression levels of genes evaluated using RT-qPCR in **H460** cancer cell line at 72 hrs following 4 Gy X-rays in normoxia (21% $O_2$) and hypoxia (0.1% $O_2$). **A)** Gene expression of **(i)** PHD2, **(ii)** HIF-1$\alpha$. **B)** Heatmap summary indicating upregulation and downregulation of investigated genes (PHD2, HIF1$\alpha$, MTCO-1, PGK1 and G6PD). **C)** Gene expression analysis of **(i)** PGK1, **(ii)** MTCO-1 and **(iii)** G6PD **D)** Schematic summary of the intracellular metabolic processes involving HIF-1$\alpha$, PHD2, PGK1 and G6PD following IR treatment. **E)** Electron transport chain (ETC) indicating the response of MTCO-1, which is a subunit of complex IV of the ETC, to radiation and oxygen level. In the schematic **D** & **E)**, a dose response is indicated by a dotted arrow and an oxygen response by a solid arrow (normoxia = blue, hypoxia = red). Up-arrow = upregulation, down-arrow = downregulation. The data was normalised to the non-IR normoxic control sample and the means and error bars (SD values) are presented. Each sample was statistically compared to the non-IR normoxic control sample (one-way ANOVA test). *P<0.05, **P<0.01, ***P<0.001 (n = 3).

**T24**

The T24 RT-qPCR results are plotted in figure 3.21. They show an increase in the mRNA levels of PHD2 following severe chronic hypoxic exposure with a fold increase from the normoxic non-IR control of 2.72 ($\pm$ 0.03), and remained constant even after the treatment with IR (2.69-fold increase ($\pm$ 0.01)) (figure 3.21A(i)). In normoxia, however, the mRNA levels of PHD2 were upregulated by 1.35-fold ($\pm$ 0.06) following IR treatment compared to the untreated normoxic control sample. In contrast to the results observed for the other two cell lines, where hypoxia induced a change in the HIF-1$\alpha$ expression levels, for chronically hypoxic T24, there were no significant changes observed between oxygen conditions, with hypoxia inducing a fold decreased of only 0.91 ($\pm$ 0.1) (figure 3.21A(ii)). However, in normoxia, the expression levels of HIF-1$\alpha$ post-IR were upregulated (1.56-fold (0.019)), which was consistent to what was seen for the previous two cell lines. In hypoxia, on the other hand, no differences were observed with the HIF-1$\alpha$ mRNA levels of the non-IR sample (0.91-fold ($\pm$ 0.1)) and IR sample (0.94-fold ($\pm$ 0.02)). This indicates that the levels of HIF-1$\alpha$ after 72 hrs from IR were not different from the normoxic control, therefore neither the prolonged severe hypoxia or the combination with IR exhibited visible effects on T24 radioresistant cells in the long run.

Concerning the expression of metabolic genes in T24, the mRNA levels of PGK1 were observed to be significantly upregulated in hypoxic conditions by 2.90-fold ($\pm$ 0.03), and were further slightly increased to 3.02-fold ($\pm$ 0.004) following IR treatment (figure 3.21C(ii)). In normoxia the expression of PGK1 was also upregulated by 1.18-fold ($\pm$ 0.004) post-IR compared with the non-IR normoxic control. Therefore, the glycolytic gene was positively regulated by low oxygen and by the IR exposure. The expression levels of MTCO-1 were, also in radioresistant T24, downregulated with a fold change of 0.72 ($\pm$ 0.04) under hypoxic exposure, which was further decreased following IR to 0.66-fold ($\pm$ 0.008) (figure 3.21C(i)). A downregulation of 0.93-fold ($\pm$ 0.02) was observed in the surviving normoxic sample compared to the normoxic non-IR control sample (figure 3.21C(ii)). These results indicate that the OXPHOS pathway was probably affected in both the T24 exposed to prolonged severe hypoxia and following IR-treatment, but also in the normoxic radioresistant T24 cells. The G6PD expression levels were also upregulated in hypoxia (1.76-fold ($\pm$ 0.004)) compared to the normoxic non-IR control sample (figure 3.21C(iii)). Moreover, IR induced an upregulation in both oxygen conditions with an increase of 1.94-fold ($\pm$ 0.03) in normoxia and 1.84-fold ($\pm$ 0.06) in hypoxia compared

to the control sample. These results therefore suggest that the flux through the PPP potentially was upregulated in response to both low oxygen and IR, which might be correlated to the enhanced glycolytic pathway observed for the T24 cell line.

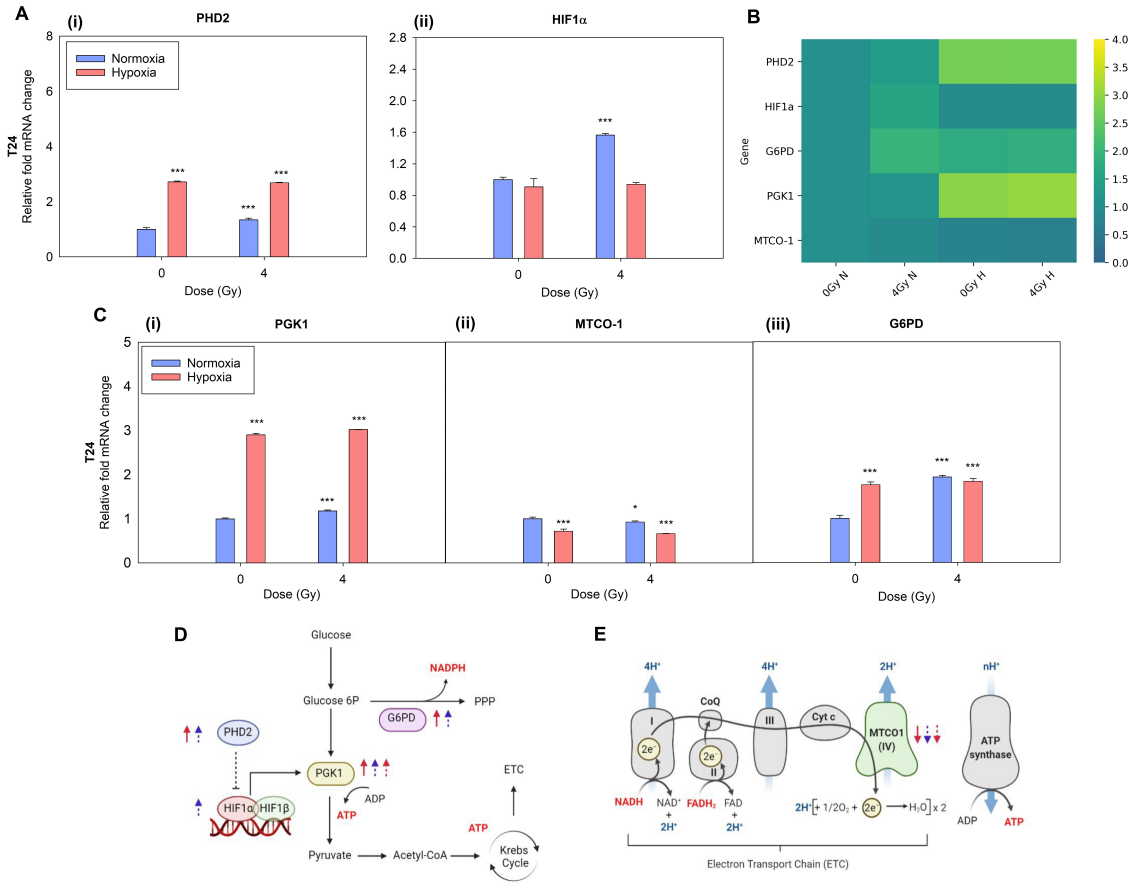


**Figure 3.21:** mRNA expression levels of genes evaluated using RT-qPCR in **T24** cancer cell line at 72 hrs following 4 Gy X-rays in normoxia (21% $O_2$) and hypoxia (0.1% $O_2$). **A)** Gene expression of **(i)** PHD2, **(ii)** HIF-1$\alpha$. **B)** Heatmap summary indicating upregulation and downregulation of investigated genes (PHD2, HIF1$\alpha$, MTCO-1, PGK1 and G6PD). **C)** Gene expression analysis of **(i)** PGK1, **(ii)** MTCO-1 and **(iii)** G6PD **D)** Schematic summary of the intracellular metabolic processes involving HIF-1$\alpha$, PHD2, PGK1 and G6PD following IR treatment. **E)** Electron transport chain (ETC) indicating the response of MTCO-1, which is a subunit of complex IV of the ETC, to radiation and oxygen level. In the schematic **D** & **E)**, a dose response is indicated by a dotted arrow and an oxygen response by a solid arrow (normoxia = blue, hypoxia = red). Up-arrow = upregulation, down-arrow = downregulation. The data was normalised to the non-IR normoxic control sample and the means and error bars (SD values) are presented. Each sample was statistically compared to the non-IR normoxic control sample (one-way ANOVA test). *P<0.05, **P<0.01, ***P<0.001 (n = 3).

**PC-3**

The RT-qPCR analysis for the PC-3 cancer cell line can be found in figure 3.22. Consistent with the results from the other cell lines, the expression levels of PHD2 were upregulated in response to chronic hypoxia with a fold change of 1.53 ($\pm$ 0.05) compared to the normoxic non-IR control sample (figure 3.22A(i)). Following IR treatment the PHD2 mRNA levels were further increased (1.93-fold increase ($\pm$ 0.038)) in hypoxia, whereas, in normoxia no significant differences between the PHD2 levels in the IR and non-IR samples were found. The mRNA levels of HIF-1$\alpha$ were downregulated by 0.52-fold ($\pm$ 0.03) in hypoxia (figure 3.22A(ii)), potentially in response to the upregulation of PHD2. However, IR induced an increase in the expression levels of HIF-1$\alpha$ in both oxygen conditions from their respective non-IR samples, with an increase of 1.12-fold ($\pm$ 0.036) in normoxia, while HIF-1$\alpha$ gene expression in radioresistant hypoxic cells remained downregulated in respect to the normoxic control sample (0.63-fold ($\pm$ 0.031)) (figure 3.22A(ii)). The expression of PGK1 was significantly upregulated by a low oxygen level with a fold change of 1.92 ($\pm$ 0.02), as well as IR, irrespective of the presence of oxygen, with a fold change of 1.13 ($\pm$ 0.03) in normoxia and 2.04 ($\pm$ 0.007) in hypoxia (figure 3.22C(ii)). Similar to the previous results of the other cell lines in hypoxia, the MTCO-1 expression levels in PC-3 chronically exposed to severe hypoxia were also significantly downregulated with a fold change of 0.87 ($\pm$ 0.031) compared to the normoxic non-IR control sample. IR induced a very slight increase in normoxia (1.073-fold ($\pm$ 0.007)) compared to the control sample, whereas there was no significant change observed in the hypoxic IR samples compared to the non-IR hypoxic sample (figure 3.22C(i)). These results potentially indicate that although the electron flux through the ETC could be reduced, thereby influencing the OXPHOS in hypoxia, it appears that it was less affected than in the other cancer cell lines investigated. The G6PD mRNA levels, on the other hand, were found to be significantly downregulated in response to severe chronic hypoxia with a 0.44-fold decrease ($\pm$ 0.047) compared to the non-IR normoxic control sample (figure 3.22C(iii)). IR, however, induced no significant change in the G6PD expression levels in normoxia, and only a slight increase was observed in the hypoxic sample in comparison to the non-IR hypoxic sample. These results indicate that although glycolysis was highly enhanced in hypoxia for the PC-3 cancer cell line, the PPP could be less active.

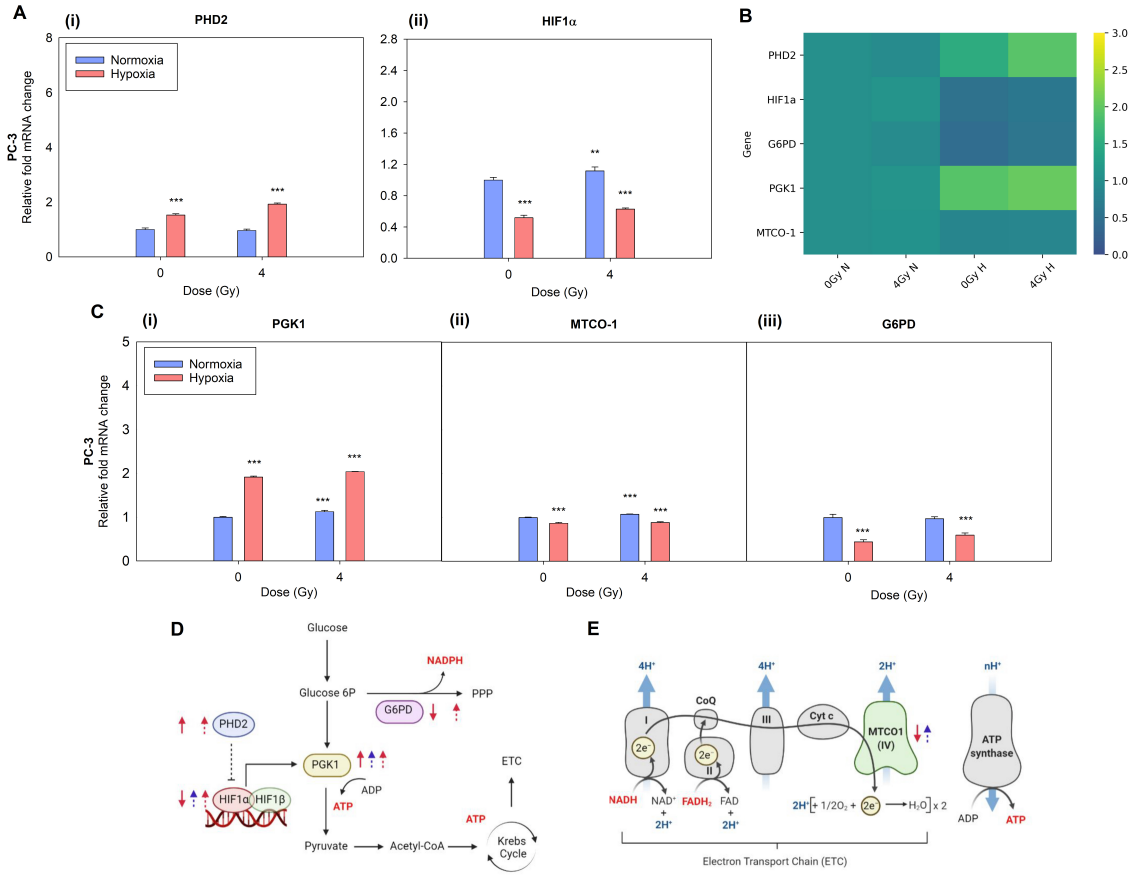


**Figure 3.22:** mRNA expression levels of genes evaluated using RT-qPCR in **PC-3** cancer cell line at 72 hrs following 4 Gy X-rays in normoxia (21% $O_2$) and hypoxia (0.1% $O_2$). **A)** Gene expression of **(i)** PHD2, **(ii)** HIF-1$\alpha$. **B)** Heatmap summary indicating upregulation and downregulation of investigated genes (PHD2, HIF1$\alpha$, MTCO-1, PGK1 and G6PD). **C)** Gene expression analysis of **(i)** PGK1, **(ii)** MTCO-1 and **(iii)** G6PD **D)** Schematic summary of the intracellular metabolic processes involving HIF-1$\alpha$, PHD2, PGK1 and G6PD following IR treatment. **E)** Electron transport chain (ETC) indicating the response of MTCO-1, which is a subunit of complex IV of the ETC, to radiation and oxygen level. In the schematic **D** & **E)**, a dose response is indicated by a dotted arrow and an oxygen response by a solid arrow (normoxia = blue, hypoxia = red). Up-arrow = upregulation, down-arrow = downregulation. The data was normalised to the non-IR normoxic control sample and the means and error bars (SD values) are presented. Each sample was statistically compared to the non-IR normoxic control sample (one-way ANOVA test). *P<0.05, **P<0.01, ***P<0.001 (n = 3).

## 3.5 Discussion

Developing tumours can be both characteristically and morphologically different, depending on the cancer type, stage, and size, as well as the location in the body, which in turn can affect how they respond to treatments such as chemo- and/or radiation therapy. For example, a tumour which is larger in size and highly proliferative, can potentially exhaust any nearby nutrient and $O_2$ supply and as a result form regions of lower oxygen concentration within the tumour mass, which are often more radio-resistant. In these conditions, cancer cells undergo further metabolic reprogramming compared to their normoxic counterparts in order to adapt to the lower oxygen conditions. For example, the enhancement of glycolysis and reduction of mitochondrial respiration for ATP production due to the lack of oxygen are possibly two of the most important of many compensatory mechanisms that exist and allow cancer cells to function at these low levels of $O_2$. Moreover, numerous clinical studies have demonstrated that low oxygenation can accelerate malignant progression and metastasis, thereby creating a poorer prognosis irrespective of which cancer treatment is used (194). These hypoxic regions, however, are often heterogeneously distributed in the tumour resulting in regions which are more hypoxic than others and consequently respond differently to treatments. Based on this, we believe it is necessary to investigate the adaptive behaviour of different types of cancer cells to different low oxygen concentrations and to obtain a deeper understanding on how it makes them more resistant to treatment. For this reason, the metabolic remodelling of four cancer cell lines, each from a different organ in the body (i.e. Brain: H4, Lung: H460, Bladder: T24, Prostate: PC-3) and exposed to different levels of hypoxia (i.e. acute and chronic), were explored in this study.

First of all, the hypoxic status of a tumour is dependant on the oxygen diffusion within the cancer mass which can be limited by the oxygen removal rate (ORR) of the cancer cells themselves. Indeed, in our study, we showed that cancer cells from various organs remove oxygen from the surrounding media at different rates, with the lung (H460) and prostate (PC-3) cancer cell lines being faster in comparison to the brain (H4) and bladder (T24) cancer cell lines which exhibited a slower removal rate (figure 3.7D). It is also worth highlighting that it took some time for the cells to reach the set hypoxic condition, meaning that only a few hours of hypoxic exposure is not a sufficient amount of time to establish a real hypoxic environment around and also inside the cells. More importantly, even though the hpoxic chamber (HC) was at a set $O_2$

level, the cells overshot this level due to their consumption and the pericellular environment inside the growth medium was therefore even more hypoxic than the set percentage in the chamber. These observations should be taken into account when performing experiments in hypoxia. In all of the experiments conducted in chronic hypoxia in the present study, cells were cultured in 1% $O_2$ for 48 hrs, allowing the cells to adapt to a mild oxygen depletion. This was followed by a period (12 hrs or 72 hrs in long-term experiments after irradiation) of severe hypoxic exposure (from 1% to 0.1%) in order to, based on the ORR measured, have an environmental oxygen content more similar to the one experienced by the cells inside the media, and thus avoiding continuous reoxygenation. Conversely, to mimic a condition of acute hypoxia (1% $O_2$ for 12 hrs), cells were exposed to 1% directly from normoxia (21%).

Since cell metabolism is restricted by intracellular transport distances and nutrient diffusion times (195), it could be logical to assume that size would also affect the diffusive processes within the cell. In fact, we found that the oxygen uptake of the cells could be loosely correlated with an inverse relationship to the cell volume (figure 3.8B(i)) after acute hypoxic exposure (i.e. 12 hrs at 0.1% $O_2$). These results are somewhat in accordance with Kleiber's Law, a universal law in biology which states an inverse relationship with body size and cell metabolism rate, and can be applied to all scale sizes including individual cells (196). In addition, Herst et al. showed that cell surface to be a major contributor to cellular oxygen consumption (197). This potentially emphasises a link between surface area-to-volume ratio (SA/V) and ORR. SA/V ratio describes the comparison between the size of the cytoplasmic membrane (SA) of a cell and the amount of the intracellular content (V). Smaller cells have internal volumes which are smaller than their external surface, resulting in larger SA/V ratio compared to bigger cells. A higher SA/V ratio (smaller volume) corresponds to a more effective transport of substances into the cells (because their surface area of the membrane is bigger in comparison with the volume). This concept clearly applied to our ORR results. In fact, in H460 and PC-3, the higher SA/V was associated with a faster oxygen (and also nutrients) removal from the culture media. Additionally, when measuring the cell Volume (cV) to nuclear Volume (nV) ratio (cV/nV), H460 and PC-3 had a smaller ratio, thus indicating that the nuclear volume in these cell lines was occupying a larger portion of the intracellular volume compared to H4 and T24. This in turn results in smaller internal distances between the surface and the intracellular components (including the nucleus), which could favour a more effective internal diffusion of $O_2$ (and nutrients). Therefore, it might be assumed that, in H460 and PC-3, the shorter internal

distances contributed to a faster $O_2$ removal from the external environment.

Since mitochondrion of the cell plays a central role in oxygen consumption and for energy generation, the ATP levels of the four cell lines were also measured acute and chronic hypoxia. Cancer cells are known to favour aerobic glycolysis as opposed to OXPHOS for ATP production, however, some cancers in fact upregulate OXPHOS as outlined in Ashton et al.'s review (177). Based on our results, under acute hypoxia all cancer cell lines maintain a level of ATP almost equivalent to that of the normoxic level, with only slight decreases. In comparison, in chronic hypoxia, only H460 showed a significant decrease compared to their normoxic counterpart. Indeed, the difference in ATP levels between acute and chronic samples, was reduced. These observations indicate that in the initial 12 hrs of hypoxic adaption, cells had sufficient $O_2$ availability and could continue to consume oxygen from the media, which is in fact confirmed in our ORR results (figure 3.7). Moreover, the cell lines which had the fastest ORR (i.e. H460 and PC-3) also exhibited the highest levels of ATP in normoxia, in contrast to T24 and H4. Therefore, the higher oxygen removal rates combined with a higher ATP content would suggest for a stronger ability to use $O_2$ to produce ATP. Additionally, since in H460 the difference between normoxic and hypoxic ATP levels was bigger, although not significant, compared to the other cell line, this might mean that cells also consumed more of the initial ATP pool in the first 12 hrs of hypoxia. However, further adaptation to hypoxic conditions (chronic hypoxia) stabilised ATP levels, which were similar to the values in acute hypoxia. This last observation was reported for all cell lines. However, hypoxia led to a slight, although not significant, decrease of the ATP content in comparison to normoxia at both time points. This might also be related to the decreased growth rate usually observed in hypoxia, as well established in literature (198) and also in the other study included in this thesis. Of note, the high level of ATP content in normoxic H460 and PC-3, and also hypoxic counterparts, potentially indicates a high reliance on the OXPHOS pathway or a high rate of glycolytic pathway. Indeed, prostate cancer cells have been shown to favour enhanced OXPHOS and limit glycolysis (199), particularly in the early stages of the cancer. However, at the moment, it is not possible to discriminate between these two processes, but further metabolic studies are ongoing to clarify this evidence.

In addition to the possible alterations in ATP production, tumours are characteristically known to have an increased reducing power which they can opt to use for redox defense as well as in

biosynthetic reactions (187, 200). In our study we showed majority of the cancer cell lines to have a significant increase in their reducing power, as defined by FADH2, FMNH2, NADPH, NADH (FFNN) levels, following acute hypoxia, which was further enhanced with increasing hypoxic severity (i.e. chronic hypoxia) (figure 3.12). One possible reason for this enhancement in the cellular redox status in hypoxia can be related to the inability of cells to use NADH, FADH2 as electron donors in the reactions involving oxygen, as an electron acceptor, along the mitochondrial ETC and thereby they would remain in their reduced form (201). Neo et al have shown an increase of NADPH in hypoxia and linked it to an associated increase in the G6PD levels and thereby in the pentose phosphate pathway (PPP), which produces NADPH (202). In addition to this, the increase in the FFNN levels can provide the necessary reducing capacity to sustain cellular glutathione pool for the elimination of toxic ROS molecules, as well as fuelling NADPH oxidase (NOX) which has been known to attenuate the consequential aftermath of redox stress (203). Taken together, it's possible that the adaption of the cancer cells to a hypoxic environment by maintaining their level of ATP production, as well as having an abundant supply of reducing agents, possibly acting as a defense against ROS, can contribute to the observed increase in radio-resistance seen for all cell lines under increasing hypoxic conditions in our clonogenic assays (figure 3.14).

The radio-resistant phenotype of cancer cells that can develop as a result of rewired metabolic demands, specifically the energy metabolism and the reducing power, was investigated on the cells which survived 4 Gy IR with photons and remained hypoxic at 0.1% $O_2$ and were then compared with the normoxic cells. In fact, it is widely accepted that failure of radiation therapy is mainly due the presence of radioresistant phenotypes which develop increased aggressiveness and invasion abilities after treatment. For this reason, we were interested in investigating the metabolic characteristics of the surviving, thus radioresistant, cells after 72 hrs from IR. Initial experiments showed an IR-induced increase more in cell volume than in nucleus volume, particularly in hypoxia thereby suggesting that the mechanisms which regulate cell morphology are more sensitive to IR at low oxygen conditions (figure 3.15). Of note, T24 cell line showed a huge increase in both cell and nuclear volume. The changes in cell size and morphology due to ionising radiation are well documented (204). In addition to this, there has been evidence suggesting a cell size checkpoint which ensures appropriate cell size throughout the cell cycle (205). Following analysis of the cell cycle progression after IR, cancer cells become blocked in either the G0-G1 or G2-M, depending on the cell line and oxygen

levels (figure 3.16). The exception was represented by T24 cells which display no arrest in their cycle, regardless of the oxygenation conditions, thus indicating a minor sensitivity toward 4 Gy irradiation. However, the cell cycle checkpoint activation were still present even under hypoxic conditions for the other cell lines (107). The increased accumulation of cells in G2-M has been associated with an increase in nuclear size 24 hrs after X-ray irradiation in normoxia (204). However, our data did not fit with this conclusion and instead for all cell lines the cell volume was mainly increased. In addition, from our results neither volume were shown to have a dependency on the $O_2$ levels. In fact, for example, there was a sensible increase only in the total cellular volume in normoxic H4 and in the hypoxic PC-3, which had cell cycle arrests in G0-G1 and G2-M, respectively. However, differences in cell type, dose and time of analysis after radiation can account for the discrepancies among studies. Therefore, these findings suggest that, at least in our study, there was no obvious correlation between cell cycle checkpoints and cellular/nuclear volume following 4 Gy radiation. However, since our results are obtained at 72 hrs post-IR, we can not exclude the possibility of nuclear or cell volume changes prior to this time point.

IR can also induce an increase in biosynthesis resulting in an increase in protein mass and thereby cell size. Indeed, from our results the cell lines which increase their cell volume in response to IR (figure 3.15) concurrently increase their reducing power (figure 3.18) which was consistent for both oxygen conditions, with the exception of PC-3 in hypoxia. Of note, in all cell lines, severe chronic hypoxia, without IR, already led to a higher reducing environment (high levels of FFNN) inside the cells compared to the normoxic counterparts. Initially thought to be due to an increased activity of the PPP, however, our results for PC-3 and H4 showed a downregulation of G6PD mRNA (i.e. the rate limiting enzyme in PPP playing a key role in NADPH production) following severely chronic hypoxic exposure (figure 3.19, 3.22 C(iii)). H460 showed no change in G6PD expression (figure 3.20 C(iii)). T24, on the other hand was the only cell line which had a significant upregulation of G6PD (figure 3.21 C(iii)) and possibly indicates an active PPP. Indeed, it is thought that G6PD is regulated by the NADPH/NADP+ ratio, so that if it increases (high level of NADPH, low level of NADP+), G6PD activity decreases (157, 169). In our study, this regulation was also detectable at a gene level, with the exception of T24. For the other cell lines, however, the high FFNN levels was attributed to processes other than the PPP, for example, the glycolytic or folate pathways (185), although the latter was shown by Raz et al. to be suppressed in severe hypoxia (206). For NADH, it can

continuously be produced by glycolysis, TCA in the mitochondria, and fatty acid oxidation (131). In fact, according to our results all the severely chronic hypoxic cancer cell lines highly upregulated PGK1 mRNA levels and therefore this suggests that the cells were pushing the glycolytic pathway, and reiterated the "metabolic shift" phenomenon under reduced oxygenation (figure 3.19, 3.20, 3.21, 3.22 C(i)). These high levels were also maintained after IR in hypoxia compared to normoxia, although the contribution of irradiation in modulating PGK1 expression was more cell-dependant. The activation of PGK1 in normoxic and hypoxic conditions has been documented in several cancers (207, 208). Interestingly, PGK1 has multi-faced functions inside cells, including DNA repair and angiogenesis, and its over-expression has been linked to cancer progression and metastasis, thus supporting chemo-and radio-resistance (208, 209, 210, 211). Notably, in all cell lines, the hypoxic surviving cells showed upregulated PGK1 compared to the normoxic non-irradiated control. This was also observed in H4, T24 and PC-3 cell lines in normoxia after IR. These observations were consistent with the fact that the cells analysed represented the surviving fractions (i.e radioresistant) after 72 hrs from irradiation. Moreover, an inter-cellular comparison revealed that hypoxic radioresistant H4 and T24 compared to PC-3 cells had a larger increase in PGK1 expression after IR. This in fact correlates with their observed radio-resistant responses in the clonogenic assays (figure 3.14). Therefore, PGK1 might participate in conferring a radioresistant phenotype. Nevertheless, in H460, the PGK1 level of expression in hypoxic radioresistant cells was similar to H4 and T24, even though they were more radio-sensitive. Also, PGK1 expression was reduced both in normoxia and in hypoxia as compared to their respective non-irradiated control cells. Hence, for H460, we did not observe a possible correlation between their clonogenic potential and PGK1 expression, indicating that this was not a possible regulation mechanism and their radiosensitivity were more dependant on other undetermined factors.

The potential increase of the glycolytic process is further confirmed in our results showing a reduction of the MTCO-1 mRNA in hypoxia for all of the cancer cell lines and thereby indirectly suggests also the activity of the OXPHOS pathway could be reduced (figure 3.19, 3.20, 3.21, 3.22 C(ii)). Furthermore, it appears that a reduction in the OXPHOS process subsequently requires a large upregulation of the glycolytic pathway to ensure an adequate supply in ATP levels and is the possible reason for the sustained ATP content for all cancer cell lines under low oxygen conditions after IR and in normoxia only for irradiated H460 (figure 3.17). However, interestingly, the radiation surviving normoxic H4, T24 and PC-3 cells had further, yet weak,

enhancement in their PGK1 expression levels, but this was not associated to their ATP content (figure 3.17). In contrast, the radioresistant normoxic H460 cells had a slight decrease in their PGK1 levels, but instead had an increase in the MTCO-1 levels, unlike the other cell lines, which might explain the significant increase in their ATP levels (figure 3.17). This is possibly due to higher ATP turnover present with OXPHOS compared with the glycolytic pathway. The mechanism by which radio-surviving H460 cell line stimulates MTCO-1 is not known, however, could be linked to the decrease in HIF-1$\alpha$ mRNA which was also observed, and interestingly not present in the other cell lines (figure 3.20 A(ii)).

Many studies have, in fact, associated metabolic changes in hypoxic cancer cells with the well-known HIF-1$\alpha$, as it is largely been reported to accumulate in hypoxic environments. Once upregulated it has been shown to activate the transcription of genes involved in the glycolytic pathway, as well as inhibiting mitochondria activity or triggering mitochondrial autophagy (212). In such a way, HIF-1$\alpha$ can reduce OXPHOS (213), thus playing an essential role in metabolic reprogramming. However, our study showed a significant downregulation of HIF-1$\alpha$ mRNA levels in the cancer cell lines H4 and PC-3 (figure 3.19, 3.22 A(ii)), while T24 experienced no change in expression following exposure to severe hypoxia for 72 hrs (figure 3.21 A(ii)). A corresponding increase in the PHD2 (known to initiate the degradation of HIF-1$\alpha$) was also observed and is therefore consistent with the reduction of HIF-1$\alpha$ (figure 3.19, 3.21, 3.22 A(i)). H460, on the other hand, was the only cell line to have an observed hypoxia-induced increase in HIF1-$\alpha$, although PHD2 levels remained high (figure 3.20 A(i) and (ii)). Therefore, based on our results the metabolic reprogramming that we have observed in relation to the PPP, glycolytic pathway and OXPHOS, at least for H4, T24 and PC-3 cell lines, can not only be attributed to an accumulation of HIF-1$\alpha$ mRNA. Other studies, including Lin et al. found that both HIF-1$\alpha$ and HIF-2$\alpha$ can in fact regulate the tumour micro-environment and showed that while both HIF proteins are stable under acute hypoxic conditions, in chronic hypoxia they, in fact, become destabilised (89). They also highlighted that the HIF-1$\alpha$ mRNA are more sensitive to the duration in hypoxia in comparison to HIF-2$\alpha$ mRNA and attributed this to the chromatin remodelling under hypoxic conditions. These results therefore show that HIF-1$\alpha$ mRNA regulation is cell-type dependant in prolonged and severe hypoxia, where in some cell line it can be downregulated, upregulated or, even not changing (figure 3.19 and 3.22). Additionally, the upregulation of PHD2 mRNA levels in severe hypoxia in all cell lines, which remained substantially stable even after irradiation, was unexpected, but it is consistent with a study

by D'Angelo et al. showing that under hypoxia PHD2 mRNA and protein levels increased, while the enzymatic activity was limited (214). These results are therefore consistent with our downregulation of HIF-1$\alpha$ that was observed in H4 and PC-3 (figure 3.19 and 3.22) and could be a possible explanation. Moreover, other studies such as Ginouvès et al. highlighted that PHDs can in fact be overactive in chronic hypoxia resulting in a desensitisation of HIF-$\alpha$ necessary to prevent cell necrosis. In their study they found an accumulation of HIF-1$\alpha$ after acute hypoxia (1% $O_2$) whereas a drastic attenuation in severely chronic hypoxia (0.1% $O_2$), which is again comparable with our results (215). However, in H460, HIF-1$\alpha$ and PHD2 expression were concordant, suggesting that, at least in this cell line, other regulation mechanisms were probably taking place. Moreover, it has been shown that HIF-1$\alpha$ regulates the expression of PGK1 (207), which in fact resulted in an upregulation concomitantly with HIF-1$\alpha$ in hypoxic control H460 cells and, accordingly, both mRNAs reduced in the radioresistant cells after 4 Gy IR exposure. Indeed, also in hypoxic radioresistant H4, T24 and PC-3 cells, the expressions of HIF-1$\alpha$ and PGK1 followed similar tendencies after IR potentially confirming the link between HIF-1$\alpha$ and the glycolytic pathway in response to IR in our cell systems and culture conditions. These results therefore highlight that the highly glycolytic behaviour, based on the PGK1 levels, observed in our hypoxic cells surviving radiation treatment, could be a key contributor to firstly, the enhancement of radiation resistance observed, and secondly, the overall differing radio-responses.

In conclusion, tumour cells have dysregulated metabolism, which is a distinct and defining trait. In the present study, we show that, under hypoxia, the need to deal with low oxygen availability requires further metabolic changes. In this scenario, also the responses to radiation treatment are further modulated compared to normoxic cells, which showed that hypoxia could elicit strong changes in the redox status and adequately alter their energy bio-energetics for enhanced survival and contribute to their resistance to irradiation treatments. This clearly highlighted the intricate complexity among the metabolic network, hypoxia and radiotherapy, and their cell type-dependency. Although the mechanistic details of these responses remain to be elucidated, identifying intercellular and intracellular variables that are modulated (or do not change) following hypoxia and radiation can help to better understand the impact of radiation treatment in hypoxic tumours.

# 4 Measurement of the radio-response of non-small cell lung cancer (NSCLC) cell lines exposed to chronic hypoxia

## 4.1 Introduction

Lung cancer is the leading cause of cancer related mortality in the US and Europe, accounting for 18% of all new cancer related deaths in 2020 (216). With an estimated 2.2 million lung cancer diagnosis and 1.8 million deaths around the globe, it is currently the second most common cancer in women after breast cancer, and the most common among men (216). Unfortunately, it has a very low relative 5-year survival rate and since patients are often asymptomatic in the early stages of lung cancer, it is more frequently than not discovered at a late and more advanced stage of the disease (217). Lung cancer can be divided into two categories: Small Cell Lung Carcinoma (SCLC) and Non-Small Cell Lung Carcinoma (NSCLC), with the latter being further subdivided into squamous cell carcinoma, adenocarcinoma, and large cell carcinoma. NSCLC accounts for 85% of lung cancer patient diagnosis' and due to its aggressive nature and highly metastatic characteristics deem it difficult to treat effectively. As a result, approximately 70% of patients die due to the uncontrolled growth and/or the formation of secondary tumours, with the brain being a highly probable lung metastasis site (218).

As with the majority of cancers, tumour hypoxia is an inevitable consequence of the excessive proliferation induced by their chaotic metabolism. For example, in healthy lung tissue the median oxygen percentage is around 5.6% which is almost 3-fold higher than that of the 1.9% oxygen content found in lung cancer (219). Many recent studies have proven that a low oxygen content correlates with poor prognosis of NSCLC due to the changes it induced in the genetic and proteomic make-up of the cancer cells, particularly in the DNA repair mechanics and the oxidant response, which can thereby enhance cancer radio-resistance (220).

NSCLC is often treated with conventional photon radiotherapy whereby the treatment success rate is largely susceptible to tumour hypoxia. Photon RT interacts with cellular bio-constructs mainly through indirect mechanisms, whereby its first point of contact is an oxygen molecule and results in the creation of highly reactive free radicals such as hydroxyl radicals ($OH^-$), superoxide anions ($O_2^-$), oxygen singlet ($O_2$) as well as hydrogen peroxide ($H_2O_2$), otherwise known as reactive oxygen species (ROS). At low levels, ROS are essential in helping to maintain physiological equilibrium by functioning as secondary messengers, regulating tissue repair and self-renewal, however, an excessive increase can result in cell toxicity (221). $H_2O_2$ is the most stable of the ROS molecules and has a much longer lifetime, allowing it to diffuse over extended distances and cause irreversible damage on the cellular biomolecules such as DNA. The induction of double strand breaks (DSBs) is the most lethal type of DNA damage and therefore the most sought after in RT. Under normal conditions (i.e. normoxia) the cell has an active antioxidant system which enables safe decomposition of reactive radicals (e.g. catalase (CAT), glutathione peroxidase (GPX1) etc.). However, since low levels of oxygen (i.e. hypoxia) are a common characteristic of NSCLC, and oxygen is a key molecule in many of the pro-oxidant and anti-oxidant processes in the cell, it is not surprising that hypoxia can induce altered redox behaviour.

Although the DNA damage response (DDR) and the repair mechanisms of cancer cells in normoxia and hypoxia have been thoroughly investigated throughout literature as outlined in Begg et al.'s recent review (107), the altered anti-oxidant behaviour which has a large association with the DDR and can therefore play a key role in the increased radio-resistance in NSCLC, has had little coverage especially in the context of hypoxic micro-evironments. Therefore, we are of the opinion that further research into the pro- and anti-oxidant capacity and damage response of lung cancer cells under low oxygenated conditions is required to provide a more substantial overview and understanding of the highly radio-resistant properties of hypoxic NSCLC tumours. For this reason, in this study three NSCLC cell lines (H460, A549, Calu-1) were irradiated using photon RT under normoxic (21% $O_2$) and chronic hypoxic (0.1% $O_2$) conditions, and the altered behaviour in their redox environment, in particular $H_2O_2$ induction, both nuclear and cytosolic, were measured. The corresponding antioxidant responses were investigated and correlated with the DNA damage response, evaluated by $\gamma$H2AX foci induction, and radio-resistances, assessed by clonogenic assays.

## 4.2 Materials & Methods

### 4.2.1 Cell Culture

Cells were cultured at 37°C in a humidified atmosphere of 5% $CO_2$ and 21% $O_2$, unless otherwise stated, and were sub-cultured using TrypLE Express (Thermo Fisher Scientific, Cat.Nr.: 12604013) when they reached 70 - 80% confluency. The cell lines used in this thesis include human non-small lung carcinoma cells: H460 (pleural) from a male (age and ethnicity unspecified), A549 (epithelial) from a 58 year Caucasian male and Calu-1 (pleura) from a 47 year old Caucasian male. All cell lines were purchased from ATCC. Calu-1 cells in McCoy's 5A (Modified) Medium (Thermo Fisher Scientific, Cat.Nr.: 16600082), H460 cells in Gibco RPMI Medium (Thermo Fisher Scientific, Cat.Nr.: 224000-89), and A549 in Ham's F-12K (Kaighn's) Medium (Thermo Fisher Scientific, Cat.Nr.: 21127-022). All media were supplemented with 10% Fetal Bovine Serum (FBS) (Thermo Fisher Scientific, Cat.Nr.: 10082147) and 1% PenStrep ((10,000 U/mL), Thermo Fisher Scientific, Cat.Nr.: 15140122). In low oxygenated conditions (i.e. hypoxia), cells were incubated in a hypoxic chamber (Sci-Tive, Baker Ruskin) as indicated in figure 4.1, where nitrogen ($N_2$) was used as a substitute. The oxygen concentration used was 0.1% - 1%, depending on the experiment. The temperature was maintained at 37°C, the $CO_2$ was 5% and the relative humidity was 75% for all experiments.


**Figure 4.1:** Image of the Sci-Tive Baker Ruskin hypoxia chamber used for low oxygen experiments.

### 4.2.2 Clonogenic Assay: Hypoxia & Normoxia

**Sample preparation prior to irradiation (IR):** A semi-confluent (60 - 70%) T75 $cm^2$ flask with a filtered cap was placed in the hypoxic chamber at 1% $O_2$ overnight (i.e. 12 hrs). The cells were then seeded at densities of 300,000, to avoid over-confluency at irradiation (IR) and incubated for a further 48 hrs at 1% $O_2$. The supply of oxygen was then reduced to 0.1% 12 hrs prior to IR. Non-filtered caps were placed on all flasks and these were sealed using parafilm to ensure the hypoxic environment was maintained in the flask during IR in normoxia. This procedure was also repeated in normoxic conditions.

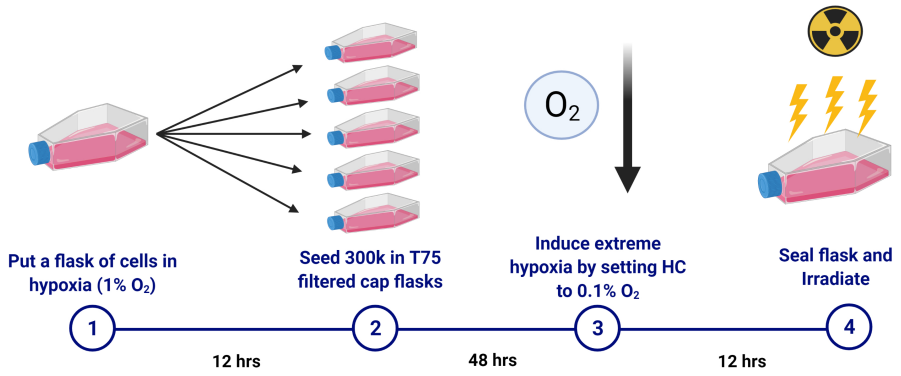


**Figure 4.2:** Schematic representation of sample preparation for inducing hypoxia in cells prior to irradiation for the clonogenic assay protocol.

**Irradiation and staining procedure:** Cells were irradiated using a 225 kVp X-ray machine (MultiRad225 Faxitron) with a field size of 20 cm x 20 cm as illustrated in figure 4.3. Following IR treatment, cells were washed with PBS (Phosphate Buffer Saline), detached using TrypyLE (2.5 mL for each T75 $cm^2$ flask) and plated in T25 $cm^2$ culture flasks using the count corresponding to a particular dose (i.e. 200 – 85,000 cells for low and high doses, respectively). Colonies were left to form over 10 to 14 days in the incubator (37°C, 5% $CO_2$) under normoxic conditions. Flasks were then fixed with 100% ethanol (EtOH) and stained using crystal violet. Stained cell clusters of more than 50 cells were considered a colony and included in the data.

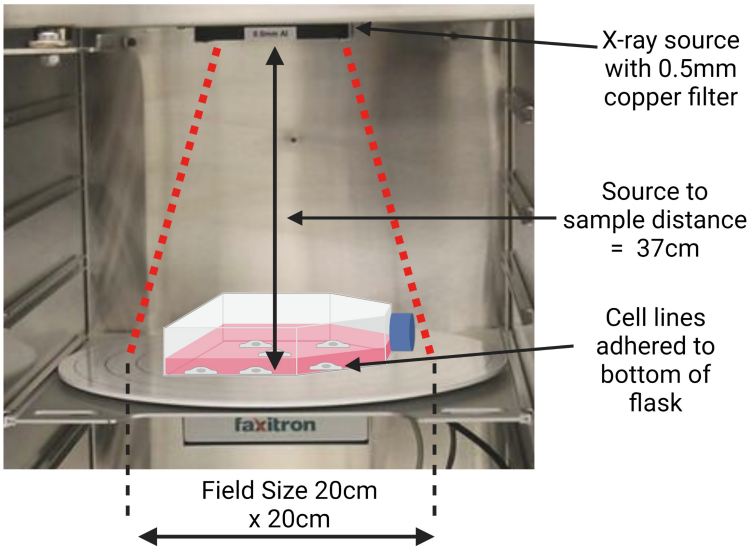


**Figure 4.3:** X-ray exposure setup in the MultiRad225 Faxitron with the cell culture flask lying perpendicular to the beam at a distance of 37 cm and a field size of 20 cm x 20 cm. A copper filter with 0.5 mm was used for all experiments.

### 4.2.3 Immunofluorescent Assay: $\gamma$H2AX Foci Staining

**Cell preparation in normoxia:** Cells were seeded on coverslips in a 6-well plate at a density of 50,000 using a media volume of 1.5 mL and were incubated at 37°C, 5% $CO_2$ and 21% $O_2$ overnight. The plates were then irradiated using the MultiRad225 Faxitron with doses varying from 0 – 8 Gy.

**Cell preparation in hypoxia:** A semi-confluent (70%) flask was incubated in the hypoxic chamber (HC) (1% $O_2$) overnight (i.e. 12 hrs). In the HC, cells were detached and seeded on coverslips in a 6-well plate using a media volume of 1.5 mL and incubated for 48 hrs. The oxygen concentration in the HC was then decreased to 0.1% $O_2$ for a further 12 hrs. The plate was then sealed with parafilm prior to removal from the HC and irradiated using the MultiRad225 Faxitron with doses varying from 0 – 16 Gy. The plates were then put back in the HC at 0.1% for timepoints of 30 min or 24 hrs post-IR.

**Immunofluorescent staining:** The media was removed from each well and the cells were washed twice with PBS. Cells were fixed using cold 4% PFA for 15 min, followed by 3 washes with PBS. Cells were then permeabilised using cold 0.25% Triton-X (1mL) for 5 min at room temperature. Following this, the cells were blocked using 4% BSA (1mL) for 45 min and then washed with cold 1% BSA (1 mL). Excess liquid was then discarded, and the cells were incubated with the primary antibody (1:1000 in 1% BSA, Anti-phospho-Histone H2A.X antibody,

Ser139, (SIGMA ALDRICH, Cat.Nr.: 05-636) for 1 hr at room temperature. Cells were washed three times with 1% BSA (1 mL) and then incubated with the secondary antibody (1:1000 in 1% BSA, AlexaFluor 647 goat anti-mouse IgG (H+L)) (Thermo Fisher Scientific; Cat.Nr.:A-21236) for 30 min in the dark at RT. The cells were then washed three times with PBS.

**Mounting Coverslip:** The coverslips with the now stained cells were left to dry for approximately 15 min. 8 µL of mounting media + DAPI was added to the glass slide and the coverslip was gently placed on top. The coverslip was then sealed with nail polish and the slides were kept at 4°C until visualised under a confocal microscope.

### 4.2.4 Nuclear $H_2O_2$ Staining/Cell cycle staining

Nuclear Peroxy Emerald 1 NucPE1 was used to measure the $H_2O_2$ levels, since it selectively localises in the nucleus of mammalian cells. It has fluorescent properties such as absorption peaks ($\gamma_{abs}$) at 468 nm ($\epsilon$ = 27,300 $M^{-1}cm^{-1}$) and 490 nm ($\epsilon$ = 26,000 $M^{-1}cm^{-1}$), and a weak emission ($\gamma_{em}$) at 530 nm ($\phi$ = 0.117). Upon interaction with $H_2O_2$, the absorption peak shifts to 505 nm and an enhanced emission peak at 530 nm ($\phi$ = 0.626) is observed as shown in figure 4.4 (222). In this study, NucPE1 is utilised to observe the $H_2O_2$ created in the nucleus of cancer cells post irradiation.

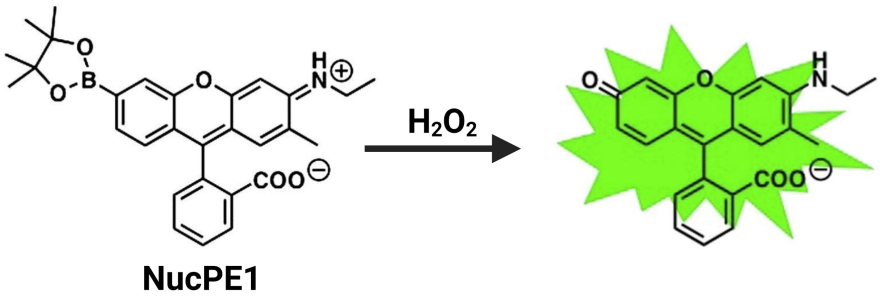


**Figure 4.4:** Illustration of the change in the chemical composition of NucPE1 molecule following interaction with $H_2O_2$, resulting in an enhanced fluorescence signal. (222)

1 x$10^6$ cells were seeded in a 100 mm petri dish the day before IR. On the day of the experiment, cells were washed with HBSS, and irradiated with a build-up of 5 mL of HBSS. Cells were stained with 10 µM of NucPE1 in HBSS solution and incubated for 20 min under a low oxygenated environment (1% $O_2$), 37°C, 5% $CO_2$, 70% humidity. Cells were washed twice with PBS and detached using TrypLE before being collected for nuclear extraction (see section 4.2.5) partially under atmospheric $O_2$ and analysed using a FACS Canto ™ II flow cytometer

as illustrated in figure 4.5. Samples were excited with a 488 nm laser and the fluorescence emission was collected at 530/30 nm. The results were analysed by using FlowJo software 8.1.

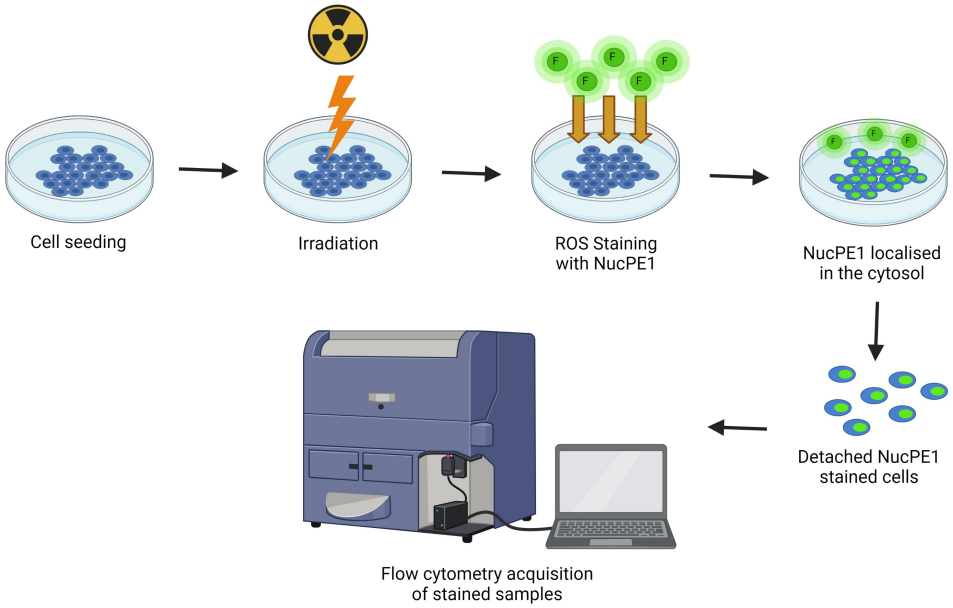


**Figure 4.5:** Schematic illustration of the NucPE1 fluorescence staining protocol prior to signal acquisition at the flow cytometer for detection of $H_2O_2$ in the nucleus of the cell.

### 4.2.5 Nuclear Extraction for Flow Cytometric Analysis

Detached cells were resuspended in 1 mL PBS and transferred to pre-chilled 1.5 mL centrifuge tubes. Samples were briefly centrifuged at 4°C for 5 - 10 seconds at 10,000 rpm. The supernatant was removed and the cell pellet was resuspended in 900 µL of ice-cold PBS containing 0.1% nonidet P40 (NP-40). The cell pellet was triturated five times on ice (step 1) and the remaining cell lysis was centrifuged again for 5 - 10 seconds at 10,000 rpm. This was repeated one more time (step 2) and on the final centrifugation step the pellet was resuspended in cold PBS and kept on ice and immediately acquired on FACs cytometer. Samples were excited with a 488 nm laser and the fluorescence emission was collected at 530 nm. The results were analysed by FlowJo software 8.1. For the hypoxic samples, all the process until step 1 included were conducted inside the Hypoxic chamber.

### 4.2.6 Cytosolic $H_2O_2$ Staining

Cells were seeded in a 60 mm petri dish at a density of 800,000 the day before IR. On the day of the experiment, cells were washed with HBSS, and irradiated with a build-up of 2 mL

of HBSS. Cells were stained with 40 µM of PY1-ME (Peroxy Yellow 1 Methyl-Ester) in HBSS solution and incubated for 20 min under a low oxygenated environment (1% $O_2$), 37°C, 5% $CO_2$, 70% humidity. Cells were washed twice with PBS and detached using TrypLE before being collected under atmospheric $O_2$ and analysed using a flow cytometer (FACS Canto II ™) as illustrated in figure 4.6. Samples were excited with a 488 nm laser and the fluorescence emission was collected at 530/30 nm. The results were analyzed by FlowJo software 8.1.

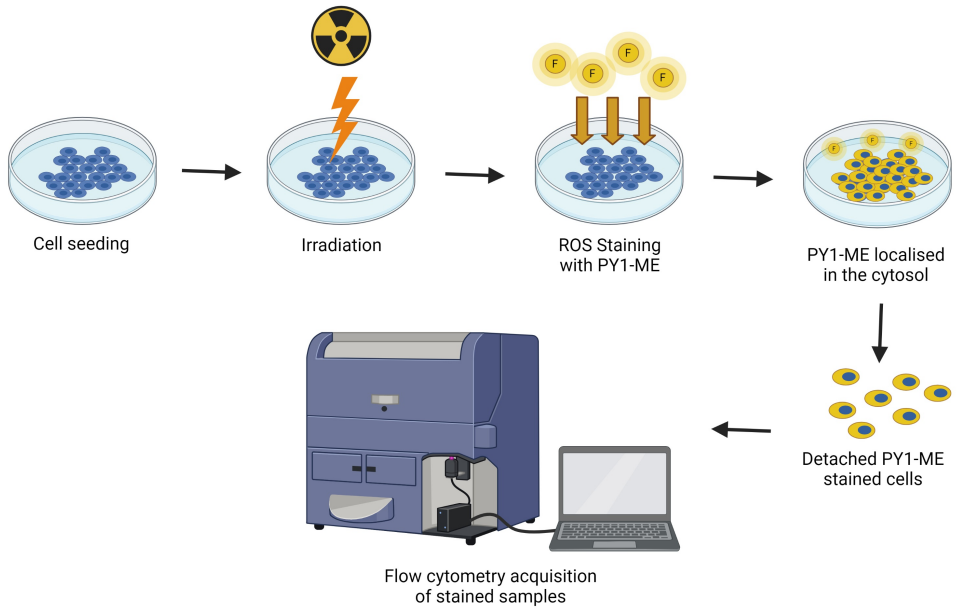


**Figure 4.6:** Schematic illustration of the PY1-ME fluorescence staining protocol prior to signal acquisition at the flow cytometer for detection of $H_2O_2$ in the cytosol of the cell.

PY1-ME is localised in the cytosol of mammalian cells. It has fluorescent properties such as absorption peaks ($\gamma_{abs}$) at 489 nm ($\epsilon$ = 18,100 $M^{-1}cm^{-1}$) and 510 nm ($\epsilon$ = 18,700 $M^{-1}cm^{-1}$), and a weak emission ($\gamma_{em}$) at 548 nm ($\phi$ = 0.0.040). Upon interaction with $H_2O_2$, the absorption peak shifts to 515 nm ($\epsilon$ = 79,900 $M^{-1}cm^{-1}$) and an enhanced emission peak at 540 nm ($\phi$ = 0.402) is observed as shown in figure 4.7 (223). In this study, PY1-ME is utilised to observe the $H_2O_2$ created in the cytosol of cancer cells post irradiation.

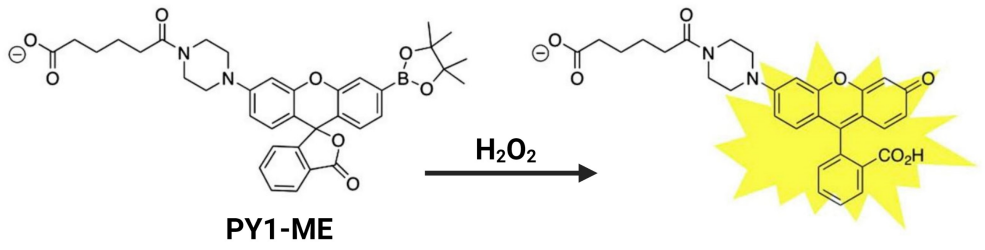


**Figure 4.7:** Illustration of the change in the chemical composition of PY1-ME molecule following interaction with $H_2O_2$, resulting in an enhanced fluorescence signal. (223)

### 4.2.7 GSH/GSSG Assay

The anti-oxidant status of the cells was determined using the GSH/GSSG-Glo™ Assay (Promega Cat.Nr.: V6611) to quantify the amount of reduced and oxidised forms of glutathione present in the samples. Cells were washed once with 5 mL of HBSS, followed by irradiation (225kV X-rays) in 5 mL of HBSS. Cells were then incubated in HBSS in a low oxygenated environment (1% $O_2$), 37°C, 70% humidity, 5% $CO_2$ for 20 min as per nuclear and cytosol ROS staining (Section 4.2.4 & Section 4.2.5). Afterwards they were washed with PBS and detached using TrypLE. Samples were collected by centrifugation, resuspended in 1 mL PBS and counted for the assay. 130,000 cells were added to each well of a 96-well plate and the assay performed following the manufacturer's instructions. The luminescence was measured at the ClarioStar plate reader.

The basic principle of the GSH/GSSG-Glo Assay is illustrated in figure 4.8, whereby glutathione S-transferase enzyme is coupled to a firefly luciferase reaction and is used to convert the Luciferin-NT (GSH probe) to luciferin. However, for more details refer to the Promega GSH/GSSG-Glo Assay technical manual (224). The assay allows measurement of the total glutathione and oxidised glutathione levels. The reduced glutathione (GSH) levels were then deduced by the removal of GSSG from the total glutathione value (i.e. Total Glutathione - Oxidised glutathione = Reduced Glutathione).

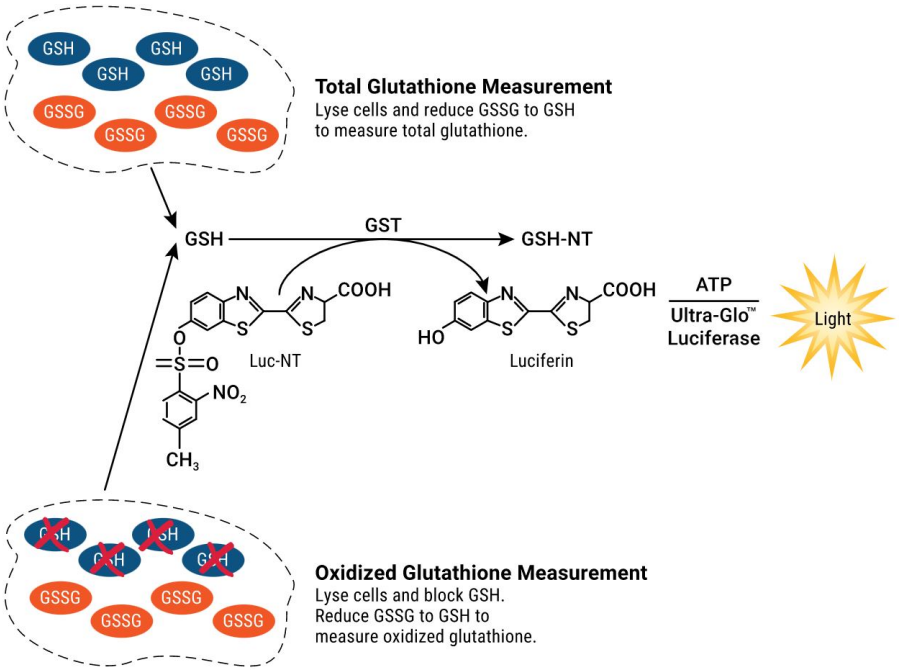


**Figure 4.8:** Illustration of GSH/GSSG assay from Promega whereby glutathione S-transferase enzyme is coupled to a firefly luciferase reaction and is used to convert the Luciferin-NT (GSH probe) to luciferin. (224)

### 4.2.8 Cell Death Assay using Propidium Iodide

Cell death analysis was performed using a Propidium Iodide (PI). Briefly, cells from each lines were cultured and prepared for the IR treatment as described in 3.2.1 and 4.2.2. Subsequently, cells and supernatants were collected, washed with cold DPBS, centrifuged and re-suspended in 1 ml of cold PBS. Each sample was acquired as "negative" using a FACS Canto ™ II flow cytometer. This enabled to set the threshold. Immediately after, 1 $\mu$L of the 100 $\mu$g/mL PI solution was added in each tube, mixed and after few minutes the samples were acquired as "positive". All samples were excited with a 488 nm laser and the fluorescence emission was collected at 585/42 nm. The results were analyzed by FlowJo software 8.1.

### 4.2.9 RNA extraction, cDNA sythesis and RT-qPCR

RNA was isolated from non-irradiated and irradiated normoxic and hypoxic cell lines (H460, A549, Calu-1) 24 hrs after irradiation using High Pure Isolation Kit (Roche, , cat.Nr.: 11828665001) as per instruction from the manufacturer. Following extraction, RNA amount, purity and integrity were checked using a Nanodrop ND-1000 (Thermo Fisher Scientific) and by running 2 $\mu$L of RNA per sample on a 1% agarose gel. 1 $\mu$g of RNA was retrotranscribed in cDNA by using RT2 First Strand Kit (Qiagen, Cat.Nr.:330404). Reverse transcription quantitative real-

time polymerase chain reaction (RT-qPCR) was then used to analyse the gene expression from the cDNA which was obtained from the isolated RNA samples.

A reaction mix (15 µL) containing 20 pmol of the forward and reverse primer pairs, Power SYBR Green PCR Master mix (Thermo Fischer Scientific) and nuclease dree water (Thermo Fischer Scientific, Cat.Nr.: 4368706) was used to amplify 25 ng of cDNA. The RT-qPCR protocol consisted of the following cycles: 1 cycle at 95°C for 10 min, 40 cycles at 95°C for 15 s and finally 60°C for 60 s. The relative gene expression was then normalised to our housekeeping gene HPRT1 (i.e gene which is expressed in all cells and not affected by IR or hypoxia). The 2-ΔΔCt method was used to perform all data analysis.

| **Gene** | **Forward Primer** | **Reverse Primer** |
|---|---|---|
| HPRT1 | TTGACACTGGCAAAACAATG | GTCCTTTTCACCAGCAAGC |
| NRF2 | CCCTCTACTTGGAAGACGAC | ATTCAACCTTGGGGCTTGG |
| KEAP1 | CTCCATATCCCATTCCCTGTAG | GAGCAGCCACTTTATTCTTACC |
| GSR | ACAGCCACCAACCACACT | GCAAAGAGACTAGATCACTGC |
| GRX | CAGTCCTCCTCAGATACCCA | AGAGCTGGCAGAAAGTAAGC |
| TRX | GAAGAAAAGGTGGTTGGGATC | GAATGGCGACTGTGTTGTC |
| GPX1 | CCCAAGCTCATCACCTGGTC | TGTCAATGGTCTGGAAGCGG |
| DNA-PKcs | AGGAACTGCTCTCAAACCTG | CCTGCGGACAATCACAAAG |
| Ku80 | GCTTCTGCCTAGCGATACC | TACCAACGGCTTGAAACCC |
| RAD51 | CACCGCCCTTTACAGAACAG | TCCACTTGAGCTACCACCTG |
| BRCA2 | CACCTCTTGAAGCCCCAGAA | AGCGATGATAAGGGCAGAGG |
| WEE1 | CCCAGCCAAAGAAGAAACCAC | GCCTCATTCAGCTCTCGGAAC |

**Table 4.1:** List of genes used in this study and their corresponding forward and reverse primers for RT-qPCR analysis

### 4.2.10 Confocal and Widefield Microscopy

Non-small cell lung cancer cell lines H460, A549 and Calu-1 were stained with AlexaFluor647 for measuring the $\gamma$H2AX foci as outlined in section 4.2.3. Zeiss LSM710 confocal microscope was used to image the $\gamma$H2AX foci using a 40x oil immersion objective. On each coverslip and for each experiment >60 cells were imaged.

### 4.2.11 Image Processing: Imagej

A z-stack was acquired for all images. They were all 12-bit and were post processed using imagej to quantify the number of $\gamma$H2AX per cell. In brief: First the background was subtracted from all images. The Hoechst image was then processed applying a set minimum area of 1000 pixels per nuclei. These ROI (regions of interest) were then saved in the ROI manager. The $\gamma$H2AX slice was then processed by background subtraction followed by despeckling and removal of noise. The minimum and maximum threshold was set and kept constant for all $\gamma$H2AX images. The maximum was then determined and the foci were segmented. Only foci which had a minimum area of 4 pixels were considered. Data from each image was then combined to determine the number of foci per cell.

### 4.2.12 Statistical Analysis

Statistical analysis was carried out using Sigmaplot software (Version 14.5). All data was statistically compared to their non-IR control for their respective oxygen conditions unless otherwise stated. Data is presented as mean $\pm$ SD or mean $\pm$ SEM and will be stated in the figure caption. Statistical significance was assessed on the mean of three individual experiments (i.e. n=3) using student t-tests and one-way ANOVA with a significance threshold of $p = 0.05$.

## 4.3 Results

This section will outline the results obtained after investigating the response of three different non-small cell lung cancer (NSCLC) cell lines to irradiation and how it is altered under chronic hypoxic conditions. Specifically, the damage response (i.e. DSB induction, repair, DDR pathways) and the pro-/anti- oxidant capacity (i.e. $H_2O_2$ induction, GSH/GSSG ratio, catalase etc.) will be investigated and evaluated against their radio-responses (clonogenic assays).

### 4.3.1 Cell growth of lung cancer cell lines under different oxygen conditions

NSCLC (H460, A549 and Calu-1) cells are commercial cell lines representing three different lung cancer sub-types (large cell, adenocarcinoma, squamous, respectively). They were cultured under 21% oxygen ($O_2$) (i.e. normal oxygenated cell culture environment) and 0.1% $O_2$ (i.e. reduced oxygen environment or hypoxia) in order to investigate how differences in growth between the cell lines in both oxygen conditions could affect cell proliferation ability. The growth of the cell lines was monitored at 24, 48 and 72 hrs and the corresponding growth profiles can be seen in figure 4.9 with the doubling times reported in table 4.2. The results showed that all three cell lines had a growth reduction in hypoxia (0.1% $O_2$) compared with normoxia (21% $O_2$) as indicated by an increase in their doubling times (figure 4.9).

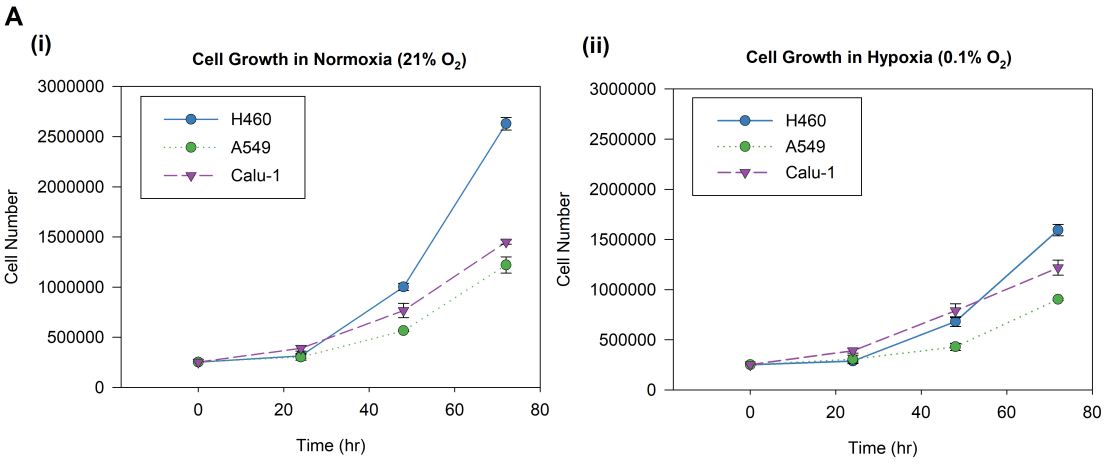


**Figure 4.9:** Cell growth of non-small lung cancer cell lines (H460, A549, Calu-1) in **A (i)** Normoxia (21% $O_2$) and **(ii)** Hypoxia (0.1% $O_2$), over a time period of 72 hrs.

Under both oxygen conditions, H460 had the fastest proliferation rate compared with the much slower proliferation rates of Calu-1 and A549, respectively. The doubling times of H460, A549 and Calu-1 in normoxia were 20.21 hrs, 30.94 hrs and 27.95 hrs, respectively, whereas in

hypoxia these increased to 25.86 hrs, 39.61 hrs and 30.54 hrs, respectively. A549, therefore, had the largest increase in doubling time in hypoxia as it increased by almost 9 hrs, followed by H460 with an approximate increase of 6 hrs and then Calu-1 which increased by only around 3 hrs (table 4.2).

| Oxygen ($O_2$) | H460 | A549 | Calu-1 |
|---|---|---|---|
| **21%** | 20.21 | 30.94 | 27.95 |
| **0.1%** | 25.86 | 39.61 | 30.54 |

**Table 4.2:** Doubling times (hours) of non-small lung cancer cells (H460, A549, Calu-1) cultured under different oxygen levels (i.e. normoxia (21% $O_2$) and hypoxia (0.1% $O_2$))

Optical microscope images of the cells at the 24 hour time-point for each cell line in normoxia and hypoxia are shown in figure 4.10, where a clear reduction in growth in the lower oxygen environment is present for all cell lines. Moreover, cell morphology appeared influenced by the lower $O_2$ levels, with H460 increasing in size, and A549 and Calu-1 displaying more elongated shapes as compared with the respective normoxic cells.

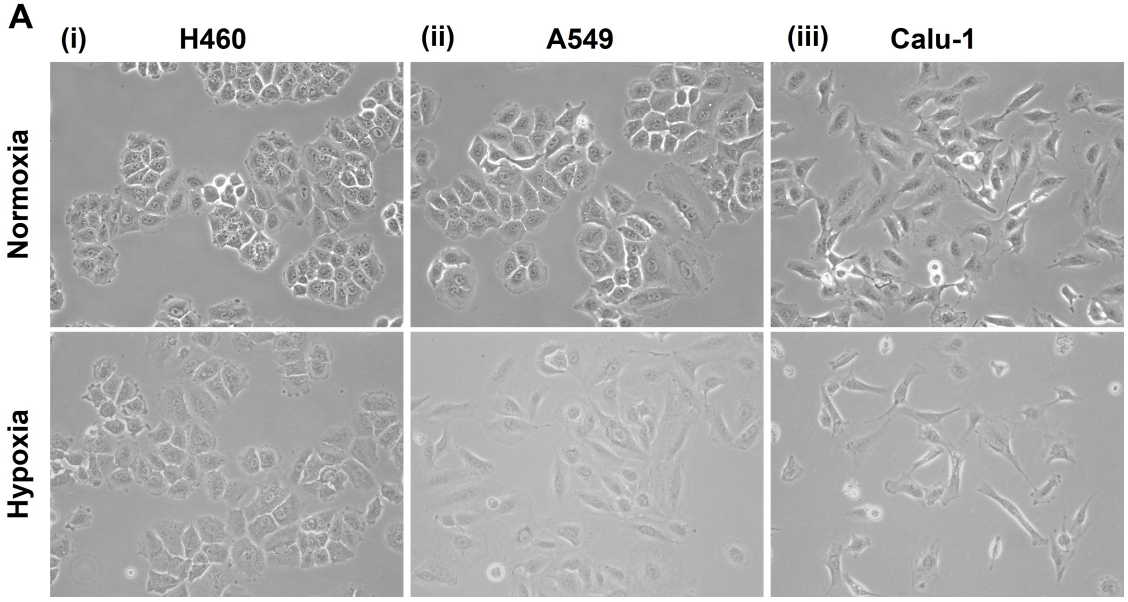


**Figure 4.10: A)** Brightfield (BF) images of NSCLC cell lines (**(i)** H460, **(ii)** A549, **(iii)** Calu-1) in normoxia (21% $O_2$) **(top)** and hypoxia (0.1% $O_2$) **(bottom)** at 24 hhrs post-seeding. Images were acquired using Nikon widefield microscope at 20X magnification.

Cancer cells have acquired a readiness to adapt to a reduced oxygen environment as it is a trait of tumours to exhibit oxygen heterogeneity throughout the tumour mass. The cell growth is indicative of this, but of course there are many cellular factors and complex mechanism involved in their hypoxic adaption which contribute to radio-resistance and will be investi-

gated throughout the thesis. The next section, however, will first focus on investigating the radio-response of the three cancer cell lines under both oxygen conditions.

### 4.3.2 Radio-response of lung cancer cell lines under different oxygen conditions

The different radio-responses of H460, A549, Calu-1 under normal oxygen and low oxygen levels were investigated in this section. Cells were irradiated using low energy photons (225keV, Faxitron) and subsequent clonogenic assays were conducted. Prior to irradiation, cells were incubated in both normoxia (21% $O_2$) and 48 hrs in hypoxia (1% $O_2$) in order to adapt the cells to oxygen depletion before exposing them to severe hypoxia (0.1% $O_2$) and IR. Although cell seeding numbers remained constant for both oxygen conditions, a higher dose with a factor increase of 2 was used for hypoxic cells compared with normoxic cells, to account for the higher cell survival in the lower oxygen condition. Therefore, while normoxic cells were irradiated with 2, 4, and 8 Gy, hypoxic (0.1% $O_2$) cells were irradiated with 4, 8 and 16 Gy. Images acquired at 24 hrs after irradiation in normoxia and hypoxia show their growth response and different morphologies post-IR (figure 4.11 and 4.12 ).

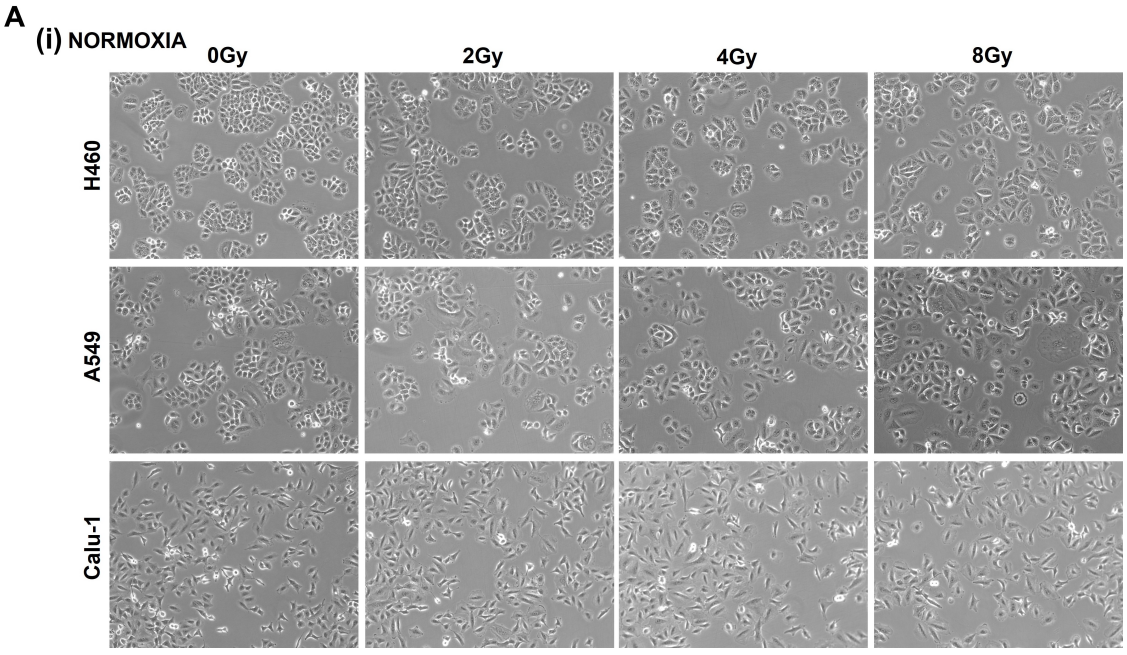


**Figure 4.11: A)** Brightfield (BF) images of NSCLC cell lines (H460, A549, Calu-1) in **(i)** normoxia (21% $O_2$) at 24 hrs post-irradiation (IR) with X-ray doses of 2, 4, 8 Gy. Images were acquired using Nikon widefield microscope at 10x magnification.

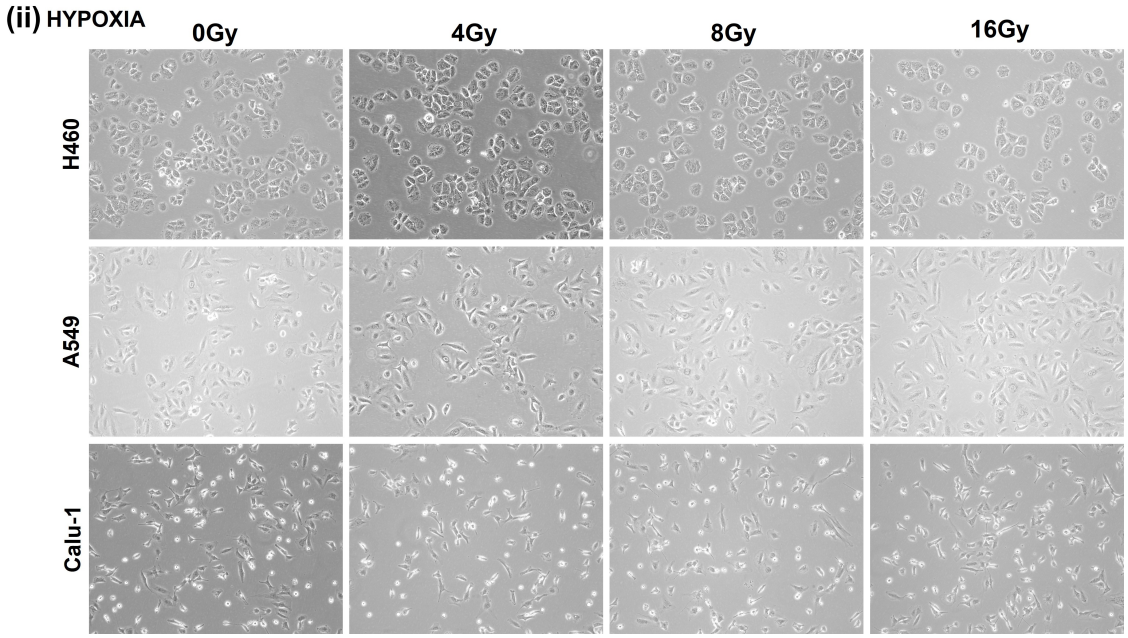


**Figure 4.12:** Brightfield (BF) images of NSCLC cell lines (H460, A549, Calu-1) in **(ii)** hypoxia (0.1% $O_2$), 24 hrs post-irradiation (IR) with X-ray doses of 4, 8, 16 Gy. Images were acquired using Nikon widefield microscope at 10x magnification.

The results from the clonogenic assays for the three lung cancer cell lines, which were analysed approximately 14 days after irradiation, are plotted in figure 4.13.

Cell survival plots in normoxia (figure 4.13) clearly indicate that H460 had the lowest cell survival ability in comparison to the other two cell lines (i.e. A549, Calu-1) after irradiation for all the doses. The survival fractions (SF) for A549 and Calu-1, on the other hand, were rather similar apart from a slightly higher SF for A549 at 8 Gy. However, after irradiation with hypoxic doses, all cell lines had similar SF profiles and exhibited a more radio-resistant response compared to their normoxic counterparts, indicating that hypoxia influenced cell radio-resistance, but at the same time the diverse intrinsic radiation sensitivity was abolished in reduced $O_2$ conditions. This is further highlighted following analysis of their $\alpha$, $\beta$ values.

The $\alpha$, $\beta$ values were then determined from the clonogenic survival curves produced and reported in 4.3. As mentioned previously the $\alpha$ and $\beta$ values are indicative for the radio-sensitivity of the cancer cells and their ratio describes the degree of curvature and thereby the killing rate of radiation. As expected, the reduced oxygen percentage causes an increase in the $\alpha$ value and a decrease in the $\beta$ value, implicating a more linear curvature with loss of the quadratic component compared with the normoxic profile (figure 4.14). However, this is only

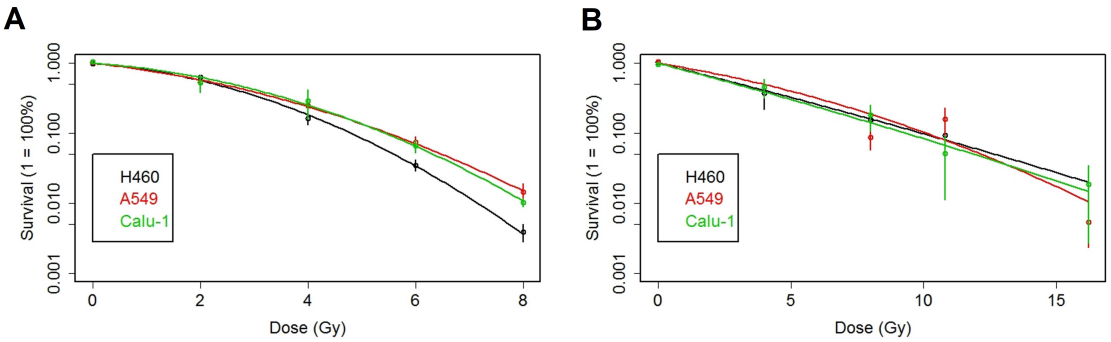


**Figure 4.13:** Clonogenic assays conducted at different oxygen conditions (**A)** 21% $O_2$ and **B)** 0.1% $O_2$ for non-small cell lung cancer cell lines: H460 (colour = black), Calu-1 (colour = red) and A549 (colour = green). Cell lines were incubated in normoxia (21% $O_2$) or hypoxia (0.1% $O_2$) prior to irradiation with doses ranging from 2 - 8 Gy and 4 - 16 Gy in normoxia and hypoxia, respectively. Survival curves were fitted with a linear quadratic equation and corresponding alpha, beta values were recorded in table 4.3

true for H460 and Calu-1 which have $\beta$ values of 0.14 (± 0.07) and 0.12 (± 0.11) in normoxia, respectively, and 0.22 (± 0.05) and 0.23(± 0.098) in hypoxia, respectively. The $\beta$ value for A549, however, decreases in hypoxia (0.14 ± 0.11) in comparison to normoxia (0.19 ± 0.06) and the $\beta$ value only decreases by a factor of 4.8, compared with the large factor decrease for the other two lung cancer cell lines (i .e. 67.3-fold for H460, and 55.4-fold for Calu-1). This indicates that H460 and Calu-1 are potentially more susceptible to oxygen changes than A549 in response to radiation.

| | **H460** | | **A549** | | **Calu-1** | |
|---|---|---|---|---|---|---|
| | **21%** | **0.1%** | **21%** | **0.1%** | **21%** | **0.1%** |
| **alpha ($\alpha$)** | 0.1436 ± 0.0717 | 0.2165 ± 0.0549 | 0.1886 ± 0.0604 | 0.1399 ± 0.1083 | 0.1196 ± 0.1099 | 0.22898 ± 0.09847 |
| **beta ($\beta$)** | 0.0699 ± 0.0141 | 0.0016 ± 0.0036 | 0.0421 ± 0.0076 | 0.0087 ± 0.0078 | 0.0558 ± 0.0141 | 0.00193 ± 0.00640 |
| **ratio ($\alpha/\beta$)** | 2.055 | 138.310 | 4.481 | 16.017 | 2.142 | 118.655 |

**Table 4.3:** Alpha and beta values for lung cancer cell lines (H460, A549, Calu-1) determined from clonogenic assays conducted at different oxygen levels (21%, 0.1% $O_2$)

Another important variable that can be obtained when comparing the survival curves of cells in normoxia and in hypoxia is the oxygen enhancement ratio (OER). The OER factor indicates the protective effects of oxygen from radiation, and is determined by calculating the ratio of doses in normoxia and hypoxia which achieve the same cell survival. The OER factor is

typically reported to be around 2.3 - 3. In this study the OER was determined from figure 4.14 by calculating the ratio of doses in normoxic and hypoxic conditions which resulted in 10% of cell survival (D10). The D50, D10 and D1 values obtained from the clonogenic profiles for each cell line are reported in table 4.4.

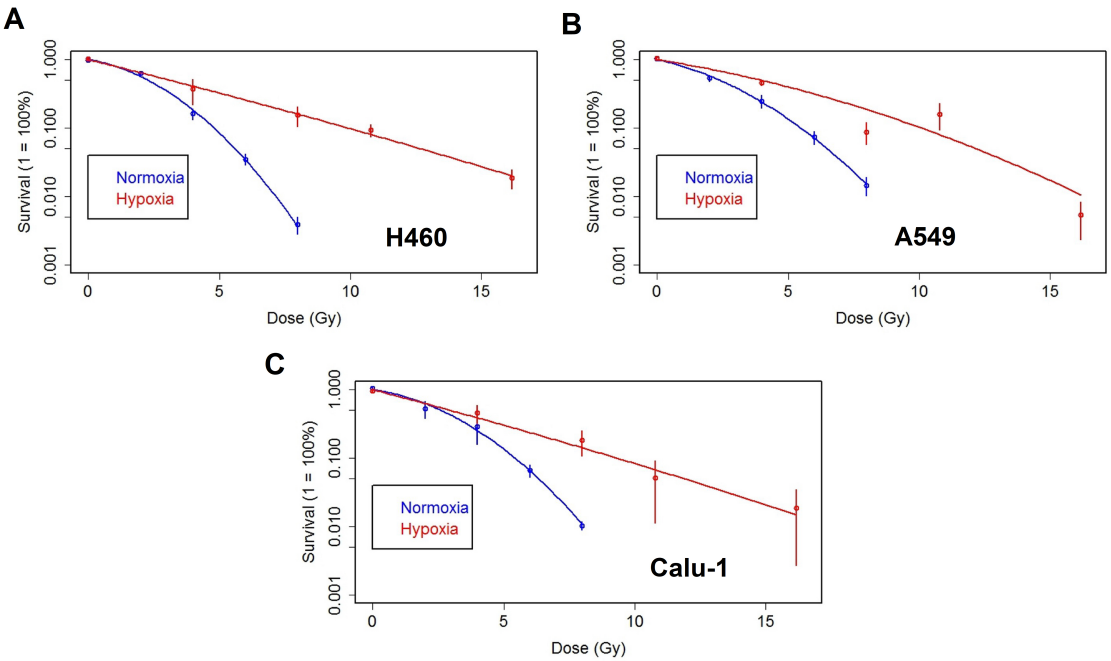


**Figure 4.14:** A) Clonogenic assays of different non-small cell lung cancer cell lines ((i) H460, (ii) A549, (iii) Calu1) in normoxia (21% $O_2$) and hypoxia (0.1% $O_2$), indicating varying radio-responses to varying oxygen levels

For H460 the D10 value was calculated as 4.8 and 9.9 in normoxia and hypoxia, respectively, which resulted in an OER of 2.07, which was highest among the three cell lines. A549 had D10 values of 5.5 (normoxia) and 10.1 (hypoxia), and therefore an OER of 1.84. Calu-1, on the other hand, had the lowest OER among the cell lines with a factor of 1.71 determined from the D10 values of 5.4 in normoxia and 9.3 in hypoxia (table 4.4).

| | **H460** | | **A549** | | **Calu-1** | |
|---|---|---|---|---|---|---|
| | **21%** | **0.1%** | **21%** | **0.1%** | **21%** | **0.1%** |
| **D1** | 7.155 | 18.732 | 8.456 | 16.313 | 8.074 | 17.524 |
| **D10** | 4.803 | 9.923 | 5.488 | 10.098 | 5.439 | 9.323 |
| **D50** | 2.285 | 3.131 | 2.395 | 3.971 | 2.612 | 2.954 |

**Table 4.4:** The dose applied to achieve a cell survival of 50% (D50), 10% (D10) and 1% (D1) for each NSCLC cell line (H460, A549, Calu-1) in normoxia (21% $O_2$) and hypoxia (0.1% $O_2$). The ratio of the D10 values in both oxygen conditions was used to calculate the OER factor.

Based on the results in this section, it is clear that the survival of NSCLC cells is dependant on the percentage of oxygen at the time of irradiation. However, in addition to oxygen level, many other factors contribute to the survival of cell post-IR, including the repair capability of the cell lines and how this is affected by low oxygen levels. For this reason, the next section investigates the initial double strand breaks induced post-IR (30 min) and also the remaining DSBs at 24 hrs post-IR which provides an indication of the repair ability of each cell line.

### 4.3.3 DSB detection after IR in normoxia and hypoxia

Ionising radiation eradicates cancer cells by inducing DNA damages including double strand breaks (DSBs), and forces cells into cycle arrest resulting ultimately in cell death if reparation is not possible. Following radiation-induced DNA DSBs, cells respond by phosphorylating multiple H2AX histones, forming $\gamma$H2AX foci at the damage site, which in turn can be detected, visualised and quantified through specific fluorescent antibodies. The majority of damage or the maximum number of foci (i.e. DSBs) occur within 30 min from the time of IR (maximal peak), after which cell responses kick-in and reparation processes begin (225) and, once repaired, $\gamma$H2AX foci are not detectable due to their dephosphorylation. The maximum and the declination of foci over time are both dose- and cell- type dependant and provide valuable information on the repair capabilities of the cells and are therefore an indication of the cellular initial radio-resistance.

In this study, the $\gamma$H2AX foci of the three lung cancer cell lines (H460, A549 and Calu-1) following photon irradiation were assessed at 30 min - to investigate the maximum number of foci induced - and at 24 hrs post-IR - to understand and provide an indication of the repair capabilities of the cells under normoxic (21% $O_2$) and hypoxic conditions (0.1% $O_2$). Samples were then fixed and stained at their respective time-points as outlined in section 4.2.3, and imaged using a confocal microscope (section 4.2.10). The number of DSB foci per cell (FPC) for each cell line 30 min and 24 hrs after X-ray irradiation under both oxygen conditions can be seen in figure 4.15A and B. Their respective representative confocal images can also be seen in figure 4.16 and 4.17 for the normoxic and hypoxic samples, respectively.

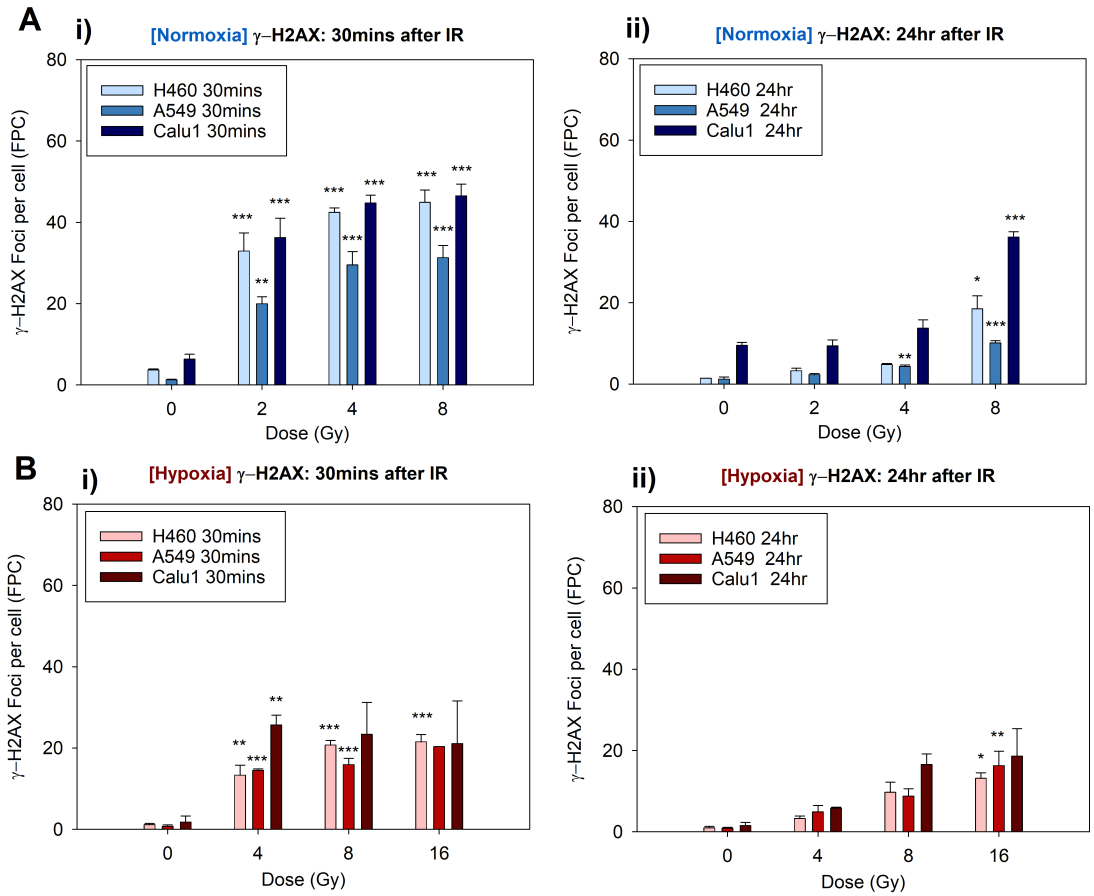


**Figure 4.15:** Detection of double strand breaks (DSBs) in NSCLC cell lines (H460, A549 and Calu-1) using immunofluorescent staining of γH2AX foci following IR under different oxygen conditions. **A.** Normoxia (21% $O_2$) samples at **i)** 30 min and **ii)** 24 hrs post-IR using doses of 2, 4, 8 Gy. **B.** Hypoxia (0.1% $O_2$) samples at **i)** 30 min and **ii)** 24 hrs post-IR using doses of 4, 8, 16 Gy. Samples were analysed using confocal microscopy with a sample size of >100 cells per replicate. The data represents mean foci count per cell with error bars (SEM) established from 3 individual experiments (n = 3). Each cell line was statistically compared to their non-IR control sample (one-way ANOVA test). *P<0.05, **P<0.01, ***P<0.001.

The normoxic DSB results at 30 min post-IR indicated a dose dependant increase for all cell lines, with H460 and Calu-1 having similar profiles and a higher number of FPC for all doses in comparison to A549. For H460, the FPC at 30 min post-IR in normoxia was 32.96 (±4.45), 42.48 (±1.07), 44.92 (±3.03) for doses of 2, 4, and 8 Gy, respectively. For Calu-1 in normoxia, the FPC obtained were 36.22 (±4.78), 44.79 (±1.90) and 46.51 (±2.87) for the same doses. The FPC for normoxic A549 post-IR, however, were slightly lower than the other two cell lines with values of 19.25 (±0.15), 29.52 (±3.28) and 31.29 (±2.99), respectively. These results are plotted in figure 4.15A(i) and all were found to be statistically significant compared to their non-IR control samples which had FPC of 3.72 (±0.21), 1.25 (±0.15) and 6.37 (±1.18) for H460, A549 and Calu-1, respectively. In hypoxia, the FPC was lower for all cell lines at 30 min post-IR, even

with the OER factor applied to the dose (figure 4.15B(i)). However, FPC were in fact similar for each cell line. The FPC for H460 following doses of 4, 8, 16 Gy were 13.31 ($\pm$2.50), 20.73 ($\pm$1.16) and 21.52 ($\pm$1.82), respectively. For A549, these were 14.51 ($\pm$0.39), 15.92 ($\pm$1.54) and 20.35, respectively, and for Calu-1 the FPC measured for each dose were 25.66 ($\pm$2.44), 23.28 ($\pm$7.84) and 21.08 ($\pm$10.51), respectively.

After 24 hrs from X-ray exposure, the normoxic samples had repaired a considerable amount of foci per cell for all cell lines compared with their peak foci count at 30 min post-IR. In fact, for H460, the FPC were reduced to 3.28 ($\pm$0.62), 4.78 ($\pm$0.29) and 18.54 ($\pm$3.16) for the normoxic doses of 2, 4 and 8 Gy, respectively. For A549, the FPC after IR with the same doses were similar to H460 with the exception of the high dose of 8 Gy. In fact, the FPC were 2.28 ($\pm$0.30), 4.33 ($\pm$0.38) and 10.14 ($\pm$0.57), respectively. Calu-1, instead, had higher FPC for each dose, possibly due to the already high basal number of foci of 9.53 ($\pm$0.71). The FPC for Calu-1 at the 24 hrs time-point under the same oxygen conditions were therefore 9.41 ($\pm$1.46), 13.75 ($\pm$2.03) and 36.15 ($\pm$1.31) following IR of 2, 4 and 8 Gy, respectively. These data can be seen plotted in figure 4.15A(ii). In hypoxia, the residual damages at 24 hrs were less than in normoxia, but the dose dependency remained consistent for all cell lines, as can be seen in figure 4.15B(ii). Following IR with doses of 4, 8, and 16 Gy, the FPC for H460 at 24 hrs time-point were 3.29 ($\pm$0.60), 9.73 ($\pm$2.51) and 13.15 ($\pm$1.39), respectively. Similarly for A549, the FPC for each dose were 4.89 ($\pm$1.61), 8.77 ($\pm$1.85) and 16.27 ($\pm$3.60), respectively. Instead, for Calu-1 at the same time-point, the FPC were slightly higher with values of 5.83 ($\pm$0.23), 16.58 ($\pm$2.60) and 18.63 ($\pm$6.74), respectively.

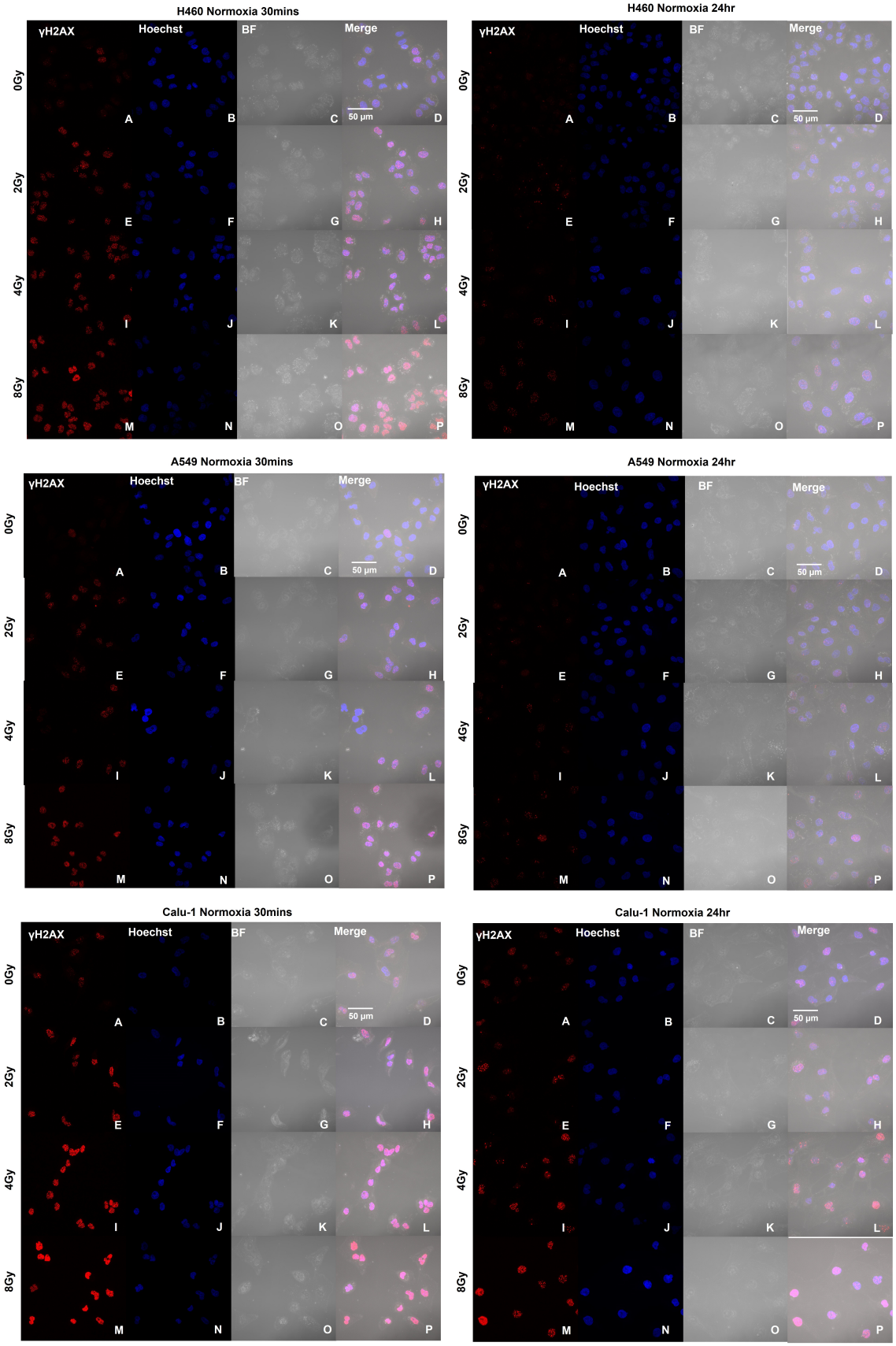


**Figure 4.16:** Representative confocal microscopy images (40x magnification) of normoxic NSCLC cell lines (**H460** (top), **A549** (middle), **Calu-1** (bottom)) in **normoxia** indicating irradiated (2, 4, 8 Gy) and control (0 Gy) samples following immunostaining of $\gamma$H2AX foci at time-points of **30 min** (left) and **24 hrs** (right) post-IR.

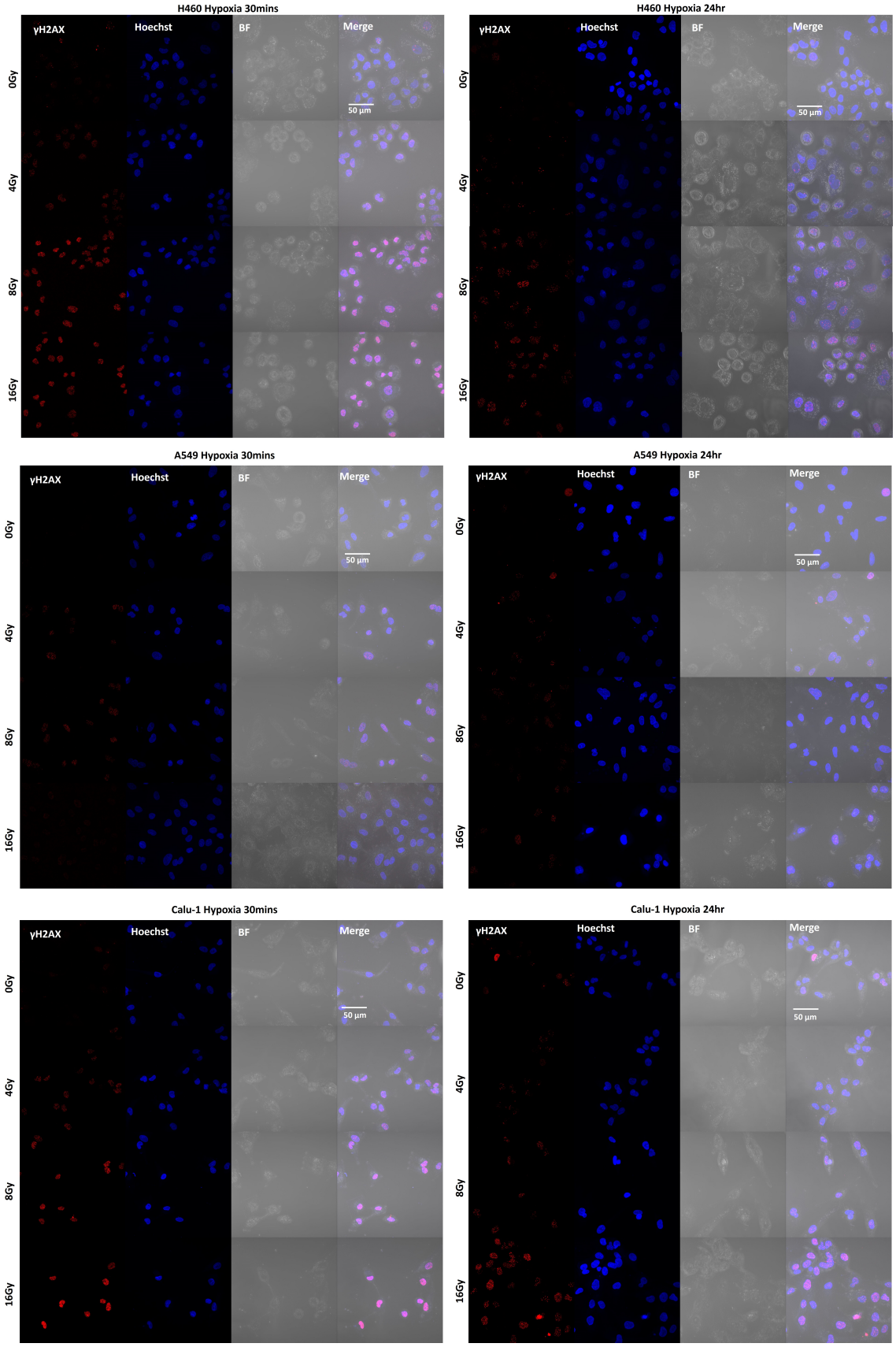


**Figure 4.17:** Representative confocal microscopy images (40x magnification) of hypoxic NSCLC cell lines (**H460** (top), **A549** (middle), **Calu-1** (bottom)) in **hypoxia** indicating irradiated (4, 8, 16 Gy) and control (0 Gy) samples following immunostaining of $\gamma$H2AX foci at time-points of **30 min** (left) and **24 hrs** (right) post-IR

The repair capacity of the cells can be determined from the ratio of foci at 30 min and 24 hrs as shown in figure 4.18A and reported in table 4.5. It is evident that with increasing doses, the repair capacity decreased for all cell lines in both oxygen conditions. However, the repair ability appeared to be significantly lower in hypoxia compared with normoxia and cell type-dependant. In fact, A549 had the highest repair ability in normoxia, whereas in hypoxia H460 had the more efficient damage repair. Calu-1, on the other hand, showed very poor ability to repair foci in both oxygen conditions, indicating potentially insufficient or unstable repair pathways that are independent from the oxygen concentration.

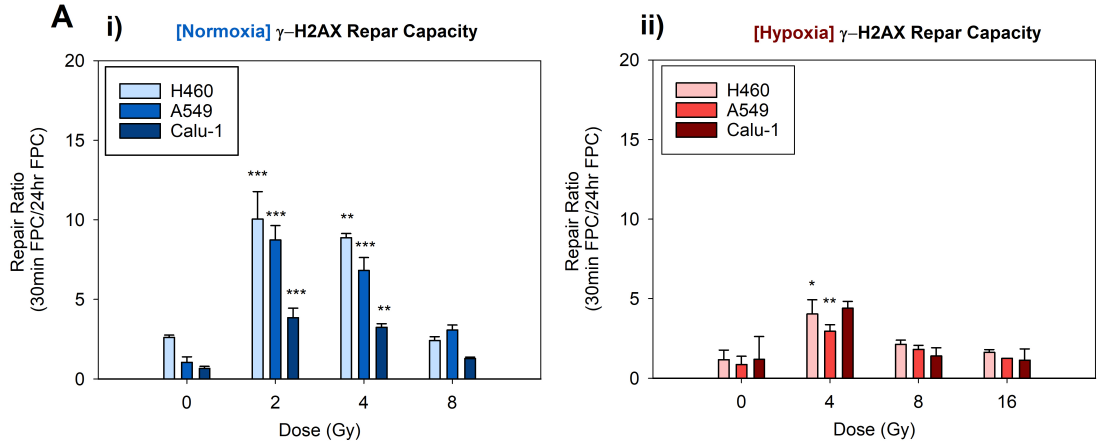


**Figure 4.18: A.** Repair capacity of the H460, A549 and Calu-1 determined by the ratio of FPC at 30 min and 24 hrs in **i)** Normoxia (21% $O_2$) and **ii)** Hypoxia (0.1% $O_2$). Samples were analysed using confocal microscopy with a sample size of >100 cells per replicate. The data represents mean foci count per cell with error bars (SEM) established from 3 individual experiments (n = 3). Each cell line was statistically compared to their non-IR control sample (one-way ANOVA test). *P<0.05, **P<0.01, ***P<0.001.

| | Normoxia | | | | Hypoxia | | | |
|---|---|---|---|---|---|---|---|---|
| | **0 Gy** | **2 Gy** | **4 Gy** | **8 Gy** | **0 Gy** | **4 Gy** | **8 Gy** | **16 Gy** |
| **H460** | 2.61 ±0.15 | 10.05 ±1.72 | 8.88 ±0.26 | 2.42 ±0.23 | 1.17 ±0.60 | 4.04 ±0.89 | 2.13 ±0.26 | 1.64 ±0.16 |
| **A549** | 1.05 ±0.34 | 8.74 ±0.90 | 6.82 ±0.81 | 3.09 ±0.31 | 0.86 ±0.52 | 2.97 ±0.40 | 1.81 ±0.26 | 1.25 ±0 |
| **Calu-1** | 0.67 ±0.13 | 3.85 ±0.60 | 3.26 ±0.21 | 1.29 ±0.08 | 1.19 ±1.43 | 4.40 ±0.43 | 1.41 ±0.51 | 1.13 ±0.71 |

**Table 4.5:** Factor reduction from peak foci at 30 min to residual foci at 24 hrs post-IR. The repair capacity of H460, A549 and Calu-1 in normoxia (21% $O_2$) and hypoxia (0.1% $O_2$) determined from the ratio of the FPC at 30 min and at 24 hrs post-IR (i.e. (FPC at 30 min)/(FPC at 24 hrs)). Normoxic samples were irradiated with doses of 2, 4 and 8 Gy, and hypoxic samples with 4, 8 and 16 Gy. Error is represented as standard error of the mean (SEM) from three independent experiments (n = 3), with the exception of A549 16 Gy hypoxia, where data represents n = 1.

In addition to evaluating the repair capacity of the cells in each oxygen condition, the protection against DSB damages that hypoxia ensued on each cell line was also measured. The corresponding plots for the initial DSBs (i.e. 30 min post-IR) and remaining DSBs (i.e. 24 hrs post-IR) can be seen in figure 4.19A and 4.19B, respectively. For each cell line a clear reduction in the initial DSB damage in hypoxia compared with normoxia was detectable. However, at 24 hrs post-IR, the lower foci number in hypoxia was only evident at higher doses of 8 Gy for H460 and Calu-1, whereas there was no difference in the amount of residual DSBs for A549 cell line in both oxygen conditions (figure 4.19B(ii)). These results showed a similar enhancement of radio-resistance observed in the clonogenic survival given by the OER. Therefore, the factor difference between the DSBs induced in normoxia compared with hypoxia can be considered as the $OER_{DSB}$. The $OER_{DSB}$ for each cell line is outlined in figure 4.19. H460 had the highest $OER_{DSB}$ at 30 min post-IR with a value of 2.099. This is followed by A549 ($OER_{DSB}$ = 1.98) and Calu-1 ($OER_{DSB}$ = 1.86), which coincides with the OER values reported for the clonogenic assays in section 4.3.2. The $OER_{DSB}$ values at 24 hrs post-IR, however, were reduced for all cell lines, indicating high repair ability in normoxia at low doses up to 4 Gy for all cell lines (figure 4.19B).

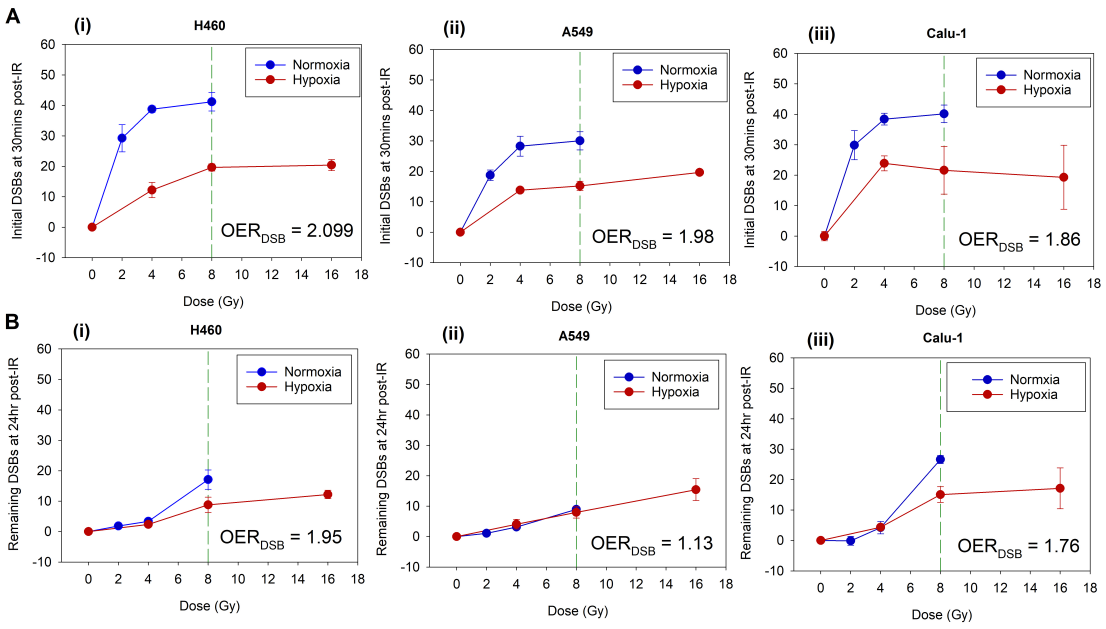


**Figure 4.19:** FPC normalised to non-IR control samples (i.e. 0 Gy) and plotted against dose (Gy) for each time-point **A)** 30 min and **B)** 24 hrs post-IR. All NSCLC cell lines (**(i)** H460, **(ii)** A549 and **iii** Calu-1) were plotted and the $OER_{DSB}$ was evaluated at 8 Gy in both oxygen conditions (normoxia (21% $O_2$) (blue) and hypoxia (0.1% $O_2$) (red)). The $OER_{DSB}$ is indicated by a green reference line on the x-axis.

### 4.3.4 Nuclear hydrogen peroxide ($H_2O_2$) levels of lung cancer cell lines evaluated in normoxia and hypoxia

As reported in previous literature, photons primarily induce indirect damage via free radical and other ROS molecule production created through water radiolysis and concomitant effects exerted on other cellular compartments. Since $H_2O_2$ has a longer half-life compared to the other ROS, it is more stable and thus is renowned as one of the key ROS inducing DSBs. Its levels following photon irradiation of the three NSCLC cell lines were measured in the nucleus of the irradiated cells. The $H_2O_2$ levels were measured under normoxic (21% $O_2$) and hypoxic (0.1% $O_2$) conditions for two different time-points: 1) directly after radiation to investigate the initial levels of $H_2O_2$ produced and potentially correlate with the DSB damages measured at 30 min, and 2) 24 hrs post-IR to investigate the prolonged production of $H_2O_2$ also correlated to secondary ROS production and consequently cells ability to combat the oxidative stress induced by radiation. For these purposes, a $H_2O_2$-specific probe known as nuclear peroxy emerald 1 (NucPE1) was used. NucPE1, developed by Dickinson et al. (222), is a boronate-based probe which accumulates in the nucleus and therefore allows selective measurement of the nucleus $H_2O_2$. Figure 4.20 confirm the localisation of NucPE1 in the nuclei for the three lung cancer cell lines under both oxygen conditions.

In order to evaluate $H_2O_2$ production after X-ray radiation, normoxic cells were irradiated with doses of 2, 4, and 8 Gy and, for the 30 min time-point, immediately stained with 10 µM NucPE1. All samples were stained under low oxygen conditions to prevent excessive oxidation of the dye prior to staining and to allow for comparison between the hypoxic stained cells. The nuclei were extracted from the cells to ensure the fluorescent signal obtained was nuclear specific. For the hypoxic samples, nuclei were extracted in hypoxia. The hypoxic samples at 24 hrs after IR were maintained in the hypoxic conditions (0.1% $O_2$) until the next day and processed as above. In order to better compare the differences between the $H_2O_2$ produced in normoxia and hypoxia in each cell line, the irradiated samples were normalised to their corresponding non-irradiated controls. The normalised plots are shown in figure 4.21.

Results obtained from the normoxic samples 30 min indicated an increasing $H_2O_2$ production with increasing irradiation dose for A549 and Calu-1, whereas for H460, although an increase was seen with 2 Gy compared to its non-irradiated control, similar signals were produced for higher doses with a clear plateau of the profile (figure 4.21A(i), (ii) and (iii)). Moreover,

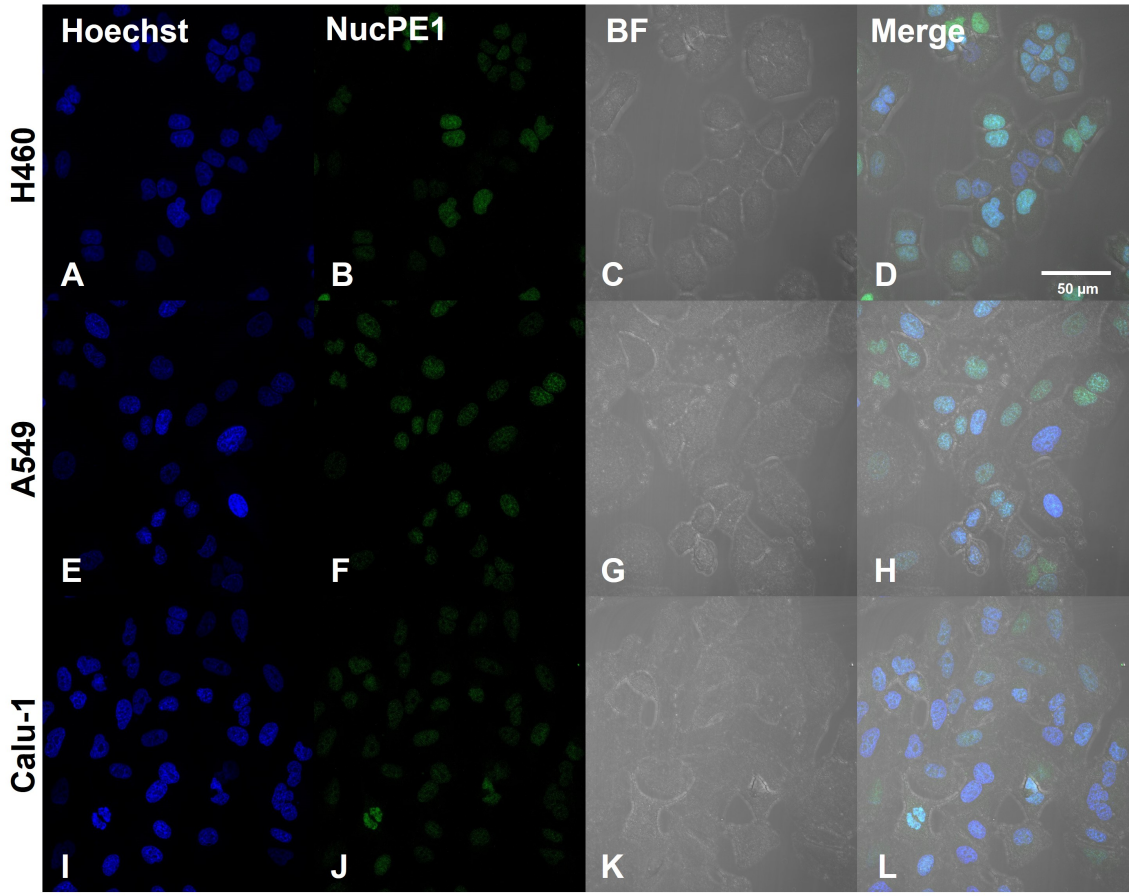


**Figure 4.20:** Nuclear hydrogen peroxide ($H_2O_2$) in normoxic H460 (Top: A-D), A549 (Middle: E-H) and Calu-1 (Bottom: I-J) after staining with Hoechst and NucPE1 (10 µM), and imaging using a confocal microscope with magnification of 40x. Scale bar represents 50 µm.

H460 and A549 appeared to have a higher nuclear $H_2O_2$ than Calu-1 when stained directly after irradiation based on their basal levels (data not shown). After 24 hrs from IR, the same trend was maintained for normoxic A549 and Calu-1 with increasing dose inducing an increase in prolonged $H_2O_2$ signal (figure 4.21B(i), (ii) and (iii)). When analysing hypoxic samples, however, there was not a clear dose induction of $H_2O_2$ production observed directly after irradiation (30 min) in all cell lines, with Calu-1 showing an increase at 8 Gy and a reduction at 16 Gy (figure 4.21A(i), (ii) and (iii)). At 24 hrs post-IR in hypoxia, Calu-1 was also the only cell line showing an increase of $H_2O_2$ levels at higher doses (8 and 16 Gy)(figure 4.21B(i), (ii) and (iii)). The results therefore highlighted that radiation can induce $H_2O_2$ production and a dose response can be observed, only if there is a sufficient amount of oxygen present for the necessary chemical reactions to occur. Therefore, in the nuclei, where the DNA as the main target of radiation therapy is localised, the hypoxic condition prevents excessive radiation-induced oxidative stress.

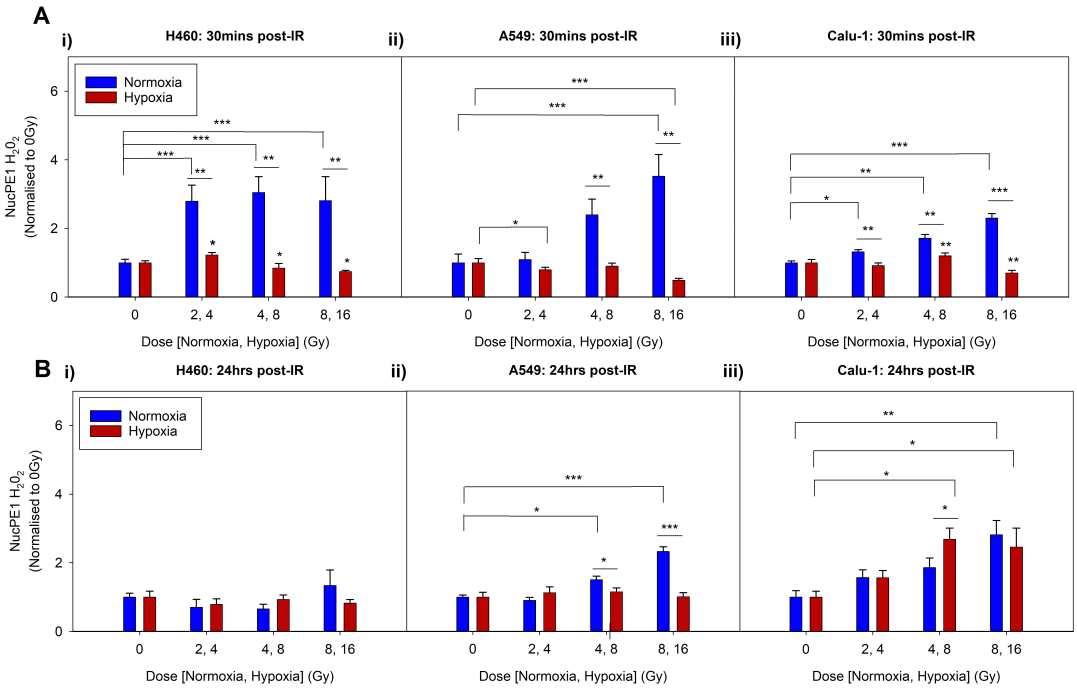


**Figure 4.21:** Normalised plot of hydrogen peroxide ($H_2O_2$) production post-IR detected using NucPE1 in the nucleus of H460, A549, Calu-1 cultured at 21% $O_2$ and 0.1% $O_2$) and measured at different timepoints. **A)(i)** H460, **(ii)** A549, and **(iii)** Calu-1 at 30 min post-IR; **B)(i)** H460, **(ii)** A549, and **(iii)** Calu-1 at 24 hrs post-IR; Cells were stained with NucPE1 (10 µM) and measured using a flow cytometer. Each sample was normalised to their non-IR control (i.e. 0 Gy) and statistically compared to their normoxic control sample (student t-test). Error bars are represented as SEM. *P<0.05, **P<0.01, ***P<0.001 (n = 3).

As mentioned previously, photons primarily induce damage on the DNA through indirect mechanisms via the creation of ROS. The immediate $H_2O_2$ data obtained post-IR for each cell line was therefore plotted against the DSB data from section 4.3.3 to determine if a correlation could be found. Each sample was again normalised to their non-irradiated control in hypoxia and normoxia and the plots can be seen in figure 4.22. In normoxia, a linear dependence of the DSBs measured at 30 min post-IR and the $H_2O_2$ produced at IR is present for all cell lines, indicating that the DSBs induced were potentially a result of the IR-induced $H_2O_2$. However, more doses would be required to confirm this positive relationship. For the hypoxic cells on the other hand, no correlation between the DSB at 30 min and the IR-induced $H_2O_2$ were observed and therefore causality can not be assumed, indicating again that hypoxia most likely played an important role in protecting cells from IR.

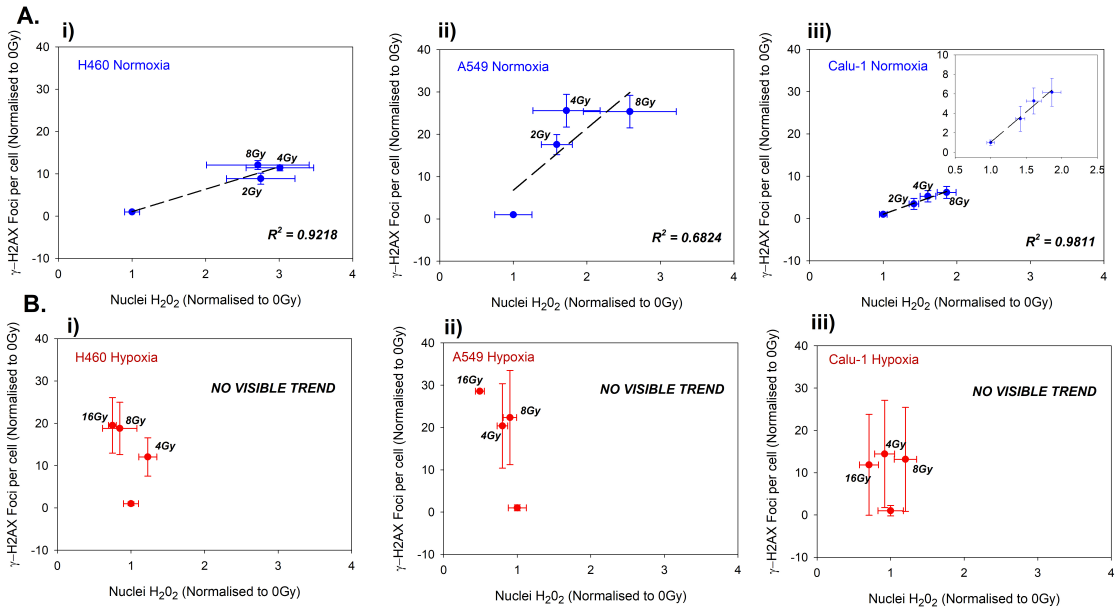


**Figure 4.22:** DSBs per cell measured at 30 min post-IR (normalised to 0 Gy control) plotted against Nuclear $H_2O_2$ levels (normalised to 0 Gy control) for doses of 2, 4, 8 Gy in **A)** Normoxia and 4, 8, 16 Gy in **B)** Hypoxia for the NSCLC cell lines **(i)** H460, **(ii)** A549 and **(iii)** Calu-1

### 4.3.5 Cytosolic hydrogen peroxide ($H_2O_2$) levels of lung cancer cell lines evaluated in normoxia and hypoxia

The cytosolic oxidative stress of the three lung cancer cell lines in normoxia and hypoxia was then investigated through using a $H_2O_2$ specific probe, peroxy yellow methyl-ester (PY1-ME (222)), that only localises in the cytosol of the cell as shown in the confocal microscopy images in figure 4.23. Cells were processed in the same way and at the same time as the NucPE1 staining as described in section 4.3.4. The normoxic cells were irradiated with 2, 4 and 8 Gy and stained with PY1-ME (40 µM), either directly after IR or 24 hrs post-IR, after which the signal of the whole cells were acquired at a FACs instrument. The hypoxic cells were incubated in the hypoxic chamber (1% - 0.1% $O_2$) for 48 hrs prior to irradiation with 4, 8, 16 Gy and stained with PY1-ME at the respective time-points. The results from the normoxic and hypoxic samples at 30 min and 24 hrs post-IR can be seen in figure 4.24.

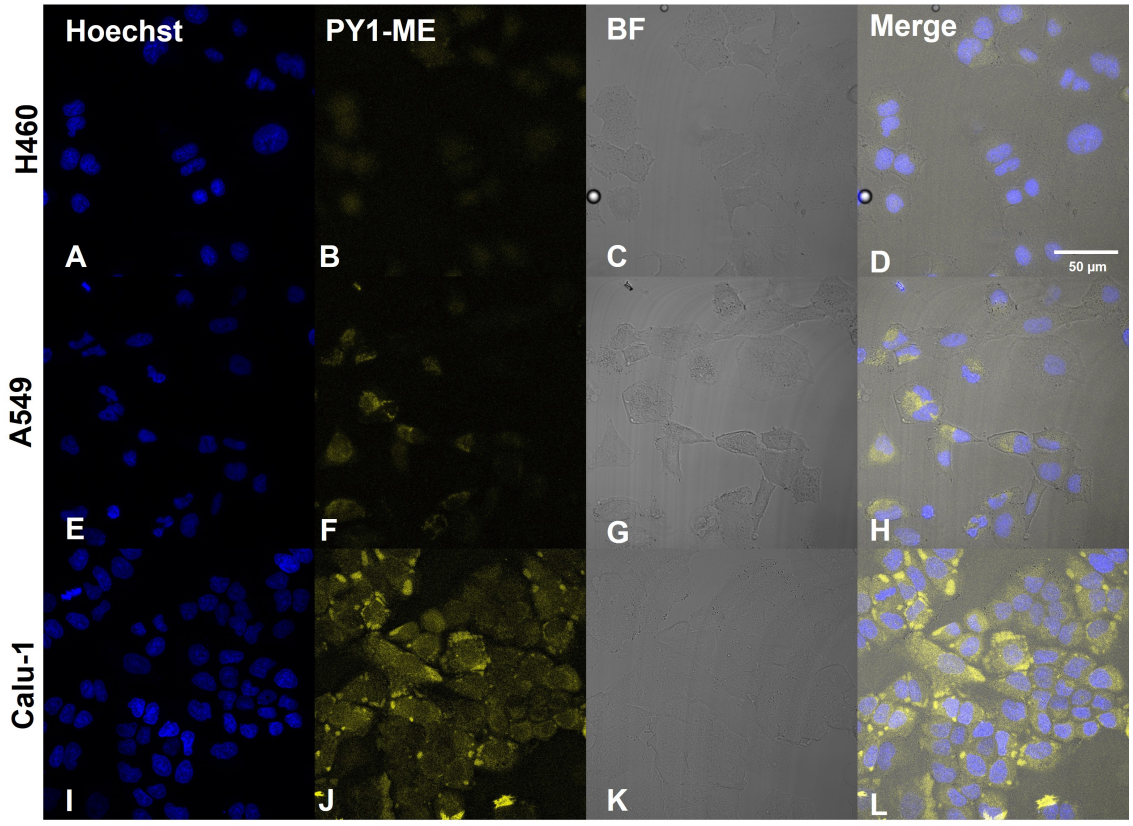


**Figure 4.23:** Cytoplasmic hydrogen peroxide ($H_2O_2$) in normoxic H460 (Top: A-D), A549 (Middle: E-H) and Calu-1 (Bottom: I-J) after staining with Hoechst and PY1-ME (40 µM), and imaging using a confocal microscope with magnification of 40x. Scale bar represents 50 µm.

Based on the results obtained following cytosolic $H_2O_2$ staining, the basal levels of cytoplasmic $H_2O_2$ were found to be different in the 3 cell lines, with Calu-1 showing the highest values, whereas A549 and H460 had similar levels (data not shown). Each sample was, however, normalised to their non-irradiated control from their respective oxygen conditions and the plots can be seen in figure 4.24. In this way, the effect radiation had on the cytosolic $H_2O_2$ production could be compared in both oxygen conditions, as well as a comparison among the three cell lines. From the results in figure 4.24, it is apparent that for H460 at both post-IR time points (30 min and 24 hrs), oxygen induced opposing effects on the cytosolic $H_2O_2$ production. In fact, in normoxia, IR caused an increase of $H_2O_2$ levels in the cytosol 30 min post-IR with increasing dose compared to the non-IR control sample (figure 4.24A(i)). In contrast, the hypoxic samples for H460 at 30 min post-IR had a significant dose-dependant decrease post-IR compared to the non-IR hypoxic control sample. At 24 hrs post-IR (figure 4.24B(i)), similar dose dependencies of $H_2O_2$ levels were observed for H460 cell line for both oxygen conditions (figure 4.24B(i)). In contrast, there were no significant differences of cytoso-

lic $H_2O_2$ production observed between irradiation doses for A549 and Calu-1, nor were there differences between the irradiated samples and their non-IR control (figure 4.24A(ii) and (iii)). For the hypoxic samples acquired at 24 hrs post-IR, however, a statistically significant dose-dependant decrease from the non-IR control sample was observed for both these cell lines (figure 4.24B(ii) and (iii)), and these results were similar to the response observed in the H460 cell line (figure 4.24B(i)).

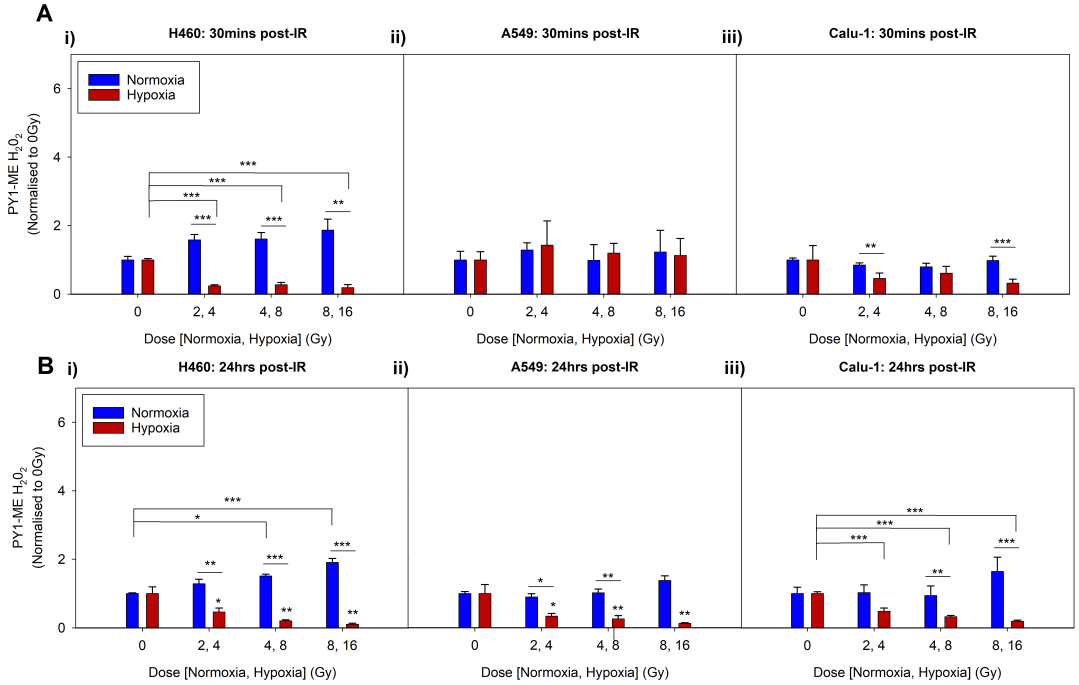


**Figure 4.24:** Normalised plot of hydrogen peroxide ($H_2O_2$) production post-IR detected using peroxy yellow methyl-ester (PY1-ME) in the cytosol of H460, A549, Calu-1 cultured in 21% $O_2$ and 0.1% $O_2$) and measured at different timepoints using flow cytometry. **A)** H460 at **i)** 30 min and **ii)** 24 hrs, post-IR. **A)** 30 min post IR for **i)** H460, **ii)** A549, and **iii)** Calu-1. **B)** 24 hrs post IR for **i)** H460, **ii)** A549, and **iii)** Calu-1. Each sample was normalised to their non-IR control (i.e. 0 Gy) and statistically compared to their normoxic control sample (student t-test) Error bars are represented as SEM. *P<0.05, **P<0.01, ***P<0.001 (n = 3).

### 4.3.6 Measurement of glutathione levels of lung cancer cells in normoxia and hypoxia

From the previous $H_2O_2$ results in section 4.3.4 and section 4.3.5, it was evident that oxidative stress following the treatment with irradiation in the three lung cancer cell lines (H460, A549, Calu-1) was cell type-specific and was affected by the oxygen condition they were exposed to. Based on that, the antioxidant responses of the cells were investigated.

Oxidative stress can induce cellular changes and damages to biological molecules (lipids, proteins and nucleic acids). However, specific $H_2O_2$ scavengers exist in cells to reduce this

stress and maintain redox homeostasis in order to preserve cell functions. One of the most important $H_2O_2$ scavengers is glutathione. Glutathione can exist in a reduced (i.e. GSH) or oxidised form (i.e. GSSG). However, it almost exclusively exists as GSH, due to the highly active and oxidative stress-inducible enzyme glutathione reductase (GSR), which reverts GSSG to GSH as shown in figure 4.25. When the oxidative stress increases, GSSG accumulates and therefore the GSH/GSSG ratio decreases. Hence, changes in the amount of GSH produced and the determination of GSH/GSSG ratio are indications of the cell health status and the oxidative stress. In fact, if there is an increase in $H_2O_2$ production, the amount of oxidised glutathione may increase, and thereby the GSH/GSSG ratio will decrease. For this reason, the ratio of the two forms of glutathione (i.e. GSH/GSSG) was measured directly (i.e. 30 min) and 24 hrs post-IR, under both oxygen conditions (i.e. normoxia 21% $O_2$ and hypoxia 0.1% $O_2$). The obtained results are presented in table 4.6 and 4.7 for normoxia and hypoxia, respectively, and plotted in figure 4.26.

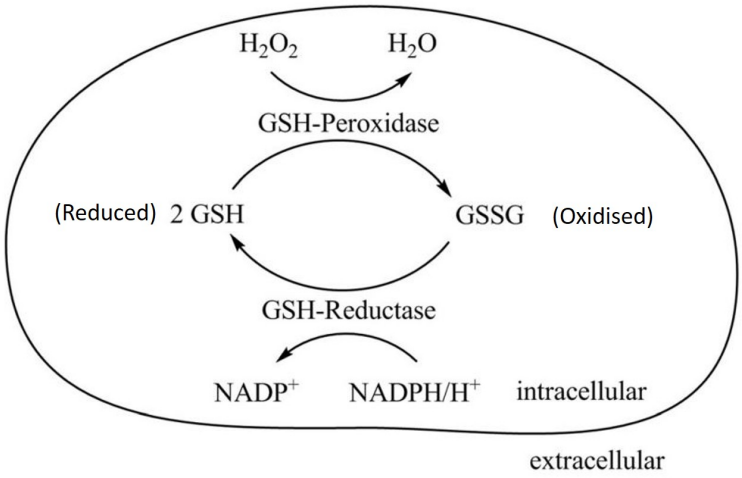


**Figure 4.25:** Schematic illustration of the oxidation of reduced glutathione (GSH) by the enzyme glutathione peroxidase (GPX) which thereby converts $H_2O_2$ to $H_2O$ to form oxidised glutathione (GSSG). GSH can be regenerated by glutathione reductase (GSR) by oxidising NADPH to $NADP^+$. (226)

The results in figure 4.26 show that in normoxia, H460 and A549 had a similar basal ratio of oxidised and reduced glutathione of 6.90 ($\pm$0.53) and 6.64 ($\pm$0.98), respectively, whereas Calu-1 had a basal ratio of almost double that with 12.87 ($\pm$0.28), indicating a low oxidative stress level or a high capacity to combat ROS in comparison to the other two cell lines. Following IR in normoxia, there was no significant change observed in the GSH/GSSG ratio at 30 min for A549 and Calu-1, while H460 showed a not linear response with the doses (figure 4.26A(i)). At 24 hrs post-IR, a dose response, although not significant except for the highest dose, was seen

for both A549 and H460 (figure 4.26A(ii) and table 4.6) in comparison to their non-IR control samples. On the contrary, Calu-1 did not show any dose dependency and their GSH/GSSG ratio still remained at higher levels (i.e. less oxidative stress) as compared to the other two cell lines.

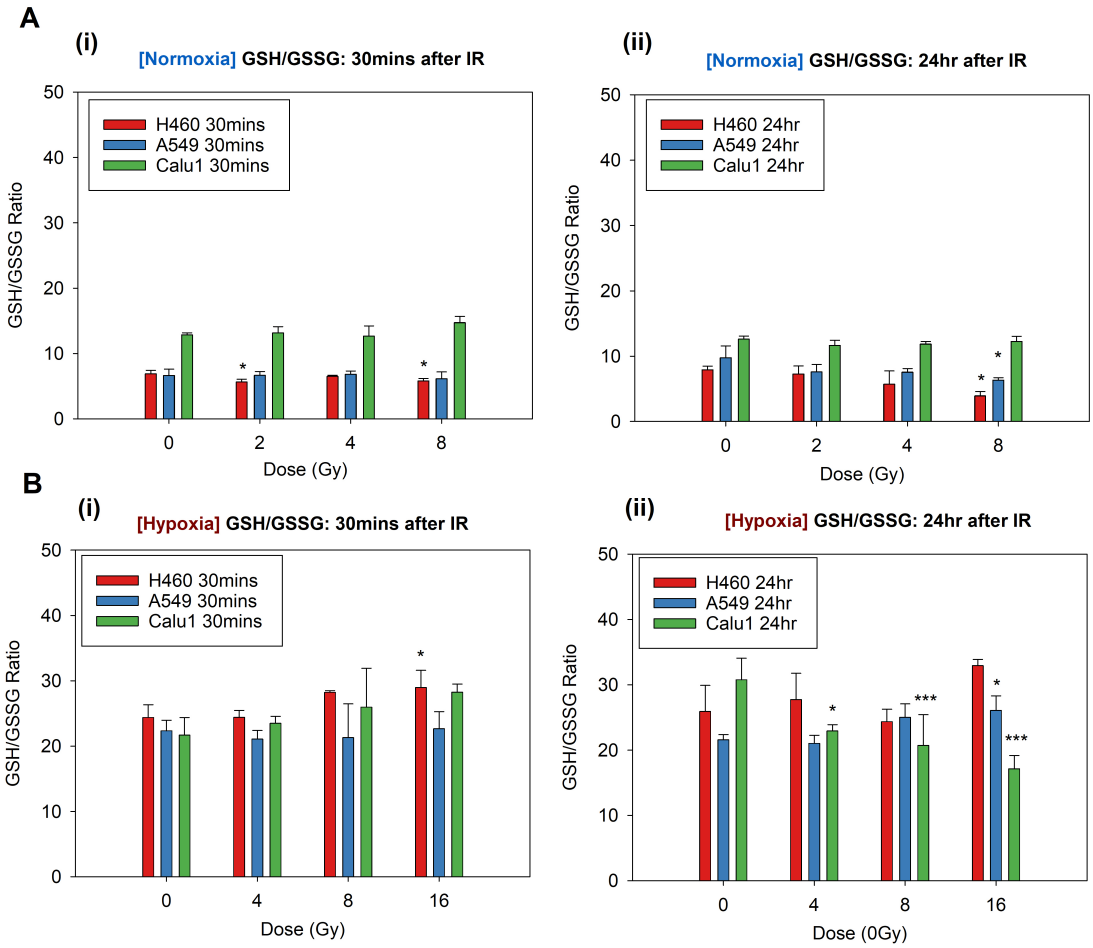


**Figure 4.26:** Ratio of reduced glutathione (GSH) and oxidised (GSSG) levels in relative luminescence units (i.e. GSH/GSSG) of H460, A549, Calu-1 following incubation in **A)** normoxia (21% $O_2$) and **B)** hypoxia (0.1% $O_2$) at time-points **(i)** 30 min and **(ii)** 24 hrs post-IR. Fluorescent signals were acquired by using a microplate reader ClarioStar. Each sample was statistically compared to the non-irradiated control sample (student t-test) and error bars are represented as SD. *P<0.05, **P<0.01, ***P<0.001 (n = 3).

When looking at the hypoxic results (figure 4.26B), a significant increase in the basal GSH/GSSG ratio was observed for all cell lines in comparison to the normoxic samples (figure 4.26B) with values of 24.40 ($\pm$1.95), 22.35 ($\pm$1.60) and 21.71 ($\pm$2.68) for H460, A549 and Calu-1, respectively (table 4.7). This increase from normoxia to hypoxia potentially indicates a large reduction of oxidative stress in the hypoxic cells, possibly due to the low amount of oxygen and therefore a reduced amount of radical production required to induce the oxidative responses. Once irradiated, the hypoxic A549 samples showed no significant change in the GSH/GSSG ratio

with all the doses tested at 30 min post-IR. Although for H460 and Calu-1 hypoxic samples a slight, not significant, increased trend was observable. However, H460 showed a reduction in oxidative stress at the very high dose of 16 Gy indicating that the high dose was the only one able to significantly change the GSH/GSSG ratio and consequently to potentially stimulate the antioxidant responses 4.26B(ii). However, 24 hrs post-IR different behaviours were detectable. While H460 did not show a dose-dependency and A549 displayed a dose increase with a significant value at 16 Gy, a clear decrease in the GSH/GSSG ratio with increasing dose was seen for the hypoxic Calu-1 cells (figure 4.26B(ii) and table 4.7).

| **Normoxia** | **30 min post-IR** | | | | **24 hrs post-IR** | | | |
|---|---|---|---|---|---|---|---|---|
| **(21% $O_2$)** | **0 Gy** | **2 Gy** | **4 Gy** | **8 Gy** | **0 Gy** | **2 Gy** | **4 Gy** | **8 Gy** |
| **H460** | 6.90 ±0.53 | 5.65 ±0.44 | 6.50 ±0.19 | 5.80 ±0.38 | 7.91 ±0.56 | 7.28 ±1.22 | 5.71 ±2.04 | 3.93 ±0.66 |
| **A549** | 6.64 ±0.98 | 6.67 ±0.58 | 6.83 ±0.50 | 6.14 ±1.04 | 9.76 ±1.81 | 7.60 ±1.13 | 7.56 ±0.55 | 6.32 ±0.39 |
| **Calu-1** | 12.87 ±0.28 | 13.17 ±0.95 | 12.67 ±1.56 | 14.73 ±0.96 | 12.62 ±0.46 | 11.65 ±0.79 | 11.85 ±0.38 | 12.26 ±0.78 |

**Table 4.6:** GSH/GSSG ratio of H460, A549, Calu-1 in normoxia (21% $O_2$) after irradiation with doses of 2, 4, 8 Gy at 30 min and 24 hrs post-IR. The ratio of reduced glutathione (GSH) to oxidised glutathione (GSSG) (GSH/GSSG) provides an indication of the oxidative stress in the cells. Each experiment was conducted 3 times (n = 3), and errors are showed as SD.

| **Hypoxia** | **30 min post-IR** | | | | **24 hrs post-IR** | | | |
|---|---|---|---|---|---|---|---|---|
| **(0.1% $O_2$)** | **0 Gy** | **2 Gy** | **4 Gy** | **8 Gy** | **0 Gy** | **2 Gy** | **4 Gy** | **8 Gy** |
| **H460** | 24.40 ±1.95 | 24.42 ±1.04 | 28.23 ±0.25 | 28.99 ±2.63 | 25.92 ±3.99 | 27.74 ±4.02 | 24.38 ±1.88 | 32.95 ±0.94 |
| **A549** | 22.35 ±1.60 | 21.07 ±1.32 | 21.31 ±5.15 | 22.66 ±2.62 | 21.57 ±0.81 | 21.04 ±1.24 | 25.02 ±2.05 | 26.08 ±2.23 |
| **Calu-1** | 21.71 ±2.68 | 23.50 ±1.06 | 25.98 ±5.94 | 28.27 ±1.23 | 30.77 ±3.30 | 22.95 ±0.95 | 20.72 ±4.71 | 17.14 ±2.04 |

**Table 4.7:** GSH/GSSG ratio of H460, A549, Calu-1 in hypoxia (0.1% $O_2$) after irradiation with doses of 2, 4, 8 Gy at 30 min and 24 hrs post-IR. Each experiment was conducted 3 times (n = 3), and errors are SD.

Figure 4.27 reports the results for the normoxic and hypoxic samples, directly comparing each cell line at each IR time-point, thus clearly showing the significant effect that oxygen exhibited on the three cancer cells. For the non-irradiated control samples at 30 min, the factor difference between normoxia and hypoxia varied for each cell line with hypoxia inducing the largest

reduction of the GSH/GSSG ratio, and thereby the oxidative stress, for H460 with a factor of around 3.5. The smallest factor decrease from normoxia to hypoxia, on the other hand, was for Calu-1 with a factor difference of 1.68. For the most part irradiation only enhanced this difference for both cell lines. Interestingly, at 24 hrs the difference between normoxia and hypoxia was increased with increasing dose for H460 and A549 due to the opposing effects irradiation induced in the two oxygen conditions. However, in contrast, Calu-1 showed a decreasing difference between oxygen conditions with increasing dose due to the stable irradiated normoxic samples across all doses.

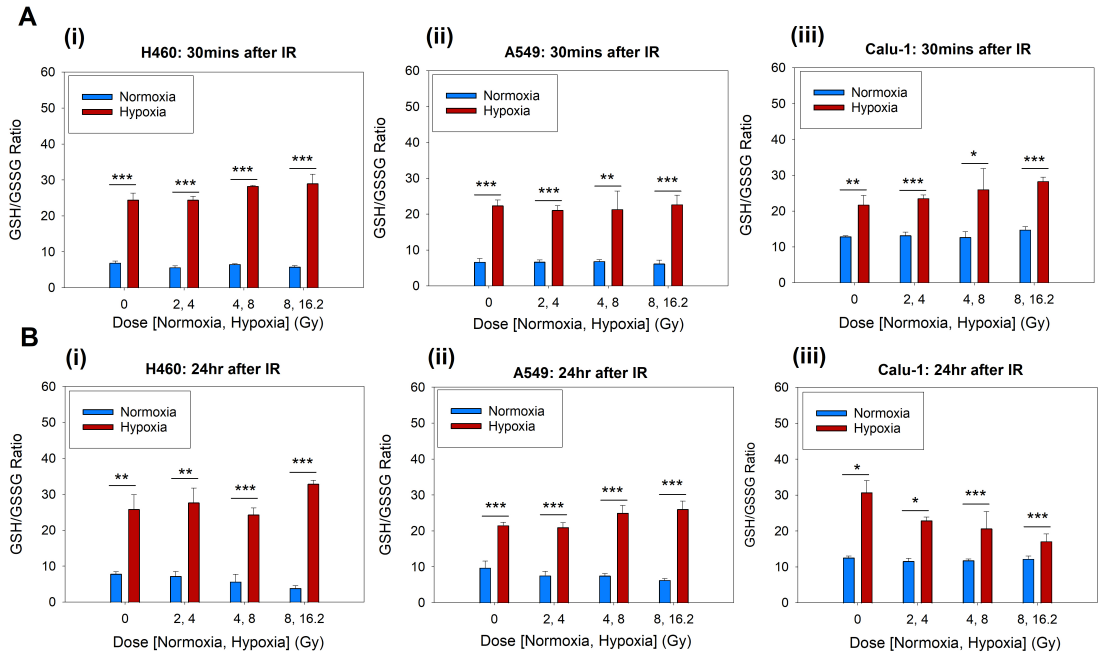


**Figure 4.27: A)** Ratio of GSH/GSSG levels. Comparison between samples incubated in normoxia (21% $O_2$) and hypoxia (0.1% $O_2$) at time-points **(A)** 30 min and **(B)** 24 hrs post-IR for **(i)** H460, **(ii)** A549 and **(iii)** Calu-1. Each sample was statistically compared to the normoxic control sample (student t-test) and error bars are represented as SD. *P<0.05, **P<0.01, ***P<0.001 (n = 3).

The immense difference in the oxidative stress between hypoxia and normoxia is dominated by the decreased amount of GSSG in hypoxia as indicated in figure 4.28 which shows the GSSG and GSH levels separately at 24 hrs after irradiation. The GSH levels were determined by subtracting the GSSG levels from the total glutathione levels (i.e. $GSH_{tot}$ = GSH + GSSG). The levels at 30 min post-IR are not shown since the genetic evaluation of the cells antioxidant capacity will only be conducted on the 24 hrs post-IR time-point. Interestingly, the GSH/GSSG ratio could be altered by changes in either GSH or GSSG contents. Here (figure 4.28), in H460 cells cultured in normoxia, the GSSG levels increased only at high doses of IR (i.e. 4, 8 Gy), whereas the total GSH levels remained unchanged. This suggests that the GSH/GSSG

ratio decreasing trend shown in figure 4.26 was mainly driven by the GSSG content at those doses, while at low doses (2 Gy) the two parameters contributed similarly as the non-irradiated control. For A549 normoxic samples, the total GSH levels dropped at a similar extent for all the doses. However, the GSSG levels remained unaffected by IR, except for the highest dose (8 Gy). In this case, therefore, the GSH/GSSG ratio was more dependant on the total GSH content, while at 8 Gy it was dependent on a combination of both GSH and GSSG. The GSH and GSSG levels for Calu-1 cells in normoxia were both increased after X-ray exposure, thus indicating that changes in both parameters contributed to the ratio.

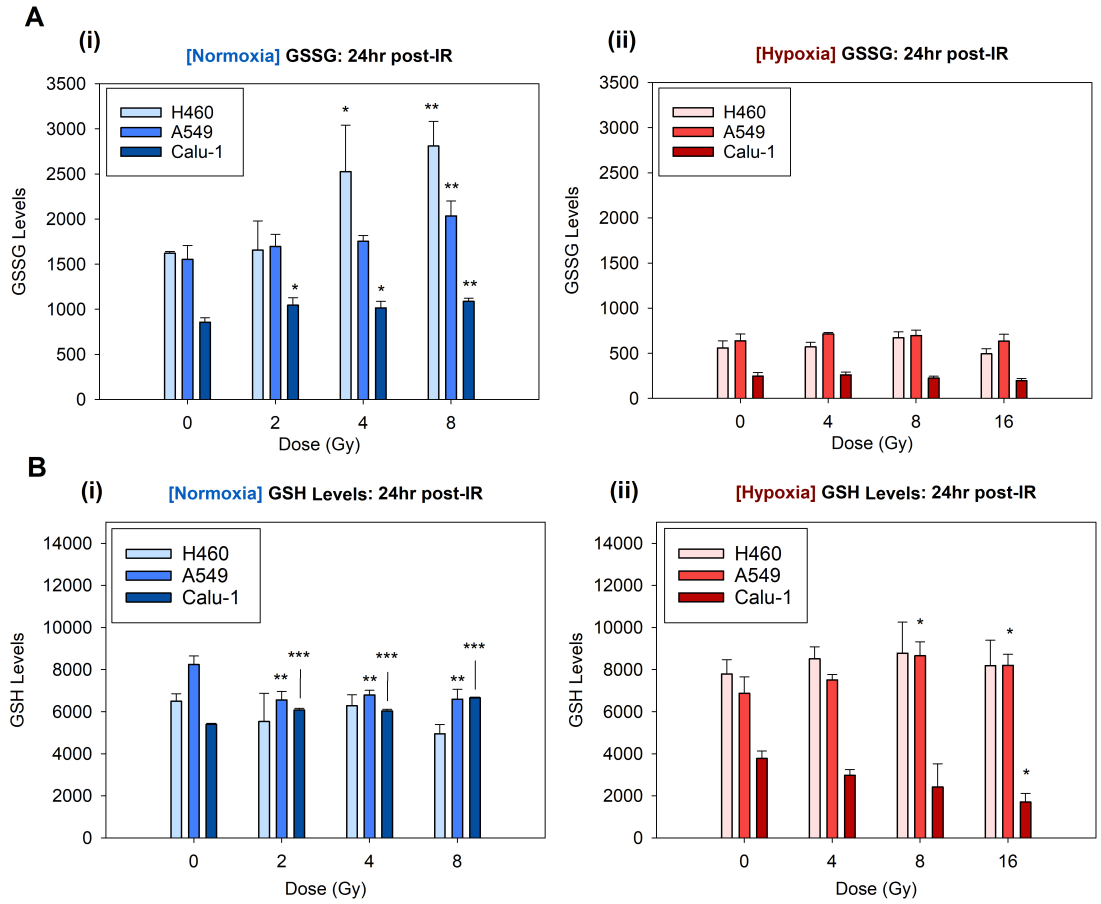


**Figure 4.28: A)** Oxidised glutathione (GSSG) and **B)** Reduced glutathione (GSH) (i.e.Total glutathione - Oxidised glutathione) values of H460, A549, Calu-1 at 24 hrs post-IR following incubation in **(i)** normoxia (21% $O_2$) and **(ii)** hypoxia (0.1% $O_2$). Each sample was statistically compared to the non-irradiated control sample (student t-test) and error bars are represented as SD. *P<0.05, **P<0.01, ***P<0.001 (n = 3).

In hypoxia, irradiation had little or no effect on the GSSG levels in any of the lung cancer cell lines. Additionally, very low $O_2$ conditions also did not exhibit profound effects on the GSH contents. In fact, the GSH levels of A549 and H460 appeared to be only mildly and not

significantly affected, with an increasing trend which only became statistically significant for 8 and 16 Gy in A549 (figure 4.28B(ii)). In normoxic Calu-1, however, an opposite decreasing trend for GSH was observed and for the highest dose (16 Gy) this reduction was significant compared to the control sample. It is therefore evident that in Calu-1 the GSH levels dominated the decrease with dose that was shown in figure 4.26D in hypoxia.

### 4.3.7 Cell cycle progression after IR in normoxia and hypoxia

Radiation is known to indirectly induce changes in the cell cycle by triggering the damage response pathway and thereby potentially blocking cells in the DNA repair checkpoints located along the cell cycle (G0-G1, S and G2-M) as outlined in section 1.3. Since in this study different DNA damage and repair abilities were observed under normoxia (21% $O_2$) and hypoxia (0.1% $O_2$), the cell cycle progression was then investigated for all lung cell lines (H460, A549, Calu-1) in both oxygen conditions (21% $O_2$ and 0.1% $O_2$) at 30 min and 24 hrs after X-ray exposure. The cell cycle of each cell line was measured by flow cytometric analysis taking advantage of nuclear peroxide emerald 1 (NucPE1) staining that is also able to interact with the DNA double helix and therefore can give information on the amount of DNA in the nuclei, which is in turn dependant on the cell cycle phase. The cell cycle results for the normoxic and hypoxic cell lines after IR can be seen in figure 4.29 and 4.30.

As expected, 30 min post-IR in normoxia (figure 4.29A) there were only slight changes observed in the cell cycle progression in comparison to the non-IR control samples. In particular, for H460, an accumulation of nuclei (i.e. cells) in the G0-G1 phase was observed for all the doses (+3.14% for 2 Gy; +5.07% for 4 Gy; +1.93% for 8 Gy) compared to non-irradiated samples, followed by a slight decrease in the S phase (-2.09% for 2 Gy; -3.07% for 4 Gy; -2% for 8 Gy) and a similar profile for all the samples in the G2-M phase, as compared to their respective controls. This indicates that this cell line was mainly, yet slightly, arrested in G0-G1 soon after IR (figure 4.29A(i)). However, this behaviour was more pronounced 24 hrs post-IR (+7.53% for 2 Gy; +14.37% for 4 Gy), which was also associated with a decrease in the S phase with the increasing doses (-4.53% for 2 Gy, -7.55% for 4 Gy). Nevertheless, with the highest dose the block was activated mainly in the G2-M phase of the cycle with a strong reduction of nuclei in the G0-G1 and S phases (-11.57% and -10.52%, respectively) and an accumulation in G2-M phase (+ 21.97% ) (figure 4.29A(i)), as compared with their respective controls.

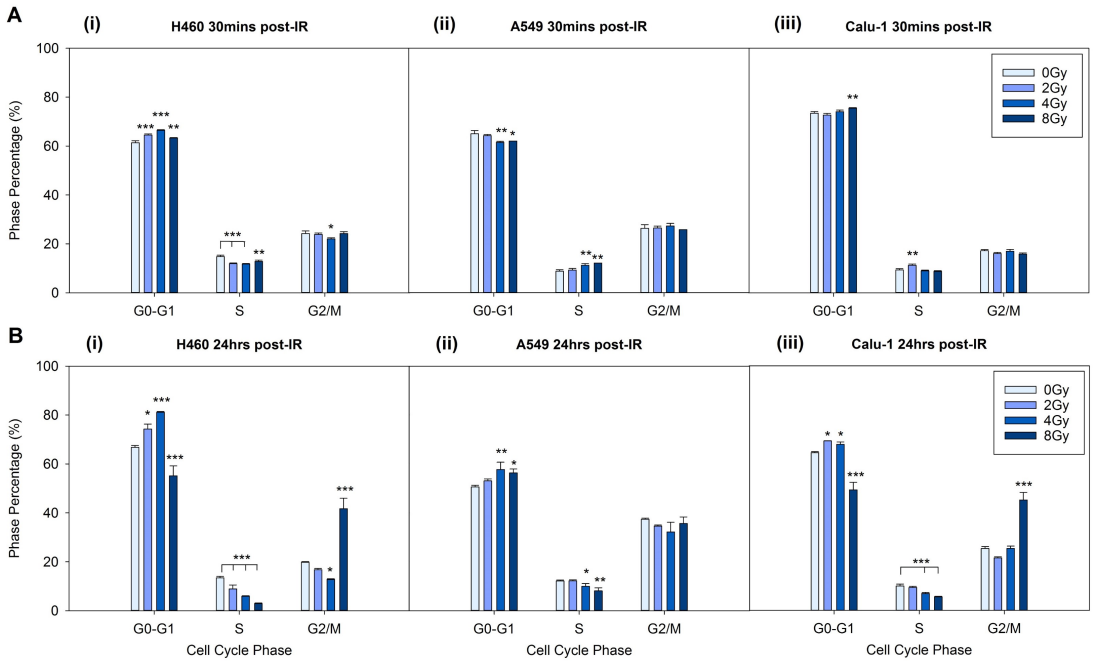


**Figure 4.29:** Cell cycle progression in normoxia (21% $O_2$) indicating the percentage of cells in phases G0-G1, S, G2-M at timepoints of **A)** 30 min post-IR and **B)** 24 hrs post-IR for NSCLC call lines **(i)** H460, **(ii)** A549 and **(iii)** Calu-1. Samples were stained with nuclear peroxy emerald 1 (NucPE1) and analysed using flow cytometry. Each sample was statistically compared to the non-irradiated control sample (student t-test) and error bars are represented as SD. *P<0.05, **P<0.01, ***P<0.001 (n = 3). NOTE: Since the staining was conducted on nuclei only, the mitotic cells are not included in the following cell cycle results.

For A549, 30 min after IR, no effects on the cell cycle were detectable, except for a decrease in the G0-G1 phase for 4 Gy and 8 Gy (-3.5% and -2.96%, respectively) and an increase in the S phase for both (+2.44% for 4 Gy; +3.35% for 8 Gy) (figure 4.29A(ii)). At 24 hrs, only the highest doses showed a slight arrest in the G0-G1 phase (+7.1% for 4 Gy; +5.72% for 8 Gy) with a correspondent decrease of cells in the S phase (-2.15% for 4 Gy; -4% for 8 Gy). However, these results showed that A549 cell cycle was not strongly affected by the X-ray irradiation, potentially indicating either a faulty or a fast repair system (figure 4.29B(ii)). As far as Calu-1 cell cycle is concerned, this cell line did not show a strong influence of the radiation treatments on cell cycle after 30 min, only a very slight increase at 8 Gy in G0-Gl phase (+2%) and for 2 Gy in the S phase (+1.93%) (figure 4.29A(iii). On the other hand, at 24 hrs post-IR, an accumulation of Calu-1 in G0-G1 was reported for 2 Gy (+4.76%) and 4 Gy (+3.33%), with a correspondent reduction of cells in the S-phase (-0.63% for 2 Gy; -3.84% for 4 Gy). Also 8 Gy-treated samples showed a reduction of cells in the S phase (-4.45%) but cells were mainly arrested in the G2-M phase (figure 4.29B(iii)).

The small changes in the cell cycle phases at 30 min post-IR are to be expected due to the cells typically having a longer cell cycle and requiring more time to initiate cell repair responses. At longer time points, the activation of cell cycle blocks showed intercellular variability and, within the same cell line, the activation was dose-dependant.

When lowering the $O_2$ level, IR induced only minor changes in the percent of cells in each phase at 30 min post-IR, as shown in figure 4.30A. For H460, a decreasing trend was observed in the cell population in G0-G1 phase which was statistically significant only at 16 Gy (-3.97%) and was accompanied by a concomitant increase of cells in the S-phase (+2.44%). Additionally, 8 Gy-treated hypoxic H460 were accumulated in the G2-M phase (+4.76%) compared to their non-IR controls (figure 4.30A(i)). Instead, 24 hrs after X-ray treatment, the decrease in G0-G1 cells was larger mainly for 8 Gy and 16 Gy (-13.24% for 8 Gy; 10% for 16 Gy) and resulted in a lot more cells blocked in the G2-M phase (+15.53% for 8 Gy; +17.97% for 16 Gy) (figure 4.30B(i)). A similar trend was also observed for the hypoxic A549 cell line but the decrease was statistically significant for all doses in the G0-G1 phase 30 min after the radiation treatments (-3.17% for 4 Gy; -3.3% for 8 Gy; -11.87% for 16 Gy). In fact, the percentage of cells in G2-M phase was increased 30 min post-IR for all the doses (+4.1% for 4 Gy; +3.5% for 8 Gy; +8.26% for 16 Gy) and only for 16 Gy also in the S phase (+3.03%). A similar profile, but to a bigger extent, was maintained at 24 hrs, where the percentage of A549 nuclei accumulated in the G0-G1 phase was reduced (-17.13% for 4 Gy; -14.2% for 8 Gy; -27.86% for 16 Gy) and it was increased in the G2-M (+17.17% for 4 Gy; +14.84% for 8 Gy; +21.7% for 16 Gy) for all treatments (figure 4.30B(ii)). This indicates that for this cell line, in hypoxic conditions, the block in G2-M was already active soon after IR and became more important after a longer time. On the contrary, Calu-1 showed a bigger portion of cells in the G0-G1 as a basal level, if compared with the other two cell lines in hypoxia. Soon after IR, Calu-1 responded by slightly decreasing the percentage of cells in the G0-G1 (-1.56% for 4 Gy; -1.86% for 16 Gy) and increasing the amount of cells in the S phase for all doses (+0.597% for 4 Gy; +0.697% for 8 Gy; +1% for 16 Gy). However, the dose response of the cell cycle fluctuated (figure 4.30A(iii)). Moreover, IR caused an accumulation of hypoxic Calu-1 cells in the G2-M phase after 24 hrs in a dose-dependant manner which was only significant for 8 Gy and 16 Gy (+7.58% and +10.92%, respectively), although the block in G2-M was much less pronounced compared to the other cell lines (figure 4.30B(iii)).

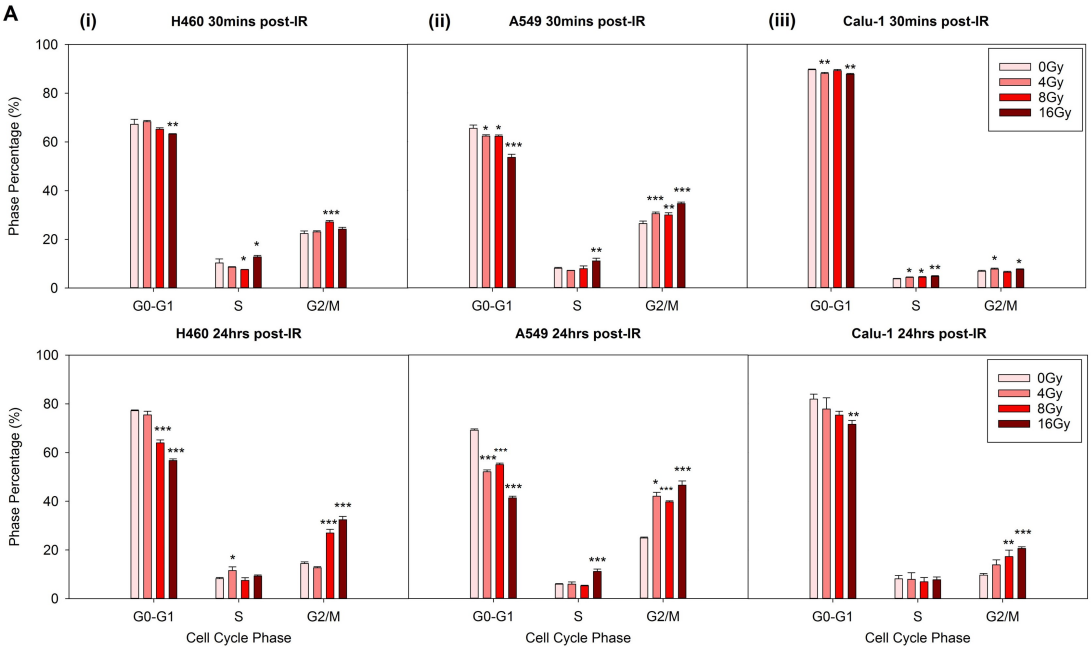


**Figure 4.30:** Cell cycle progression in hypoxia (0.1% $O_2$) indicating the percentage of cells in phases G0-G1, S, G2-M at timepoints of **A)** 30 min post-IR and **B)** 24 hrs post-IR for NSCLC call lines **(i)** H460, **(ii)** A549 and **(iii)** Calu-1. Samples were stained with nuclear peroxy emerald 1 (NucPE1) and analysed using flow cytometry. Each sample was statistically compared to the non-irradiated control sample (student t-test) and error bars are represented as SD. *P<0.05, **P<0.01, ***P<0.001 (n = 3). NOTE: Since the staining was conducted on nuclei only, the mitotic cells are not included in the following cell cycle results.

Since a block in the G2-M was observed in some cases, particularly after IR with high doses in normoxia and hypoxia, the possibility that cells could exit from G2-M arrest and be induced to die after 48 hrs from radiation was tested. This was done by staining with propidium iodide (PI) and analysing the fluorescent signal at the flow cytometer. PI is a membrane impermeable dye which therefore does not accumulate in viable cells, however, in damaged or dying and dead cells it can bind to the DNA by intercalating between base pairs. In this way, it can be determined whether the cells will progress through the cell cycle or die following the G2-M block. It is worth noting that this analysis takes into account all the cell death processes involved, without distinguishing among all the possible mechanisms (i.e. necrosis, apoptosis, or autophagy). The corresponding results can be seen in figure 4.31.

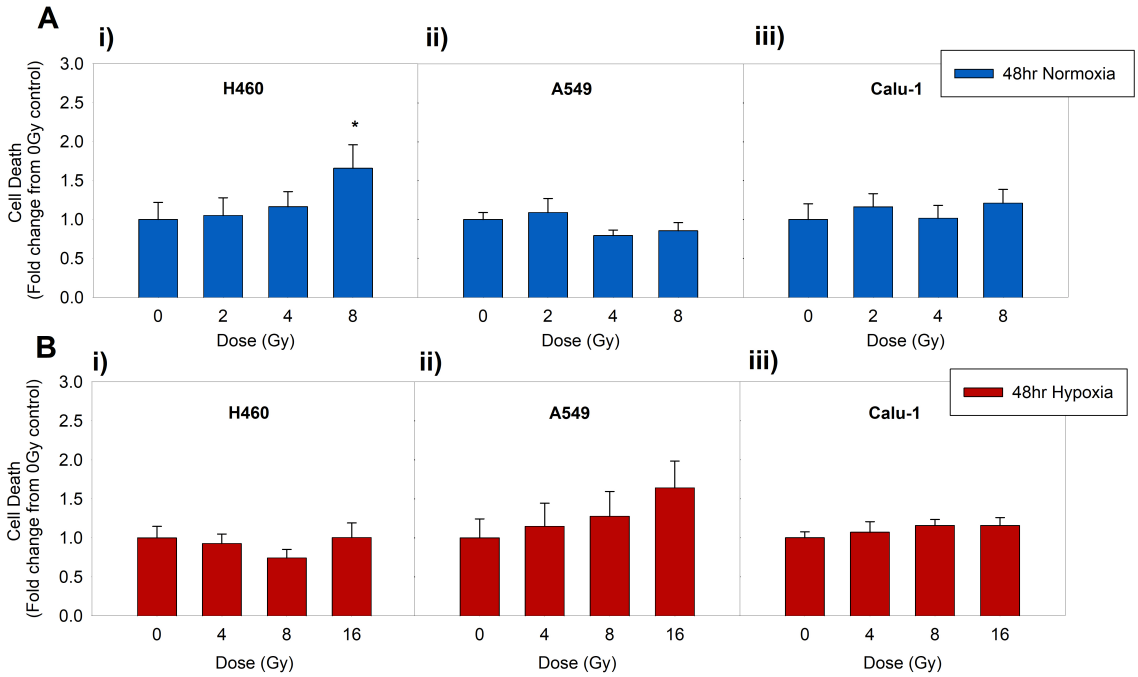


**Figure 4.31:** Cell death assay for H460, A549, Calu-1 using propidium iodide (PI) staining at 48 hrs post-IR in **A. i) - iii)** Normoxia (21% $O_2$) using doses of 2, 4, 8 Gy and **B. i) - iii)** Hypoxia (0.1% $O_2$) using doses of 4, 8, 16 Gy. Samples were measured by flow cytometry. The percentage of Propidium positive cells for each oxygen condition and and X-ray dose was normalised to the non-IR controls and the means and error bars (SD values) from 3 experiments were presented. Each sample was statistically compared to the non-IR control sample (one-way ANOVA test). *P<0.05, **P<0.01, ***P<0.001 (n = 3).

In normoxia, a high number of dying cells were seen at 48 hrs post-8 Gy IR for H460, with a 66% increase in death compared to the non-IR (0 Gy) control sample (figure 4.31A(i)). This potentially indicates that the cells blocked in the G2-M phase of the cell cycle in figure 4.29B(i) were unable to recover from IR damage, and were programmed to die. For A549, 48 hrs after X-ray treatment, dying cells were comparable with the untreated control. This result, in association with the percentage of cells that increased in G0-G1 at 24 hrs for the two highest doses (figure 4.31B(ii)) and no changes in the G2-M, might be explained by the ability of the cells to resolve the damages after the accumulation in the G0-G1 and would therefore allow cells to progress into the cycle without causing death.

Similarly, in normoxic Calu-1, where a block at 24 hrs was observed in the G0-G1 for 2 Gy and 4 Gy and in the G2-M for 8 Gy (figure 4.29B(iii)), cells were able to exit from the respective arrest points as suggested by the fact that there was no cell death induction at 48 hrs post-IR (figure 4.31A(iii)). Interestingly, in hypoxia, on the other hand, the radiation-induced G2-M arrest observed with highest doses for all the cell lines did not result in cell death in our culture conditions. A549 showed an increase in cell death with increasing dose but differences

were found to be statistically insignificant compared with the non-IR control sample (4.31B(i-iii)). This potentially indicates that, even though IR induced a block in the G2-M phase of the cell cycle for the cell lines as shown in figure 4.30B(i-iii), the repair kinetics remained active and contribute to the radio-resistance observed in section 4.3.2. The two main repair pathways (non-homologous end-joining (NHEJ) and homologous recombination (HR)) will be investigated on a genetic level for all cell lines in section 4.3.9.

### 4.3.8 RT-qPCR analysis of gene alteration in the antioxidant pathways after irradiation in normoxia and hypoxia

The results from sections 4.3.4, 4.3.5, and 4.3.6 indicate that both oxygen and radiation play a role in the oxidant and antioxidant capacity of the cell. This was further investigated at a genetic level using RT-qPCR technique to analyse the expression of key antioxidant components, such as NRF2 and catalase. Moreover, based on the results of glutathione assay, the mRNA expressions of GSR, GPX1, GRX and TRX were also investigated. In fact, all of these genes are directly or indirectly involved in $H_2O_2$ detoxification. Since the majority of the changes from the previous analysis were observed at 24 hrs from the radiation treatments, the expression of all the genes was analysed at this time point. The mRNA results obtained for H460, A549 and Calu1 under both oxygen conditions can be seen in figure 4.32, 4.33 and 4.34, respectively. Each figure also includes a heatmap (figure 4.32F, 4.33F and 4.34F) and a summary schematic (figure 4.32E, 4.33E and 4.34E) outlining the statistically significant up- and down-regulation of the antioxidant genes in their respective chemical process for the removal of $H_2O_2$. All data presented in this section represents a fold-change from the non-IR normoxic control sample.

**H460**

The H460 results in figure 4.32A indicated that NRF2 mRNA, a master regulator of many antioxidant genes, was significantly upregulated by irradiation in normoxia, with a clear dose dependant response. Interestingly, NRF2 was strongly up-regulated by the low $O_2$ exposure and its mRNA expression was slightly decreased with the IR compared to the hypoxic untreated sample, but it still remained higher than the normoxic cells. However, NRF2 binding cofactor KEAP1 (figure 4.32A), was found to be completely unaffected by both IR and hypoxia. As expected, and possibly due to the downstream effects of NRF2, antioxidant genes including TRX and GRX were all also upregulated in normoxia with increasing dose (figure 4.32C and E, respectively). TRX and GRX were also upregulated in hypoxia with a fold increase of 1.7 and 3.4, respectively. The irradiation did not substantially change the levels of mRNA for TRX as compared to the hypoxic control (figure 4.32C for TRX and E for GRX), and it reduced them for GRX at 8 Gy and 16 Gy, even though the gene expression was maintained at higher levels than the normoxic samples. Instead, GPX1 expression appeared to be less influenced by the $O_2$ level, while it showed a dose dependency both in normoxia and in hypoxia (figure 4.32C). Indeed, the mRNA expression for GPX1 was almost the same when comparing the doses with the OER factor applied, except for the highest hypoxic dose which, however, was still able to induce gene expression changes (figure 4.32C). On the other hand, GSR expression for the most part appeared to be unchanged by IR in normoxia, while it was down-regulated by the hypoxic condition by 50% with no dose-response (figure 4.32E). Of note, no Catalase expression (Ct values above 35, which was imposed as the detection limit of the RT-qPCR) was detectable in normoxia, and in hypoxia a very weak increase was observed as compared to normoxia. However, this was considered "not expressed" since it was still above the threshold level (data not shown). These results correlate with the increasing oxidative stress observed in the normoxic samples in section 4.3.6. In fact, the redox scavenging system is enhanced to counteract the excessive IR-induced oxidative stress and prevent damage to biological structures. However, besides GPX1 and GSR, the other antioxidant scavengers analysed in the present study resulted upregulated in conditions of low oxygen.

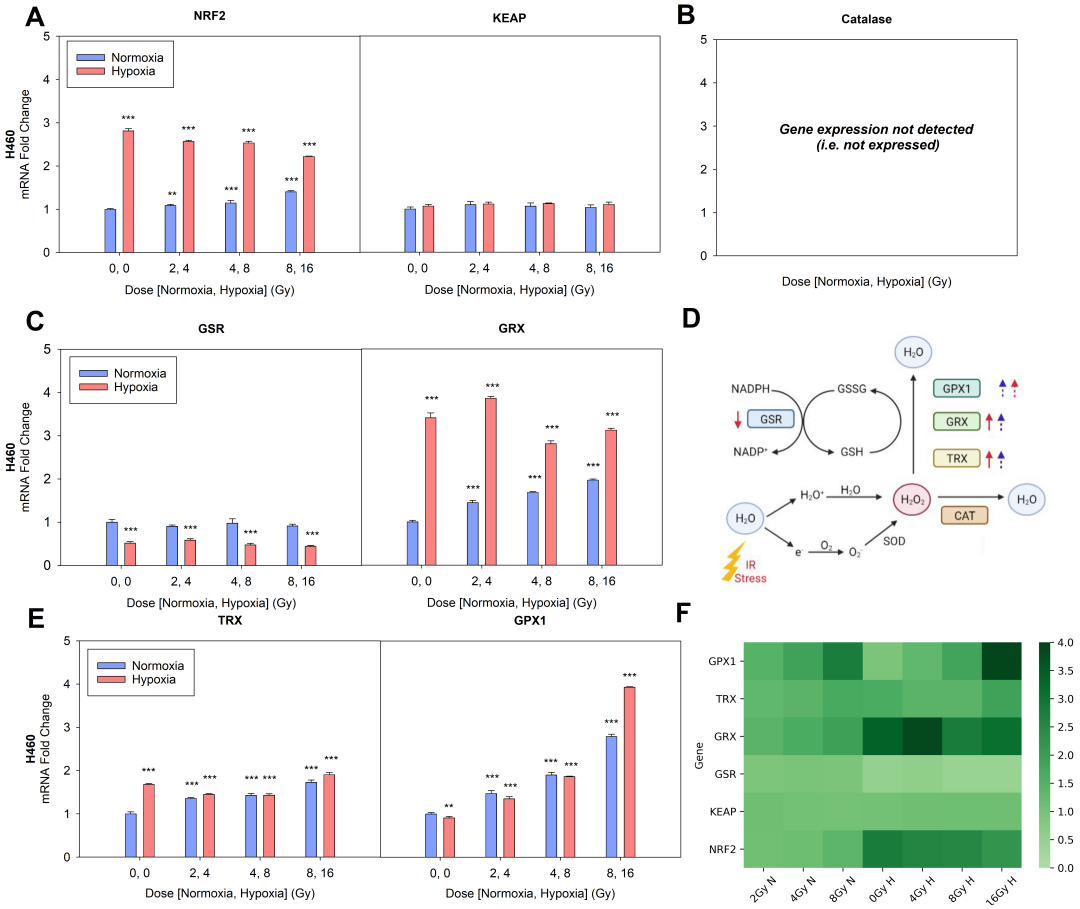


**Figure 4.32:** mRNA expression levels of intracellular antioxidant system evaluated using RT-qPCR of H460 lung cancer cell line at 24 hrs following treatment with IR using doses of 2, 4, 8 Gy in normoxia (21% $O_2$) and 4, 8, 16 Gy in hypoxia (0.1% $O_2$). The following genes were evaluated: **A)** NRF2 (nuclear factor erythroid 2-related factor 2) and KEAP1 (kelch-like ECH-associated protein 1), **B)** CAT (catalase), **C)** TRX (Thioredoxin), GPX1 (glutathione peroxidase), and **E)** GSR (glutathione-disulfide reductase), (GRX) glutaredoxins; **D)** Schematic summary of the intracellular antioxidant mechanisms of $H_2O_2$ removal involving CAT, TRX, GPX1, GSR and GRX following an insult of IR. A dose response is indicated by a dotted arrow and an oxygen response by a solid arrow (normoxia = blue, hypoxia = red). Up-arrow = upregulation, down-arrow = downregulation; **F)** Heatmap summary indicating upregulated and downregulation antioxidant genes. The data was normalised to the non-IR control sample for each oxygen condition and the means and error bars (SD values) of three replicates are presented. Each sample was statistically compared to the non-IR control sample (one-way ANOVA test). *P<0.05, **P<0.01, ***P<0.001 (n = 3).

**A549**

The A549 results in figure 4.33A, show that NRF2 was weakly up-regulated with the highest doses in normoxia and strongly in the hypoxic samples in comparison to the normoxic counterparts. Of note, the hypoxic upregulation of NRF2, which supposedly regulates the expression of Catalase and GPX1, was not correlated with a higher expression of them at 0 Gy in hypoxia (figure 4.33B and C, respectively). Further, although a dose-response was observed in hypoxia, the mRNA expressions of GPX1 and Catalase remained lower than the normoxic control (0 Gy). They became upregulated only at 8 Gy for Catalase and 16 Gy for GPX1 (figure 4.33B and C, respectively). In normoxia, instead, the mRNA levels of these two genes showed a dose-increase (figure 4.33B for Catalase and C for GPX1). However, in normoxia, the levels of NRF2 expression were only slightly upregulated for 4 Gy and 8 Gy (figure 4.33A). This suggests that the regulation of GPX1 and Catalase genes in A549 in response to X-ray radiation involves most likely other genes and also that the $O_2$ plays a central role. Moreover, KEAP1 expression in normoxia did not change with the doses, while hypoxia down-regulated it (0 Gy hypoxia vs 0 Gy normoxia) and the IR exposure stimulated KEAP1 transcription (figure 4.33A). TRX also resulted upregulated with the IR in normoxia, while its levels increased only with the high doses in hypoxia (figure 4.33C). Radiation also induced an upregulation in the TRX mRNA levels for this cell line in normoxia, which was higher than in hypoxia, where it became significant only for the high doses of 8 and 16 Gy (figure 4.33C). Instead, GRX increased by 50% in normoxia in a dose-dependant manner, and it was upregulated in hypoxia where its expression still followed a dose-response increase (figure 4.33E). However, GRX upregulation following radiation treatments were higher in normoxia than in hypoxia. Moreover, at 16 Gy in hypoxia a drop of GRX expression was observed. This drop was also visible at the highest doses for catalase both in normoxia and in hypoxia. Thus, those doses had a negative effect on the mRNA levels of these genes in A549. Then, also in this cell line, GSR expression decreased by approximately 46% in hypoxia (figure 4.33E).

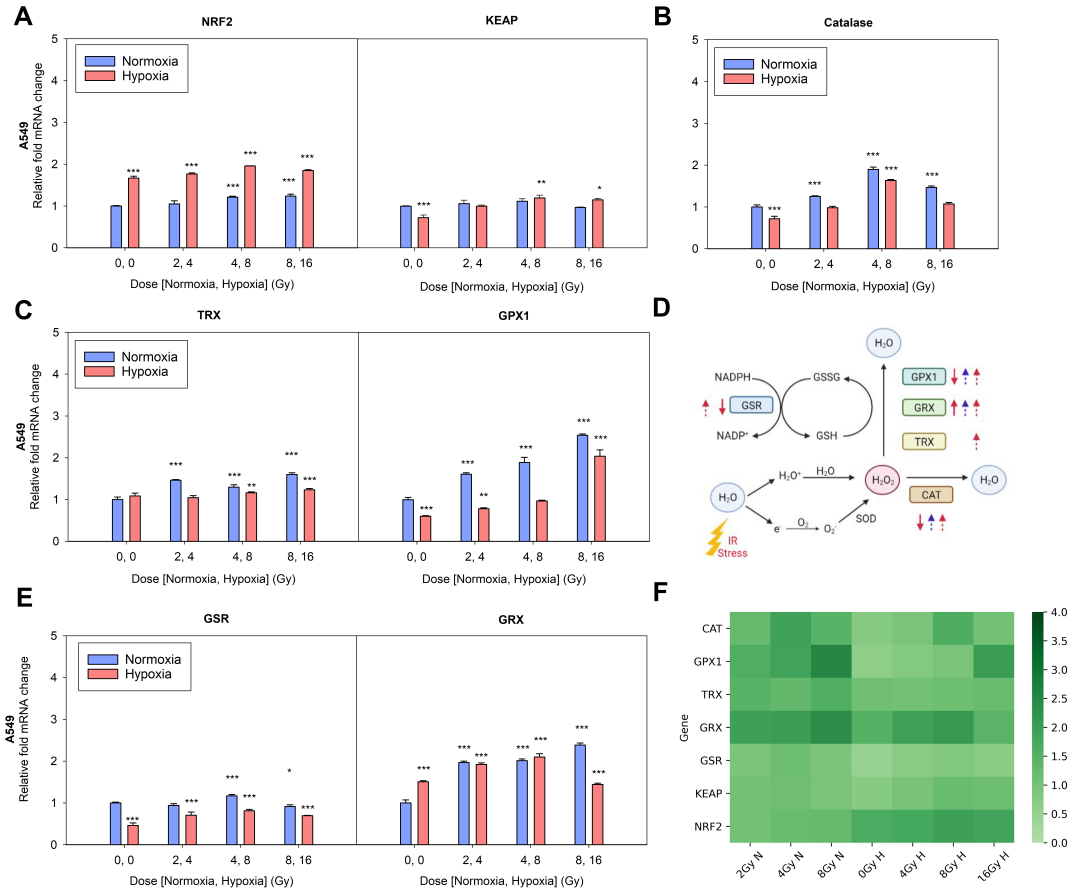


**Figure 4.33:** mRNA expression levels of intracellular antioxidant system evaluated using RT-qPCR of A549 lung cancer cell line at 24 hrs following treatment with IR using doses of 2, 4, 8 Gy in normoxia (21% $O_2$) and 4, 8, 16 Gy in hypoxia (0.1% $O_2$). The following genes were evaluated: **A)** NRF2 (nuclear factor erythroid 2-related factor 2) and KEAP1 (kelch-like ECH-associated protein 1), **B)** CAT (catalase), **C)** TRX (Thioredoxin), GPX1 (glutathione peroxidase), and **E)** GSR (glutathione-disulfide reductase), (GRX) glutaredoxins; **D)** Schematic summary of the intracellular antioxidant mechanisms of $H_2O_2$ removal involving CAT, TRX, GPX1, GSR and GRX following an insult of IR. A dose response is indicated by a dotted arrow and an oxygen response by a solid arrow (normoxia = blue, hypoxia = red). Up-arrow = upregulation, down-arrow = downregulation; **F)** Heatmap summary indicating upregulated and downregulation antioxidant genes. The data was normalised to the non-IR control sample for each oxygen condition and the means and error bars (SD values) of three replicates are presented. Each sample was statistically compared to the non-IR control sample (one-way ANOVA test). *P<0.05, **P<0.01, ***P<0.001 (n = 3).

**Calu-1**

The genetic expression levels of Calu-1 are shown in figure 4.34. Similarly to A549 and H460, there was a significant upregulation of NRF2 in hypoxia compared to the non-irradiated normoxic control, and only a slight increase for the highest dose in normoxia (figure 4.34A). In hypoxia, however, the NRF2 expression levels appeared to fall off with increasing dose from 4 Gy to 16 Gy (figure 4.34A). The mRNA levels of KEAP1 in the Calu-1 cell line were unaffected by hypoxic conditions, however, were statistically significantly upregulated by irradiation with a dose dependant response in normoxia (figure 4.34A). The expression levels of catalase, GPX1 and especially GRX (figure 4.34C and E, respectively) were upregulated by radiation in a dose-dependant manner in normoxia and by hypoxia where the dose-dependency was less evident. In low oxygen condition, then, similarly to A549, Calu-1 showed a drop in the expression of catalase after 24 hrs from 16 Gy irradiation (figure 4.34B) and were therefore consistent with the NRF2 results. In contrast, for TRX, only the higher dose induced a significant increase under both oxygen conditions compared to the non-IR control sample, and in hypoxia its expression was downregulated compared to the normoxic control sample (figure 4.34C). In line with the other two cell lines, also GSR mRNA levels for Calu-1 were down-regulated in hypoxia compared to the non-IR control in normoxia (figure 4.34E).

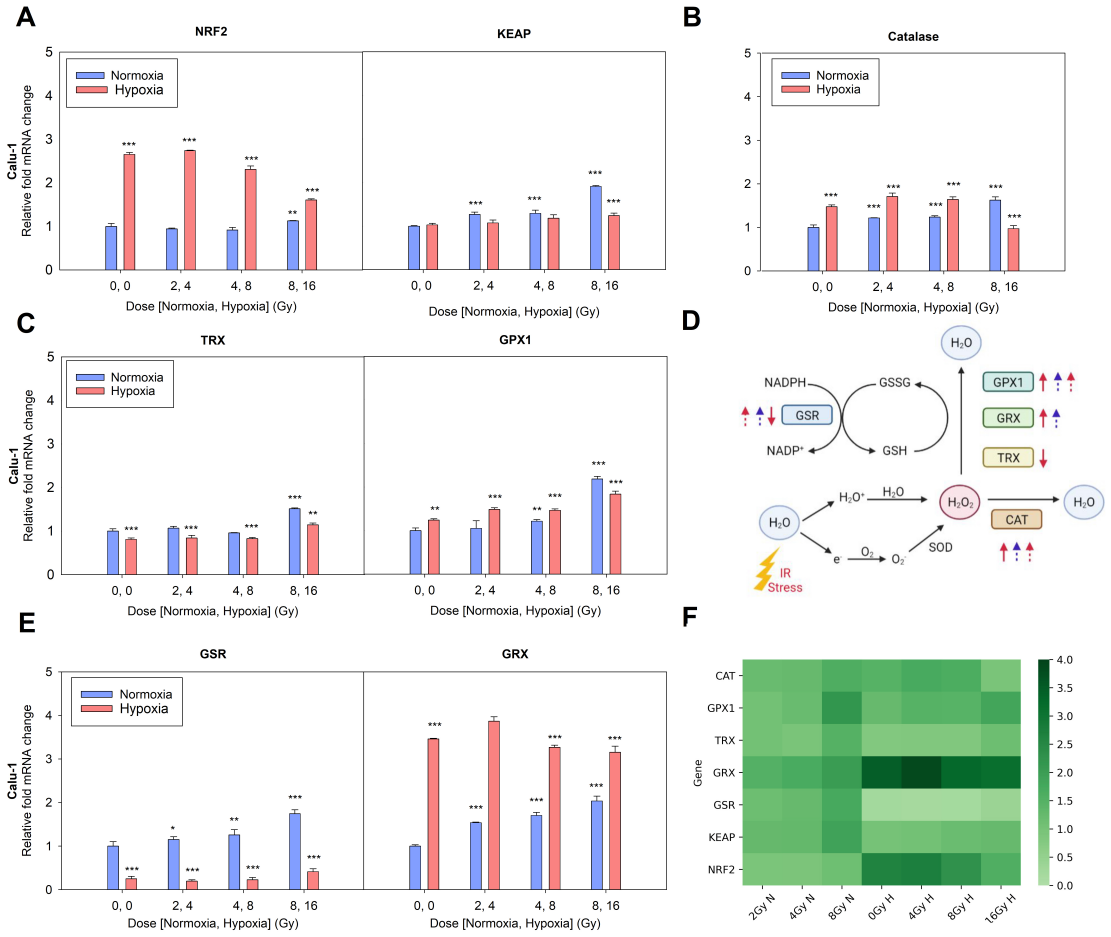


**Figure 4.34:** mRNA expression levels of intracellular antioxidant system evaluated using RT-qPCR of Calu-1 lung cancer cell line at 24 hrs following treatment with IR using doses of 2, 4, 8 Gy in normoxia (21% $O_2$) and 4, 8, 16 Gy in hypoxia (0.1% $O_2$). The following genes were evaluated: **A)** NRF2 (nuclear factor erythroid 2-related factor 2) and KEAP1 (kelch-like ECH-associated protein 1), **B)** CAT (catalase), **C)** TRX (Thioredoxin), GPX1 (glutathione peroxidase), and **E)** GSR (glutathione-disulfide reductase), (GRX) glutaredoxins; **D)** Schematic summary of the intracellular antioxidant mechanisms of $H_2O_2$ removal involving CAT, TRX, GPX1, GSR and GRX following an insult of IR. A dose response is indicated by a dotted arrow and an oxygen response by a solid arrow (normoxia = blue, hypoxia = red). Up-arrow = upregulation, down-arrow = downregulation; **F)** Heatmap summary indicating upregulated and downregulation antioxidant genes. The data was normalised to the non-IR control sample for each oxygen condition and the means and error bars (SD values) of three replicates are presented. Each sample was statistically compared to the non-IR control sample (one-way ANOVA test). *P<0.05, **P<0.01, ***P<0.001 (n = 3).

In summary, taken all together, the data from this gene analysis show that hypoxia and IR treatments exhibited different effects on different cell lines. In some cases, the dominant role was played by the $O_2$ levels (for example, NRF2, GRX and GSR), in others the increasing radiation dose was the main factor (for example, TRX A549), and in many others the combination of hypoxia and radiation modulated the gene expression. Moreover, a common feature in all cell lines was the upregulation of NRF2 in non-irradiated samples (0 Gy hypoxia vs 0 Gy normoxia) with Calu-1 and H460 showing the largest increase for this gene (approximately 2.65 and 2.8 fold change, respectively), whereas A549 increased by a factor of 1.67.

### 4.3.9 RT-qPCR analysis of gene alteration in the repair pathways after irradiation in normoxia and hypoxia

The genetic expression of important genes involved in the DNA repair mechanics, specifically in NHEJ (Non-homologous End Joining) and HR (Homologous Recombination) pathways, was evaluated in order to investigate their involvement in repairing DSBs following irradiation and the hypoxia-modulating effects on these pathways. The NHEJ genes evaluated in this study include DNA-PKcs (DNA-dependant protein kinase catalytic subunit i.e. main regulator of a number of proteins in DSB repair in the NHEJ pathway) and Ku-80 (i.e. heterodimer protein which, along with Ku70, recognises DNA damage, binds to strand breaks and recruits DNA-PKc). For the HR pathway, the gene expression levels of RAD51 (RAD51 Recombinase) and BRCA2 (Breast cancer type 2) were evaluated. BRCA2 is a tumour suppressor protein which binds to the DNA damage site to facilitate the loading of RAD51. RAD51 is a protein which then determines and facilitates homologous DNA strand exchange to repair the damaged DNA. Other genes that were investigated included WEE1 (WEE1 G2 Checkpoint Kinase), which is an important protein active in the G2 phase of the cell cycle as its role is to prevent cells from entering mitosis too early. The mRNA results obtained for H460, A549 and Calu-1 under both oxygen conditions can be seen in figure 4.35, 4.36 and 4.37, respectively. Each figure also include a heatmap (figure 4.35F, 4.36F and 4.37F) and a summary schematic (figure 4.35E, 4.36E and 4.37E) outlining the statistically significant up- and down-regulation of the repair genes in their respective repair pathways (i.e. NHEJ, HR) following DNA damage induced by IR in normoxia (21% $O_2$) and hypoxia (0.1% $O_2$).

**H460**

The RT-qPCR repair results obtained for H460 can be seen in figure 4.35. For this cell line in normoxia, the mRNA levels of the DNA-PKcs did not significantly change with low radiation doses, but increased with the higher dose of 8 Gy, whereas Ku-80 mRNA expression levels were largely unaffected by IR and remained stable for all doses (figure 4.35A). It is possible that the basal expression of these two genes was already sufficient to sense the DNA damages after low dose exposure or that 24 hrs post-IR was a long time point to catch significant changes in genes involved in a faster repair mechanism. On the contrary, the mRNA levels of RAD51 showed a dose-dependant decrease following IR in normoxia. BRCA2 also decreased significantly and was stable with all doses (figure 4.35C). In hypoxia, all of the repair genes investigated in this study for H460 cells were downregulated when compared to the normoxic non-IR control sample (figure 4.35A and C). Moreover, it seems that the X-ray exposure induced a stronger down-regulation at the lowest dose (4 Gy) with increasing dose-dependant effects, potentially to compensate for the higher level of damages induced at higher doses and thereby to ensure sufficient repair. These results suggest that for H460, which is the most sensitive cell line investigated in this study, the HR pathway is far more affected by the low oxygen condition compared with the NHEJ repair pathway. However, in spite of the severe hypoxic condition, cells were still able to activate this pathway even under increased stress. When analysing the mRNA expression levels of WEE1, an essential protein in the G2 phase of the cell cycle, they were unaffected in normoxia and highly upregulated by 59% in hypoxia for the H460 cell line compared to the 0 Gy normoxic control (figure 4.35D). WEE1 delays the G2-M transition in response to DNA damages and recently it has been suggested a role in regulating the intra S phase checkpoint. Therefore, its over-expression might correlate with the slower proliferation rate observed in hypoxia (figure 4.9) and with a better ability to sense the IR-induced damages and to provide the cells with more time for repairing in a less metabolically active state. Although there was not a dose dependency observed and at the very high dose of 16 Gy the levels decreased.

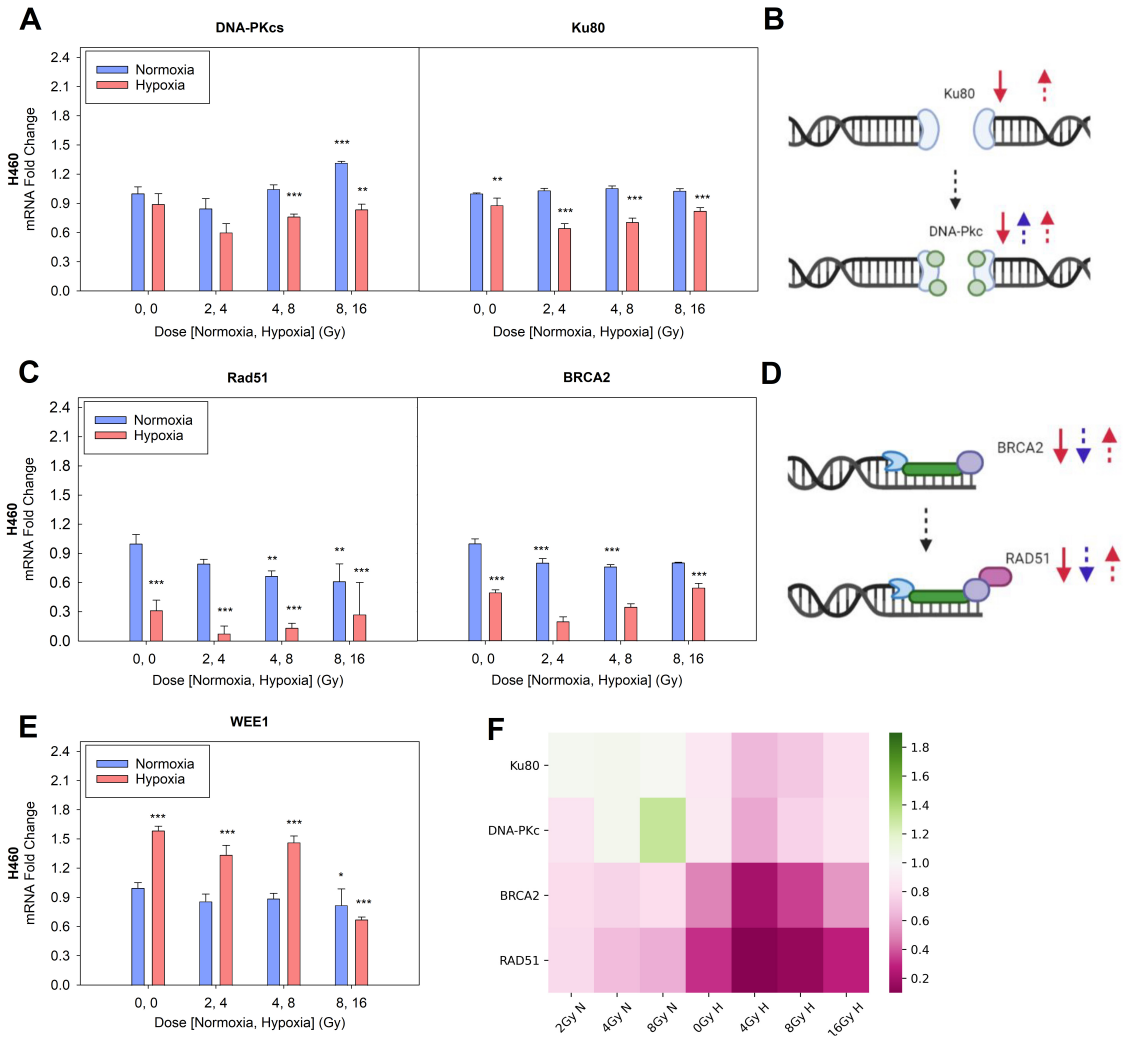


**Figure 4.35:** mRNA expression levels of intracellular repair system evaluated using RT-qPCR of H460 lung cancer cell line at 24 hrs following treatment with IR using doses of 2, 4, 8 Gy in normoxia (21% $O_2$) and 4, 8, 16 Gy in hypoxia (0.1% $O_2$). **A)** Expression profiles of DNA-PKcs and Ku80 genes, involved in the non-homologous end joining (NHEJ) pathway; **B)** Schematic summary of the DNA-PKcs and Ku80 mechanism, of action combined with the results obtained (dose response= dotted arrow; oxygen response= solid arrow; normoxia = blue, hypoxia= red); **C)** Expression profiles of RAD51 and BRCA2; **D)** Schematic summary of RAD51 and BRCA2 mechanism, combined with the results obtained (dose response = dotted arrow; oxygen response = solid arrow; normoxia = blue, hypoxia = red). **E)** mRNA fold change of WEE1 **F)** Heatmap summary indicating upregulated and downregulation repair genes 24 hrs after IR in normoxia and hypoxia. The data was normalised to the non-IR control sample for each oxygen condition and the means and error bars (SD values) of triplicates are presented. Each sample was statistically compared to the non-IR control sample (one-way ANOVA test). *P<0.05, **P<0.01, ***P<0.001 (n = 3).

**A549**

The RT-qPCR repair results obtained for A549 are shown in figure 4.36. For A549, the repair genes investigated in this study which are involved in the NHEJ and HR were all significantly downregulated under low oxygen conditions in comparison to the non-IR normoxic control (figure 4.36A). These results are consistent with the previous data observed for the H460 cell line (figure 4.35). In normoxia, DNA-PKcs levels fluctuated and a slight decrease was observed for DNA-PKcs until 4 Gy. In contrast, a somewhat dose-dependant increase with increasing dose was observed for Ku-80 under normoxic conditions, and all IR samples were statistically significantly different to the normoxic non-IR control sample (figure 4.36A). The HR genes (RAD51 and BRCA2), on the other hand, both decreased in a dose-dependant manner under normoxic conditions (figure 4.36C). As far as the WEE1 expression levels are concerned, there was a significant enhancement in hypoxia for the A549 cells (figure 4.36E), as already observed in the H460 results. However, in A549 cell line, irradiation increased the expression levels of WEE1 in hypoxia for 4 Gy and 8 Gy but decreased at 16 Gy. Unlike H460, however, in normoxia where the mRNA levels of WEE1 were unfazed by IR at low doses, the WEE1 expression was downregulated in A549 following IR of 2 Gy and 4 Gy compared to the non-IR sample and was further decreased at a high dose of 8 Gy.

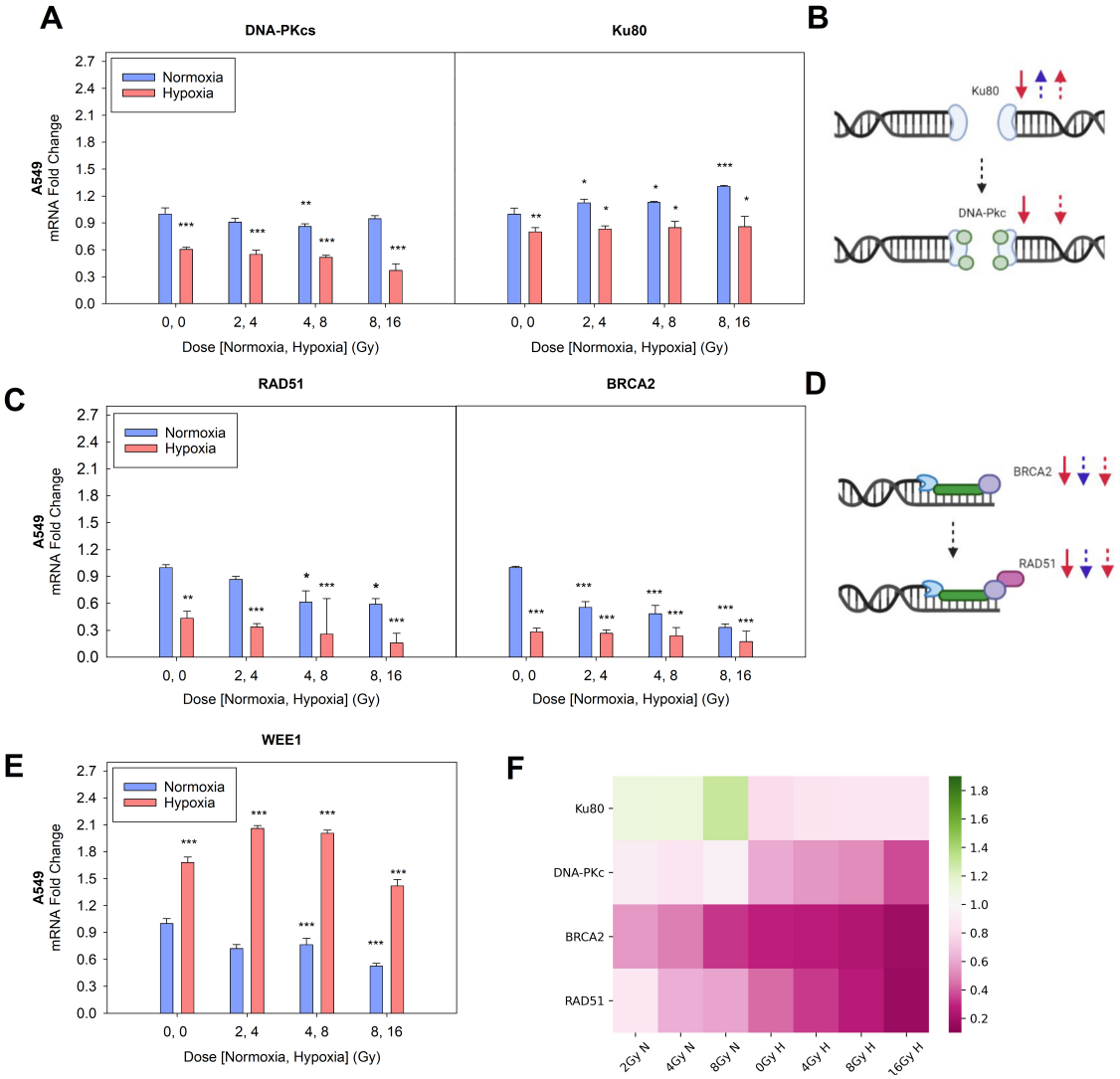


**Figure 4.36:** mRNA expression levels of intracellular repair system evaluated using RT-qPCR of A549 lung cancer cell line at 24 hrs following treatment with IR using doses of 2, 4, 8 Gy in normoxia (21% $O_2$) and 4, 8, 16 Gy in hypoxia (0.1% $O_2$). **A)** Expression profiles of DNA-PKcs and Ku80 genes, involved in the non-homologous end joining (NHEJ) pathway; **B)** Schematic summary of the DNA-PKcs and Ku80 mechanism, of action combined with the results obtained (dose response= dotted arrow; oxygen response= solid arrow; normoxia = blue, hypoxia= red); **C)** Expression profiles of RAD51 and BRCA2; **D)** Schematic summary of RAD51 and BRCA2 mechanism, combined with the results obtained (dose response = dotted arrow; oxygen response = solid arrow; normoxia = blue, hypoxia = red). **E)** mRNA fold change of WEE1 **F)** Heatmap summary indicating upregulated and downregulation repair genes 24 hrs after IR in normoxia and hypoxia. The data was normalised to the non-IR control sample for each oxygen condition and the means and error bars (SD values) of triplicates are presented. Each sample was statistically compared to the non-IR control sample (one-way ANOVA test). *P<0.05, **P<0.01, ***P<0.001 (n = 3).

**Calu-1**

The RT-qPCR results evaluating the repair response for Calu-1 can be seen in figure 4.37. These results showed that the NHEJ repair pathway genes, DNA-PKcs and Ku-80, were both downregulated in the hypoxic Calu-1 samples in comparison to the normoxic non-IR control, however, the mRNA expression levels then appeared to fluctuate with IR dose for both genes (figure 4.37A). In normoxia, a similar fluctuating dose response was observed for the mRNA levels of DNA-PKcs and Ku-80, with a significant upregulation found after IR of 2 Gy and 8 Gy for DNA-PKcs, whereas, for Ku-80, only 8 Gy induced a significant upregulation in comparison to the normoxic non-IR control (figure 4.37A). The selected genes involved in the HR repair pathway (RAD51, BRCA2) were both downregulated in hypoxia with a similar trend (figure 4.37C). In Calu-1, irradiation increased the mRNA expression of both genes in hypoxia with increasing dose, but at the high dose of 16 Gy the mRNA expression levels of both genes dropped almost to the same level as the 0 Gy hypoxic sample. This indicates that the highest dose reduced the expression of RAD51 and BRCA2 or the stability of their mRNAs. The WEE1 mRNA expression levels of the hypoxic samples were severely upregulated also for Calu-1 cells, while fluctuating differences were detectable for the normoxic samples (figure 4.37E). Irradiation only appeared to enhance the upregulation, as indicated by the increasing dose trend, with the exception of the high dose of 16 Gy which showed a drop, however, the over-expression remained statistically significant compared to the normoxic 0 Gy.

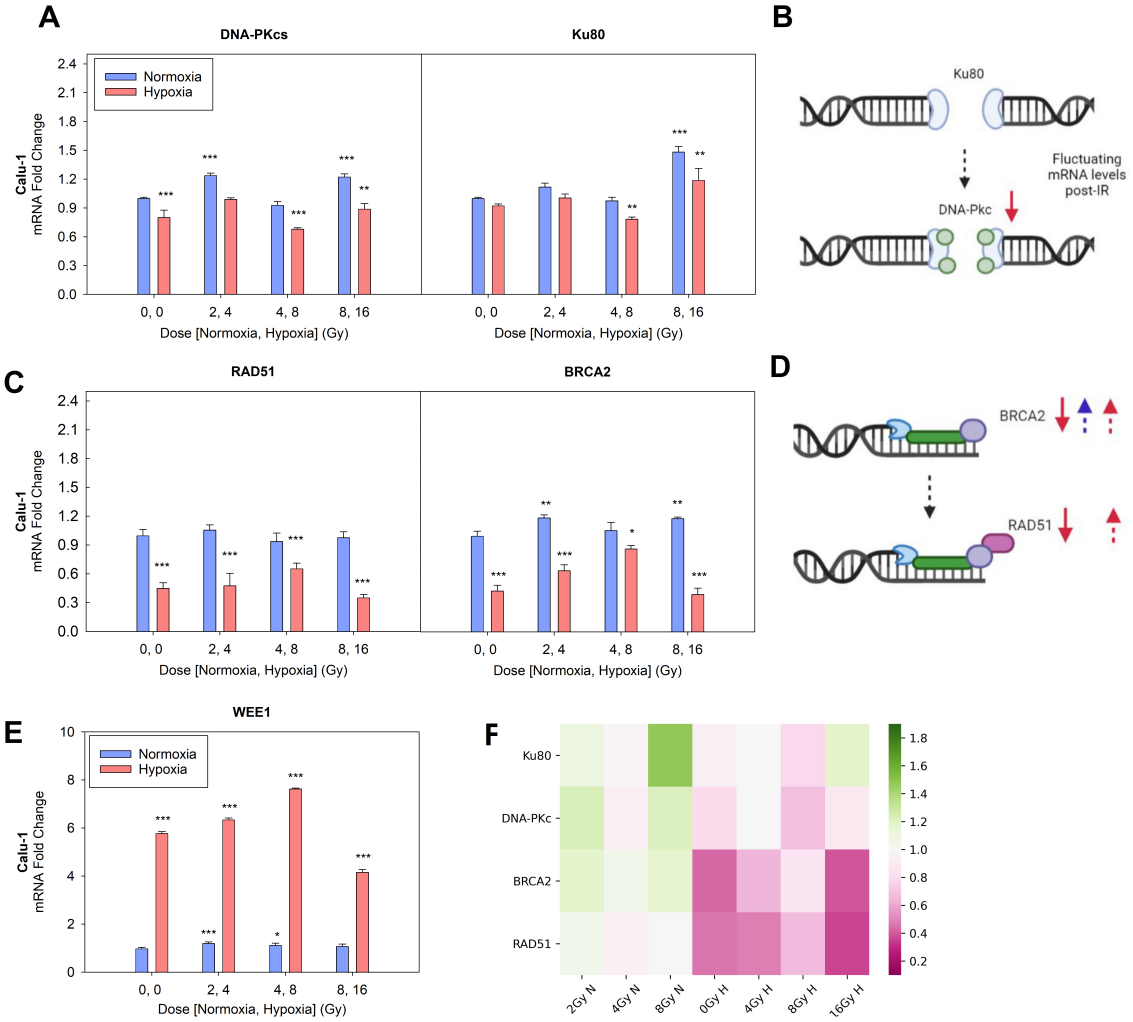


**Figure 4.37:** mRNA expression levels of intracellular repair system evaluated using RT-qPCR of Calu-1 lung cancer cell line at 24 hrs following treatment with IR using doses of 2, 4, 8 Gy in normoxia (21% $O_2$) and 4, 8, 16 Gy in hypoxia (0.1% $O_2$). **A)** Expression profiles of DNA-PKcs and Ku80 genes, involved in the non-homologous end joining (NHEJ) pathway; **B)** Schematic summary of the DNA-PKcs and Ku80 mechanism, of action combined with the results obtained (dose response= dotted arrow; oxygen response= solid arrow; normoxia = blue, hypoxia= red); **C)** Expression profiles of RAD51 and BRCA2; **D)** Schematic summary of RAD51 and BRCA2 mechanism, combined with the results obtained (dose response = dotted arrow; oxygen response = solid arrow; normoxia = blue, hypoxia = red). **E)** mRNA fold change of WEE1 **F)** Heatmap summary indicating upregulated and downregulation repair genes 24 hrs after IR in normoxia and hypoxia. The data was normalised to the non-IR control sample for each oxygen condition and the means and error bars (SD values) of triplicates are presented. Each sample was statistically compared to the non-IR control sample (one-way ANOVA test). *P<0.05, **P<0.01, ***P<0.001 (n = 3).

Overall, after evaluating the repair gene expressions (DNA-PKcs, Ku-80, RAD51, BRCA2) in normoxia (21% $O_2$) and hypoxia (0.1% $O_2$) for the lung cancer cell lines (H460, A549, Calu-1), it becomes clear that for all cell lines the genes involved in both the NHEJ (DNA-PKcs, Ku-80) and the HR (RAD51, BRCA2) repair pathways were downregulated in hypoxic conditions. However, in general, the HR pathway appeared to be more affected by the low oxygen level. Also, for the most part, IR induced an increasing dose response in the repair kinetics for all cell lines under both oxygen conditions. WEE1, on the other hand, was highly upregulated for all cell lines in hypoxia, possibly restricting cells from entering mitosis too early and thereby potentially contributing to the slower proliferation observed in hypoxia compared to normoxia.

## 4.4 Discussion

Radiotherapy is often used in the treatment of non-small cell lung cancer (NSCLC), however, many NSCLC cell lines are highly radio-resistant (RR) and therefore have a reduced treatment success rate (220). This is especially problematic when the NSCLC develops regions of hypoxia in which cells activate adaptive responses characterised by altered redox and energy metabolisms, as well as repair mechanisms, which all contribute to RR (220). Different lung cancer cell lines (H460 (p53-wt, K-Ras mutant), A549 (p53-wt, K-Ras mutant) and Calu-1 (p53-null) were therefore investigated in this radiobiological study which aimed to highlight potential common and cell-type specific features in hypoxic lung tumour cell lines (i.e. 0.1% $O_2$, chronic hypoxia) which are inherently more resistant to radiotherapy treatments, and how their altered responses in hypoxia, in terms of their damage repair and antioxidant capacity contribute to their ability to survive photon treatment. The three lung cell lines were chosen due to their differing aggressiveness determined by their proliferation profiles as indicated in section 4.9, radio-responses as reported in section 4.3.2. and different invasiveness as outlined by Rudisch et al. (227).

In the present study, it is shown that the three lung cancer cell lines had different growth rates in normal culture conditions (normoxia), with H460 being more proliferative, followed by Calu-1 and A549. However, in hypoxic conditions, although maintaining a similar trend, all three cell lines had a growth reduction. According to literature, H460 and Calu-1 are considered more aggressive in nature with highly proliferative characteristics compared to the slower growing A549. Faster cycling cells have the possibility to accumulate more DNA damages if their repair systems do not work properly. This is especially true in cancer cells where often inactivation or over-activation of cell cycle checkpoints due to mutations result in failure of the cell cycle control and aberrant responses. When exposed to IR treatments, the radio-responses of the three cell lines in normoxia show that A549 and Calu-1 are more radio-resistant with similar survival profiles, whereas H460 was more radio-sensitive. Interestingly, however, the radio-responses of all three cell lines in hypoxia were similar, thus implying that hypoxia induced varying "protectiveness" for each of the cell lines, with a higher protection observed for the hypoxic and more proliferative H460 cell line, as indicated by the OER factor. The OER factor for these cell lines, which was calculated at 10% survival fraction, fell between 1.7 and 2.1. In general, these OER values were slightly lower in comparison to previous studies

conducted in hypoxia with photon IR, which have estimated OER values between 2.3 and 3.3 as outlined by Carlson et al. (228). However, comparison between studies is difficult since the OER is dependant on many factors, including the cell type, LET (229), the oxygen percentage and how it is obtained and stably maintained, and also largely on the survival percentage that OER is evaluated at, which is often not reported.

Survival ability of cells is linked to the amount of IR-induced DNA damages and to cell ability to repair them. When analysing the DNA damages (by staining of $\gamma$H2AX foci) soon after exposure, an increasing dose response was obtained, with an observed saturation at high doses for all cell lines in both oxygen conditions, albeit a much lower amount of foci was induced in hypoxia. Interestingly, the reduction of the initial DSB foci from normoxic to hypoxic for each cell line is within the same range as the OER values obtained from the clonogenic profile (section 4.3.2), which is consistent with studies from Carlson et al. (228) and Stewart et al. (230). It is possible that the measured DSB damage is a combination of isolated (iDSB) and clustered (cDSB) DNA DSBs as outlined and incorporated in a survival model developed by Mairani et al. (231). In this model, the authors suggested that the combination of the two DSB types can describe the lethality of damage as a function of dose and, with the incorporation of an OER (or as they call it hypoxia reduction factor (HRF)), oxygen level. We suspect that the observed increasing profile for all cell lines is potentially attributed to the inhomogeneous induction/distribution of iDSB and cDSB at low and high doses (232). In fact, DSBs at 24 hrs post-IR for H460 and Calu-1 exhibited an increasing quadratic dose response, which according to Mairini's study, would account for the cDSB which were unable to be repaired (231). The reduction of DSB induction at 30 min post-IR that was observed in hypoxia, possibly attributed to the fact that low LET radiation (i.e. photons) more so relies on indirect damage of DNA, and therefore requires the creation of oxygen radicals or reactive oxygen species (ROS) to induce damage (16). However, since the oxygen concentration is reduced in the cell under hypoxic conditions, there is possibly a lower probability of ROS generation and thereby a reduced amount of indirect damage. For this reason, the $H_2O_2$ production in the three lung cancer cell lines was evaluated, both in the nucleus and in the cytoplasm, at two time points: soon after irradiation to analyse the possibility of direct $H_2O_2$ formation, and 24 hrs post-IR which allows to mainly consider the secondary $H_2O_2$ formation. As expected, there was an increase in the nuclear $H_2O_2$ levels post-IR with increasing IR dose in normoxia (i.e. oxygen enriched environment) for all cell lines (figure 4.21). However, in normoxic H460 the lower

dose was already able to induce high levels of nuclear $H_2O_2$, which might explain the highest radiosensitivity observed in normoxia. Instead, in normoxic A549 cells, only the highest doses stimulated high nuclear $H_2O_2$ production, which was correlated with higher $\gamma$H2AX foci, but was still less compared to H460. Interestingly, Calu-1 cells were less prone to producing nuclear $H_2O_2$, and in fact, they showed the lowest increase in normoxia compared to the other cell lines. Despite this, Calu-1 cells induced a high level of $\gamma$H2AX foci soon after IR with a dose dependency, although their basal level was already higher than the other cells, which might be related to their p53-null condition. Moreover, when the nuclear $H_2O_2$ levels (normalised to 0 Gy) were plotted as a function of DSB (normalised to 0 Gy) at 30 min post-IR (figure 4.19), a somewhat linear dependency with increasing doses was found for all lung cancer cell lines in normoxia (except for H460 8 Gy), potentially indicating that there was a direct correlation of DSB damage induced by $H_2O_2$ inside a single cell line (figure 4.19A). However, when comparing all the cell lines, the data from Calu-1 cells (lower nuclear $H_2O_2$ but higher foci count compared to the other cell lines) indicated that the extent of DNA damages was dependant on the cell type and that producing less nuclear $H_2O_2$ did not necessarily correspond to having less DNA damages. It is possible therefore that in this case the direct DNA damage was a predominant factor and/or different forms of ROS were involved.

Additionally, as expected, the ability of all cell lines to repair the IR-induced DNA damages was inversely linked to the dose, as shown by the foci number after 24 hrs. At this time point, the delayed $H_2O_2$ production varied depending on the cell type, with normoxic H460 and A549 cells being able to markedly reduce the level of $H_2O_2$ in the nuclei with a trend similar to the residual $\gamma$H2AX foci profile. On the contrary, Calu-1 cells, although having a higher basal level of foci, were able to repair the damages, as compared to the 30 min time point. This, however, was associated with a stronger increase in secondary $H_2O_2$ production in the nucleus, when compared with the other two cell lines (figure 4.21B(iii)). While studies have investigated a relationship between ROS and corresponding DSB damage (233, 234, 235), to the best of our knowledge, our study is the first time that measured nuclear $H_2O_2$ was found to directly correlate with IR-induced DSBs in cancer cell lines. Moreover, in addition to ours, we have only found one other study which managed to measure the nuclear $H_2O_2$ (236) and therefore highlights the importance of these findings.

On the other hand, in hypoxia, the basal level of $H_2O_2$ in the nucleus was lower for NSCLC cell lines compared to the normoxic counterparts (data not shown), indicating that the mechanisms by which $H_2O_2$ was produced in the nucleus were potentially less active in low oxygen conditions. Hypoxic cell irradiation did not lead to important changes in the nuclear $H_2O_2$ production both soon after IR and at 24 hrs in any cell line (figure 4.21A and B), except for weak changes at the higher doses and in a cell-dependant manner. Moreover, in hypoxia, there was no visible trend between the $H_2O_2$ created after IR and the DSBs induced (figure 4.19B), indicating that additional factors, which could be altered in chronic hypoxia compared to normoxia, were possibly affecting either the induction of DNA damage by IR or the $H_2O_2$ production in these lung cancer cell lines, or perhaps a combination of the two. The delayed $H_2O_2$ production was associated with an ability to repair which resulted to be less clear in hypoxia than in normoxia (figure 4.15B), and was probably due to the lower amount of damages produced in hypoxia. Altogether this evidence indicates that radiosensitivity among cancer cells derived from the same organ was higher in normoxia than in hypoxia and show an intra-organ heterogeneity, which seemed to be less pronounced in hypoxia than in normoxia.

Since X-ray exposure causes damages also to other cellular organelles with ROS increase in the cytosol, the specific analysis for cytosolic $H_2O_2$ was also performed. In contrast to the $H_2O_2$ levels measured in the nucleus where a clear dose increase was observed with increasing IR dose, the cytosolic $H_2O_2$ results, except for mild fluctuations, showed no dose response for any of the NSCLC cell lines at 30 min post-IR (figure 4.24A). This could be due to a potentially high scavenging ability present in the cytosol (237), which perhaps efficiently and promptly removed the excess IR-induced $H_2O_2$. In fact, since we were able to detect the initial excess of IR-induced $H_2O_2$ in the nucleus and not in the cytosol, it potentially highlights the strong antioxidant capacity in the cytosol compared to the limited, albeit existing, one present in the nucleus (238). More interestingly, a slight increasing dose response of the cytosolic $H_2O_2$ levels were observed at 24 hrs post-IR for H460 in comparison to its non-IR control, whereas for Calu-1 and A549, an increase in $H_2O_2$ levels were only seen at high doses (figure 4.24B). These findings suggest that the three lung cancer cell lines could have differing antioxidant capacity, with A549 and Calu-1 having a stronger ability to combat the oxidants at low doses compared to H460. This, in turn, might contribute to the higher radio-resistance observed for A549 and Calu-1 compared to H460 cells. According to a recent study by Diehn et al., increased production of free radical scavenging enzymes leads to low ROS levels and contributes to

tumour radio-resistance (239). Indeed, the analysis of the reduced/oxidised glutathione ratio, and the gene expression in normoxia showed a tendency, although not significant, to increased oxidative stress in H460 after 24 hrs from IR, as shown by the increase in the GSSG levels. Glutathione is a central antioxidant molecule involved in $H_2O_2$ detoxification by glutathione peroxidase (GPX). The gene expression analysis of GPX1 showed that in normoxia the mRNA levels were upregulated in a dose-dependant manner for H460. It is reasonable to hypothesise that increased levels of $H_2O_2$ could stimulate GPX1 expression in order to favour the detoxification of $H_2O_2$, which results in increasing levels of GSSG ($H_2O_2$ + GSH (Catalase by GPX) $\rightarrow$ $H_2O$ + GSSG). Increased GSSG can be also generated in cases of high oxidative stress following the reduction of the Glutaredoxin enzyme (GRX), in a reaction involving GSH and proteins with oxidised thiol-disulfide groups. Based on that, in normoxia the level of GRX mRNA were increased after IR, which thus could be correlated with the increase of the GSSG levels. Another enzyme for $H_2O_2$ removal is catalase, which is often referred to as the strongest $H_2O_2$ cellular scavenger (240). Surprisingly, in H460 the expression of catalase was undetectable, which might contribute to the high basal levels of $H_2O_2$ observed in this cell line. Indeed, Kang et al. (241) confirmed the reduced levels of catalase in H460, which therefore most likely relied more on the GPX1 system to remove the $H_2O_2$. To the best of our knowledge, there are very few publications reporting a gene downregulation of catalase in the H460-wt (wild type) cell line, and this could potentially be an interesting avenue for further research. However, in this cell line, despite the increasing levels of GPX1 and GRX mRNAs with increasing doses, it seemed that the balance between IR-induced $H_2O_2$ production and elimination was unfavourable resulting in accumulation of $H_2O_2$ and GSSG with IR doses. Indeed, no change was observed in the expression of GSR, which is used to convert the oxidised glutathione back to it reduced form for further scavenging of the $H_2O_2$ molecule.

Another central gene regulating many of the antioxidant responses is NRF2. NRF2 is an important protein which usually becomes unbound from its negative regulator, KEAP1, when there is an increase in oxidative stress within the cell. NRF2 in fact directly regulates the transcription of antioxidant genes, including GSR, GPX, TRX1 and genes involved in GSH synthesis. NRF2 was slightly upregulated by radiation treatment in H460 with a linear correlation with GPX, TRX1, but not with GSR. Taken together, these findings are in line with the idea that in H460 the antioxidant systems, although upregulated, could be less efficient, which would make the cells more sensitive to irradiation, compared with the other two cell lines.

This evidence could potentially shed light on the more radio-sensitive response observed for the H460 cell line compared with the other two more radio-resistant NSCLC cell lines. In normoxic A549, the GSH/GSSG ratio showed a marginal not significant decrease, associated with unperturbed levels of $H_2O_2$, except for the very high dose of 8 Gy. Similarly to H460, in A549, NFR2 upregulation was observed after IR, together with GPX, TRX1, but not with GSR. This, associated with the upregulated levels of GPX1 and catalase mRNAs, indicated that the antioxidant systems worked better than in H460 cells. In normoxic Calu-1 cells, the $H_2O_2$ levels were unchanged (figure 4.24B(iii)), although also for this cell line at 8 Gy the $H_2O_2$ increased, and the GSH/GSSG ratio at 24 hrs were was largely unaffected (because both GSH and GSSG levels increased) (figure 4.27B(iii) and 4.28A(i) and B(i)). In Calu-1 no effect of IR on NRF2 was visible, excluding again the highest dose, and the same was observed for TRX1 and GPX1. In this cell line, 24 hrs post IR in normoxia, the gene expression levels of GPX1 and catalase, as well as GSR, tended to be upregulated with increasing doses. Consequently, it can be inferred that in Calu-1 the antioxidant systems analysed were not particularly influenced by irradiation and were able to keep the levels of $H_2O_2$ produced following IR under control. Of note, the dose of 8 Gy represents a very high insult for cells and, although the gene expression is still influenced, cells most likely were severely compromised making the interpretation of the data difficult.

Unexpectedly in hypoxia, the cytoplasmic $H_2O_2$ levels were lower than in the normoxic samples (data not shown). Indeed, according to many publications, hypoxia would cause an increase in the ROS levels of cancer cells (242), with some specifying an increase in $H_2O_2$ (243, 244), which was not seen in this study. This increase has been attributed to the fact that electron transfer across the ETC in the mitochondria slows down under hypoxia, thereby resulting in a larger leak of electrons from the ETC which in turn interact with $O_2$ and thus create ROS (104, 146). However, another body of evidence supports the notion that hypoxic tumour regions are more radioresistant because of the reduction in ROS generation ((142)). Results from Sgarbi et al. who investigated the modulation of ROS levels in fibroblast and osteosarcoma cancer cell lines under 0.5% $O_2$ showed a significant decrease in the ROS levels compared to normoxia which was even further decreased after prolonged hypoxia (245). They associated this decrease, at least in part, to the decrease in superoxide levels which they also observed in hypoxia (245). It is worth to note that comparison among studies is difficult, as many parameters, such as $O_2$%, the time of exposure and cell lines, often differ from one to

each other, but these parameters strongly influence the responses of the cells. In our study, the cells were cultured in hypoxia at 1% and subsequently exposed to lower $O_2$ levels (0.1%) for more than 24 hrs so to obtain cells which had almost completely adapted to the hypoxic environment and avoid stress due to acute conditions with varying $O_2$ gradients.

To support the results, when investigating the oxidative stress in hypoxic control cells (0 Gy), the GSH/GSSG ratio was much higher in hypoxia than in normoxia for all lines (figure 4.26B), due to higher levels of GSH compared to GSSG. This was indicative of a reduced oxidative stress condition. However, when $O_2$ was depleted, the genes involved in the antioxidant systems were differentially regulated. In fact, we noticed a strong basal upregulation of the master antioxidant gene, NRF2, for all cancer cell lines, simultaneously with a basal increase in the mRNA levels for GRX and a reduction of GSR genes. Instead, for GPX1, its expression was reduced in H460 and A549, but increased in Calu-1. While reduced levels of GPX and $H_2O_2$ in H460 and A549 might support the hypothesis that GPX expression can be modulated by $H_2O_2$, this does not apply to Calu-1. The analysis of the responses in hypoxic samples after IR showed that the IR induced cytosolic $H_2O_2$ at 24 hrs to decrease with doses for all NSCLC lines (figure 4.24B). A study by Hennessy et al. also showed a decrease of ROS levels in their hypoxic prostate cell lines (at 0.5% $O_2$) after irradiation with 4 Gy photons (246). Hennessey attributed the decrease to an associated reduction in the GSH levels and hypothesised that it could also be due to a reduced capacity of oxygen compounds present to "fix" the DNA damage allowing repair to happen (246). However, in our study, the GSH/GSSG ratio results were not particularly affected by IR in H460 and A549, apart from at the high doses where it increased and corresponded to the larger decrease in $H_2O_2$. These observations indicated a condition with less oxidative stress, which was associated in fact to a dose-reduction of the cytosolic $H_2O_2$. Conversely, in Calu-1, an appreciable decrease in intracellular GSH/GSSG ratio was observed, indicating, on the contrary, a condition of oxidative stress but this was associated to a reduced $H_2O_2$ content in the cytoplasm. The RT-qPCR analysis of antioxidant genes in the hypoxic conditions used in this study showed that NRF2 expression was maintained at high levels after IR, with variable trends depending on the cell type (figures 4.32A, 4.33A, 4.34A). It is possible that, after irradiating the cells, the upregulation of NRF2 mRNA levels in hypoxia initiated a strong cytosolic antioxidant response in the cells to combat the flux of $H_2O_2$. This would explain the dose-dependant decrease of the $H_2O_2$ levels, which, in turn, would reduce the NRF2 levels with IR, as observed in H460 and Calu-1 cell lines. In

several studies NRF2 depletion has been associated with enhanced radio-sensitisation and ROS accumulation (173, 247, 248). In a study by Singh et al. on A549 and H460 in normoxia, it was shown that reduced function of NRF2 promoted radiosensitivity by favouring ROS accumulation and lowering the mRNA levels of GSR and TRX1. This is partially consistent with our results on ROS content and with the reported upregulation of TRX1 in hypoxic H460 and A549, but not in Calu-1, in which it was downregulated, albeit over-expressed compared to the normoxic samples. By contrast, the GSR levels were downregulated in hypoxia in all NSCLC lines, which in fact correlated with the low levels of GSSG. The reason why hypoxic cells needed to upregulate some of the antioxidants from their basal levels, even though less $H_2O_2$ content and lower oxidative stress was measured as indicated by the GSH/GSSG ratio, is not clear and needs deeper investigations. However, it should noted that the oxidative stress is a phenomenon that is not only linked to $H_2O_2$, although it is the more stable among ROS, and thereof it is possible that other ROS were also playing an active role. In addition, the mechanistic regulation of the antioxidant genes and their downstream effects in prolonged severe hypoxia might be totally different from what happens in normoxia (174).

The higher radio-resistance observed in hypoxia compared to normoxia might be influenced by the upregulation of NRF2, which is also involved in cell survival. On this regard, NRF2 has been shown participate also in DDR pathways, in particular in the HR. It has been shown that in A549, NRF2 depletion led to a slowdown of the DNA repair associated to a reduction of RAD51 expression and radiosensitivity (247). However, these observations were in contrast with our data in normoxia. In fact, our results in normoxia, showed that NRF2 expression was inversely associated with RAD51 and BRCA2 levels, with increasing doses, both in H460 and in A549. In Calu-1, on the other hand, where NRF-2 was not sensibly affected by X-ray treatment, also the expressions of RAD51 did not change while for BRCA2 there were fluctuations. This behaviour was even more pronounced in severe prolonged hypoxia, where, in A549, both genes were down-regulated with the doses, whereas in Calu-1 they were upregulated. Therefore, the HR genes in these cell lines responded differently to IR. The dose-dependant increase in the HR repair pathway genes exhibited in Calu-1 could be associated with the corresponding increased unrepaired foci observed in our $\gamma$H2AX results at 24 hrs after IR. In H460 instead, RAD51 and BRCA2 were both down-regulated at 4 Gy, but then increased in a dose-dependant manner. This suggested that, depending on the dose, opposite effects could be stimulated. The transcriptional repression of RAD51 in both chronic hypoxic (0.5% and

0.01% $O_2$) and post-hypoxic conditions was reported by Bindra et al., where they also found that A549 had the largest decrease in gene expression compared to the other investigated cell lines in their study (249). As far as the NHEJ pathway is concerned, the analysis of DNA-PKcs and Ku-80 showed strong variability with doses and cell type in normoxia. In hypoxia, these genes maintained similar trends within each cell lines. However, in general also NHEJ pathway resulted downregulated at a gene level compared to normoxia, except for Ku-80 in Calu-1. This was in agreement with studies by Meng et al. on pancreatic cancer cells reporting the down-regulation of DSB repair genes in both pathways under long hypoxic exposure (48-72 hrs of 0.2% $O_2$) (113). It is a well-established observation that cancerous cells alter their DNA damage response and repair systems in hypoxia resulting in genomic instability and thereby resistance to therapy treatments (112, 250, 251). Our results re-emphasise this for the three NSCLC cell lines investigated in this study, where we observed a downregulation of both NHEJ and HR repair pathway related genes in response to chronic hypoxia. However, the decrease was more evident for the genes related to the HR pathway compared with the NHEJ pathway for all cell lines. Although many studies have reported a downregulation of HR in hypoxia, the consensus on the response of NHEJ repair pathway is less well defined and understood (113).

The two main DSB repair pathways, NHEJ and HR, are known to be utilised by the cell at different phases in the cell cycle (i.e. NHEJ: throughout the cell cycle but mainly in G0-G1 (252); HR: only in S- and G2-phase (253)) and activated to delay the progression of cell cycle and, if necessary, induce cell death. At 24 hrs time point the main effects were observed. As expected, the changes in the expression levels of the repair genes (section 4.3.9) in normoxia, for the most part, corroborated with the observed changes in the normoxic cell cycle results, where an arrest was mainly activated in the G0-G1 for H460 cell line and with this the NHEJ pathway was more activated. However, Calu-1 appeared to continue to rely on both the HR and the NHEJ repair pathways following irradiation with no downregulation observed for the investigated genes in either of the pathways (figure 4.37). It is important to mention that Calu-1 cells are p53 null, thereof they should be less dependant on the G0-G1 checkpoint. Nonetheless, the p53 status of the Calu-1 did not explain the discrepant observed accumulation of cells in G0-G1. To possibly reconciliate these data, indeed a strong link between p53 and HR machinery, in particular BRCA1, has been reported (254) and a role of p53 in choosing the DSB repair pathway and striking a balance between HR and NHEJ was also proposed (255).

However, for the highest dose, H460 and Calu-1 cells accumulated mainly in G2-M phase (figure 4.29). This did not correlate with the results in H460, since the HR genes were less expressed. It is possible that, for this cell line, a main role can be played by other genes, that have not been included in this studied. On the other hand, these data also coincides with the high number of DSBs measured (figure 4.15), possibly residual cDSBs, at this dose for both these two cell lines. In fact, analysis from the cell death assay (figure 4.31) showed that the more radio-sensitive cell line, H460, had a considerable amount of cell death after 8 Gy at 48 hrs post-IR, whereas, Calu-1 had no increase in cell death compared to the non-IR sample. It might be that Calu-1 has a slower repair system. A549, on the other hand, exhibited no block in the cell cycle and also no quadratic increase of DSBs at high doses. Interestingly, however, the genetic results in section 4.3.9 showed a decreasing expression of WEE1 with increasing IR for the A549 cell line, although no change in expression was observed for the other two cell lines. Since one of WEE1s main roles is preventing cells from entering mitosis too early by activating cell cycle arrest in the G2 or S-phase of the cell cycle (256), then these observations could potentially explain the lack of the expected block at these cell cycle checkpoints in the A549 cell line. Nevertheless, no increase in cell death was observed for this radio-resistant cell line at 48 hrs post-IR (figure 4.31). When exposed to long-term hypoxia after IR, surprisingly all cell lines activated mainly the G2-M phase which was correlated with a strong over-expression of WEE1 for all cell types. G2-M is also reported to be the phase where the expression of RAD51 is maximal. Nevertheless, in hypoxia, RAD51 resulted downregulated at all doses. This block, however, was not associated with cell death at least up until 48 hrs after IR, which has been shown to be a sufficient time point to notice a tendency of cells towards cell death (257, 258). This further demonstrated the high radio-resistance of the hypoxic lung cancer cells. Moreover, as reported above, all the genes for the NHEJ and HR investigated were downregulated, in all cell lines, but cells were still able to activate a block before entering mitosis.

In conclusion, our data support the concept that hypoxia might favour genetic instability and the selection of more resistant and aggressive phenotype. In fact, the adaptive responses to hypoxia in the context of radiation treatment, including the downregulation of repair genes, the activation of the antioxidant systems, and the block in G2-M with no induction of cell death following IR, resulted in less DNA damages and higher survival rates in NSCLC cell lines.

# 5 Conclusion and Future Perspectives

Cancer is a detrimental disease affecting millions of people worldwide, however, there has been increasing amounts of research into understanding the characteristics of cancer cells and the mechanisms behind their erratic behaviour which makes them more prone to being resistant to treatments such as radiation therapy. Cancer cells, in general, are highly proliferative which can cause an accumulation of DNA mutations, driven by the creation of reactive oxygen species (ROS) and thereby resulting in genetic instability and/or changes in the cell's DNA damage response (DDR). In addition, they can also develop low oxygenated or nutrient deprived environments which they can willingly adapt to by altering their, already rewired, metabolism. Both of these cancer traits, genomic instability (i.e. ROS, DDR, antioxidants) and metabolic reprogramming (OXPHOS, glycolysis etc.), are in fact emerging hallmarks in cancer and contribute to their therapy resistance. However, these attributes are largely influenced by the environmental conditions, in addition to being cell- and organ-type dependent, and therefore need to be further explored for developing a more personalised and cell specific treatment regime.

The initial section of this study showcased the adaptive processes of cancer cell lines from different bodily organs under various levels of hypoxia, to account for the tumour scenario of short- and long-term nutrient deprivation. The first results highlighted that cancer cell lines can have varying consumption rates (defined by the removal rate of oxygen (ORR) from the media) which in turn could be related to the metabolic processes which they use, for example cancer cell lines that still uses OXPHOS would probably need more oxygen than a cell line that has a tendency towards glycolysis. The morphological properties of the cell were also found to have a correlation with the ORR as it had a somewhat linear dependence on the surface-to-volume ratio, indicating a faster $O_2$ consumption/removal with a larger surface area-to-volume ratio (i.e. with more volume and less surface area diffusion of oxygen into

the cell is slower). Impressively, in both hypoxic conditions the cells were able to maintain an oxic-like cell progression as well as ATP production, albeit a small decrease for most cell lines, reiterating their ability to modify their cellular processes, possibly assisted by their increased reducing potential observed and thereby contributing to their enhanced survival after irradiation (IR). Severely chronic hypoxic cells, in fact, were observed to have a potential enhancement of glycolysis (i.e. as indicated by PGK1 mRNA levels) and a possible decrease of OXPHOS (i.e. as indicated by MTCO-1 mRNA levels) compared to normally oxygenated cells, with IR inducing a slight increase in the glycolytic pathway, and a subsequent increase in the cellular ATP content, with the exception of the lung cancer cell line, H460. Nonetheless, admittedly, the possibility that cells were also not consuming ATP and FFNN, which would result in their accumulation, cannot be ruled out, although negative regulatory feedbacks might then occur. This provides a hint and stimulates further research to better elucidate these responses. The reducing power was already strongly upregulated in hypoxia and resulted in only a minor stimulation by IR. Interestingly, the downregulation of the HIF-1$\alpha$ mRNA for majority of cell lines highlights that the metabolic reprogramming in relation to the PPP, glycolytic pathway and OXPHOS, can not only be attributed to an accumulation of HIF-1$\alpha$ mRNA, in addition to the fact that it is largely depending on cell type and the hypoxic severity. Moreover, we show a possible link between HIF-1$\alpha$ and the glycolytic pathway in the radio-resistant hypoxic cells, as indicated by PGK1 mRNA levels, and highlight that highly glycolytic behaviour of hypoxic cancer cells can be a contributing factor to their resistance to radiation in hypoxia.

We have therefore demonstrated that the combination of hypoxia and IR leads to alterations in the metabolic processes of different tumour tissue cell lines. However, this inadvertently can also affect the production of reactive oxygen species (ROS) within the cell, thereby influencing the DNA through damages or by manipulating the damage responses which can result in the cells becoming genomically unstable and more resistant to therapies. Looking to one particular tumour type, lung, the nuclear $H_2O_2$ levels (i.e. most stable and long-lived ROS) were in fact induced by IR under normoxic conditions, and directly correlated with the DNA DSB damages. However, the observed reduction of nuclear $H_2O_2$ in hypoxia appeared to be unaffected by IR and thus highlights a possible reason for the reduced DNA damage, and subsequent downregulation of DNA repair genes and enhanced radio-resistance of the hypoxic cells. Moreover, for the most part, after the initial dose of IR, lung cancer cell lines

appeared to increase their repair gene expression with increasing dose, although, the balance between the repair pathways varied among cell lines. Deepening this aspect can improve our understanding of the strategies that different tumours put into action to deal with IR-induced damages and how they increase their radio-resistance ability. The cytosolic $H_2O_2$ in normoxic lung cancer cells, on the other hand, was unaltered by lower, and possibly more clinically relevant, doses, potentially due to the upregulation of the cellular antioxidant capacity. In addition, the master regulator of anti-oxidants, NRF2, was highly upregulated in hypoxia in all NSCLC cell lines and therefore possibly elicited a surge of scavenging ROS potential, which thereby contributed to the higher survival of the hypoxic NSCLC cell lines.

In conclusion, our present study showed that cancer cell metabolism is further altered under low oxygen availability (i.e. hypoxia), and also in response to irradiation treatment. The significant changes in the redox state of the cells in hypoxia, in addition to the sufficient alteration in their bio-energetics, can participate in enhancing cell survival and in contributing to radiation resistances of cancer cell lines. It would therefore be interesting to conduct a more in depth analysis of the metabolic profiling of cancer cells to specifically define which metabolites are driving their treatment resistant behaviour and could be potential targets for therapy. Moreover, this study highlighted that hypoxic cells have altered oxidant and antioxidant capacity as well as changes in their DNA damage response, which resulted in reduced DNA damage and higher probability of cell survival. These findings therefore provide information on the more aggressive phenotype of resistant hypoxic cancer cells which could be further developed on in future studies.

# List of Scientific Contributions

**Peer Reviewed Articles**

P.I Tirinato, L., Marafioti, M. G., Pagliari, F., Jansen, J., Aversa, I., **Hanley, R.**, Nisticò, C., Garcia-Calderón, D., Genard, G., Guerreiro, J. F., Costanzo, F. S., Seco, J. (2021). Lipid droplets and ferritin heavy chain: A devilish liaison in human cancer cell radioresistance. ELife. https://doi.org/10.7554/ELIFE.72943

P.II Nisticò, C., Pagliari, F., Chiarella, E., Guerreiro, J. F., Marafioti, M. G., Aversa, I., Genard, G., **Hanley, R**., Garcia-Calderón, D., Bond, H. M., Mesuraca, M., Tirinato, L., Spadea, M. F., Seco, J. C. (2021). Lipid Droplet Biosynthesis Impairment through DGAT2 Inhibition Sensitizes MCF7 Breast Cancer Cells to Radiation. International Journal of Molecular Sciences. https://doi.org/10.3390/IJMS221810102

P.III Jansen, J., Knoll, J., Beyreuther, E., Pawelke, J., Skuza, R., **Hanley, R.** , Brons, S., Pagliari, F., Seco, J. (2021). Does FLASH deplete oxygen? Experimental evaluation for photons, protons, and carbon ions. Medical Physics. 3982–3990. https://doi.org/10.1002/MP.14917

P.IV Jansen, J., Vieten, P., Pagliari, F., **Hanley, R.**, Marafioti, M. G., Tirinato, L., Seco, J. (2021). A Novel Analysis Method for Evaluating the Interplay of Oxygen and Ionizing Radiation at the Gene Level. Frontiers in Genetics. https://doi.org/10.3389/FGENE.2021.597635

P.V Guerreiro, J. F., Gomes, M. A. G. B., Pagliari, F., Jansen, J., Marafioti, M. G., Nistico, C., **Hanley, R.**, Costa, R. O., Ferreira, S. S., Mendes, F., Fernandes, C., Horn, A., Tirinato, L., Seco, J. (2020). Iron and copper complexes with antioxidant activity as inhibitors of the metastatic potential of glioma cells. 12699–12710. https://doi.org/10.1039/D0RA00166J

# Conference Contributions

C.I Jansen,J., Knoll, J., Beyreuther, E., Pawelke, J., Skuza, **R., Hanley**, R., Brons, S., Pagliari, F., Seco, J.: **Oral presentation:** Does oxygen depletion occur in FLASH-RT? Experimental evaluation for photons, protons and carbon ions. *PTCOG59, 59th annual meeting of the Particle Therapy Co-Operative Group (PTCOG) 2021*

C.II J. Jansen, J. Knoll, R. Skuza, **R. Hanley**, L. Hehn, G. Echner, S. Brons, F. Pagliari, J. Seco: **Oral presentation:** Implementation of an online oxygen meter for studying oxygen removal during FLASH irradiation. *PTCOG59, 59th annual meeting of the Particle Terapy Co-Operative Group (PTCOG) 2020*

C.III **Hanley, R.**, Pagliari, F., Dias, M.F., Marafioti, M.G., Jansen, J., Guerreiro, J., Tirinato, L., Seco, J. **Poster Presentation:** Evaluation of Novel Optical $O_2$ Sensor Spots: Oxygen Consumption Rate of Cancer Cells in Radio-Biology, *PhD Retreat 2019*

C.IV Jansen, J., Tirinato, L., Maraoti, M.G., **Hanley, R.**, Yao, X.Q., Pagliari, F., Seco, J.: **Oral Presentation:** Preliminary gene expression results of cancer cells in hypoxic and normoxic environment under irradiation (doi: 10.15129/GSI-2019-00596) *International Biophysics Collaboration Meeting 2019*

C.V J.F. Guerreiro, **R. Hanley**, L. Tirinato, F. Pagliari, M.G. Marafioti, O.M. Gil, F. Mendes, J. Seco. **Poster presentation:** Study of the effectiveness of low-densely ionizing radiation as a DNA-damaging anticancer treatment in different cancer cell lines *The 3rd International Conference on Dosimetry and its Applications (ICDA-3) 2019*

C.VI J. Jansen, L. Tirinato, M.G. Marafioti, **R. Hanley**, X.Q. Yao, F. Pagliari, J. Seco. **Poster presentation:** Gene expression of cancer cells in hypoxic and normoxic environment under irradiation. *PTCOG58, 58th annual meeting of the Particle Therapy Co-Operative Group (PTCOG) 2019*

C.VII Jansen, J., Tirinato, L., Maraoti, M.G., Yao, X.Q., **Hanley, R.**, Ribeiro, T., Pagliari, F., Seco, J. **Poster Presentation:** Gene Expression of SK-BR-3 in Hypoxic and Normoxic Environment under Photon Radiation, *3rd Heidelberg Symposium on Novel Techniques in Ion Beam Radiotherapy 2018*

C.VIII **Hanley, R.**, Pagliari, F., Dias, M.F., Tirinato, L., Seco, J. **Poster Presentation:** Evaluation of Optical $O_2$ Sensors for in-vitro Radiation Biology, *3rd Heidelberg Symposium on Novel Techniques in Ion Beam Radiotherapy 2018*

C.IX Marafioti, M.G., Tirinato, L., Pagliari, F., Jansen, J., Hanley, R., Yao, X.Q., Ribeiro, T., Costanzo, F.S., Seco, J. **Poster presentation:** Lipid Droplets: A new player in radioresistance of breast and lung cancer cells. *Frontiers in Cancer Research Conference Heidelberg 2018*

# Acronyms

**AP** Apurinic sites. 11

**ARE** Antioxidant response element. 15

**ATP** Adenosine triphosphate. 41, 46, 57, 58, 60, 62, 70–72, 75, 84, 86, 87, 89, 90

**BD** Base damage. 11

**BRCA2** Breast cancer type 2. 141, 142, 144, 146, 148, 156

**BSA** Bovine serum albumin. 96, 97

**CAT** Catalase. 15, 93

**COX1** Cytochrome c oxidase 1. 75

**DDR** DNA damage repair. 17, 18, 21–23, 28, 29, 93

**DNA** Deoxyribonucleic acid. 10–12, 93, 110, 119

**DNA-PKcs** DNA-dependent protein kinase catalytic subunit. 141, 142, 144, 146, 148, 157

**DSBs** Double strand breaks. 11, 19, 20, 22, 28, 38, 93, 110, 116, 117, 119, 141

**ETC** Electron transport chain. 16, 31–34, 59, 82

**FADH2** Flavin adenine dinucleotide. 59, 60, 73

**FFNN** FADH2, FMNH2, NADH and NADPH. 60–62, 73–75, 87, 88

**FMNH2** The reduced form of flavin mononucleotide. 60

**FPC** DSB foci per cell. 110–112

**G6P** Glucose-6-phosphate. 35

**G6PD** Glucose-6-phosphate dehydrogenase. 22, 35–37, 75–78, 80, 82, 87, 88

**GPX** Glutathione peroxidase. 15, 16

**GPX1** Glutathione peroxidase 1. 93, 133, 134, 136, 138, 153–155

**GRX** Glutaredoxin. 133, 134, 136, 138, 140, 153, 155

**GSH** Glutathione. 15, 16, 36, 100, 123, 126–128

**GSR** Glutathione reductase. 36, 123, 133, 134, 136, 138, 140, 153–156

**GSSG** Glutathione (oxidised). 16, 36, 100, 123, 126, 127

**HBSS** Hanks' balanced salt solution. 97–100

**HC** Hypoxic chamber. 43, 51, 52, 96

**HIF** Hypoxia inducible factor. 24–29, 33–35, 37, 75, 76, 78, 80, 82, 90, 91

**HR** Homologous recombination. 19, 20, 28, 38, 133, 141, 142, 144, 146, 148, 156–158

**IR** Ionizing radiation. 95, 97, 98, 106, 110, 112, 117, 119

**KEAP1** Kelch-like ECH associated protein 1. 15, 134, 136, 138, 153

**KERMA** Kinetic energy released per unit mass. 7, 8

**Ku-80** Heterodimer protein. 141, 142, 144, 146, 148, 157

**LET** Linear energy transfer. 5, 8–11, 64

**LINAC** Linear accelerator. 2, 3

**LQM** Linear quadratic model. 9

**mRNA** Messenger ribonucleic acid. 26, 36, 75, 76, 78, 80, 82, 89, 90, 133, 134, 136, 138, 141, 142, 144, 146, 153–156

**MTCO-1** Cytochrome c oxidase 1.. 75, 76, 78, 80, 82, 89, 90

**NADH** Nicotinamide adenine dinucleotide. 46, 59, 60, 73, 87, 88

**NADPH** Nicotinamide adenine dinucleotide phosphate. 14, 16, 22, 29, 34–37, 46, 59, 60, 73, 75, 79, 87, 88

**NHEJ** Non-homologous end-joining. 18–20, 28, 38, 133, 141, 142, 144, 146, 148, 157, 158

**NOX** NADPH oxidase. 14, 16

**NRF2** Nuclear erythroid 2-related factor. 15, 133, 134, 136, 138, 140, 153–156

**NSCLC** Non-small cell lung carcinoma. 28, 40, 92, 93, 104, 110, 117

**NucPE1** Nuclear Peroxy Emerald 1. 97, 117, 120, 128

**OCR** Oxygen consumption rate. 52, 54

**OER** Oxygen enhancement ratio. 10, 47, 64, 108, 109, 112, 116, 134, 149, 150

**ORR** Oxygen removal rate. 52, 86

**OXPHOS** Oxidative phosphorylation. 27, 29, 30, 33, 35, 41, 57–59, 72, 75, 76, 78, 80, 82, 86, 89, 90

**PBS** Phosphate buffered saline. 45, 47, 48, 95–100

**PFA** Paraformaldehyde. 45, 96

**PGK1** Phosphoglycerate kinase 1. 75, 76, 78, 80, 82, 89, 90

**PHD2** HIF-1 alpha regulator. 75, 76, 78, 80–82, 90

**PHDs** Proline hydroxylation domain proteins. 25

**PI** Propidium iodide. 131

**PPP** Pentose phosphate pathway. 22, 27, 29, 35, 37, 60, 75, 77, 78, 81, 82, 88, 90

**PY1-ME** Peroxy yellow 1 methyl-ester. 99, 120

**RAD51** RAD51 Recombinase. 141, 142, 144, 146, 148, 156, 158

**RNA** Ribonucleic acid. 48, 101

**ROI** Region of interest. 49, 103

**ROS** Reactive oxygen species. 11, 13–16, 21, 22, 24, 27, 31–40, 60, 87, 93, 100, 117, 119, 123

**RT** Radiation therapy. 1, 2, 7, 8, 14, 93

**RT-qPCR** reverse transcription quantitative real-time PCR. 48, 75, 78, 80, 82, 102, 133, 134, 155

**Ru5P** Ribulose-5-phosphate. 35

**SCLC** Small cell lung carcinoma. 92

**SF** Survival fraction. 107

**SOD** Superoxide dismutase. 13, 15

**SSBs** Single strand breaks. 11

**TR** Thioredoxin reductase. 36

**TRX** Thioredoxin. 15, 16, 36, 133, 134, 136, 138, 140

**WEE1** WEE1 G2 Checkpoint Kinase. 141, 142, 144, 146, 148, 158

# List of Figures


1.1 Schematic of the ionisation of an atom . . . . . 2
1.2 Dominant processes of photon interaction with matter . . . . . 4
1.3 Schematic of the Compton scattering after an incident photon interacts with matter 5
1.4 Photon attenuation coefficients in water. . . . . 7
1.5 Representative graph of the Linear quadratic model (LQM) . . . . . 9
1.6 Illustration of DNA structure . . . . . 10
1.7 Illustration of direct and indirect action to damage DNA . . . . . 11
1.8 Illustration of water radiolysis . . . . . 13
1.9 Schematic overview of the antioxidant response of cancer cells . . . . . 15
1.10 Schematic overview of ROS production and antioxidant system, and how it relates to DNA damage . . . . . 17
1.11 Cell cycle progression and the dominant repair pathways . . . . . 19
1.12 Illustration of DNA damage repair pathways, non-homologous end joining (NHEJ) and homologous recombination (HR), after DSB induction . . . . . 21
1.13 Overview of ROS and the DNA damage repair response (DDR) . . . . . 22
1.14 Illustration of the tumour vasculature and OER . . . . . 25
1.15 Illustration of HIF-$\alpha$ activation under hypoxic conditions . . . . . 26
1.16 Illustration of cell metabolism, highlighting important processes including glycolysis, mitochondrial tricarboxylic (TCA) cycle and the pentose phosphate pathway (PPP) . . . . . 30
1.17 Mitochondrial activity and complexes . . . . . 31
1.18 Mitochondrial electron transport chain (ETC) and protein complexes (I - IV) where reactive oxygen species are produced . . . . . 32
1.19 Pentose Phosphate Pathway . . . . . 36

3.1 Hypoxic chamber used in this project by Sci-Tive, Baker Ruskin. . . . . 43
3.2 Oxygen concentration in-vitro measurement using PyroScience sensor spots. . . 44
3.3 CellTiter-Glo® Luminescent Cell Viability Assay by Promega . . . . . 46
3.4 PrestoBlue assay . . . . . 47
3.5 X-ray exposure setup using the 6 MV Siemens linear accelerator (LINAC), with the cell culture flask lying perpendicular to the beam at a source to skin distance (SSD) of 100 cm and a field size of 20 cm x 20 cm. . . . . 48
3.6 IMARIS reconstructed images of cell and nucleus volumes for cancer cell lines H4, T24, H460 and PC-3 in hypoxia. . . . . 50
3.7 Oxygen concentration measurements in-vitro using $O_2$ sensor spots and Firesting oxygen meter . . . . . 53
3.8 Nucleus and cell volume measurements of cancer cell lines (H4, H460, T24, PC-3) in acute (12hrs at 1% $O_2$) and chronic (72 hrs at 1% $O_2$) hypoxia . . . . . 55
3.9 Nucleus and cell size measurements of cancer cell lines (H4, H460, T24, PC-3) in acute hypoxia (12 hrs at 1% $O_2$) related to the ORR . . . . . 56
3.10 Cell cycle progression of cancer cell lines (H4, H460, T24, PC-3) in acute and chronic hypoxia . . . . . 57
3.11 Energy metabolism of cancer cell lines (H4, H460, T24, PC-3) in acute and chronic hypoxia . . . . . 59
3.12 Reducing power of cancer cell lines (H4, H460, T24, PC-3) in acute and chronic hypoxia . . . . . 61
3.13 Clonogenic assays of cancer cell lines (H4, H460, T24, PC-3) under different oxygen conditions: 21% $O_2$, 0.6% $O_2$ and 0.1% $O_2$ . . . . . 63
3.14 Clonogenic assays of cancer cell lines (H4, H460, T24, PC-3) indicating their enhanced survival under hypoxic conditions (i.e. 0.6% $O_2$ and 0.1% $O_2$) . . . . . 65
3.15 Cell and nucleus volume measurements of cancer cell lines (H4, H460, T24, PC-3) 72 hrs post-IR in normoxia and hypoxia . . . . . 68
3.16 Cell cycle progression of cancer cell lines (H4, H460, T24, PC-3) 72 hrs post-IR in normoxia and hypoxia . . . . . 69
3.17 Energy metabolism of cancer cell lines (H4, H460, T24, PC-3) 72 hrs post-IR in normoxia and hypoxia . . . . . 71

3.18 Reducing power of cancer cell lines (H4, H460, T24, PC-3) 72 hrs post-IR in normoxia and hypoxia . . . . . 74
3.19 H4 genetic evaluation of metabolism 72 hrs post-IR in normoxia and hypoxia . . 77
3.20 H460 genetic evaluation of metabolism 72 hrs post-IR in normoxia and hypoxia . 79
3.21 T24 genetic evaluation of metabolism 72 hrs post-IR in normoxia and hypoxia . . 81
3.22 PC-3 genetic evaluation of metabolism 72 hrs post-IR in normoxia and hypoxia . 83

4.1 Image of the Sci-Tive Baker Ruskin hypoxia chamber used for low oxygen experiments. . . . . 94
4.2 Schematic representation of sample preparation for inducing hypoxia in cells prior to irradiation for the clonogenic assay protocol. . . . . 95
4.3 X-ray exposure setup in the MultiRad225 Faxitron with the cell culture flask lying perpendicular to the beam at a distance of 37 cm and a field size of 20 cm x 20 cm. A copper filter with 0.5 mm was used for all experiments. . . . . 96
4.4 Illustration of the change in the chemical composition of NucPE1 molecule following interaction with $H_2O_2$, resulting in an enhanced fluorescence signal. (222) 97
4.5 Schematic illustration of the NucPE1 fluorescence staining protocol prior to signal acquisition at the flow cytometer for detection of $H_2O_2$ in the nucleus of the cell. . . . . 98
4.6 Schematic illustration of the PY1-ME fluorescence staining protocol prior to signal acquisition at the flow cytometer for detection of $H_2O_2$ in the cytosol of the cell. . . . . 99
4.7 Illustration of the change in the chemical composition of PY1-ME molecule following interaction with $H_2O_2$, resulting in an enhanced fluorescence signal. (223) 99
4.8 Illustration of GSH/GSSG assay from Promega whereby glutathione S-transferase enzyme is coupled to a firefly luciferase reaction and is used to convert the Luciferin-NT (GSH probe) to luciferin. (224) . . . . . 101
4.9 Cell growth profiles of NSCLC over 72hours in normoxia and hypoxia . . . . . 104
4.10 Brightfield images of NSCLC at 24 hrs in normoxia and hypoxia . . . . . 105
4.11 Brightfield images of NSCLC post-IR at 24 hrs in normoxia . . . . . 106
4.12 Brightfield images of NSCLC post-IR at 24 hrs in hypoxia . . . . . 107
4.13 Clonogenic assays of NSCLC cell lines conducted in normoxia and hypoxia . . . 108

4.14 Clonogenic assays of NSCLC cell lines conducted in normoxia and hypoxia indicating OER . . . 109
4.15 DSBs detected by immunoflourescent staining of $\gamma$H2AX foci of NSCLC cell lines post-IR at 30 min and 24 hrs in normoxia and hypoxia . . . 111
4.16 Confocal images of $\gamma$H2AX foci post-IR in normoxia for NSCLC cell lines. . . . 113
4.17 Confocal images of $\gamma$H2AX foci post-IR in hypoxia for NSCLC cell lines. . . . 114
4.18 Repair capacity of DSBs detected by immunoflourescent staining of $\gamma$H2AX foci of NSCLC cell lines post-IR at 30 min and 24 hrs in normoxia and hypoxia . . . 115
4.19 Determination of $OER_{DSB}$ for NSCLC in hypoxia and normoxia at 30 min and 24 hrs post-IR. . . . 116
4.20 Confocal microscopy images of localisation of NucPE1 in the nuclei of NSCLC cell lines in normoxia . . . 118
4.21 Normalised plot of nuclear $H_2O_2$ production post-IR at 30 min and 24 hrs detected using NucPE1 of NSCLC cell lines in normoxia and hypoxia . . . 119
4.22 Normalised DSBs per cell vs Nuclei $H_2O_2$ for NSCLC cell lines (H460, A549, Calu-1) at 30 min post-IR in normoxia (21% $O_2$) and hypoxia (0.1% $O_2$) . . . 120
4.23 Confocal microscopy images of localisation of PY1-ME in the cytosol of NSCLC cell lines in normoxia . . . 121
4.24 Normalised plot of cytosolic $H_2O_2$ production post-IR at 30 min and 24 hrs detected using PY1-ME of NSCLC cell lines in normoxia and hypoxia . . . 122
4.25 Schematic illustration of the production of oxidised (GSSG) and reduced glutathione (GSH) . . . 123
4.26 GSH/GSSG ratio comparing NSCLC cell lines (H460, A549, Calu-1) in normoxia (21% $O_2$) and hypoxia (0.1% $O_2$) at 30 min and 24 hrs post-IR . . . 124
4.27 GSH/GSSG ratio for NSCLC comparing normoxia (21% $O_2$) and hypoxia (0.1% $O_2$) at 30 min and 24 hrs post-IR . . . 126
4.28 Glutathione levels (oxidised and reduced) of NSCLC cell lines at 24 hrs in normoxia and hypoxia . . . 127
4.29 Cell cycle progression of NSCLC cell lines at 30 min and 24 hrs post IR in normoxia 129
4.30 Cell cycle progression of NSCLC cell lines at 30 min and 24 hrs post IR in hypoxia 131
4.31 Cell death assay for H460, A549, Calu-1 using propidium iodide (PI) staining at 48 hrs post-IR in normoxia and hypoxia . . . 132

4.32 H460 antioxidant genes 24 hrs post-IR in normoxia and hypoxia . . . . . 135
4.33 A549 antioxidant genes 24 hrs post-IR in normoxia and hypoxia . . . . . 137
4.34 Calu-1 antioxidant genes 24 hrs post-IR in normoxia and hypoxia . . . . . 139
4.35 H460 repair genes 24 hrs post-IR in normoxia and hypoxia . . . . . 143
4.36 A549 repair genes 24 hrs post-IR in normoxia and hypoxia . . . . . 145
4.37 Calu-1 repair genes 24 hrs post-IR in normoxia and hypoxia . . . . . 147

# List of Tables

1.1 Water radiolysis yields in µmol $J^{-1}$ following exposure of water (pH 3 - 11) to gamma radiation and electrons with LETs of 0.2 - 0.3 keV $\mu m^{-1}$. Adapted from (19). . . . . 13

3.1 Median oxygen percentage ($O_2$%) in healthy tissue and tumour tissue from different organs in the body including brain, lung, bladder, and prostate. Table adapted from Mckeown et. al (183) . . . . . 41

3.2 List of genes used in this study and their corresponding forward and reverse primers for RT-qPCR analysis . . . . . 49

3.3 OER cancer cell lines (H460, PC-3, T24, H4) determined from clonogenic results conducted at normoxic oxygen levels (21% $O_2$) . . . . . 64

3.4 $\alpha$ and $\beta$ values for cancer cell lines (H460, PC-3, T24, H4) determined from clonogenic results conducted at normoxic oxygen levels (21% $O_2$) . . . . . 66

3.5 $\alpha$ and $\beta$ values for cancer cell lines (H460, PC-3, T24, H4) determined from clonogenic results conducted at hypoxic oxygen levels (0.6% $O_2$) . . . . . 66

3.6 $\alpha$ and $\beta$ values for cancer cell lines (H460, PC-3, T24, H4) determined from clonogenic results conducted at hypoxic oxygen levels (0.1% $O_2$) . . . . . 66

4.1 List of genes used in this study and their corresponding forward and reverse primers for RT-qPCR analysis . . . . . 102

4.2 Doubling times (hours) of non-small lung cancer cells (H460, A549, Calu-1) cultured under different oxygen levels (i.e. normoxia (21% $O_2$) and hypoxia (0.1% $O_2$)) . . . . . 105

4.3 Alpha and beta values for lung cancer cell lines (H460, A549, Calu-1) determined from clonogenic assays conducted at different oxygen levels (21%, 0.1% $O_2$) . . . . . 108
4.4 The dose applied to achieve a cell survival of 50% (D50), 10% (D10) and 1% (D1) for each NSCLC cell line (H460, A549, Calu-1) in normoxia (21% $O_2$) and hypoxia (0.1% $O_2$). The ratio of the D10 values in both oxygen conditions was used to calculate the OER factor. . . . . 109
4.5 Factor reduction of DSBs from peak foci at 30 min to residual foci at 24 hrs post-IR. 115
4.6 GSH/GSSG Ratio of NSCLC in normoxia (21% $O_2$) at 30 min and 24 hrs post-IR. 125
4.7 GSH/GSSG Ratio of NSCLC in hypoxia (0.1% $O_2$) at 30 min and 24 hrs post-IR. . 125

# Bibliography


[1] E J Hall and A J Giaccia. *Radiobiology for the Radiologist*. Online access with subscription: LWW Classic Book Collection. Lippincott Williams & Wilkins, 2006. ISBN 9780781741514. URL https://books.google.de/books?id=6HhjwRyqBzgC.

[2] Lesson Explainer: Ionization Energy | Nagwa. URL https://www.nagwa.com/en/explainers/840185315807/.

[3] Wolfgang Schlegel, Christian P. Karger, and Oliver Jaeckel. Medizinische physik. 2018. doi: https://doi.org/10.1007/978-3-662-54801-1.

[4] Ervin D. Podgorsak and International Atomic Energy Agency. *Radiation oncology physics : a handbook for teachers and students.* International Atomic Energy Agency, 2005. ISBN 9201073046.

[5] James E. Turner. Atoms, Radiation, and Radiation Protection: Third Edition. *Atoms, Radiation, and Radiation Protection: Third Edition*, pages 1–585, oct 2007. doi: 10.1002/9783527616978. URL https://onlinelibrary.wiley.com/doi/book/10.1002/9783527616978.

[6] Principles of Radiologic Physics and Dosimetry. *Manual of Interventional Oncology*, apr 2018. doi: 10.1055/B-0038-160294. URL https://oncohemakey.com/principles-of-radiologic-physics-and-dosimetry/.

[7] Samuel J. Ling, Jeff Sanny, and William Moebs. University Physics Volume 3, sep 2016.

[8] International Atomic Energy Agency. *Diagnostic Radiology Physics: A Handbook for Teachers and Students*. STI/PUB. International Atomic Energy Agency, 2014. ISBN 9789201310101.

[9] Basics of Radiation Therapy | Clinical Gate. URL https://clinicalgate.com/basics-of-radiation-therapy-2/.

[10] National Institute of Standards and Technology. XCOM: Photon Cross Sections Database | NIST. URL https://www.nist.gov/pml/xcom-photon-cross-sections-database.

[11] Wazir Muhammad, Amjad Hussain, and Muhammad Maqbool. Basic Concepts in Radiation Dosimetry. pages 9–41, 2017. doi: 10.1007/978-3-319-61540-0_2.

[12] Stephen Joseph McMahon. The linear quadratic model: Usage, interpretation and challenges. *Physics in Medicine and Biology*, 64(1):01TR01, jan 2019. ISSN 13616560. doi: 10.1088/1361-6560/aaf26a. URL https://doi.org/10.1088/1361-6560/aaf26a.

[13] Helen Kreuzer and Adrianne Massey. DNA Structure, 2014. URL https://www2.nau.edu/lrm22/lessons/dna{_}notes/dna{_}notes.html.

[14] Jose G. Bazan, Quynh-Thu Le, and Daniel Zips. Radiobiology of Lung Cancer. *IASLC Thoracic Oncology*, pages 330–336.e2, 2018. doi: 10.1016/B978-0-323-52357-8.00035-4.

[15] Alexandra C. Vítor, Pablo Huertas, Gaëlle Legube, and Sérgio F. de Almeida. Studying DNA Double-Strand Break Repair: An Ever-Growing Toolbox. *Frontiers in Molecular Biosciences*, 7:24, feb 2020. ISSN 2296889X. doi: 10.3389/fmolb.2020.00024.

[16] Ryoichi Hirayama, Atsushi Ito, Masanori Tomita, Teruyo Tsukada, Fumio Yatagai, Miho Noguchi, Yoshitaka Matsumoto, Yuki Kase, Koichi Ando, Ryuichi Okayasu, and Yoshiya Furusawa. Contributions of direct and indirect actions in cell killing by high-LET radiations. *Radiation research*, 171(2):212–218, feb 2009. ISSN 0033-7587 (Print). doi: 10.1667/RR1490.1.

[17] Cláudio M. Lousada, Inna L. Soroka, Yuriy Yagodzinskyy, Nadezda V. Tarakina, Olga Todoshchenko, Hannu Hänninen, Pavel A. Korzhavyi, and Mats Jonsson. Gamma radiation induces hydrogen absorption by copper in water. *Scientific Reports*, 6, apr 2016. ISSN 20452322. doi: 10.1038/SREP24234.

[18] Hermann Dertinger and Horst Jung. *Molecular Radiation Biology*. Heidelberg Science Library. Springer US, New York, NY, 1970. ISBN 978-0-387-90013-1. doi: 10.1007/978-1-4684-6247-0.

[19] Sophie Le Caër. Water radiolysis: Influence of oxide surfaces on H2 production under ionizing radiation. *Water (Switzerland)*, 3(1):235–253, 2011. ISSN 20734441. doi: 10.3390/w3010235.

[20] Helmut SIES. Strategies of antioxidant defense. *European Journal of Biochemistry*, 215 (2):213–219, 1993. ISSN 14321033. doi: 10.1111/J.1432-1033.1993.TB18025.X/FORMAT/PDF.

[21] Nan Yang, Wanyue Xiao, Xuejiao Song, Wenjun Wang, and Xiaochen Dong. Recent advances in tumor microenvironment hydrogen peroxide-responsive materials for cancer photodynamic therapy. *Nano-Micro Letters*, 12:1–27, 1 2020. ISSN 21505551. doi: 10.1007/S40820-019-0347-0/FIGURES/14. URL `https://link.springer.com/article/10.1007/s40820-019-0347-0`.

[22] Jennifer J. Hu, Neil Dubin, Deirdre Kurland, Bing Li Ma, and George C. Roush. The effects of hydrogen peroxide on DNA repair activities. *Mutation research*, 336(2):193–201, 1995. ISSN 0027-5107. doi: 10.1016/0921-8777(94)00054-A. URL `https://pubmed.ncbi.nlm.nih.gov/7885389/`.

[23] Upadhyayula Sai Srinivas, Bryce W.Q. Tan, Balamurugan A. Vellayappan, and Anand D. Jeyasekharan. ROS and the DNA damage response in cancer, jul 2019. ISSN 22132317.

[24] Helmut Sies and Dean P. Jones. Reactive oxygen species (ROS) as pleiotropic physiological signalling agents. *Nature reviews. Molecular cell biology*, 21(7):363–383, jul 2020. ISSN 1471-0080. doi: 10.1038/S41580-020-0230-3. URL `https://pubmed.ncbi.nlm.nih.gov/32231263/`.

[25] Wanyeon Kim, Sungmin Lee, Danbi Seo, Dain Kim, Kyeongmin Kim, Eun Gi Kim, Ji Hoon Kang, Ki Moon Seong, Hye Sook Youn, and Bu Hyun Youn. Cellular Stress Responses in Radiotherapy. *Cells*, 8(9), sep 2019. ISSN 2073-4409. doi: 10.3390/CELLS8091105. URL `https://pubmed.ncbi.nlm.nih.gov/31540530/`.

[26] Haotian Yang, Rehan M. Villani, Haolu Wang, Matthew J. Simpson, Michael S. Roberts, Min Tang, and Xiaowen Liang. The role of cellular reactive oxygen species in cancer chemotherapy. *Journal of experimental & clinical cancer research : CR*, 37(1), nov 2018. ISSN 1756-9966. doi: 10.1186/S13046-018-0909-X. URL https://pubmed.ncbi.nlm.nih.gov/30382874/.

[27] Jie Wang and Jing Yi. Cancer cell killing via ROS: to increase or decrease, that is the question. *Cancer biology & therapy*, 7(12):1875–1884, 2008. ISSN 1555-8576. doi: 10.4161/CBT.7.12.7067. URL https://pubmed.ncbi.nlm.nih.gov/18981733/.

[28] Dilip Narayanan, Sana Ma, and Dennis Özcelik. Targeting the redox landscape in cancer therapy. *Cancers*, 12:1–31, 7 2020. ISSN 2072-6694. doi: 10.3390/CANCERS12071706. URL https://pubmed.ncbi.nlm.nih.gov/32605023/.

[29] R. S. Patwardhan, D. Sharma, R. Checker, M. Thoh, and S. K. Sandur. Spatio-temporal changes in glutathione and thioredoxin redox couples during ionizing radiation-induced oxidative stress regulate tumor radio-resistance. *Free radical research*, 49(10):1218–1232, oct 2015. ISSN 1029-2470. doi: 10.3109/10715762.2015.1056180. URL https://pubmed.ncbi.nlm.nih.gov/26021764/.

[30] Suna Zhou, Wenguang Ye, Qiuju Shao, Mingxin Zhang, and Jun Liang. Nrf2 is a potential therapeutic target in radioresistance in human cancer. *Critical reviews in oncology/hematology*, 88(3):706–715, dec 2013. ISSN 1879-0461. doi: 10.1016/J.CRITREVONC.2013.09.001. URL https://pubmed.ncbi.nlm.nih.gov/24126138/.

[31] Anju Singh, Manish Bodas, Nobunao Wakabayashi, Fred Bunz, and Shyam Biswal. Gain of Nrf2 Function in Non-Small-Cell Lung Cancer Cells Confers Radioresistance. *Antioxidants & Redox Signaling*, 13(11):1627, dec 2010. ISSN 15230864. doi: 10.1089/ARS.2010.3219. URL /pmc/articles/PMC3541552//pmc/articles/PMC3541552/?report=abstracthttps://www.ncbi.nlm.nih.gov/pmc/articles/PMC3541552/.

[32] Donnie R. Stacy, Kim Ely, Pierre P. Massion, Wendell G. Yarbrough, Dennis E. Hallahan, Konjeti R. Sekhar, and Michael L. Freeman. Increased expression of nuclear factor E2 p45-related factor 2 (NRF2) in head and neck squamous cell carcinomas. *Head & neck*, 28(9):813–818, sep 2006. ISSN 1043-3074. doi: 10.1002/HED.20430. URL https://pubmed.ncbi.nlm.nih.gov/16637057/.

[33] C. J. Harvey, R. K. Thimmulappa, A. Singh, D. J. Blake, G. Ling, N. Wakabayashi, J. Fujii, A. Myers, and S. Biswal. Nrf2-regulated glutathione recycling independent of biosynthesis is critical for cell survival during oxidative stress. *Free radical biology & medicine*, 46(4):443–453, feb 2009. ISSN 1873-4596. doi: 10.1016/J.FREERADBIOMED.2008.10.040. URL https://pubmed.ncbi.nlm.nih.gov/19028565/.

[34] Claudia Tonelli, Iok In Christine Chio, and David A. Tuveson. Transcriptional regulation by nrf2. *Antioxidants Redox Signaling*, 29:1727, 12 2018. ISSN 15577716. doi: 10.1089/ARS.2017.7342. URL /pmc/articles/PMC6208165//pmc/articles/PMC6208165/?report=abstracthttps://www.ncbi.nlm.nih.gov/pmc/articles/PMC6208165/.

[35] Vaishali Aggarwal, Hardeep Singh Tuli, Ayşegül Varol, Falak Thakral, Mukerrem Betul Yerer, Katrin Sak, Mehmet Varol, Aklank Jain, Md Asaduzzaman Khan, and Gautam Sethi. Role of Reactive Oxygen Species in Cancer Progression: Molecular Mechanisms and Recent Advancements. *Biomolecules 2019, Vol. 9, Page 735*, 9(11):735, nov 2019. ISSN 2218273X. doi: 10.3390/BIOM9110735. URL https://www.mdpi.com/2218-273X/9/11/735/htmhttps://www.mdpi.com/2218-273X/9/11/735.

[36] Rui Xue Huang and Ping Kun Zhou. DNA damage response signaling pathways and targets for radiotherapy sensitization in cancer, dec 2020. ISSN 20593635. URL https://doi.org/10.1038/s41392-020-0150-x.

[37] Mark J. O'Connor. Targeting the DNA Damage Response in Cancer. *Molecular Cell*, 60 (4):547–560, nov 2015. ISSN 10974164. doi: 10.1016/j.molcel.2015.10.040. URL http://dx.doi.org/10.1016/j.molcel.2015.10.040.

[38] Bert Vogelstein, David Lane, and Arnold J. Levine. Surfing the p53 network. *Nature 2000 408:6810*, 408(6810):307–310, 2000. ISSN 1476-4687. doi: 10.1038/35042675. URL https://www.nature.com/articles/35042675.

[39] Kathryn T. Bieging, Stephano Spano Mello, and Laura D. Attardi. Unravelling mechanisms of p53-mediated tumour suppression. *Nature reviews. Cancer*, 14(5):359–370, 2014. ISSN 1474-1768. doi: 10.1038/NRC3711. URL https://pubmed.ncbi.nlm.nih.gov/24739573/.

[40] Camilla R Elbæk, Valdemaras Petrosius, and Claus S Sørensen. Mutat Res Fund Mol Mech Mutagen WEE1 kinase limits CDK activities to safeguard DNA replication and mitotic entry. *Mutat Res Fund Mol Mech Mutagen*, 819-820(February):111694, 2020. ISSN 0027-5107. doi: 10.1016/j.mrfmmm.2020.111694. URL https://doi.org/10.1016/j.mrfmmm.2020.111694.

[41] Cell Cycle Analysis Assays - Tools to help simplify cell division, mitosis and cell cycle research - DE. URL //www.thermofisher.com/de/de/home/life-science/cell-analysis/cell-viability-and-regulation/cell-cycle.html.

[42] Nimrat Chatterjee and Graham C. Walker. Mechanisms of DNA damage, repair, and mutagenesis. *Environmental and Molecular Mutagenesis*, 58(5):235–263, jun 2017. ISSN 10982280. doi: 10.1002/em.22087. URL /pmc/articles/PMC5474181/ /pmc/articles/PMC5474181/?report=abstracthttps://www.ncbi.nlm.nih.gov/pmc/articles/PMC5474181/.

[43] Shideng Bao, Qiulian Wu, Roger E. McLendon, Yueling Hao, Qing Shi, Anita B. Hjelmeland, Mark W. Dewhirst, Darell D. Bigner, and Jeremy N. Rich. Glioma stem cells promote radioresistance by preferential activation of the DNA damage response. *Nature*, 444(7120):756–760, dec 2006. ISSN 1476-4687. doi: 10.1038/NATURE05236. URL https://pubmed.ncbi.nlm.nih.gov/17051156/.

[44] Linlin Yang, Changxian Shen, Adriana Estrada-Bernal, Ryan Robb, Moumita Chatterjee, Nikhil Sebastian, Amy Webb, Xiaokui Mo, Wei Chen, Sunil Krishnan, and Terence M Williams. Oncogenic KRAS drives radioresistance through upregulation of NRF2-53BP1-mediated non-homologous end-joining repair. *Nucleic Acids Research*, 49(19): 11067–11082, nov 2021. ISSN 0305-1048. doi: 10.1093/NAR/GKAB871. URL https://academic.oup.com/nar/article/49/19/11067/6381135.

[45] Nikolaos Givalos, Hariklia Gakiopoulou, Melina Skliri, Katerina Bousboukea, Anastasia E. Konstantinidou, Penelope Korkolopoulou, Maria Lelouda, Gregory Kouraklis, Efstratios Patsouris, and Gabriel Karatzas. Replication protein A is an independent prognostic indicator with potential therapeutic implications in colon cancer. *Modern Pathology 2007 20:2*, 20(2):159–166, feb 2007. ISSN 1530-0285. doi: 10.1038/modpathol.3800719. URL https://www.nature.com/articles/3800719.

[46] Jan H.J. Hoeijmakers. Genome maintenance mechanisms for preventing cancer. *Nature*, 411(6835):366–374, may 2001. ISSN 00280836. doi: 10.1038/35077232. URL https://pubmed.ncbi.nlm.nih.gov/11357144/.

[47] Alberto Ciccia and Stephen J. Elledge. The DNA Damage Response: Making It Safe to Play with Knives. *Molecular Cell*, 40(2):179–204, oct 2010. ISSN 10972765. doi: 10.1016/j.molcel.2010.09.019. URL /pmc/articles/PMC2988877//pmc/articles/PMC2988877/?report=abstracthttps://www.ncbi.nlm.nih.gov/pmc/articles/PMC2988877/.

[48] Inger Brandsma and Dik C. Gent. Pathway choice in DNA double strand break repair: Observations of a balancing act. *Genome Integrity*, 3(1):1–10, nov 2012. ISSN 20419414. doi: 10.1186/2041-9414-3-9. URL http://www.genomeintegrity.com/content/3/1/9.

[49] Jeremy S. Myers and David Cortez. Rapid activation of ATR by ionizing radiation requires ATM and Mre11. *The Journal of biological chemistry*, 281(14):9346–9350, apr 2006. ISSN 0021-9258. doi: 10.1074/JBC.M513265200. URL https://pubmed.ncbi.nlm.nih.gov/16431910/.

[50] David Cortez, Yi Wang, Jun Qin, and Stephen J. Elledge. Requirement of ATM-dependent phosphorylation of brca1 in the DNA damage response to double-strand breaks. *Science (New York, N.Y.)*, 286(5442):1162–1166, nov 1999. ISSN 0036-8075. doi: 10.1126/SCIENCE.286.5442.1162. URL https://pubmed.ncbi.nlm.nih.gov/10550055/.

[51] Malgorzata Krajewska, Rudolf S.N. Fehrmann, Elisabeth G.E. De Vries, and Marcel A.T.M. van Vugt. Regulators of homologous recombination repair as novel targets for cancer treatment. *Frontiers in Genetics*, 6(MAR):96, 2015. ISSN 16648021. doi: 10.3389/FGENE.2015.00096/BIBTEX.

[52] Xuan Li and Wolf Dietrich Heyer. Homologous recombination in DNA repair and DNA damage tolerance. *Cell research*, 18(1):99–113, jan 2008. ISSN 1748-7838. doi: 10.1038/CR.2008.1. URL https://pubmed.ncbi.nlm.nih.gov/18166982/.

[53] Patrick Sung and Hannah Klein. Mechanism of homologous recombination: mediators and helicases take on regulatory functions. *Nature Reviews Molecular Cell Biology 2006 7:10*, 7(10):739–750, aug 2006. ISSN 1471-0080. doi: 10.1038/nrm2008. URL https://www.nature.com/articles/nrm2008.

[54] Hannes Lans, Jurgen A. Marteijn, and Wim Vermeulen. Atp-dependent chromatin remodeling in the dna-damage response. *Epigenetics Chromatin*, 5:4, 2012. ISSN 17568935. doi: 10.1186/1756-8935-5-4. URL /pmc/articles/PMC3275488//pmc/articles/PMC3275488/?report=abstracthttps://www.ncbi.nlm.nih.gov/pmc/articles/PMC3275488/.

[55] Pierpaola Davalli, Gaetano Marverti, Angela Lauriola, and Domenico D'Arca. Targeting oxidatively induced DNA damage response in cancer: Opportunities for novel cancer therapies. *Oxidative Medicine and Cellular Longevity*, 2018, 2018. ISSN 19420994. doi: 10.1155/2018/2389523.

[56] Tao Shi and Tobias B. Dansen. Reactive Oxygen Species Induced p53 Activation: DNA Damage, Redox Signaling, or Both?, oct 2020. ISSN 15577716. URL https://www.liebertpub.com/doi/abs/10.1089/ars.2020.8074.

[57] Yunxiao Meng, Chi Wei Chen, Mingo M.H. Yung, Wei Sun, Jing Sun, Zhuqing Li, Jing Li, Zongzhu Li, Wei Zhou, Stephanie S. Liu, Annie N.Y. Cheung, Hextan Y.S. Ngan, John C. Braisted, Yan Kai, Weiqun Peng, Alexandros Tzatsos, Yiliang Li, Zhijun Dai, Wei Zheng, David W. Chan, and Wenge Zhu. DUOXA1-mediated ROS production promotes cisplatin resistance by activating ATR-Chk1 pathway in ovarian cancer. *Cancer letters*, 428:104–116, aug 2018. ISSN 1872-7980. doi: 10.1016/J.CANLET.2018.04.029. URL https://pubmed.ncbi.nlm.nih.gov/29704517/.

[58] Sergei V. Kozlov, Ashley J. Waardenberg, Kasper Engholm-Keller, Jonathan W. Arthur, Mark E. Graham, and Martin Lavin. Reactive Oxygen Species (ROS)-Activated ATM-Dependent Phosphorylation of Cytoplasmic Substrates Identified by Large-Scale Phosphoproteomics Screen. *Molecular & cellular proteomics : MCP*, 15(3):1032–1047, mar 2016. ISSN 1535-9484. doi: 10.1074/MCP.M115.055723. URL https://pubmed.ncbi.nlm.nih.gov/26699800/.

[59] Zhi Guo, Sergei Kozlov, Martin F. Lavin, Maria D. Person, and Tanya T. Paull. ATM activation by oxidative stress. *Science*, 330(6003):517–521, oct 2010. ISSN 10959203. doi: 10.1126/SCIENCE.1192912/SUPPL_FILE/GUO.SOM.PDF. URL https://www.science.org/doi/abs/10.1126/science.1192912.

[60] Dong Xiao, Anna Herman-Antosiewicz, Jedrzej Antosiewicz, Hui Xiao, Marni Brisson, John S. Lazo, and Shivendra V. Singh. Diallyl trisulfide-induced G2–Mphase cell cycle arrest in human prostate cancer cells is caused by reactive oxygen species-dependent destruction and hyperphosphorylation of Cdc25C. *Oncogene 2005 24:41*, 24(41):6256–6268, may 2005. ISSN 1476-5594. doi: 10.1038/sj.onc.1208759. URL https://www.nature.com/articles/1208759.

[61] Oscar Fernandez-Capetillo, Alicia Lee, Michel Nussenzweig, and André Nussenzweig. H2AX: the histone guardian of the genome. *DNA repair*, 3(8-9):959–967, aug 2004. ISSN 1568-7864. doi: 10.1016/J.DNAREP.2004.03.024. URL https://pubmed.ncbi.nlm.nih.gov/15279782/.

[62] L. J. Mah, A. El-Osta, and T. C. Karagiannis. $\gamma$H2AX: a sensitive molecular marker of DNA damage and repair. *Leukemia 2010 24:4*, 24(4):679–686, feb 2010. ISSN 1476-5551. doi: 10.1038/leu.2010.6. URL https://www.nature.com/articles/leu20106.

[63] M. A. Kang, E. Y. So, A. L. Simons, D. R. Spitz, and T. Ouchi. DNA damage induces reactive oxygen species generation through the H2AX-Nox1/Rac1 pathway. *Cell Death & Disease 2012 3:1*, 3(1):e249–e249, jan 2012. ISSN 2041-4889. doi: 10.1038/cddis.2011.134. URL https://www.nature.com/articles/cddis2011134.

[64] Barbara Muz, Pilar de la Puente, Feda Azab, and Abdel Kareem Azab. The role of hypoxia in cancer progression, angiogenesis, metastasis, and resistance to therapy. *Hypoxia*, 3:83, 12 2015. ISSN 2324-1128. doi: 10.2147/HP.S93413. URL /pmc/articles/PMC5045092//pmc/articles/PMC5045092/?report=abstracthttps://www.ncbi.nlm.nih.gov/pmc/articles/PMC5045092/.

[65] R. H. Thomlinson and L. H. Gray. The Histological Structure of Some Human Lung Cancers and the Possible Implications for Radiotherapy. *British Journal of Cancer*, 9(4):539, 1955. doi: 10.1038/BJC.1955.55. URL https://www.ncbi.nlm.nih.gov/pmc/articles/PMC2073776/.

[66] Irma Telarovic, Roland H. Wenger, and Martin Pruschy. Interfering with tumor hypoxia for radiotherapy optimization. *Journal of Experimental Clinical Cancer Research 2021 40:1*, 40:1–26, 6 2021. ISSN 1756-9966. doi: 10.1186/S13046-021-02000-X. URL https://jeccr.biomedcentral.com/articles/10.1186/s13046-021-02000-x.

[67] Mark W. Dewhirst, Yiting Cao, and Benjamin Moeller. Cycling hypoxia and free radicals regulate angiogenesis and radiotherapy response. *Nature Reviews Cancer*, 8(6):425–437, 6 2008. ISSN 1474175X. doi: 10.1038/nrc2397.

[68] Li Zhang and Richard P. Hill. Hypoxia enhances metastatic efficiency by up-regulating mdm2 in kht cells and increasing resistance to apoptosis. *Cancer research*, 64:4180–4189,

6 2004. ISSN 0008-5472. doi: 10.1158/0008-5472.CAN-03-3038. URL https://pubmed.ncbi.nlm.nih.gov/15205329/.

[69] Peter Vaupel. Hypoxia and aggressive tumor phenotype: implications for therapy and prognosis. *The oncologist*, 13 Suppl 3:21–26, 5 2008. ISSN 1083-7159. doi: 10.1634/THEONCOLOGIST.13-S3-21. URL https://pubmed.ncbi.nlm.nih.gov/18458121/.

[70] Hiroshi Harada. Hypoxia-inducible factor 1-mediated characteristic features of cancer cells for tumor radioresistance. 2016. doi: 10.1093/jrr/rrw012.

[71] Peter Vaupel and Louis Harrison. Tumor hypoxia: causative factors, compensatory mechanisms, and cellular response. *The oncologist*, 9 Suppl 5:4–9, 11 2004. ISSN 1083-7159. doi: 10.1634/THEONCOLOGIST.9-90005-4. URL https://pubmed.ncbi.nlm.nih.gov/15591417/.

[72] Peter Vaupel. Tumor microenvironmental physiology and its implications for radiation oncology. *Seminars in Radiation Oncology*, 14:198–206, 7 2004. ISSN 1053-4296. doi: 10.1016/J.SEMRADONC.2004.04.008.

[73] Michael R. Horsman and Jens Overgaard. The impact of hypoxia and its modification of the outcome of radiotherapy. *Journal of radiation research*, 57 Suppl 1:i90–i98, 8 2016. ISSN 1349-9157. doi: 10.1093/JRR/RRW007. URL https://pubmed.ncbi.nlm.nih.gov/26983987/.

[74] Colin H. Richards, Zahra Mohammed, Tahir Qayyum, Paul G. Horgan, and Donald C. McMillan. The prognostic value of histological tumor necrosis in solid organ malignant disease: a systematic review. *http://dx.doi.org/10.2217/fon.11.99*, 7:1223–1235, 10 2011. ISSN 14796694. doi: 10.2217/FON.11.99. URL https://www.futuremedicine.com/doi/abs/10.2217/fon.11.99.

[75] Marianne Nordsmark, Søren M. Bentzen, Volker Rudat, David Brizel, Eric Lartigau, Peter Stadler, Axel Becker, Markus Adam, Michael Molls, Juergen Dunst, David J. Terris, and Jens Overgaard. Prognostic value of tumor oxygenation in 397 head and neck tumors after primary radiation therapy. an international multi-center study. *Radiotherapy and Oncology*, 77:18–24, 10 2005. ISSN 0167-8140. doi: 10.1016/J.RADONC.2005.06.038. URL http://www.thegreenjournal.com/article/S0167814005002823/fulltext.

[76] Joiner M.C. and A.J. Van der Kogel. *Basic Clinical Radiobiology*. CRC Press, 8 2018. doi: https://doi.org/10.1201/9780429490606.

[77] A. Weidemann and R. S. Johnson. Biology of hif-1. *Cell Death Differentiation 2008 15:4*, 15:621–627, 2 2008. ISSN 1476-5403. doi: 10.1038/cdd.2008.12. URL https://www.nature.com/articles/cdd200812.

[78] Gregg L. Semenza. Targeting hif-1 for cancer therapy. *Nature Reviews Cancer 2003 3:10*, 3:721–732, 2003. ISSN 1474-1768. doi: 10.1038/nrc1187. URL https://www.nature.com/articles/nrc1187.

[79] Kiichi Hirota. Basic biology of hypoxic responses mediated by the transcription factor hifs and its implication for medicine. *Biomedicines*, 8(2):32, 2 2020. ISSN 22279059. doi: 10.3390/biomedicines8020032.

[80] Gregg L. Semenza. Hif-1 mediates metabolic responses to intratumoral hypoxia and oncogenic mutations. *The Journal of clinical investigation*, 123:3664–3671, 9 2013. ISSN 1558-8238. doi: 10.1172/JCI67230. URL https://pubmed.ncbi.nlm.nih.gov/23999440/.

[81] Alyssa Vito, Nader El-Sayes, and Karen Mossman. Hypoxia-Driven Immune Escape in the Tumor Microenvironment, apr 2020. ISSN 20734409. URL www.mdpi.com/journal/cells.

[82] Mei Yee Koh and Garth Powis. Passing the baton: The hif switch. *Trends in biochemical sciences*, 37:364, 9 2012. ISSN 09680004. doi: 10.1016/J.TIBS.2012.06.004. URL /pmc/articles/PMC3433036//pmc/articles/PMC3433036/?report=abstracthttps://www.ncbi.nlm.nih.gov/pmc/articles/PMC3433036/.

[83] Mei Yee Koh, Robert Lemos, Xiuping Liu, and Garth Powis. The hypoxia-associated factor switches cells from hif-1- to hif-2-dependent signaling promoting stem cell characteristics, aggressive tumor growth and invasion. *Cancer Research*, 71(11):4015–4027, 6 2011. ISSN 00085472. doi: 10.1158/0008-5472.CAN-10-4142.

[84] Kritika Saxena and Mohit Kumar Jolly. Acute vs. chronic vs. cyclic hypoxia: Their differential dynamics, molecular mechanisms, and effects on tumor progression. *Biomolecules*, 9(8), 8 2019. ISSN 2218273X. doi: 10.3390/biom9080339.

[85] David M. Poitz, Antje Augstein, Kathleen Hesse, Marian Christoph, Karim Ibrahim, Rüdiger C. Braun-Dullaeus, Ruth H. Strasser, and Alexander Schmeißer. Regulation of the hif-system in human macrophages – differential regulation of hif- subunits under sustained hypoxia. *Molecular Immunology*, 57:226–235, 2 2014. ISSN 0161-5890. doi: 10.1016/J.MOLIMM.2013.10.001.

[86] Tokujiro Uchida, Fabrice Rossignol, Michael A. Matthay, Rémi Mounier, Sylvianne Couette, Eric Clottes, and Christine Clerici. Prolonged hypoxia differentially regulates hypoxia-inducible factor (hif)-1alpha and hif-2alpha expression in lung epithelial cells: implication of natural antisense hif-1alpha. *The Journal of biological chemistry*, 279:14871–14878, 4 2004. ISSN 0021-9258. doi: 10.1074/JBC.M400461200. URL https://pubmed.ncbi.nlm.nih.gov/14744852/.

[87] Rafal Bartoszewski, Adrianna Moszyńska, Marcin Serocki, Aleksandra Cabaj, Andreas Polten, Renata Ochocka, Louis Dell'Italia, Sylwia Bartoszewska, Jarosław Króliczewski, Michał Dąbrowski, and James F. Collawn. Primary endothelial-specific regulation of hypoxiainducible factor (hif)-1 and hif-2 and their target gene expression profiles during hypoxia. *FASEB Journal*, 33(7), 2019. ISSN 15306860. doi: 10.1096/fj.201802650RR.

[88] Linda Holmquist-Mengelbier, Erik Fredlund, Tobias Löfstedt, Rosa Noguera, Samuel Navarro, Helén Nilsson, Alexander Pietras, Johan Vallon-Christersson, Åke Borg, Katarina Gradin, Lorenz Poellinger, and Sven Påhlman. Recruitment of hif-1 and hif-2 to common target genes is differentially regulated in neuroblastoma: Hif-2 promotes an aggressive phenotype. *Cancer Cell*, 10(5):413–423, 11 2006. ISSN 15356108. doi: 10.1016/j.ccr.2006.08.026.

[89] Qun Lin, Xiangyu Cong, and Zhong Yun. Differential hypoxic regulation of hypoxia-inducible factors 1 and 2. *Molecular Cancer Research*, 9(6):757–765, 6 2011. ISSN 15417786. doi: 10.1158/1541-7786.MCR-11-0053.

[90] A. Giatromanolaki, M. I. Koukourakis, E. Sivridis, H. Turley, K. Talks, F. Pezzella, K. C. Gatter, and A. L. Harris. Relation of hypoxia inducible factor 1 and 2 in operable non-small cell lung cancer to angiogenic/molecular profile of tumours and survival. *British Journal of Cancer*, 85(6):881–890, 9 2001. ISSN 00070920. doi: 10.1054/bjoc.2001.2018.

[91] Autumn L Jackson, Bing Zhou, and William Y Kim. Hif, hypoxia and the role of angiogenesis in non-small cell lung cancer. 2010. doi: 10.1517/14728222.2010.511617.

[92] David Zagzag, Hua Zhong, Joanne M. Scalzitti, Erik Laughner, Jonathan W. Simons, and Gregg L. Semenza. Expression of hypoxia-inducible factor 1 in brain tumors: Association with angiogenesis, invasion, and progression. *Cancer*, 88(11):2606–2618, 6 2000. ISSN 0008543X. doi: 10.1002/1097-0142(20000601)88:11{\textless}2606::AID-CNCR25{\textgreater}3.0.CO;2-W.

[93] Daniele M. Gilkes and Gregg L. Semenza. Role of hypoxia-inducible factors in breast cancer metastasis. *Future Oncology*, 9(11):1623–1636, 11 2013. ISSN 14796694. doi: 10.2217/fon.13.92.

[94] Hua Zhong, Gregg L Semenza, Jonathan W Simons, and Angelo M De Marzo. Up-regulation of hypoxia-inducible factor 1alpha is an early event in prostate carcinogenesis. *Cancer detection and prevention*, 28(2):88–93, 2004. ISSN 0361-090X (Print). doi: 10.1016/j.cdp.2003.12.009.

[95] K. L. Talks, H. Turley, K. C. Gatter, P. H. Maxwell, C. W. Pugh, P. J. Ratcliffe, and A. L. Harris. The expression and distribution of the hypoxia-inducible factors hif-1 and hif-2 in normal human tissues, cancers, and tumor-associated macrophages. *American Journal of Pathology*, 157(2):411–421, 2000. ISSN 00029440. doi: 10.1016/S0002-9440(10)64554-3.

[96] Chang Sheng Lin, Tu Chen Liu, Ming Tsung Lee, Shun Fa Yang, and Thomas Chang Yao Tsao. Independent prognostic value of hypoxia-inducible factor 1-alpha expression in small cell lung cancer. *International Journal of Medical Sciences*, 14(8):785–790, 2017. ISSN 14491907. doi: 10.7150/ijms.19512.

[97] Roy Vergis, Catherine M Corbishley, Andrew R Norman, Jaclyn Bartlett, Sameer Jhavar, Michael Borre, Sara Heeboll, Alan Horwich, Robert Huddart, Vincent Khoo, Ros Eeles, Colin Cooper, Matthew Sydes, David Dearnaley, and Chris Parker. Intrinsic markers of tumour hypoxia and angiogenesis in localised prostate cancer and outcome of radical treatment: a retrospective analysis of two randomised radiotherapy trials and one surgical cohort study. *The Lancet. Oncology*, 9(4):342–351, 4 2008. ISSN 1474-5488 (Electronic). doi: 10.1016/S1470-2045(08)70076-7.

[98] Daniel M. Aebersold, Philipp Burri, Karl T. Beer, Jean Laissue, Valentin Djonov, Richard H. Greiner, and Gregg L. Semenza. Expression of hypoxia-inducible factor-1: A novel predictive and prognostic parameter in the radiotherapy of oropharyngeal cancer. *Cancer Research*, 61(7):2911–2916, 4 2001. ISSN 00085472.

[99] Qi Liu and Peicheng Cao. Clinical and prognostic significance of hif-1 in glioma patients: a meta-analysis. *International journal of clinical and experimental medicine*, 8(12):22073–22083, 12 2015. ISSN 1940-5901.

[100] H. Harada, S. Itasaka, Y. Zhu, L. Zeng, X. Xie, A. Morinibu, K. Shinomiya, and M. Hiraoka. Treatment regimen determines whether an hif-1 inhibitor enhances or inhibits the effect of radiation therapy. *British Journal of Cancer*, 100(5):747–757, 3 2009. ISSN 00070920. doi: 10.1038/sj.bjc.6604939.

[101] B. J. Moeller and M. W. Dewhirst. Hif-1 and tumour radiosensitivity. *British Journal of Cancer*, 95(1):1–5, 7 2006. ISSN 15321827. doi: 10.1038/sj.bjc.6603201.

[102] Hiroshi Harada, Satoshi Itasaka, Shinae Kizaka-Kondoh, Keiko Shibuya, Akiyo Morinibu, Kazumi Shinomiya, and Masahiro Hiraoka. The Akt/mTOR pathway assures the synthesis of HIF-1$\alpha$ protein in a glucose- and reoxygenation-dependent manner in irradiated tumors. *Journal of Biological Chemistry*, 284(8):5332–5342, feb 2009. ISSN 00219258. doi: 10.1074/jbc.M806653200. URL `http://www.ncbi.nlm.nih.gov/pubmed/19098000`.

[103] Benjamin J. Moeller, Yiting Cao, Chuan Y. Li, and Mark W. Dewhirst. Radiation activates hif-1 to regulate vascular radiosensitivity in tumors: Role of reoxygenation, free radicals, and stress granules. *Cancer Cell*, 5(5):429–441, 5 2004. ISSN 15356108. doi: 10.1016/S1535-6108(04)00115-1.

[104] N. S. Chandel, D. S. McClintock, C. E. Feliciano, T. M. Wood, J. A. Melendez, A. M. Rodriguez, and P. T. Schumacker. Reactive oxygen species generated at mitochondrial Complex III stabilize hypoxia-inducible factor-1$\alpha$ during hypoxia: A mechanism of O2 sensing. *Journal of Biological Chemistry*, 275(33):25130–25138, aug 2000. ISSN 00219258. doi: 10.1074/jbc.M001914200. URL https://pubmed.ncbi.nlm.nih.gov/10833514/.

[105] T. Klimova and N. S. Chandel. Mitochondrial complex iii regulates hypoxic activation of hif. *Cell death and differentiation*, 15:660–666, 4 2008. ISSN 1350-9047. doi: 10.1038/SJ.CDD.4402307. URL https://pubmed.ncbi.nlm.nih.gov/18219320/.

[106] Shahrzad Movafagh, Sean Crook, and Kim Vo. Regulation of hypoxia-inducible factor-1a by reactive oxygen species: new developments in an old debate. *Journal of cellular biochemistry*, 116:696–703, 2015. ISSN 1097-4644. doi: 10.1002/JCB.25074. URL https://pubmed.ncbi.nlm.nih.gov/25546605/.

[107] Katheryn Begg and Mahvash Tavassoli. Inside the hypoxic tumour: reprogramming of the DDR and radioresistance. *Cell Death Discovery 2020 6:1*, 6(1):1–15, aug 2020. ISSN 2058-7716. doi: 10.1038/s41420-020-00311-0. URL https://www.nature.com/articles/s41420-020-00311-0.

[108] Andria Rakotomalala, Alexandre Escande, Alessandro Furlan, Samuel Meignan, and Eric Lartigau. Hypoxia in solid tumors: How low oxygenation impacts the "six rs" of radiotherapy. *Frontiers in Endocrinology*, 12:1084, 9 2021. ISSN 16642392. doi: 10.3389/FENDO.2021.742215/BIBTEX.

[109] Ranjit S. Bindra, Meredith E. Crosby, and Peter M. Glazer. Regulation of dna repair in hypoxic cancer cells. *Cancer and Metastasis Reviews 2007 26:2*, 26:249–260, 4 2007. ISSN 1573-7233. doi: 10.1007/S10555-007-9061-3. URL https://link.springer.com/article/10.1007/s10555-007-9061-3.

[110] Ester M. Hammond, Nicholas C. Denko, Mary Jo Dorie, Robert T. Abraham, and Amato J. Giaccia. Hypoxia Links ATR and p53 through Replication Arrest. *Molecular and Cellular Biology*, 22(6):1834, mar 2002. doi: 10.1128/MCB.22.6.1834-1843.2002. URL /pmc/articles/PMC135616//pmc/articles/PMC135616/?report=abstracthttps://www.ncbi.nlm.nih.gov/pmc/articles/PMC135616/.

[111] Ester M. Hammond, Mary Jo Dorie, and Amato J. Giaccia. ATR/ATM Targets Are Phosphorylated by ATR in Response to Hypoxia and ATM in Response to Reoxygenation *. *Journal of Biological Chemistry*, 278(14):12207–12213, apr 2003. ISSN 0021-9258. doi: 10.1074/JBC.M212360200. URL http://www.jbc.org/article/S002192581964812X/fulltexthttp://www.jbc.org/article/S002192581964812X/abstracthttps://www.jbc.org/article/S0021-9258(19)64812-X/abstract.

[112] Robert G. Bristow and Richard P. Hill. Hypoxia, dna repair and genetic instability. *Nature Reviews Cancer 2008 8:3*, 8:180–192, 3 2008. ISSN 1474-1768. doi: 10.1038/nrc2344. URL https://www.nature.com/articles/nrc2344https://www.nature.com/articles/nrc2344/boxes/bx2.

[113] Alice X. Meng, Farid Jalali, Andrew Cuddihy, Norman Chan, Ranjit S. Bindra, Peter M. Glazer, and Robert G. Bristow. Hypoxia down-regulates dna double strand break

repair gene expression in prostate cancer cells. *Radiotherapy and Oncology*, 76:168–176, 8 2005. ISSN 0167-8140. doi: 10.1016/J.RADONC.2005.06.025. URL http://www.thegreenjournal.com/article/S0167814005002690/fulltext.

[114] Cowman S, Fan YN, Pizer B, and Sée V. Decrease of Nibrin expression in chronic hypoxia is associated with hypoxia-induced chemoresistance in some brain tumour cells. *BMC cancer*, 19(1), apr 2019. ISSN 1471-2407. doi: 10.1186/S12885-019-5476-9. URL https://pubmed.ncbi.nlm.nih.gov/30943920/.

[115] Saki M, Makino H, Javvadi P, Tomimatsu N, Ding LH, Clark JE, Gavin E, Takeda K, Andrews J, Saha D, Story MD, Burma S, and Nirodi CS. EGFR Mutations Compromise Hypoxia-Associated Radiation Resistance through Impaired Replication Fork-Associated DNA Damage Repair. *Molecular cancer research : MCR*, 15(11):1503–1516, nov 2017. ISSN 1557-3125. doi: 10.1158/1541-7786.MCR-17-0136. URL https://pubmed.ncbi.nlm.nih.gov/28801308/.

[116] Shannon L. Gibson, Ranjit S. Bindra, and Peter M. Glazer. Hypoxia-induced phosphorylation of chk2 in an ataxia telangiectasia mutated-dependent manner. *Cancer research*, 65:10734–10741, 12 2005. ISSN 0008-5472. doi: 10.1158/0008-5472.CAN-05-1160. URL https://pubmed.ncbi.nlm.nih.gov/16322218/.

[117] Meng AX, Jalali F, Cuddihy A, Chan N, Bindra RS, Glazer PM, and Bristow RG. Hypoxia down-regulates DNA double strand break repair gene expression in prostate cancer cells. *Radiotherapy and oncology : journal of the European Society for Therapeutic Radiology and Oncology*, 76(2):168–176, aug 2005. ISSN 0167-8140. doi: 10.1016/J.RADONC.2005.06.025. URL https://pubmed.ncbi.nlm.nih.gov/16026872/.

[118] Yan Ren, Piliang Hao, Bamaprasad Dutta, Esther Sok Hwee Cheow, Kae Hwan Sim, Chee Sian Gan, Sai Kiang Lim, and Siu Kwan Sze. Hypoxia Modulates A431 Cellular Pathways Association to Tumor Radioresistance and Enhanced Migration Revealed by Comprehensive Proteomic and Functional Studies. *Molecular & Cellular Proteomics : MCP*, 12(2):485, feb 2013. doi: 10.1074/MCP.M112.018325. URL /pmc/articles/PMC3567868//pmc/articles/PMC3567868/?report=abstracthttps://www.ncbi.nlm.nih.gov/pmc/articles/PMC3567868/.

[119] Um JH, Kang CD, Bae JH, Shin GG, Kim DW, Kim DW, Chung BS, and Kim SH. Association of DNA-dependent protein kinase with hypoxia inducible factor-1 and its implication in resistance to anticancer drugs in hypoxic tumor cells. *Experimental & molecular medicine*, 36(3):233–242, jun 2004. ISSN 1226-3613. doi: 10.1038/EMM.2004.32. URL https://pubmed.ncbi.nlm.nih.gov/15272235/.

[120] Yuhong Lu, Adrian Chu, Mitchell S. Turker, and Peter M. Glazer. Hypoxia-Induced Epigenetic Regulation and Silencing of the BRCA1 Promoter. *Molecular and Cellular Biology*, 31(16):3339, aug 2011. doi: 10.1128/MCB.01121-10. URL /pmc/articles/PMC3147797//pmc/articles/PMC3147797/?report=abstracthttps://www.ncbi.nlm.nih.gov/pmc/articles/PMC3147797/.

[121] Ranjit S. Bindra, Shannon L. Gibson, Alice Meng, Ulrica Westermark, Maria Jasin, Andrew J. Pierce, Robert G. Bristow, Marie K. Classon, and Peter M. Glazer. Hypoxia-Induced Down-regulation of BRCA1 Expression by E2Fs. *Cancer Research*, 65(24):11597–11604, dec 2005. ISSN 0008-5472. doi: 10.1158/0008-5472.CAN-05-2119. URL https://cancerres.aacrjournals.org/content/65/24/11597https://cancerres.aacrjournals.org/content/65/24/11597.abstract.

[122] Naima Hammoudi, Kausar Begam Riaz Ahmed, Celia Garcia-Prieto, and Peng Huang. Metabolic alterations in cancer cells and therapeutic implications. *Chinese Journal of Cancer*, 30(8):508–525, 2011. ISSN 1000467X. doi: 10.5732/cjc.011.10267. URL /pmc/articles/PMC4013402//pmc/articles/PMC4013402/?report=abstracthttps://www.ncbi.nlm.nih.gov/pmc/articles/PMC4013402/.

[123] Otto Warburg, Franz Wind, and Erwin Negelein. Über den stoffwechsel von tumoren im körper. *Klinische Wochenschrift 1926 5:19*, 5:829–832, 5 1926. ISSN 1432-1440. doi: 10.1007/BF01726240. URL https://link.springer.com/article/10.1007/BF01726240.

[124] Ralph J. De Berardinis and Navdeep S. Chandel. Fundamentals of cancer metabolism. *Science Advances*, 2, 5 2016. ISSN 23752548. doi: 10.1126/SCIADV.1600200. URL /pmc/articles/PMC4928883//pmc/articles/PMC4928883/?report=abstracthttps://www.ncbi.nlm.nih.gov/pmc/articles/PMC4928883/.

[125] Matthew G.Vander Heiden, Lewis C. Cantley, and Craig B. Thompson. Understanding the warburg effect: The metabolic requirements of cell proliferation. *Science*, 324:1029–1033, 5 2009. ISSN 00368075. doi: 10.1126/SCIENCE.1160809. URL https://www.researchgate.net/publication/24445138_Understanding_the_Warburg_Effect_The_Metabolic_Requirements_of_Cell_Proliferation.

[126] Luis Gustavo Saboia Ponte, Isadora Carolina Betim Pavan, Mariana Camargo Silva Mancini, Luiz Guilherme Salvino Da Silva, Ana Paula Morelli, Matheus Brandemarte Severino, Rosangela Maria Neves Bezerra, and Fernando Moreira Simabuco. The hallmarks of flavonoids in cancer. *Molecules*, 26(7), apr 2021. doi: 10.3390/MOLECULES26072029.

[127] Emma McCann, Jacintha O'Sullivan, and Simone Marcone. Targeting cancer-cell mitochondria and metabolism to improve radiotherapy response. *Translational oncology*, 14, 1 2021. ISSN 1936-5233. doi: 10.1016/J.TRANON.2020.100905. URL https://pubmed.ncbi.nlm.nih.gov/33069104/.

[128] Winnie Wai Ying Kam and Richard B. Banati. Effects of ionizing radiation on mitochondria. *Free Radical Biology and Medicine*, 65:607–619, 12 2013. ISSN 0891-5849. doi: 10.1016/J.FREERADBIOMED.2013.07.024.

[129] Nick Lane. *Power, sex, suicide : mitochondria and the meaning of life*. Oxford University Press, 2005. ISBN 0199205647.

[130] Kyra J. Cowan. The mitochondria: Powerhouse of the cell. In *Functional Metabolism*, pages 211–241. John Wiley Sons, Inc., 1 2005. doi: 10.1002/047167558x.ch8.

[131] Inmaculada Martínez-Reyes and Navdeep S. Chandel. Mitochondrial tca cycle metabolites control physiology and disease. *Nature Communications 2020 11:1*, 11:1–11, 1 2020. ISSN 2041-1723. doi: 10.1038/s41467-019-13668-3. URL https://www.nature.com/articles/s41467-019-13668-3.

[132] Brett A. Wagner, Sujatha Venkataraman, and Garry R. Buettner. The rate of oxygen utilization by cells. *Free Radical Biology and Medicine*, 51(3):700–712, 8 2011. ISSN 08915849. doi: 10.1016/j.freeradbiomed.2011.05.024.

[133] Garry R. Buettner. Superoxide Dismutase in Redox Biology: The Roles of Superoxide and Hydrogen Peroxide. *Anti-Cancer Agents in Medicinal Chemistry*, 11(4):341–346, nov 2012. ISSN 18715206. doi: 10.2174/187152011795677544. URL https://pubmed.ncbi.nlm.nih.gov/21453242/.

[134] Kátia C. Carvalho, Isabela W. Cunha, Rafael M. Rocha, Fernanda R. Ayala, Mariana M. Cajaíba, Maria D. Begnami, Rafael S. Vilela, Geise R. Paiva, Rodrigo G. Andrade, and Fernando A. Soares. Glut1 expression in malignant tumors and its use as an immunodiagnostic marker. *Clinics*, 66(6):965–972, 2011. ISSN 18075932. doi: 10.1590/S1807-59322011000600008.

[135] Cory U Lago, Ho Joong Sung, Wenzhe Ma, Ping-yuan Wang, and Paul M Hwang. p53, aerobic metabolism, and cancer. *Antioxidants redox signaling*, 15(6):1739–1748, 9 2011. ISSN 1557-7716. doi: 10.1089/ars.2010.3650.

[136] Satoaki Matoba, Ju Gyeong Kang, Willmar D. Patino, Andrew Wragg, Manfred Boehm, Oksana Gavrilova, Paula J. Hurley, Fred Bunz, and Paul M. Hwang. p53 regulates mitochondrial respiration. *Science*, 312(5780):1650–1653, 6 2006. ISSN 00368075. doi: 10.1126/science.1126863.

[137] Iñigo San-Millán and George A Brooks. Reexamining cancer metabolism: lactate production for carcinogenesis could be the purpose and explanation of the warburg effect. *Carcinogenesis*, 38(2):119–133, 2017. doi: 10.1093/carcin/bgw127.

[138] William W. Wheaton and Navdeep S. Chandel. Hypoxia. 2. hypoxia regulates cellular metabolism. *American Journal of Physiology - Cell Physiology*, 300: C385, 3 2011. ISSN 03636143. doi: 10.1152/AJPCELL.00485.2010. URL /pmc/articles/PMC3063979//pmc/articles/PMC3063979/?report=abstracthttps://www.ncbi.nlm.nih.gov/pmc/articles/PMC3063979/.

[139] Jung Whan Kim, Irina Tchernyshyov, Gregg L. Semenza, and Chi V. Dang. Hif-1-mediated expression of pyruvate dehydrogenase kinase: a metabolic switch required for cellular adaptation to hypoxia. *Cell metabolism*, 3:177–185, 3 2006. ISSN 1550-4131. doi: 10.1016/J.CMET.2006.02.002. URL https://pubmed.ncbi.nlm.nih.gov/16517405/.

[140] Ioanna Papandreou, Rob A. Cairns, Lucrezia Fontana, Ai Lin Lim, and Nicholas C. Denko. Hif-1 mediates adaptation to hypoxia by actively downregulating mitochondrial oxygen consumption. *Cell metabolism*, 3:187–197, 3 2006. ISSN 1550-4131. doi: 10.1016/J.CMET.2006.01.012. URL https://pubmed.ncbi.nlm.nih.gov/16517406/.

[141] Chris E. Cooper. The steady-state kinetics of cytochrome c oxidation by cytochrome oxidase. *Biochimica et Biophysica Acta (BBA) - Bioenergetics*, 1017:187–203, 6 1990. ISSN 0005-2728. doi: 10.1016/0005-2728(90)90184-6.

[142] Pearl Lee, Navdeep S. Chandel, and M. Celeste Simon. Cellular adaptation to hypoxia through hypoxia inducible factors and beyond. *Nature reviews. Molecular cell biology*, 21:268–283, 5 2020. ISSN 1471-0080. doi: 10.1038/S41580-020-0227-Y. URL https://pubmed.ncbi.nlm.nih.gov/32144406/.

[143] Gregg L. Semenza, Peter H. Roth, Hon Ming Fang, and Guang L. Wang. Transcriptional regulation of genes encoding glycolytic enzymes by hypoxia-inducible factor 1. *Journal of Biological Chemistry*, 269:23757–23763, 9 1994. ISSN 0021-9258. doi: 10.1016/S0021-9258(17)31580-6. URL http://www.jbc.org/article/S0021925817315806/fulltexthttp://www.jbc.org/article/S0021925817315806/abstracthttps://www.jbc.org/article/S0021-9258(17)31580-6/abstract.

[144] Ruixue Huang and Ping-Kun Zhou. Hif-1 signaling: A key orchestrator of cancer radioresistance. *Radiation Medicine and Protection*, 3 2020. ISSN 26665557. doi: 10.1016/j.radmp.2020.01.006.

[145] Toshio Suda, Keiyo Takubo, and Gregg L. Semenza. Metabolic regulation of hematopoietic stem cells in the hypoxic niche. *Cell stem cell*, 9:298–310, 10 2011. ISSN 1875-9777. doi: 10.1016/J.STEM.2011.09.010. URL https://pubmed.ncbi.nlm.nih.gov/21982230/.

[146] Eric L. Bell, Tatyana A. Klimova, James Eisenbart, Carlos T. Moraes, Michael P. Murphy, G. R.Scott Budinger, and Navdeep S. Chandel. The Qo site of the mitochondrial complex III is required for the transduction of hypoxic signaling via reactive oxygen species production. *Journal of Cell Biology*, 177(6):1029–1036, jun 2007. ISSN 00219525. doi: 10.1083/jcb.200609074. URL https://pubmed.ncbi.nlm.nih.gov/17562787/.

[147] Joslyn K. Brunelle, Eric L. Bell, Nancy M. Quesada, Kristel Vercauteren, Valeria Tiranti, Massimo Zeviani, Richard C. Scarpulla, and Navdeep S. Chandel. Oxygen sensing requires mitochondrial ros but not oxidative phosphorylation. *Cell metabolism*, 1:409–414, 6 2005. ISSN 1550-4131. doi: 10.1016/J.CMET.2005.05.002. URL https://pubmed.ncbi.nlm.nih.gov/16054090/.

[148] Robert D. Guzy, Beatrice Hoyos, Emmanuel Robin, Hong Chen, Liping Liu, Kyle D. Mansfield, M. Celeste Simon, Ulrich Hammerling, and Paul T. Schumacker. Mitochondrial complex iii is required for hypoxia-induced ros production and cellular oxygen sensing. *Cell metabolism*, 1:401–408, 6 2005. ISSN 1550-4131. doi: 10.1016/J.CMET.2005.05.001. URL https://pubmed.ncbi.nlm.nih.gov/16054089/.

[149] Kathrin Doege, Sandra Heine, Inga Jensen, Wolfgang Jelkmann, and Eric Metzen. Inhibition of mitochondrial respiration elevates oxygen concentration but leaves regulation of hypoxia-inducible factor (hif) intact. *Blood*, 106:2311–2317, 10 2005. ISSN 0006-4971. doi: 10.1182/BLOOD-2005-03-1138. URL https://pubmed.ncbi.nlm.nih.gov/15947089/.

[150] Yee Liu Chua, Eric Dufour, Emmanuel P. Dassa, Pierre Rustin, Howard T. Jacobs, Cormac T. Taylor, and Thilo Hagen. Stabilization of hypoxia-inducible factor-1 protein in hypoxia occurs independently of mitochondrial reactive oxygen species production. *The Journal of Biological Chemistry*, 285:31277, 10 2010. ISSN 00219258. doi: 10.1074/JBC.M110.158485. URL /pmc/articles/PMC2951202//pmc/articles/PMC2951202/?report=abstracthttps://www.ncbi.nlm.nih.gov/pmc/articles/PMC2951202/.

[151] Anne Tulard, Françoise Hoffschir, Florence Hillairet De Boisferon, Catherine Luccioni, and Anne Bravard. Persistent oxidative stress after ionizing radiation is involved in inherited radiosensitivity. *Free Radical Biology and Medicine*, 35:68–77, 7 2003. ISSN 0891-5849. doi: 10.1016/S0891-5849(03)00243-0.

[152] Tohru Yamamori, Hironobu Yasui, Masayuki Yamazumi, Yusuke Wada, Yoshinari Nakamura, Hideo Nakamura, and Osamu Inanami. Ionizing radiation induces mitochondrial reactive oxygen species production accompanied by upregulation of mitochondrial electron transport chain function and mitochondrial content under control of the cell cycle checkpoint. *Free Radical Biology and Medicine*, 53:260–270, 7 2012. ISSN 0891-5849. doi: 10.1016/J.FREERADBIOMED.2012.04.033.

[153] Shinko Kobashigawa, Keiji Suzuki, and Shunichi Yamashita. Ionizing radiation accelerates drp1-dependent mitochondrial fission, which involves delayed mitochondrial reactive oxygen species production in normal human fibroblast-like cells. *Biochemical and Biophysical Research Communications*, 414:795–800, 11 2011. ISSN 0006-291X. doi: 10.1016/J.BBRC.2011.10.006.

[154] Kasumi Kawamura, Fei Qi, and Junya Kobayashi. Potential relationship between the biological effects of low-dose irradiation and mitochondrial ros production. *Journal of*

*radiation research*, 59:ii91–ii97, 4 2018. ISSN 1349-9157. doi: 10.1093/JRR/RRX091. URL https://pubmed.ncbi.nlm.nih.gov/29415254/.

[155] Sudip Banerjee, Nukhet Aykin-Burns, Kimberly J. Krager, Sumit K. Shah, Stepan B. Melnyk, Martin Hauer-Jensen, and Snehalata A. Pawar. Loss of C/EBP$\delta$ enhances IR-induced cell death by promoting oxidative stress and mitochondrial dysfunction. *Free Radical Biology and Medicine*, 99:296–307, oct 2016. ISSN 18734596. doi: 10.1016/J.FREERADBIOMED.2016.08.022.

[156] Ruilong Liu, Wenfeng Li, Bangbao Tao, Xiongjun Wang, Zhuo Yang, Yajuan Zhang, Chenyao Wang, Rongzhi Liu, Hong Gao, Ji Liang, and Weiwei Yang. Tyrosine phosphorylation activates 6-phosphogluconate dehydrogenase and promotes tumor growth and radiation resistance. *Nature communications*, 10(1):991, 3 2019. ISSN 2041-1723. doi: 10.1038/s41467-019-08921-8.

[157] Marta Anna Kowalik, Amedeo Columbano, and Andrea Perra. Emerging role of the pentose phosphate pathway in hepatocellular carcinoma. *Frontiers in Oncology*, 7(MAY), 5 2017. ISSN 2234943X. doi: 10.3389/fonc.2017.00087.

[158] Xiongjian Rao, Xiaotao Duan, Weimin Mao, Xuexia Li, Zhonghua Li, Qian Li, Zhiguo Zheng, Haimiao Xu, Min Chen, Peng G. Wang, Yingjie Wang, Binghui Shen, and Wen Yi. O-glcnacylation of g6pd promotes the pentose phosphate pathway and tumor growth. *Nature Communications*, 6:8468, 9 2015. ISSN 20411723. doi: 10.1038/ncomms9468.

[159] E. Panieri and M. M. Santoro. Ros homeostasis and metabolism: a dangerous liason in cancer cells. *Cell Death Disease 2016 7:6*, 7:e2253–e2253, 6 2016. ISSN 2041-4889. doi: 10.1038/cddis.2016.105. URL https://www.nature.com/articles/cddis2016105.

[160] Krushna C. Patra and Nissim Hay. The pentose phosphate pathway and cancer. *Trends in biochemical sciences*, 39(8):347, 2014. doi: 10.1016/J.TIBS.2014.06.005. URL /pmc/articles/PMC4329227//pmc/articles/PMC4329227/?report=abstracthttps://www.ncbi.nlm.nih.gov/pmc/articles/PMC4329227/.

[161] Jing Fan, Jiangbin Ye, Jurre J. Kamphorst, Tomer Shlomi, Craig B. Thompson, and Joshua D. Rabinowitz. Quantitative flux analysis reveals folate-dependent nadph production. *Nature*, 510:298–302, 2014. ISSN 14764687. doi: 10.1038/NATURE13236.

[162] Harvey J. Cohen, Adolfo Elizalde, and Sherwood P. Miller. Cytologic studies of glucose-6-phosphate dehydrogenase in malignancy. *Cancer*, 21(6):1055–1060, 6 1968. ISSN 1097-0142. doi: 10.1002/1097-0142(196806)21:6{\textless}1055::AID-CNCR2820210605{\textgreater}3.0.CO;2-1.

[163] Michael P. Gamcsik, Mohit S. Kasibhatla, Stephanie D. Teeter, and O. Michael Colvin. Glutathione levels in human tumors. *Biomarkers : biochemical indicators of exposure, response, and susceptibility to chemicals*, 17:671, 12 2012. ISSN 1354750X. doi: 10.3109/1354750X.2012.715672. URL /pmc/articles/PMC3608468//pmc/articles/PMC3608468/?report=abstracthttps://www.ncbi.nlm.nih.gov/pmc/articles/PMC3608468/.

[164] Sarah L. Blair, Paul Heerdt, Sonu Sachar, Amir Abolhoda, Steven Hochwald, Huiming Cheng, and Michael Burt. Glutathione metabolism in patients with non-small cell lung cancers. *Cancer Research*, 57, 1997.

[165] Sue Goo Rhee, Hyun Ae Woo, In Sup Kil, and Soo Han Bae. Peroxiredoxin functions as a peroxidase and a regulator and sensor of local peroxides. *The Journal of biological chemistry*, 287:4403–4410, 2 2012. ISSN 1083-351X. doi: 10.1074/JBC.R111.283432. URL https://pubmed.ncbi.nlm.nih.gov/22147704/.

[166] Albena T. Dinkova-Kostova and Andrey Y. Abramov. The emerging role of nrf2 in mitochondrial function. *Free Radical Biology and Medicine*, 88:179–188, 11 2015. ISSN 0891-5849. doi: 10.1016/J.FREERADBIOMED.2015.04.036.

[167] Yun Jeong Kim, Ji Yeon Ahn, Ping Liang, Clement Ip, Yuesheng Zhang, and Young Mee Park. Human prx1 gene is a target of nrf2 and is up-regulated by hypoxia/reoxygenation: implication to tumor biology. *Cancer research*, 67:546–554, 1 2007. ISSN 0008-5472. doi: 10.1158/0008-5472.CAN-06-2401. URL https://pubmed.ncbi.nlm.nih.gov/17234762/.

[168] Michael Cox and David L. Nelson. Lehninger Principles of Biochemistry. page 1200, 2008. URL http://www.amazon.co.uk/Lehninger-Principles-Biochemistry-Michael-Cox/dp/0716743396.

[169] Chiara Riganti, Elena Gazzano, Manuela Polimeni, Elisabetta Aldieri, and Dario Ghigo. The pentose phosphate pathway: an antioxidant defense and a crossroad in tumor cell fate. *Free radical biology medicine*, 53:421–436, 8 2012. ISSN 1873-4596. doi: 10.1016/J.FREERADBIOMED.2012.05.006. URL https://pubmed.ncbi.nlm.nih.gov/22580150/.

[170] Jiangang Zhao, Xu Lin, Di Meng, Liping Zeng, Runzhou Zhuang, Sha Huang, Wang Lv, and Jian Hu. Nrf2 mediates metabolic reprogramming in non-small cell lung cancer. *Frontiers in oncology*, 10, 11 2020. ISSN 2234-943X. doi: 10.3389/FONC.2020.578315. URL https://pubmed.ncbi.nlm.nih.gov/33324555/.

[171] Peng Jiang, Wenjing Du, Xingwu Wang, Anthony Mancuso, Xiang Gao, Mian Wu, and Xiaolu Yang. P53 regulates biosynthesis through direct inactivation of glucose-6-phosphate dehydrogenase. *Nature Cell Biology*, 13(3):310–316, 3 2011. ISSN 14657392. doi: 10.1038/ncb2172.

[172] Ayako Nagao, Minoru Kobayashi, Sho Koyasu, Christalle C.T. Chow, and Hiroshi Harada. Hif-1-dependent reprogramming of glucose metabolic pathway of cancer cells and its therapeutic significance. *International Journal of Molecular Sciences*, 20, 2019. ISSN 14220067. doi: 10.3390/IJMS20020238. URL /pmc/articles/PMC6359724//pmc/articles/PMC6359724/?report=abstracthttps://www.ncbi.nlm.nih.gov/pmc/articles/PMC6359724/.

[173] Davinder Singh, Rohit Arora, Pardeep Kaur, Balbir Singh, Rahul Mannan, and Saroj Arora. Overexpression of hypoxia-inducible factor and metabolic pathways: Possible targets of cancer. *Cell and Bioscience*, 7(1), 11 2017. ISSN 20453701. doi: 10.1186/s13578-017-0190-2.

[174] Lin Gao, Rebeca Mejías, Miriam Echevarría, and José López-Barneo. Induction of the glucose-6-phosphate dehydrogenase gene expression by chronic hypoxia in pc12 cells. *FEBS Letters*, 569(1-3):256–260, 7 2004. ISSN 00145793. doi: 10.1016/j.febslet.2004.06.004.

[175] Niamh Lynam-Lennon, Stephen G. Maher, Aoife Maguire, James Phelan, Cian Muldoon, John V. Reynolds, and Jacintha O'Sullivan. Altered mitochondrial function and energy metabolism is associated with a radioresistant phenotype in oesophageal adenocarcinoma. *PloS one*, 9, 6 2014. ISSN 1932-6203. doi: 10.1371/JOURNAL.PONE.0100738. URL https://pubmed.ncbi.nlm.nih.gov/24968221/.

[176] Paolo Ettore Porporato, Nicoletta Filigheddu, José Manuel Bravo San Pedro, Guido Kroemer, and Lorenzo Galluzzi. Mitochondrial metabolism and cancer. *Cell Research 2017 28:3*, 28:265–280, 12 2017. ISSN 1748-7838. doi: 10.1038/cr.2017.155. URL https://www.nature.com/articles/cr2017155.

[177] Thomas M. Ashton, W. Gillies McKenna, Leoni A. Kunz-Schughart, and Geoff S. Higgins. Oxidative phosphorylation as an emerging target in cancer therapy. *Clinical Cancer Research*, 24(11):2482–2490, 6 2018. ISSN 15573265. doi: 10.1158/1078-0432.CCR-17-3070.

[178] Peter Vaupel, Michael Höckel, and Arnulf Mayer. Detection and Characterization of Tumor Hypoxia Using pO2 Histography. *https://home.liebertpub.com/ars*, 9(8):1221–1235, jul 2007. doi: 10.1089/ARS.2007.1628. URL https://www.liebertpub.com/doi/abs/10.1089/ars.2007.1628.

[179] Le QT, Chen E, Salim A, Cao H, Kong CS, Whyte R, Donington J, Cannon W, Wakelee H, Tibshirani R, Mitchell JD, Richardson D, O'Byrne KJ, Koong AC, and Giaccia AJ. An evaluation of tumor oxygenation and gene expression in patients with early stage non-small cell lung cancers. *Clinical cancer research : an official journal of the American Association for Cancer Research*, 12(5):1507–1514, mar 2006. ISSN 1078-0432. doi: 10.1158/1078-0432.CCR-05-2049. URL https://pubmed.ncbi.nlm.nih.gov/16533775/.

[180] Yang X, Cheng Y, Li P, Tao J, Deng X, Zhang X, Gu M, Lu Q, and Yin C. A lentiviral sponge for miRNA-21 diminishes aerobic glycolysis in bladder cancer T24 cells via the PTEN/PI3K/AKT/mTOR axis. *Tumour biology : the journal of the International Society for Oncodevelopmental Biology and Medicine*, 36(1):383–391, jan 2015. ISSN 1423-0380. doi: 10.1007/S13277-014-2617-2. URL https://pubmed.ncbi.nlm.nih.gov/25266796/.

[181] Movsas B, Chapman JD, Horwitz EM, Pinover WH, Greenberg RE, Hanlon AL, Iyer R, and Hanks GE. Hypoxic regions exist in human prostate carcinoma. *Urology*, 53(1):11–18, jan 1999. ISSN 0090-4295. doi: 10.1016/S0090-4295(98)00500-7. URL https://pubmed.ncbi.nlm.nih.gov/9886581/.

[182] Chris Parker, Michael Milosevic, Ants Toi, Joan Sweet, Tony Panzarella, Rob Bristow, Charles Catton, Pamela Catton, Juanita Crook, Mary Gospodarowicz, Michael McLean, Padraig Warde, and Richard P. Hill. Polarographic electrode study of tumor oxygenation in clinically localized prostate cancer. *International Journal of Radiation Oncology*Biology*Physics*, 58(3):750–757, mar 2004. ISSN 0360-3016. doi: 10.1016/S0360-3016(03)01621-3.

[183] McKeown SR. Defining normoxia, physoxia and hypoxia in tumours-implications for treatment response. *The British journal of radiology*, 87(1035), mar 2014. ISSN 1748-880X. doi: 10.1259/BJR.20130676. URL https://pubmed.ncbi.nlm.nih.gov/24588669/.

[184] David Robert Grimes and Frederick J. Currell. Oxygen diffusion in ellipsoidal tumour spheroids. *Journal of The Royal Society Interface*, 15, 2018. ISSN 17425662. doi: 10.1098/RSIF.2018.0256. URL https://royalsocietypublishing.org/doi/abs/10.1098/rsif.2018.0256.

[185] K L Eales, K E R Hollinshead, and D A Tennant. Hypoxia and metabolic adaptation of cancer cells. *Oncogenesis*, 5(1):e190, 2016. ISSN 2157-9024. doi: 10.1038/oncsis.2015.50.

[186] Hamilton. Optical Oxygen Sensors, 2013. URL https://www.pyroscience.com/en/products/theory/optical-oxygen-sensors.

[187] Huai Qiang Ju, Jin Fei Lin, Tian Tian, Dan Xie, and Rui Hua Xu. NADPH homeostasis in cancer: functions, mechanisms and therapeutic implications, dec 2020. ISSN 20593635. URL https://doi.org/10.1038/s41392-020-00326-0.

[188] Peng Jiang, Wenjing Du, and Mian Wu. Regulation of the pentose phosphate pathway in cancer. *Protein & cell*, 5(8):592–602, 2014. ISSN 1674-8018. doi: 10.1007/s13238-014-0082-8.

[189] Sephra N. Rampersad. Multiple Applications of Alamar Blue as an Indicator of Metabolic Function and Cellular Health in Cell Viability Bioassays. *Sensors (Basel, Switzerland)*, 12(9):12347, sep 2012. doi: 10.3390/S120912347. URL /pmc/articles/PMC3478843//pmc/articles/PMC3478843/?report=abstracthttps://www.ncbi.nlm.nih.gov/pmc/articles/PMC3478843/.

[190] C. M. van Leeuwen, A. L. Oei, J. Crezee, A. Bel, N. A.P. Franken, L. J.A. Stalpers, and H. P. Kok. The alfa and beta of tumours: a review of parameters of the linear-quadratic model, derived from clinical radiotherapy studies. *Radiation Oncology (London, England)*, 13(1), may 2018. ISSN 1748717X. doi: 10.1186/S13014-018-1040-Z. URL /pmc/articles/PMC5956964//pmc/articles/PMC5956964/?report=abstracthttps://www.ncbi.nlm.nih.gov/pmc/articles/PMC5956964/.

[191] PGK1 gene: MedlinePlus Genetics. URL https://medlineplus.gov/genetics/gene/pgk1/.

[192] Cytochrome Oxidase. URL https://chem.libretexts.org/@go/page/97882.

[193] Hung-Chi Yang, Yi-Hsuan Wu, Wei-Chen Yen, Hui-Ya Liu, Tsong-Long Hwang, Arnold Stern, and Daniel Tsun-Yee Chiu. The Redox Role of G6PD in Cell Growth, Cell Death, and Cancer. *Cells*, 8(9), sep 2019. doi: 10.3390/CELLS8091055. URL /pmc/articles/PMC6770671//pmc/articles/PMC6770671/?report=abstracthttps://www.ncbi.nlm.nih.gov/pmc/articles/PMC6770671/.

[194] J M Brown. The hypoxic cell: a target for selective cancer therapy–eighteenth bruce f. cain memorial award lecture. *Cancer research*, 59(23):5863–5870, 12 1999. ISSN 0008-5472 (Print).

[195] Richard J. McMurtrey. Analytic models of oxygen and nutrient diffusion, metabolism dynamics, and architecture optimization in three-dimensional tissue constructs with applications and insights in cerebral organoids. *Tissue Engineering. Part C, Methods*, 22:221, 3 2016. ISSN 19373392. doi: 10.1089/TEN.TEC.2015.0375. URL /pmc/articles/PMC5029285//pmc/articles/PMC5029285/?report=abstracthttps://www.ncbi.nlm.nih.gov/pmc/articles/PMC5029285/.

[196] Geoffrey B. West, William H. Woodruff, and James H. Brown. Allometric scaling of metabolic rate from molecules and mitochondria to cells and mammals. *Proceedings of the National Academy of Sciences of the United States of America*, 99(SUPPL. 1):2473–2478, 2 2002. ISSN 00278424. doi: 10.1073/pnas.012579799.

[197] Patries M. Herst and V. Michael Berridge. Cell surface oxygen consumption: A major contributor to cellular oxygen consumption in glycolytic cancer cell lines. *Biochimica et Biophysica Acta - Bioenergetics*, 1767(2):170–177, 2 2007. ISSN 00052728. doi: 10.1016/j.bbabio.2006.11.018.

[198] Maimon E. Hubbi and Gregg L. Semenza. Regulation of cell proliferation by hypoxia-inducible factors. *American Journal of Physiology - Cell Physiology*, 309:C775, 12 2015. ISSN 15221563. doi: 10.1152/AJPCELL.00279.2015. URL /pmc/articles/PMC4683214//pmc/articles/PMC4683214/?report=abstracthttps://www.ncbi.nlm.nih.gov/pmc/articles/PMC4683214/.

[199] Fahim Ahmad, Murali Krishna Cherukuri, and Peter L Choyke. Metabolic reprogramming in prostate cancer. *British Journal of Cancer*, page 125, 2021. ISSN 1185-1196. doi: 10.1038/s41416-021-01435-5. URL https://doi.org/10.1038/s41416-021-01435-5.

[200] Sheng Hao. Nadph promotes the rapid growth of the tumor. *Infection International*, 6: 57–60, 2017. doi: 10.1515/ii-2017-0164.

[201] Manish Mittal, Markus Roth, Peter König, Simone Hofmann, Eva Dony, Parag Goyal, Anne Christin Selbitz, Ralph Theo Schermuly, Hossein Ardeschir Ghofrani, Grazyna Kwapiszewska, Wolfgang Kummer, Walter Klepetko, Mir Ali Reza Hoda, Ludger Fink, Jörg Hänze, Werner Seeger, Friedrich Grimminger, Harald H.H.W. Schmidt, and Norbert Weissmann. Hypoxia-dependent regulation of nonphagocytic nadph oxidase subunit nox4 in the pulmonary vasculature. *Circulation Research*, 101:258–267, 8 2007. ISSN 00097330. doi: 10.1161/CIRCRESAHA.107.148015.

[202] Hwa Neo, Dhara Patel, Sharath Kandhi, and Michael S Wolin. Roles for cytosolic nadph redox in regulating pulmonary artery relaxation by thiol oxidation-elicited subunit dimerization of protein kinase g1. *Am J Physiol Heart Circ Physiol*, 305:330–343, 2013. doi: 10.1152/ajpheart.01010.2011.-The. URL www.ajpheart.org.

[203] Qiujun Yu, Chi Fung Lee, Wang Wang, Georgios Karamanlidis, Junya Kuroda, Shouji Matsushima, Junichi Sadoshima, and Rong Tian. Elimination of nadph oxidase activity promotes reductive stress and sensitizes the heart to ischemic injury. *Journal of the American Heart Association*, 3, 2014. ISSN 2047-9980. doi: 10.1161/JAHA.113.000555. URL https://pubmed.ncbi.nlm.nih.gov/24470522/.

[204] Patrick Voos, Sebastian Fuck, Fabian Weipert, Laura Babel, Dominique Tandl, Tobias Meckel, Stephanie Hehlgans, Claudia Fournier, Anna Moroni, Franz Rödel, and Gerhard Thiel. Ionizing radiation induces morphological changes and immunological modulation of jurkat cells. *Frontiers in immunology*, 9, 4 2018. ISSN 1664-3224. doi: 10.3389/FIMMU.2018.00922. URL https://pubmed.ncbi.nlm.nih.gov/29760710/.

[205] Alison C. Lloyd. The regulation of cell size. *Cell*, 154:1194–1205, 9 2013. ISSN 0092-8674. doi: 10.1016/J.CELL.2013.08.053. URL http://www.cell.com/article/S0092867413010842/fulltexthttp://www.cell.com/article/S0092867413010842/abstracthttps://www.cell.com/cell/abstract/S0092-8674(13)01084-2.

[206] S. Raz, D. Sheban, N. Gonen, M. Stark, B. Berman, and Y. G. Assaraf. Severe hypoxia induces complete antifolate resistance in carcinoma cells due to cell cycle arrest. *Cell Death Disease 2014 5:2*, 5:e1067–e1067, 2 2014. ISSN 2041-4889. doi: 10.1038/cddis.2014.39. URL https://www.nature.com/articles/cddis201439.

[207] Yadong Zhang, Hongshi Cai, Yan Liao, Yue Zhu, Fang Wang, and Jinsong Hou. Activation of pgk1 under hypoxic conditions promotes glycolysis and increases stem cell-like properties and the epithelial-mesenchymal transition in oral squamous cell carcinoma cells via the akt signalling pathway. *International journal of oncology*, 57:743–755, 9 2020. ISSN 1791-2423. doi: 10.3892/IJO.2020.5083. URL https://pubmed.ncbi.nlm.nih.gov/32705252/.

[208] Yu He, Yang Luo, Dan Zhang, Xixi Wang, Peng Zhang, Haocheng Li, Samina Ejaz, and Shufang Liang. Pgk1-mediated cancer progression and drug resistance. *American journal of cancer research*, 9:2280–2302, 11 2019. ISSN 2156-6976. URL https://pubmed.ncbi.nlm.nih.gov/31815035https://www.ncbi.nlm.nih.gov/pmc/articles/PMC6895440/.

[209] Huijun Xie, Guihui Tong, Yupei Zhang, Shu Liang, Kairui Tang, and Qinhe Yang. Pgk1 drives hepatocellular carcinoma metastasis by enhancing metabolic process. *International Journal of Molecular Sciences*, 18, 8 2017. ISSN 14220067. doi: 10.3390/IJMS18081630. URL /pmc/articles/PMC5578020//pmc/articles/PMC5578020/?report=abstracthttps://www.ncbi.nlm.nih.gov/pmc/articles/PMC5578020/.

[210] Hao Ding, Yi Jun Cheng, Hua Yan, Rui Zhang, Jin Bing Zhao, Chun Fa Qian, Wen Bin Zhang, Hong Xiao, and Hong Yi Liu. Phosphoglycerate kinase 1 promotes radioresistance in u251 human glioma cells. *Oncology reports*, 31:894–900, 2 2014. ISSN 1791-2431. doi: 10.3892/OR.2013.2874. URL https://pubmed.ncbi.nlm.nih.gov/24284928/.

[211] Chan Ho Jang, In Ae Lee, Young Ran Ha, Jinkyu Lim, Mi Kyung Sung, Sung Joon Lee, and Jong Sang Kim. Pgk1 induction by a hydrogen peroxide treatment is suppressed by antioxidants in human colon carcinoma cells. *Bioscience, biotechnology, and biochemistry*, 72:1799–1808, 2008. ISSN 1347-6947. doi: 10.1271/BBB.80079. URL https://pubmed.ncbi.nlm.nih.gov/18603805/.

[212] Gregg L. Semenza, Bing Hua Jiang, Sandra W. Leung, Rosa Passantino, Jean Paul Concordat, Pascal Maire, and Agata Giallongo. Hypoxia response elements in the aldolase a, enolase 1, and lactate dehydrogenase a gene promoters contain essential binding sites for hypoxia-inducible factor 1. *Journal of Biological Chemistry*, 271(51):32529–32537, 1996. ISSN 00219258. doi: 10.1074/jbc.271.51.32529.

[213] Gregg L. Semenza. Hif-1: upstream and downstream of cancer metabolism. *Current opinion in genetics development*, 20:51, 2 2010. ISSN 0959437X. doi: 10.1016/J.GDE.2009.10.009. URL /pmc/articles/PMC2822127//pmc/articles/PMC2822127/?report=abstracthttps://www.ncbi.nlm.nih.gov/pmc/articles/PMC2822127/.

[214] Gisela D'Angelo, Eric Duplan, Nicole Boyer, Paul Vigne, and Christian Frelin. Hypoxia up-regulates prolyl hydroxylase activity: a feedback mechanism that limits hif-1 responses during reoxygenation. *The Journal of biological chemistry*, 278:38183–38187, 10 2003. ISSN 0021-9258. doi: 10.1074/JBC.M302244200. URL https://pubmed.ncbi.nlm.nih.gov/12876291/.

[215] Amandine Ginouvè, Karine Ilc, Nuria Macías, Jacques Pouyssé, and Edurne Berra. Phds overactivation during chronic hypoxia "desensitizes" hif and protects cells from necrosis. *CELL BIOLOGY*, 105:4745–4750, 2008. URL www.pnas.orgcgidoi10.1073pnas.0705680105.

[216] Hyuna Sung, Jacques Ferlay, Rebecca L. Siegel, Mathieu Laversanne, Isabelle Soerjomataram, Ahmedin Jemal, and Freddie Bray. Global cancer statistics 2020: Globocan estimates of incidence and mortality worldwide for 36 cancers in 185 countries. *CA: A Cancer Journal for Clinicians*, 71:209–249, 5 2021. ISSN 1542-4863. doi: 10.3322/CAAC.21660. URL https://onlinelibrary.wiley.com/doi/full/10.3322/caac.21660https://onlinelibrary.wiley.com/doi/abs/10.3322/caac.21660https://acsjournals.onlinelibrary.wiley.com/doi/10.3322/caac.21660.

[217] Sean Blandin Knight, Phil A. Crosbie, Haval Balata, Jakub Chudziak, Tracy Hussell, and Caroline Dive. Progress and prospects of early detection in lung cancer. *Open Biology*, 7, 2017. ISSN 20462441. doi: 10.1098/RSOB.170070. URL /pmc/articles/PMC5627048//pmc/articles/PMC5627048/?report=abstracthttps://www.ncbi.nlm.nih.gov/pmc/articles/PMC5627048/.

[218] Jill S. Barnholtz-Sloan, Andrew E. Sloan, Faith G. Davis, Fawn D. Vigneau, Ping Lai, and Raymond E. Sawaya. Incidence proportions of brain metastases in patients diagnosed

(1973 to 2001) in the metropolitan detroit cancer surveillance system. *Journal of clinical oncology : official journal of the American Society of Clinical Oncology*, 22:2865–2872, 2004. ISSN 0732-183X. doi: 10.1200/JCO.2004.12.149. URL https://pubmed.ncbi.nlm.nih.gov/15254054/.

[219] S. R. McKeown. Defining normoxia, physoxia and hypoxia in tumours - implications for treatment response. *British Journal of Radiology*, 87(1035):1–12, 2014. ISSN 00071285. doi: 10.1259/bjr.20130676.

[220] Yufeng Liu, Xiang Chen, Qingqing Hu, Jinhong Huang, and Chunhua Ling. Resistance to radiotherapy in lung cancer. *Int J Clin Exp Med*, 11(8):7628–7642, 2018. URL www.ijcem.com/.

[221] Bruno Perillo, Marzia Di Donato, Antonio Pezone, Erika Di Zazzo, Pia Giovannelli, Giovanni Galasso, Gabriella Castoria, and Antimo Migliaccio. Ros in cancer therapy: the bright side of the moon. *Experimental molecular medicine*, 52:192–203, 2 2020. ISSN 2092-6413. doi: 10.1038/S12276-020-0384-2. URL https://pubmed.ncbi.nlm.nih.gov/32060354/.

[222] Bryan C. Dickinson, Yan Tang, Zengyi Chang, and Christopher J. Chang. A Nuclear-Localized Fluorescent Hydrogen Peroxide Probe for Monitoring Sirtuin-Mediated Oxidative Stress Responses In Vivo. *Chemistry & Biology*, 18(8):943–948, aug 2011. ISSN 1074-5521. doi: 10.1016/J.CHEMBIOL.2011.07.005.

[223] Evan W. Miller, Bryan C. Dickinson, and Christopher J. Chang. Aquaporin-3 mediates hydrogen peroxide uptake to regulate downstream intracellular signaling. *Proceedings of the National Academy of Sciences of the United States of America*, 107(36):15681–15686, sep 2010. ISSN 00278424. doi: 10.1073/pnas.1005776107. URL /pmc/articles/PMC2936599//pmc/articles/PMC2936599/?report=abstracthttps://www.ncbi.nlm.nih.gov/pmc/articles/PMC2936599/.

[224] GSH/GSSG-Glo™ Assay| Measure Ratio of GSH to GSSG | Promega. URL https://www.promega.de/en/products/cell-health-assays/oxidative-stress-assays/gsh{_}gssg{_}glo-assay/?catNum=V6611.

[225] Christophe E Redon, Jennifer S Dickey, William M Bonner, and Olga A Sedelnikova. $\gamma$-H2AX as a biomarker of DNA damage induced by ionizing radiation in human peripheral blood lymphocytes and artificial skin. *Advances in space research : the official journal of the Committee on Space Research (COSPAR)*, 43(8):1171–1178, 2009. ISSN 0273-1177. doi: 10.1016/j.asr.2008.10.011.

[226] Katarzyna Gach, Angelika Długosz, and Anna Janecka. The role of oxidative stress in anticancer activity of sesquiterpene lactones. *Naunyn-Schmiedeberg's Archives of Pharmacology*, 388(5):477–486, apr 2015. ISSN 14321912. doi: 10.1007/S00210-015-1096-3.

[227] Albin Rudisch, Matthew Richard Dewhurst, Luminita Gabriela Horga, Nina Kramer, Nathalie Harrer, Meng Dong, Heiko van der Kuip, Andreas Wernitznig, Andreas Bernthaler, Helmut Dolznig, and Wolfgang Sommergruber. High EMT Signature Score of Invasive Non-Small Cell Lung Cancer (NSCLC) Cells Correlates with NF$\kappa$B Driven Colony-Stimulating Factor 2 (CSF2/GM-CSF) Secretion by Neighboring Stromal Fibroblasts. *PloS one*, 10(4):e0124283–e0124283, apr 2015. ISSN 1932-6203. doi: 10.1371/journal.pone.0124283. URL https://pubmed.ncbi.nlm.nih.gov/25919140https://www.ncbi.nlm.nih.gov/pmc/articles/PMC4412534/.

[228] David J. Carlson, Robert D. Stewart, and Vladimir A. Semenenko. Effects of oxygen on intrinsic radiation sensitivity: A test of the relationship between aerobic and hypoxic linear-quadratic (LQ) model parameters. *Medical Physics*, 33(9):3105–3115, 2006. ISSN 00942405. doi: 10.1118/1.2229427.

[229] Tatiana Wenzl and Jan J. Wilkens. Theoretical analysis of the dose dependence of the oxygen enhancement ratio and its relevance for clinical applications. *Radiation Oncology*, 6(1):171, dec 2011. ISSN 1748717X. doi: 10.1186/1748-717X-6-171. URL /pmc/articles/PMC3283483//pmc/articles/PMC3283483/?report=abstracthttps://www.ncbi.nlm.nih.gov/pmc/articles/PMC3283483/.

[230] Robert D. Stewart, Victor K. Yu, Alexandros G. Georgakilas, Constantinos Koumenis, Joo Han Park, and David J. Carlson. Effects of radiation quality and oxygen on clustered DNA lesionsand cell death. *Radiation Research*, 176(5):587–602, nov 2011. ISSN 00337587. doi: 10.1667/RR2663.1. URL https://pubmed.ncbi.nlm.nih.gov/21823972/.

[231] Andrea Mairani, Till T. Böhlen, Ivana Dokic, Gonzalo Cabal, Stephan Brons, and Thomas Haberer. Modelling of cell killing due to sparsely ionizing radiation in normoxic and hypoxic conditions and an extension to high LET radiation. *International Journal of Radiation Biology*, 89(10):782–793, oct 2013. ISSN 09553002. doi: 10.3109/09553002.2013.800247. URL https://www.tandfonline.com/doi/abs/10.3109/09553002.2013.800247.

[232] Thomas Friedrich, Marco Durante, and Michael Scholz. Modeling cell survival after irradiation with ultrasoft x rays using the giant loop binary lesion model. *Radiation Research*, 181:485–494, 2014. ISSN 19385404. doi: 10.1667/RR13518.1. URL https://www.researchgate.net/publication/261799592_Modeling_Cell_Survival_after_Irradiation_with_Ultrasoft_X_Rays_using_the_Giant_Loop_Binary_Lesion_Model.

[233] Annahita Sallmyr, Jinshui Fan, Kamal Datta, Kyu Tae Kim, Dan Grosu, Paul Shapiro, Donald Small, and Feyruz Rassool. Internal tandem duplication of flt3 (flt3/itd) induces increased ros production, dna damage, and misrepair: Implications for poor prognosis in aml. *Blood*, 111:3173–3182, 3 2008. ISSN 00064971. doi: 10.1182/BLOOD-2007-05-092510.

[234] Feyruz V. Rassool, Terry J. Gaymes, Nader Omidvar, Nicola Brady, Stephanie Beurlet, Marika Pla, Murielle Reboul, Nicholas Lea, Christine Chomienne, Nicholas S.B. Thomas, Ghulam J. Mufti, and Rose Ann Padua. Reactive oxygen species, dna damage, and error-prone repair: a model for genomic instability with progression in myeloid leukemia? *Cancer research*, 67:8762–8771, 9 2007. ISSN 0008-5472. doi: 10.1158/0008-5472.CAN-06-4807. URL https://pubmed.ncbi.nlm.nih.gov/17875717/.

[235] Zarir E. Karanjawala, Niamh Murphy, David R. Hinton, Chih Lin Hsieh, and Michael R. Lieber. Oxygen metabolism causes chromosome breaks and is associated with the neuronal apoptosis observed in dna double-strand break repair mutants. *Current Biology*, 12:397–402, 3 2002. ISSN 09609822. doi: 10.1016/S0960-9822(02)00684-X/ATTACHMENT/B6728D64-A56A-45EE-AFAE-A89452E66AE0/MMC1.PDF. URL http://www.cell.com/article/S096098220200684X/fulltexthttp://www.cell.com/article/S096098220200684X/abstracthttps://www.cell.com/current-biology/abstract/S0960-9822(02)00684-X.

[236] Christine S. Gibhardt, Bastian Roth, Indra Schroeder, Sebastian Fuck, Patrick Becker, Burkhard Jakob, Claudia Fournier, Anna Moroni, and Gerhard Thiel. X-ray irradiation activates K+ channels via H2O2 signaling. *Scientific Reports 2015 5:1*, 5(1):1–11, sep 2015. ISSN 2045-2322. doi: 10.1038/srep13861. URL https://www.nature.com/articles/srep13861.

[237] Swati Dey, Agnieszka Sidor, and Brian O'Rourke. Compartment-specific control of reactive oxygen species scavenging by antioxidant pathway enzymes. *The Journal of Biological Chemistry*, 291:11185, 5 2016. ISSN 1083351X. doi: 10.1074/JBC.M116.726968. URL /pmc/articles/PMC4900267//pmc/articles/PMC4900267/?report=abstracthttps://www.ncbi.nlm.nih.gov/pmc/articles/PMC4900267/.

[238] Young Mi Go and Dean P. Jones. Redox control systems in the nucleus: Mechanisms and functions. *Antioxidants Redox Signaling*, 13:489, 8 2010. ISSN 15230864. doi: 10.1089/ARS.2009.3021. URL /pmc/articles/PMC2935340//pmc/articles/PMC2935340/?report=abstracthttps://www.ncbi.nlm.nih.gov/pmc/articles/PMC2935340/.

[239] Maximilian Diehn, Robert W. Cho, Neethan A. Lobo, Tomer Kalisky, Mary Jo Dorie, Angela N. Kulp, Dalong Qian, Jessica S. Lam, Laurie E. Ailles, Manzhi Wong, Benzion Joshua, Michael J. Kaplan, Irene Wapnir, Frederick M. Dirbas, George Somlo, Carlos Garberoglio, Benjamin Paz, Jeannie Shen, Sean K. Lau, Stephen R. Quake, J. Martin Brown, Irving L. Weissman, and Michael F. Clarke. Association of reactive oxygen species levels and radioresistance in cancer stem cells. *Nature*, 458:780–783, 4 2009. ISSN 0028-0836. doi: 10.1038/NATURE07733. URL https://profiles.wustl.edu/en/publications/association-of-reactive-oxygen-species-levels-and-radioresistance.

[240] Ankita Nandi, Liang Jun Yan, Chandan Kumar Jana, and Nilanjana Das. Role of catalase in oxidative stress- and age-associated degenerative diseases. *Oxidative Medicine and Cellular Longevity*, 2019, 2019. ISSN 19420994. doi: 10.1155/2019/9613090.

[241] M. Y. Kang, H. B. Kim, C. Piao, K. H. Lee, J. W. Hyun, I. Y. Chang, and H. J. You. The critical role of catalase in prooxidant and antioxidant function of p53. *Cell Death Differentiation 2013 20:1*, 20:117–129, 8 2012. ISSN 1476-5403. doi: 10.1038/cdd.2012.102. URL https://www.nature.com/articles/cdd2012102.

[242] Iman Azimi, Rosalie M. Petersen, Erik W. Thompson, Sarah J. Roberts-Thomson, and Gregory R. Monteith. Hypoxia-induced reactive oxygen species mediate N-cadherin and SERPINE1 expression, EGFR signalling and motility in MDA-MB-468 breast cancer cells. *Scientific Reports*, 7(1):1–11, nov 2017. ISSN 20452322. doi: 10.1038/s41598-017-15474-7. URL https://www.nature.com/articles/s41598-017-15474-7.

[243] Dwight J. Klemm, Susan M. Majka, Joseph T. Crossno, John C. Psilas, Jane Eb Reusch, and Chrystelle V. Garat. Reduction of reactive oxygen species prevents hypoxia-induced CREB depletion in pulmonary artery smooth muscle cells. *Journal of Cardiovascular Pharmacology*, 58(2):181–191, aug 2011. ISSN 01602446. doi: 10.1097/FJC.0b013e31821f2773. URL /pmc/articles/PMC3155008//pmc/articles/PMC3155008/?report=abstracthttps://www.ncbi.nlm.nih.gov/pmc/articles/PMC3155008/.

[244] Ricardo Vergara, Francisca Parada, Sebastián Rubio, and Francisco J. Pérez. Hypoxia induces H2O2 production and activates antioxidant defence system in grapevine buds through mediation of H 2O2 and ethylene. *Journal of Experimental Botany*, 63(11):4123–4131, jun 2012. ISSN 00220957. doi: 10.1093/jxb/ers094. URL https://pubmed.ncbi.nlm.nih.gov/22451722/.

[245] Gianluca Sgarbi, Giulia Gorini, Francesca Liuzzi, Giancarlo Solaini, and Alessandra Baracca. Hypoxia and IF1 Expression Promote ROS Decrease in Cancer Cells. *Cells*, 7(7):64, jun 2018. ISSN 20734409. doi: 10.3390/cells7070064. URL /pmc/articles/PMC6071258//pmc/articles/PMC6071258/?report=abstracthttps://www.ncbi.nlm.nih.gov/pmc/articles/PMC6071258/.

[246] Derek Hennessey, Lynn M. Martin, Anne Atzberger, Thomas H. Lynch, Donal Hollywood, and Laure Marignol. Exposure to hypoxia following irradiation increases radioresistance in prostate cancer cells. *Urologic Oncology: Seminars and Original Investigations*, 31(7):1106–1116, 2013. ISSN 10781439. doi: 10.1016/j.urolonc.2011.10.008. URL http://dx.doi.org/10.1016/j.urolonc.2011.10.008.

[247] Sundarraj Jayakumar, Debojyoti Pal, and Santosh K. Sandur. Nrf2 facilitates repair of radiation induced dna damage through homologous recombination repair pathway in a ros independent manner in cancer cells. *Mutation Research/Fundamental and Molecular Mechanisms of Mutagenesis*, 779:33–45, 9 2015. ISSN 0027-5107. doi: 10.1016/J.MRFMMM.2015.06.007.

[248] Alina Küper, Jennifer Baumann, Kirsten Göpelt, Melanie Baumann, Christopher Sänger, Eric Metzen, Philip Kranz, and Ulf Brockmeier. Overcoming hypoxia-induced resistance of pancreatic and lung tumor cells by disrupting the perk-nrf2-hif-axis. *Cell death disease*, 12:82, 1 2021. ISSN 20414889. doi: 10.1038/S41419-020-03319-7.

[249] Ranjit S. Bindra, Paul J. Schaffer, Alice Meng, Jennifer Woo, Kårstein Måseide, Matt E. Roth, Paul Lizardi, David W. Hedley, Robert G. Bristow, and Peter M. Glazer. Down-regulation of rad51 and decreased homologous recombination in hypoxic cancer cells. *Molecular and cellular biology*, 24:8504–8518, 10 2004. ISSN 0270-7306. doi: 10.1128/MCB.24.19.8504-8518.2004. URL https://pubmed.ncbi.nlm.nih.gov/15367671/.

[250] Kaisa R. Luoto, Ramya Kumareswaran, and Robert G. Bristow. Tumor hypoxia as a driving force in genetic instability. *Genome integrity*, 4, 10 2013. ISSN 2041-9414. doi: 10.1186/2041-9414-4-5. URL https://pubmed.ncbi.nlm.nih.gov/24152759/.

[251] Ramya Kumareswaran, Olga Ludkovski, Alice Meng, Jenna Sykes, Melania Pintilie, and Robert G. Bristow. Chronic hypoxia compromises repair of dna double-strand breaks to drive genetic instability. *Journal of cell science*, 125:189–199, 1 2012. ISSN 1477-9137. doi: 10.1242/JCS.092262. URL https://pubmed.ncbi.nlm.nih.gov/22266907/.

[252] Ludovic Deriano and David B. Roth. Modernizing the nonhomologous end-joining repertoire: Alternative and classical nhej share the stage. *http://dx.doi.org/10.1146/annurev-genet-110711-155540*, 47:433–455, 11 2013. ISSN 15452948. doi: 10.1146/ANNUREV-GENET-110711-155540. URL https://www.annualreviews.org/doi/abs/10.1146/annurev-genet-110711-155540.

[253] Maria Jasin and Rodney Rothstein. Repair of strand breaks by homologous recombination. *Cold Spring Harbor perspectives in biology*, 5, 2013. ISSN 1943-0264. doi: 10.1101/CSHPERSPECT.A012740. URL https://pubmed.ncbi.nlm.nih.gov/24097900/.

[254] Chao Dong, Fengmei Zhang, Yue Luo, Hui Wang, Xipeng Zhao, Gongshe Guo, Simon N. Powell, and Zhihui Feng. p53 suppresses hyper-recombination by modulating brca1 function. *DNA repair*, 33:60, 9 2015. ISSN 15687856. doi: 10.1016/J.DNAREP.2015.06.005. URL /pmc/articles/PMC4960982//pmc/articles/PMC4960982/?report=abstracthttps://www.ncbi.nlm.nih.gov/pmc/articles/PMC4960982/.

[255] Sylvie Moureau, Janna Luessing, Emma Christina Harte, Muriel Voisin, and Noel Francis Lowndes. A role for the p53 tumour suppressor in regulating the balance between homologous recombination and non-homologous end joining. *Open biology*, 6, 9 2016. ISSN 2046-2441. doi: 10.1098/RSOB.160225. URL https://pubmed.ncbi.nlm.nih.gov/27655732/.

[256] Andrea Ghelli Luserna Di Rorà, Claudio Cerchione, Giovanni Martinelli, and Giorgia Simonetti. A WEE1 family business: Regulation of mitosis, cancer progression, and therapeutic target. *Journal of Hematology and Oncology*, 13(1), sep 2020. ISSN 17568722. doi: 10.1186/S13045-020-00959-2.

[257] Y. Q. Li, Y. P. Guo, V. Jay, P. A. Stewart, and C. S. Wong. Time course of radiation-induced apoptosis in the adult rat spinal cord. *Radiotherapy and Oncology*, 39(1):35–42, apr 1996. ISSN 0167-8140. doi: 10.1016/0167-8140(96)01705-7. URL `http://www.thegreenjournal.com/article/0167814096017057/fulltext`.

[258] H. J. Park, J. C. Lyons, T. Ohtsubo, and C. W. Song. Cell cycle progression and apoptosis after irradiation in an acidic environment. *Cell death and differentiation*, 7(8):729–738, 2000. ISSN 1350-9047. doi: 10.1038/SJ.CDD.4400702. URL `https://pubmed.ncbi.nlm.nih.gov/10918447/`.

**Acknowledgements**

I would first like to thank my supervisor Prof. Dr. Joao Seco for giving me the opportunity work in his group on this project at DKFZ for the past four years. I thank him for his continued support and enthusiasm throughout the PhD, as well as being a member of my thesis advisory committee (TAC) and a referee for my thesis. I would like to also thank Prof. Dr. Christian Karger for agreeing to be my second thesis referee and for being a valued member of my TAC. In addition, I would like to thank the other members of my TAC, Prof. Dr. Oliver Jäkel and Prof. Dr. Michael Hausmann. Thank you all for offering important and useful advice throughout the PhD years.

I would like to convey my sincerest gratitude to Dr. Francesca Pagliari, without whom honestly this thesis and work would not have been possible. Thank you for being there with me and this project from (almost) the start. Your unconditional support and encouragement are what got me through until the end. Thank you for all of your advice and help throughout, from the experiments to the thesis, you were the driving force. Hopefully all of those countless late nights, weekends in the lab and sitting in hypoxia were finally worth it! You are both a mentor and a friend - Go raibh míle míle maith agat Fra!

Many thanks to current and past members from the division of Biomedical Physics in Radiation Oncology (E041) at the German Cancer Research Center. You all have made my time here so enjoyable. From the many dinners to the endless amounts of cake eaten, it's been an absolute pleasure sharing this experience with you all. In particular, I would like to say thank to Dr. Joana Guerreiro for her teaching and advice in the early stages of the PhD which helped to start one of the main areas of focus in the thesis. I would also like thank my fellow PhD students Daniel Garcia and Jeannette Jansen for being there to help throughout some of the inevitable PhD struggles.

To Jonah, from the bottom of my heart, I would like to say a BILLION thanks for everything you've done for me these past few years - From being my emotional support and motivating me when I needed it, especially in the last few weeks, to helping with formatting and proof-reading the thesis right up until submission. You have been amazing and I don't think I could have done it without you.

Finally, I would like to thank my family and friends. Special thanks to my family for supporting me from Ireland and always being on the other end of the phone. Thanks to my friends and all my WG 2.8 flatmates for always being there through the good and the bad times. It has been an emotional rollercoaster throughout these past four years but you all have made it such an amazing and unforgettable experience and definitely worth it.

**Declaration**

I, Rachel A. Hanley, declare that this Ph.D. thesis is the result of my own research, and that all sources used in this work have been duly referenced. This thesis has not been submitted to any other university or institute for a degree award.

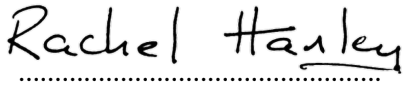

Heidelberg, December 6$^{th}$ 2021

Rachel A. Hanley